UNIVERSITY OF CALIFORNIA

Los Angeles

Economic Model Predictive Control Using Data-Based Empirical Models

A dissertation submitted in partial satisfaction of the

requirements for the degree Doctor of Philosophy

in Chemical Engineering

by

Anas Wael Alanqar

2017

ABSTRACT OF THE DISSERTATION

Economic Model Predictive Control Using Data-Based Empirical Models

by

Anas Wael Alanqar

Doctor of Philosophy in Chemical Engineering

University of California, Los Angeles, 2017

Professor Panagiotis D. Christofides, Chair

The increasingly competitive and continuously changing world economy has made it necessary to exploit the economic potential of chemical processes which has led engineers to economically optimize process operation to provide long-term economic growth. Approaches for increasing the profitability of industrial processes include directly incorporating process economic considerations into the system's operation and control policy. A fairly recent control strategy, termed economic model predictive control (EMPC), is capable of coordinating dynamic economic plant optimization with a feedback control policy to allow real-time energy management. The key underlying assumption to design and apply an EMPC is that a process/system dynamic model is available to predict the future process state evolution. Constructing models of dynamical systems is done either through first-principles and/or from process input/output data. First-principle models attempt to account for the essential mechanisms behind the observed physico-chemical phenomena. However, arriving at a first-principles model may be a challenging task for complex and/or poorly understood processes in which system identification serves as a suitable alternative. Motivated by this, the first part of my doctoral research has focused on introducing novel economic model predictive control schemes that are designed utilizing models obtained from advanced system identification methods. Various system identification schemes were investigated in the EMPC designs including linear

modeling, multiple models, and on-line model identification. On-line model identification is used to obtain more accurate models when the linear empirical models are not capable of capturing the nonlinear dynamics as a result of significant plant disturbances and variations, actuator faults, or when it is desired to change the region of operation. An error-triggered on-line model identification approach is introduced where a moving horizon error detector is used to quantify prediction error and trigger model re-identification when necessary. The proposed EMPC schemes presented great economic benefit, precise predictions, and significant computational time reduction. These benefits indicate the effectiveness of the proposed EMPC schemes in practical industrial applications. The second part of the dissertation focuses on EMPC that utilizes well-conditioned polynomial nonlinear state-space (PNLSS) models for processes with nonlinear dynamics. A nonlinear system identification technique is introduced for a broad class of nonlinear processes which leads to the construction of polynomial nonlinear state-space dynamic models which are well-conditioned with respect to explicit numerical integration methods. This development allows using time steps that are significantly larger than the ones required by nonlinear state-space models identified via existing techniques. Finally, the dissertation concludes by investigating the use of EMPC in tracking a production schedule. Specifically, given that only a small subset of the total process state vector is typically required to track certain production schedules, a novel EMPC is introduced scheme that forces specific process states to meet the production schedule and varies the rest of the process states in a way that optimizes process economic performance.

The dissertation of Anas Wael Alanqar is approved.

Lieven Vandenberghe

Dante A. Simonetti

James Davis

Panagiotis D. Christofides, Committee Chair

University of California, Los Angeles

2017

Contents

List of Figures

ACKNOWLEDGEMENTS

I would like to gratefully thank my advisor, Professor Panagiotis D. Christofides, for his remarkable support throughout my doctoral work. I was very fortunate to have him as my Ph.D. advisor. His research field is of very high interest for me and has numerous applications in both academia and industry. Professor Christofides was always supportive and encouraging. His dedication and passion to his work have always motivated me to aim to do better and to be humble about my work. I would like to thank Professor James Davis, Professor Dante A. Simonetti and Professor Lieven Vandenberghe for agreeing to serve on my doctoral committee.

I would like to thank Dr. Matthew James Ellis for being an excellent colleague at the beginning of my graduate studies. I greatly appreciate his valuable guidance that helped me to start my research work. I would like to also thank Helen Durand for being an outstanding colleague who worked closely with me on many of my research projects. Her comments and detailed oriented personality have strengthened the quality of my work. Also, I would like to thank all my lab mates during my graduate career for being great colleagues and close friends throughout my time at UCLA.

Financial support from the Department of Energy (DOE) and the National Science Foundation (NSF) is gratefully acknowledged.

Finally and most importantly, I would like to thank my father, Wael I. Alanqar, and my mother, Wafa Al-Farra, for their faith in me and their nonstop support and encouragement. My father's ambition in life and appreciation for knowledge has inspired me to always seek knowledge and try to go beyond the disciplinary boundaries. My parents have always supported me in being successful in life. Witnessing their dedication and determination on a daily basis motivated me to always try to learn and improve myself. They started me on my path to success which I am extremely grateful and fortunate to have.

Chapter 2 is a version of: A. Alanqar, M. Ellis, and P. D. Christofides. Economic model predictive control of nonlinear process systems using empirical models. *AIChE J.*, 61:816-830, 2015.

Chapter 3 is a version of: A. Alanqar, H. Durand, and P. D. Christofides. On identification of wellconditioned nonlinear systems: Application to economic model predictive control of nonlinear processes. *AIChE J.*, 61:3353-3373, 2015.

Chapter 4 is a version of: A. Alanqar, H. Durand, and P. D. Christofides. Error-triggered online model identification for modelbased feedback control. *AIChE J.*, 63:949–966, 2017.

Chapter 5 is a version of: A. Alanqar, H. Durand, and P. D. Christofides. Fault-Tolerant Economic Model Predictive Control Using Error-Triggered On-line Model Identification. *Industrial & Engineering Chemistry Research J.*, submitted, 2017.

Chapter 6 is a version of: A. Alanqar, H. Durand, F. Albalaw, and P. D. Christofides. An economic model predictive control approach to integrated production management and process operation. *AIChE J.*, in press, 2017.

VITA

2008–2013	Bachelor of Science, Chemical Engineering Department of Chemical and Petroleum Engineering Kansas University
2013	Graduation Distinction Kansas University
2013–2017	Graduate Student Researcher / Teaching Assistant Department of Chemical and Biomolecular Engineering University of California, Los Angeles
2017	Teaching Assistant and Associate Department of Chemical and Biomolecular Engineering University of California, Los Angeles

PUBLICATIONS

1. A. Alanqar, M. Ellis, and P. D. Christofides, "Economic model predictive control of nonlinear process systems using empirical models," *AIChE Journal*, 2015, **61**, 816-830.

2. A. Alanqar, H. Durand, and P. D. Christofides, "On identification of wellconditioned nonlinear systems: Application to economic model predictive control of nonlinear processes," *AIChE Journal*, 2015, **61**, 3353-3373.

3. A. Alanqar, H. Durand, and P. D. Christofides, "Error-triggered online model identification for modelbased feedback control," *AIChE Journal*, 2017, **63**, 949-966.

4. A. Alanqar, H. Durand, and P. D. Christofides, "Fault-Tolerant Economic Model Predictive Control Using Error-Triggered On-line Model Identification," *Industrial & Engineering Chemistry Research Journal*, 2017, submitted.

5. A. Alanqar, H. Durand, F. Albalaw and P. D. Christofides, "An economic model predictive control approach to integrated production management and process operation," *AIChE Journal*, 2017, in press.

Chapter 1

Introduction

1.1 Development of Economic Model Predictive Control

The chemical industry plays a vital role in the US economy. The competitive market and continuously changing consumer demand have made it necessary to find reliable and flexible operation strategies to meet the consumer demand while maximizing economics. The traditional paradigm in achieving optimal operations is done through two layers. In the upper layer, real-time optimization (RTO) is carried out in order to find optimal process set-points utilizing the steady-state models of the plant. These set-points are then sent to the lower layer which forces the plant to operate at these steady states. Increasing operational efficiency is one of the most important determinants of success of the chemical and petrochemical industry, which has led engineers to develop cost effective operational strategies to optimize plant management. Integration of economic considerations and process control serves as one approach for optimizing process operation. A fairly recent control strategy that coordinates dynamic economic plant optimization with a feedback control policy, termed economic model predictive control (EMPC), has gained attention due to its ability to promote optimal time-varying operation while accounting for constraints and ensuring closed-loop stability.

The EMPC structure shares many of its characteristics with the traditional tracking model

predictive control (MPC). Both control strategies utilize the process model to predict the future evolution of the process state over a certain horizon. Then, dynamic optimization problems are solved on-line in order to calculate optimal control actions that achieve the desired objective of the controller. In MPC, the objective is to track certain operating set-points (steady-states) that are determined by the RTO layer. MPC is typically formulated with a quadratic cost function that penalizes both: 1) Deviations of the process state from the desired steady-state, and 2) The energy utilized in order to drive the system into this desired steady-state. On the other hand, EMPC framework deals with a reformulation of the conventional MPC quadratic cost function in which an economic (not necessarily quadratic) cost function is used directly as the cost in MPC, and thus, it may, in general, lead to time-varying process operation policies (instead of steady-state operation), which directly optimizes process economics on-line. This allows for real-time energy management and avoids delays in optimization that occur in the two layer RTO-MPC structure. Several EMPC formulations have been proposed in recenrt years in order to guarantee closed-loop stability including EMPC with terminal constrains, EMPC with terminal regions and EMPC with Lyapunov-based constraints.

1.2 MPC and EMPC in Industrial Process Systems Using Empirical Models

As mentioned in the previous section, economic model predictive control (EMPC) is a feedback control technique that attempts to tightly integrate economic optimization and feedback control since it is a predictive control scheme that is formulated with an objective function representing the process economics. Numerous research works have considered applying EMPC to realistic chemical engineering examples including large-scale chemical process networks and catalytic reactors. As its name implies, EMPC requires the availability of a dynamic model to compute its control actions. Most applications assumed the availability of a first-principles process model that accurately describes the plant dynamics. However, in industrial practice, obtaining accurate first-

principles models is a challenging task for complex and/or poorly understood processes in which case empirical models constructed using process data may be used in the design of the feedback controller.

In the past ten years, significant work has been done on the application of MPC using empirical models. To enable the application of EMPC to complex industrial processes, EMPC designed with empirical modeling must be introduced. Recent research in the area of system identification has led to the development of various advanced linear and nonlinear model identification techniques that are able to capture process dynamics within large regions of operation. Having such advanced model identification methods facilitates the application of EMPC in industrial practice. The effectiveness of applying empirical model-based EMPC schemes in practical industrial applications can present great economic benefit, precise predictions, and significant computational time reduction when the empirical model that captures the important process dynamics is significantly simpler than the first principles model.

A variety of input/output system identification methods (e.g., (nonlinear) autoregressive moving average with exogenous input ((N)ARMAX) methods, or methods that identify polynomial and neural-network models[7,51,69]) have been developed. Input/output models, such as Hammerstein models,[17] Wiener models,[70] Hammerstein-Wiener models,[8,34] polynomial ARX models,[6,74] and neural Wiener models[47,60,61] have been used in tracking model predictive control (MPC) applications

Another type of empirical modeling that is also widely used is empirical state-space modeling. System identification techniques have been developed to identify linear and nonlinear state-space models. Several linear state-space system identification methods based on input/output data, such as optimization-based methods and subspace model identification, have been developed that can be used for multiple-input/multiple-output (MIMO) systems because of their ability to model interactions among process states.[4,5,9,37,56,71,73,76] Subspace model identification has been investigated for use in model predictive control[65] and can be carried out through a variety of techniques such as the canonical variate algorithm (CVA),[59] the multivariable output error state-space algo-

rithm (MOESP),[16,42–44] and numerical algorithms for subspace state-space system identification (N4SID).[39] Using subspace model identification within the context of EMPC is expected to be beneficial since the EMPC requires the use of a state-space model, and the EMPC cost function depends on most of the states (if not all).

In both input/output and state-space empirical modeling, a wide variety of polynomial functions have been used to identify nonlinear models. Polynomial functions used in input/output system identification include Chebyshev polynomials,[58] Volterra polynomials,[62,69] polynomial ARX models,[74] Laguerre polynomials,[63] and polynomial neural networks.[69] Traditional empirical modeling approaches focus on a certain class of nonlinear systems like Wiener-Hammerstein or neural networks but nonlinear state-space models cover a much larger class of systems. The need for a general nonlinear system identification technique that can represent many classes of nonlinear systems led to the development of state-space nonlinear system identification techniques based on input/output data. The polynomial nonlinear state-space (PNLSS) approach is a system identification method for MIMO systems that leads to a model of a multivariable nonlinear system based purely on input/output data.[52,64,67,68,75,77] PNLSS is a promising all-purpose nonlinear system identification method that can be used for many different types of systems, including those that are described by bilinear models, Wiener-Hammerstein models, and models with nonlinearities appearing in the states or inputs, or appearing in both.[64,67,68,75] Therefore, using PNLSS models in the EMPC design can result in improved economic performance since PNLSS models allow operation over a wider region in state-space.

In the case that the process is subject to significant plant disturbances and variations, actuator faults, or when it is desired to change the region of operation, the empirical models may not be able to capture the resulting dynamics in the new conditions. Therefore, re-identified of the process model on-line, when significant prediction errors occur, is necessary in order to compensate for the changes in the plant. Thus, when operating conditions change, on-line model re-identification may be used within the EMPC design in order to compensate for changes in the plant model which would result in better economic performance.

1.3 Production Management in the Chemical Industry

Managing production schedules and tracking time-varying demand of certain products while optimizing process economics are subjects of central importance in industrial applications.[90–93] The rapidly changing demand of chemical products has made it necessary to exploit dynamic optimization methods in order to cope the changing markets. Shifts in demand and supply of certain products occur constantly and finding reliable methods to achieve the desired production has become necessary.[94,95] In the chemical industry, it has become common to produce multiple products from the same plant in both batch and continuous processes.[91,93] Several frameworks that use optimization strategies have been proposed for scheduling in order to optimize the decision-making process while accounting for practical constraints and limitations.[93,94] Scheduling and control are two crucial elements that serve the same overall goal of maximizing plant economics while meeting the customer demand. After solving the scheduling problem, process control strategies are used to drive the plant to follow the desired production schedule. Extensive research efforts have been dedicated recently to develop reliable methods that could track desired production setpoints corresponding to different operating conditions.[91,105,106] The use of MPC in tracking the desired production schedule while accounting for input/output constraints has also been considered.[90,91,105]

Generally, only a subset of the total process state vector is requested to follow production schedules. Therefore, there is a potential in many processes to meet the desired schedule while achieving economically optimal process operation. Thus, it is expected that introducing a novel EMPC framework can lead a control strategy that meets the production schedule for the desired states while maximizing economics with respect to the rest of the states.

1.4 Dissertation Objectives and Structure

Motivated by the above considerations, this dissertation focuses on the development of novel EMPC designs that utilize empirical models and the application of EMPC in production man-

agement. Various system identification schemes were investigated in the EMPC designs including linear modeling, non-linear modeling, multiple models, and on-line model identification. On-line model identification is used to obtain more accurate models when the linear empirical models are not capable of capturing the nonlinear dynamics as a result of significant plant disturbances and variations, actuator faults, or when it is desired to change the region of operation. Finally, the use of EMPC in tracking a production schedule is investigated. Conditions to guarantee feasibility and closed stability of the proposed schemes are derived. The dissertation has the following structure:

Chapter 2 focuses on the development of a Lyapunov-based economic model predictive control (LEMPC) designed with an empirical model that allows for closed-loop stability guarantees in the context of nonlinear chemical processes. Specifically, when the linear model provides a sufficient degree of accuracy in the region where time-varying economically optimal operation is considered, conditions for closed-loop stability under the LEMPC scheme based on the empirical model are derived. The LEMPC scheme is applied to a chemical process example to demonstrate its closed-loop stability and performance properties as well as significant computational advantages.

Chapter 3 focuses on the development of EMPC that utilizes well-conditioned polynomial nonlinear state-space models for processes with nonlinear dynamics. Specifically, the chapter initially addresses the development of a nonlinear system identification technique for a broad class of nonlinear processes which leads to the construction of polynomial nonlinear state-space dynamic models which are well-conditioned over a broad region of process operation in the sense that they can be correctly integrated in real-time using explicit numerical integration methods via time steps that are significantly larger than the ones required by nonlinear state-space models identified via existing techniques. Working within the framework of polynomial nonlinear state-space (PNLSS) models, additional constraints are imposed in the identification procedure to ensure well-conditioning of the identified nonlinear dynamic models. This development is key because it enables the design of Lyapunov-based EMPC (LEMPC) systems for nonlinear processes using the well-conditioned nonlinear models that can be readily implemented in real-time since the computational burden required to compute the control actions within the process sampling period is reduced. A stability

analysis for this LEMPC design is provided that guarantees closed-loop stability of a process under certain conditions when an LEMPC based on a nonlinear empirical model is used. Finally, a classical chemical engineering reactor example demonstrates both the system identification and LEMPC design techniques, and the significant advantages in terms of computation time reduction in LEMPC calculations when using the nonlinear empirical model.

Chapter 4 addresses the fact that linear empirical models may not capture the nonlinear dynamics over a wide region of state-space and may also perform poorly when significant plant variations and disturbances occur. Therefore, an error-triggered on-line model identification approach is introduced for closed-loop systems under model-based feedback control strategies. The linear models are re-identified on-line when significant prediction errors occur. A moving horizon error detector is used to quantify the model accuracy and to trigger the model re-identification on-line when necessary. The proposed approach is demonstrated through two chemical process examples using a Lyapunov-based economic model predictive control (LEMPC). The chemical process examples illustrate that the proposed error-triggered on-line model identification strategy can be used to obtain more accurate state predictions to improve process economics while maintaining closed-loop stability of the process.

Chapter 5 presents a data-driven methodology to overcome actuator faults in empirical model-based feedback control. More specifically, the chapter introduces the use of a moving horizon error detector that quantifies prediction errors and triggers updating of the model used in the controller on-line when significant prediction errors occur due to the loss of one of the actuators. Model re-identification is conducted on-line using the most recent input/output data collected after the fault occurrence. The error-triggered on-line model identification approach can be applied to overcome various types of actuator faults, including the case where the value at which the actuator is stuck is known and the case where the value at which the actuator is stuck is unknown. The proposed methodology is applied in economic model predictive control (EMPC). Two different chemical process examples are considered in order to demonstrate the application of the proposed strategy. In the first example, application of the proposed scheme for the case where the value at which

the actuator is stuck is known is demonstrated through a benchmark catalytic chemical reactor example where the actuator faults occur in the heat input causing shifts and variations in plant operating conditions. The second example demonstrates the case where the value at which the actuator is stuck is unknown through a typical chemical reactor example. The proposed scheme was able to compensate for the variations in the plant caused by the actuator loss by obtaining more accurate models that are suitable for the new conditions and updating them in the EMPC architecture. Improved economic performance was obtained as the updated models were able to capture process dynamics under the new conditions and provide better state predictions.

Chapter 6 investigates the use of economic model predictive control (EMPC) in tracking a production schedule. Specifically, given that only a small subset of the total process state vector is typically required to track certain scheduled values, a novel EMPC scheme is designed, through proper construction of the objective function and constraints, that forces specific process states to meet the production schedule and varies the rest of the process states in a way that optimizes process economic performance. Conditions under which feasibility and closed-loop stability of a nonlinear process under such an EMPC for schedule management can be guaranteed are developed. The proposed EMPC scheme is demonstrated through a chemical process example in which the product concentration is requested to follow a certain production schedule.

Finally, Chapter 7 summarizes the contributions of this dissertation.

Chapter 2

Economic Model Predictive Control of Nonlinear Process Systems Using Empirical Models

2.1 Introduction

The economic success of chemical and petrochemical industry relies heavily on optimal process operation which has led to the emergence of an overall process control goal to translating process/system economic considerations into feedback control objectives.[15] One key development towards achieving this goal is economic model predictive control (EMPC). EMPC is a feedback control technique that attempts to tightly integrate economic optimization and feedback control since it is a predictive control scheme that is formulated with an objective function representing the process/system economics[2,20,22] (see, also,[14] for an overview of recent results on EMPC). While initial efforts on EMPC have focused on closed-loop stability considerations recent developments have addressed economic performance improvement over conventional (tracking) model predictive control (MPC) including: formulating a Lyapunov-based EMPC with closed-loop performance guarantees over finite-time and infinite-time operating intervals,[13] investigating the tran-

sient performance and closed-loop stability of EMPC formulated without terminal constraints,[18] and studying the closed-loop performance of EMPC formulated with a self-tuning terminal cost and generalized terminal constraint.[32]

The key underlying assumption to design and apply an EMPC is that a process/system dynamic model is available to predict the future process state evolution. Constructing models of dynamical systems is done either through first principles and/or from process input/output data.[79] First-principle models are developed from conservation equations and attempt to account for the essential mechanisms behind the observed physico-chemical phenomena. However, arriving at a first principles model requires sufficient process knowledge which maybe a challenging task for complex industrial processes. On the other hand, system identification serves as an alternative to first principles models when first-principles models are unavailable and/or too complex to use on-line in model predictive control. Over the past thirty years, numerous methods have been developed to construct linear or nonlinear empirical models from input/output data (see, for example,[3,7,28,36,51] and the references contained therein for an overview of these methods). Perhaps, the most common type of empirical model is a linear model. When a process system exhibits significant nonlinearities as is the case in most chemical processes, the use of multiple linear models has been employed to improve the accuracy of prediction over a larger operating region.[19,23,33] One potential grouping of the various methods of system identification is to group the methods on the basis of the type of empirical model derived which may be either an input-output model or a state-space model. It is important to note that when the output vector is the entire state vector, input-output modeling methods may be used to construct a state-space model.

Within the context of input-output models, (nonlinear) autoregressive moving average with exogenous input models ((N)ARMAX), Volterra models, and neural-network models are some of the types of input-output models commonly used (see, for instance,[7,51] and the references therein for more details on input-output modeling). Numerous works on integrating input-output models within the context of tracking MPC, which is formulated with a cost function that is positive definite with respect to a set-point or steady-state, have been investigated. For instance, the use

of Hammerstein, Wiener, and Hammerstein-Wiener models within MPC[8,17,34] has been considered, the use of multiple-models within MPC constructed from autoregressive with exogenous input (ARX) models has been investigated for batch processes (e.g.,[6]), and multiple-model adaptive predictive control has been formulated for mean arterial pressure and cardiac output regulation (e.g.,[46]).

On the other hand, empirical state-space modeling methods are another type of empirical modeling techniques. Within this context, linear subspace system identification is a very widely known and used empirical modeling method that is based on input/output data.[37,39,42–44,56,76] In particular, subspace model identification (SMI) are non-iterative methods that take into account multivariable interactions and result in models that have great numerical stability for multiple-input multiple-output (MIMO) systems.[9,39,76] Some of the various subspace system identification algorithms in the literature include multi-variable output error state-space algorithm (MOESP),[16,42–44] the Canonical Variate Algorithm (CVA),[59] and numerical algorithms for subspace state-space system identification (N4SID).[39] Identifying the deterministic part of a MIMO state-space model using SMI methods has proven to be successful in the context of industrial settings.[1,16,29,41,43] Combining subspace methods with MPC has also been considered (see, for instance,[56] and the references contained therein).

To date, no work on formulating an EMPC scheme using an empirical model with guaranteed closed-loop stability properties has been completed. In this chapter, an integrated view of system modeling, feedback control, and process/system economics is undertaken. Specifically, an LEMPC formulated with an empirical model is considered. The type of empirical model is restricted to state-space models given the fact that the economic cost function typically depends on at least some (if not all) of the state variables. While the linear model may be derived from any system identification technique, it must be sufficiently close (in a sense to be made precise below) to the linearization of the nonlinear process model at the steady-state around which time-varying operation is considered. Under this assumption, sufficient conditions for closed-loop stability (boundedness of the closed-loop state in a compact state-space set) under the LEMPC with

the empirical linear model applied to the nonlinear chemical process are derived. The LEMPC with empirical model method is applied to a chemical process example and extensive closed-loop simulations are performed that demonstrate the closed-loop stability and performance properties. Furthermore, a significant reduction in the on-line computation time with LEMPC formulated with an empirical model is realized over LEMPC formulated with a nonlinear first-principles model.

2.2 Preliminaries

2.2.1 Notation

The Euclidean norm of a vector is denoted by the operator $|\cdot|$ and the (any) norm of a matrix is denoted as $\|\cdot\|$. A continuous function $\alpha : [0,a) \rightarrow [0,\infty)$ is said to belong to class $\mathscr{K}$ if it is strictly increasing and is zero when evaluated at zero. The symbol Ω_ρ is used to denote the set $\Omega_\rho := \{x \in R^{n_x} : V(x) \leq \rho\}$ where V is a continuously differentiable positive definite scalar function and $\rho > 0$. The symbol x^T denotes the transpose of the vector x.

2.2.2 Class of Systems

The class of nonlinear process systems considered can be written in the following continuous-time state-space form:

$$\dot{x}(t) = f(x(t), u(t), w(t)) \tag{2.1}$$

where $x \in R^n$ is the state vector of the system, $u \in R^m$ is the control (manipulated) input vector, and $w \in R^l$ is the disturbance vector. The vector function f is assumed to be locally Lipschitz on $R^n \times R^m \times R^l$. The control actions are bounded by the physical constraints on the control actuators and thus, are restricted to belong to a nonempty convex set $U := \{u \in R^m : u_i^{\min} \leq u_i \leq u_i^{\max},\ i = 1,\ \ldots,\ m\}$. The norm of the disturbance vector is bounded (i.e., $|w(t)| \leq \theta$ for all t where $\theta > 0$ bounds the norm). The equilibrium of the system of Eq. 2.1 is considered to be the origin, i.e., $f(0,0,0) = 0$. The state of the system of Eq. 2.1 is assumed to be synchronously sampled and

available at sampling time instances $t_k = k\Delta$, $k = 0,\ 1,\ \ldots$ where $\Delta > 0$ is the sampling period.

We restrict the class of nonlinear systems of Eq. 2.1 considered to a class of stabilizable nonlinear systems. Specifically, we assume the existence of a Lyapunov-based controller $h(x) \in U$ that renders the origin of the closed-loop nominal system ($w(t) \equiv 0$) of Eq. 2.1 asymptotically stable for all x in an open neighborhood of the origin. This assumption implies the existence of a continuously differentiable Lyapunov function, $V : R^n \rightarrow R_+$, for the closed-loop system of Eq. 2.1 under $u(t) = h(x(t))$ that satisfies:[30,111]

$$\alpha_1(|x|) \leq V(x) \leq \alpha_2(|x|), \tag{2.2a}$$

$$\frac{\partial V(x)}{\partial x} f(x, h(x), 0) \leq -\alpha_3(|x|), \tag{2.2b}$$

$$\left| \frac{\partial V(x)}{\partial x} \right| \leq \alpha_4(|x|) \tag{2.2c}$$

for all $x \in D \subseteq R^{n_x}$ where D is an open neighborhood of the origin and $\alpha_i(\cdot)$, $i = 1,\ 2,\ 3,\ 4$ are functions of class $\mathscr{K}$. For various classes of nonlinear systems, several stabilizing control laws that explicitly account for input constraints have been developed (see, for example,[10,12,27,83] for results in this direction). The stability region (i.e., the set of points in state-space where convergence to the origin under the Lyapunov-based controller is guaranteed) may be estimated as the level set of the Lyapunov function where the time-derivative of the Lyapunov function is negative, and is denoted as $\Omega_\rho \subset D$. Moreover, the origin of the sampled-data system resulting from the system of Eq. 2.1 under the Lyapunov-based controller when implemented in a sample-and-hold fashion is practically stable (i.e., the closed-loop state will converge to a small compact, forward invariant set containing the origin in its interior) when a sufficiently small sampling period is used and the disturbance vector is sufficiently small.[31]

In this chapter, empirical models will be constructed to predict the evolution of the state of the system of Eq. 2.1 using data-based modeling techniques. Specifically, the type of empirical models constructed for the system of Eq. 2.1 are linear time-invariant (LTI) state-space models which have

the following form:

$$\dot{x}(t) = Ax(t) + Bu(t) \tag{2.3}$$

where $x \in R^n$ is the state vector, $u \in R^m$ is the input vector, and A and B are constant matrices of appropriate dimensions. When the nominal nonlinear model of Eq. 2.1 is unavailable, the Lyapunov-based controller needs to be designed on the basis of the empirical model of Eq. 2.3. We assume that the pair (A,B) is stabilizable in the sense that there exists a state feedback controller $h_L(x) \in U$ that renders the origin of the closed-loop system of Eq. 2.3 exponentially stable for all initial conditions $x \in D_L$ where D_L is some open neighborhood of the origin. Furthermore, the controller $h_L(x) \in U$ is assumed to be locally Lipschitz on R^n in the sense that there exists a $K > 0$ such that $|h_L(x)|$ can be bounded by $K|x|$ for all x in a compact set containing the origin in its interior. When the controller $h_L(x)$ is applied to the nominal nonlinear system of Eq. 2.1, there are two factors that affect closed-loop stability: the closeness of the model of Eq. 2.3 to the linearization of the nominal model of Eq. 2.1 at the origin and the effect of the nonlinearities of the system of Eq. 2.1. Locally, we can show that the controller $h_L(x)$ possesses a robustness margin to overcome these two effects and render the origin of the nominal closed-loop nonlinear system asymptotically stable. This is stated in the following proposition.

Proposition 1 *If the origin of closed-loop system of Eq. 2.3 under the controller $h_L(x)$ is exponentially stable and there exist $\hat{\rho} > 0$ and $\delta > 0$ such that:*

$$\|\bar{A} - A\| + \|\bar{B} - B\|K \leq \delta \tag{2.4}$$

where the matrices $\bar{A}$ and $\bar{B}$ denote the linearization of $f(x,u,0)$ at the origin:

$$\bar{A} := \frac{\partial f}{\partial x}(0,0,0), \quad \bar{B} := \frac{\partial f}{\partial u}(0,0,0)\ . \tag{2.5}$$

then the origin of the nominal closed-loop system of Eq. 2.1 is exponentially stable for all $x \in \Omega_{\hat{\rho}} \subset D_L$.

Proof 2.1 *To prove the result of Proposition 1, we will show that there exists a Lyapunov function for the closed-loop system of Eq. 2.1 under the controller $h_L(x)$ when $\hat{\rho} > 0$ and $\delta > 0$ are sufficiently small. Owing to the fact that the origin of closed-loop system of Eq. 2.3 under the controller $h_L(x)$ is exponentially stable, there exists a continuously differentiable Lyapunov function $\hat{V} : R^n \to R_+$ such that:*[111]

$$c_1|x|^2 \leq \hat{V}(x) \leq c_2|x|^2, \tag{2.6a}$$

$$\frac{\partial \hat{V}(x)}{\partial x}\left(Ax + Bh_L(x)\right) \leq -c_3|x|^2, \tag{2.6b}$$

$$\left|\frac{\partial \hat{V}(x)}{\partial x}\right| \leq c_4|x| \tag{2.6c}$$

for all $x \in D_L$ where c_i, $i = 1,\ 2,\ 3,\ 4$ are positive constants. Define

$$g(x) := f(x, h_L(x), 0) - \bar{A}x - \bar{B}h_L(x) \tag{2.7}$$

which contains terms of second-order and higher in x. Consider the following closed-loop system:

$$\dot{x} = Ax + Bh_L(x) + f(x, h_L(x)) - Ax - Bh_L(x)\ . \tag{2.8}$$

and the time-derivative of $\hat{V}$ along the trajectory of the closed-loop system of Eq. 2.8:

$$\begin{aligned}
\dot{\hat{V}} &= \frac{\partial \hat{V}(x)}{\partial x}\left(Ax + Bh_L(x)\right) + \frac{\partial \hat{V}(x)}{\partial x}\left(f(x, h_L(x), 0) - Ax - Bh_L(x)\right) \\
&\overset{(5.4b)}{\leq} -c_3|x|^2 + \left|\frac{\partial \hat{V}(x)}{\partial x}\right| \left|\left(\bar{A} - A\right)x + \left(\bar{B} - B\right)h_L(x) + g(x)\right| \\
&\overset{(5.4c)}{\leq} -c_3|x|^2 + c_4|x|\left(\left|\left(\bar{A} - A\right)x + \left(\bar{B} - B\right)h_L(x)\right| + |g(x)|\right)
\end{aligned} \tag{2.9}$$

for all $x \in D_L$. Since the controller $h_L(x)$ is locally Lipschitz, there exists a $K > 0$ such that:

$$\begin{aligned}
\dot{\hat{V}} &\leq -c_3|x|^2 + c_4|x|\left(\left(\left\|\bar{A} - A\right\||x| + \|\bar{B} - B\|\,|h_L(x)|\right) + |g(x)|\right) \\
&\leq -c_3|x|^2 + c_4|x|\left(\left(\left\|\bar{A} - A\right\| + \|\bar{B} - B\|K\right)|x| + |g(x)|\right)
\end{aligned} \tag{2.10}$$

for all $x \in B_R = \{x \in R^n : |x| \leq R\}$ where R is any $R > 0$ such that $B_R \subset D_L$. If the condition of Eq. 2.4 is satisfied, there exits a $\delta > 0$ such that:

$$\dot{\hat{V}} \leq -c_3|x|^2 + c_4\delta|x|^2 + c_4|x||g(x)| \tag{2.11}$$

for all $x \in B_R$. Since $g(x)$ contains terms of second-order and higher in x and vanishes at the origin, there exists a $\gamma > 0$ such that:

$$|g(x)| < \gamma|x|^2 \tag{2.12}$$

for all $x \in B_R$. Thus,

$$\dot{\hat{V}} \leq -c_3|x|^2 + c_4\delta|x|^2 + c_4\gamma|x|^3 \tag{2.13}$$

for all $x \in B_R$. For any $B_r \subset B_R$, the time-derivative of $\hat{V}$ can be bounded by the following:

$$\dot{\hat{V}} \leq -c_3|x|^2 + c_4(\delta + \gamma r)|x|^2 \tag{2.14}$$

for all $x \in B_r$ where $r < R$. If $\delta > 0$ and $r > 0$ are chosen to satisfy $c_3/c_4 > (\delta + \gamma r)$, then there exists a $\hat{c}_3 > 0$ such that:

$$\dot{\hat{V}} = \frac{\partial \hat{V}(x)}{\partial x}\left(f(x, h_L(x), 0)\right) \leq -\hat{c}_3|x|^2 \tag{2.15}$$

for all $|x| < r$. Let $\hat{\rho} > 0$ be such that $\hat{\rho} \leq \min\{\hat{V}(x) : |x| < r\}$ which completes the proof.

We will make use of the following properties in the "Stability Analysis" subsection. Owing to the locally Lipschitz property assumed for the vector function $f(\cdot,\cdot,\cdot)$ as well as the fact that the Lyapunov function $V(\cdot)$ is a continuously differentiable function, the following inequalities hold:

$$|f(x_1, u, w) - f(x_2, u, 0)| \leq L_x|x_1 - x_2| + L_w|w|, \tag{2.16}$$

$$\left|\frac{\partial V(x_1)}{\partial x} f(x_1, u, w) - \frac{\partial V(x_2)}{\partial x} f(x_2, u, 0)\right| \leq L'_x|x_1 - x_2| + L'_w|w| \tag{2.17}$$

for all $x_1, x_2 \in \Omega_{\hat{\rho}}$, $u \in U$ and $|w| \leq \theta$ where L_x, L_w, L'_x, and L'_w are positive constants. Additionally,

there exists $M > 0$ that bounds the vector field:

$$|f(x,u,w)| \leq M \tag{2.18}$$

for all $x \in \Omega_{\hat{\rho}}$, $u \in U$ and $|w| \leq \theta$ because $f(\cdot,\cdot,\cdot)$ is a locally Lipschitz vector function of its arguments and Ω_ρ and U are compact sets. For the linear model of Eq. 2.3, there exist $M_L > 0$ and $L_L > 0$ such that:

$$|Ax_1 + Bu| \leq M_L \tag{2.19}$$

$$\left| \frac{\partial V(x_1)}{\partial x}(Ax_1 + Bu) - \frac{\partial V(x_2)}{\partial x}(Ax_2 + Bu) \right| \leq L_L |x_1 - x_2| \tag{2.20}$$

for all $x_1, x_2 \in \Omega_{\hat{\rho}}$ and $u \in U$.

2.2.3 Lyapunov-based EMPC

A specific type of EMPC will be considered in this chapter. Specifically, we consider Lyapunov-based EMPC (LEMPC)[20] which utilizes the Lyapunov-based controller $h(x)$ in the design of two constraints. The two constraints allow for provable guarantees on closed-loop stability (the closed-loop state is always bounded in Ω_ρ). Each constraint defines an operating mode of the LEMPC.

The formulation of LEMPC is given by the following optimization problem:

$$\min_{u\in S(\Delta)} \quad \int_{t_k}^{t_{k+N}} L_e(\tilde{x}(\tau),u(\tau))\,d\tau \tag{2.21a}$$

$$\text{s.t.} \quad \dot{\tilde{x}}(t) = f(\tilde{x}(t),u(t),0) \tag{2.21b}$$

$$\tilde{x}(t_k) = x(t_k) \tag{2.21c}$$

$$u(t) \in U,\ \forall\, t \in [t_k,t_{k+N}) \tag{2.21d}$$

$$V(\tilde{x}(t)) \leq \rho_e,\ \forall\, t \in [t_k,t_{k+N}) \quad \text{if } x(t_k) \in \Omega_{\rho_e} \tag{2.21e}$$

$$\frac{\partial V(x(t_k))}{\partial x} f(x(t_k),u(t_k),0) \leq \frac{\partial V(x(t_k))}{\partial x} f(x(t_k),h(x(t_k)),0) \quad \text{if } x(t_k) \notin \Omega_{\rho_e} \tag{2.21f}$$

where the input trajectory over the prediction horizon $N\Delta$ is the decision variable in the optimization problem. The notation $\tilde{x}(t)$ denotes the predicted behavior of the state trajectory under the input trajectory computed by the LEMPC. The region Ω_{ρ_e} is a subset of the stability region Ω_ρ where time-varying operation is allowed (ρ_e which defines a level set of the Lyapunov function is chosen to make Ω_ρ invariant; see[20] for details regarding this point).

The objective function of the optimization problem of Eq. 2.21a is formulated with a stage cost derived from the economics of the system of Eq. 2.1 (e.g., the operating cost, energy cost, the negative of the operating profit, the negative of the production rate). The initial value problem embedded in the optimization problem (Eq. 2.21b-2.21c) is used to predict the evolution of the system over the prediction horizon where the initial condition is obtained through a state measurement at the current time step. The input constraint of Eq. 2.21d bounds the computed input trajectory to be within the admissible input set. Depending on where the current state is in state-space, mode 1, which is defined by the constraint of Eq. 2.21e, or mode 2, which is defined by the constraint of Eq. 2.21f, are active. Under mode 1 operation of the LEMPC, the computed input trajectory is allowed to force a potentially transient (time-varying) state trajectory while maintaining the predicted state in a subset of the stability region. The region $\Omega_{\rho_e} \subset \Omega_\rho$ is chosen on the basis of

closed-loop stability in the presence of uncertainty, i.e., $w(t) \not\equiv 0$. Under mode 2 operation of the LEMPC, the constraint of Eq. 2.21f forces the control action for the first sampling period in the prediction horizon to decrease the Lyapunov function by at least as much as the decrease forced by the control action computed by the Lyapunov-based controller. This contractive constraint will guarantee that any state starting in $\Omega_\rho \setminus \Omega_{\rho_e}$ will be eventually forced back to Ω_{ρ_e}. For more details and discussion of LEMPC along with a complete closed-loop stability analysis, the interested reader may refer to.[20]

2.3 Economic Model Predictive Control using Empirical Models

In this section, we summarize the formulation and implementation of an LEMPC formulated with an empirical model as well as derive sufficient conditions such that the closed-loop nonlinear system under the LEMPC formulated with an empirical model will be stable in a sense to be made precise below.

2.3.1 Formulation with Empirical Models and Implementation

The formulation of the LEMPC with the empirical model is similar to the LEMPC of Eq. 2.21 except it is formulated with the empirical model of Eq. 2.3, the stabilizing controller $h_L(x)$, and the

Lyapunov function $\hat{V}(x)$. The formulation of the LEMPC using an empirical model is given by:

$$\min_{u\in S(\Delta)} \quad \int_{t_k}^{t_{k+N}} L_e(\hat{x}(\tau),u(\tau))\,d\tau \tag{2.22a}$$

$$\text{s.t.} \quad \dot{\hat{x}}(t) = A\hat{x}(t)+Bu(t) \tag{2.22b}$$

$$\hat{x}(t_k) = x(t_k) \tag{2.22c}$$

$$u(t)\in U,\ \forall\, t\in[t_k,t_{k+N}) \tag{2.22d}$$

$$\hat{V}(\hat{x}(t))\le \hat{\rho}_e,\ \forall\, t\in[t_k,t_{k+N}) \quad \text{if } x(t_k)\in\Omega_{\hat{\rho}_e} \tag{2.22e}$$

$$\frac{\partial \hat{V}(x(t_k))}{\partial x}\left(Ax(t_k)+Bu(t_k)\right) \le \frac{\partial \hat{V}(x(t_k))}{\partial x}\left(Ax(t_k)+Bh_L(x(t_k))\right) \quad \text{if } x(t_k)\notin\Omega_{\hat{\rho}_e} \tag{2.22f}$$

where the notation $\hat{x}(t)$ is used to distinguish that the LEMPC predicts the evolution of the system of Eq. 2.1 with the empirical model of Eq. 2.3 and $\Omega_{\hat{\rho}_e}\subset\Omega_{\hat{\rho}}$ is the subset where time-varying operation under the LEMPC may dictate a time-varying operating policy (the other constraints are similar to that used in Eq. 2.21). The optimal solution of the optimization problem of Eq. 2.22 is denoted as $u^*(t|t_k)$ defined for $t\in[t_k,t_{k+N})$.

The LEMPC of Eq. 2.22 is implemented in a receding horizon fashion. At a sampling instance, the LEMPC is solved for an input trajectory $u^*(t|t_k)$ for $t\in[t_k,t_{k+N})$, but only applies the control action for the first sampling period of the prediction horizon to the system. The control action to be applied over the first sampling period is denoted as $u^*(t_k|t_k)$. The implementation strategy of the LEMPC is summarized in the following algorithm:

1. Receive a state measurement $x(t_k)$. Go to Step 2.

2. If $x(t_k)\in\Omega_{\hat{\rho}_e}$, go to Step 2.1. Else, go to Step 2.2.

   2.1 The mode 1 constraint of Eq. 2.22e is active and the mode 2 constraint of Eq. 2.22f is inactive. Go to Step 3.

   2.2 The mode 2 constraint of Eq. 2.22f is active and the mode 1 constraint of Eq. 2.22e is

inactive. Go to Step 3.

3. The optimization problem of Eq. 2.22 solves for its optimal input trajectory defined for $t \in [t_k, t_{k+N})$. Go to Step 4.

4. The first control action of the input trajectory $u^*(t_k|t_k)$ is applied to the system of Eq. 2.1. Go to Step 5.

5. $k := k+1$ and go to Step 1.

2.3.2 Stability Analysis

In this subsection, the stability properties of the LEMPC formulated with the empirical model are analyzed. The following proposition bounds the difference between the actual state trajectory of the system of Eq. 2.1 in the presence of uncertainty ($w(t) \not\equiv 0$) and the predicted state trajectory from the model of Eq. 2.3 over a time period from $t = 0$ to $t = T$.

Proposition 2 *Consider the solutions, denoted as $x(t)$ and $\hat{x}(t)$, respectively, of the following dynamic equations:*

$$\dot{x}(t) = f(x(t), u(t), w(t)), \quad x(0) = x_0, \tag{2.23}$$

$$\dot{\hat{x}}(t) = A\hat{x}(t) + Bu(t), \quad \hat{x}(0) = x_0, \tag{2.24}$$

where $u(t) \in U$ and $|w(t)| \leq \theta$ for all $t \in [0, T]$ and initial condition $x(0) = \hat{x}(0) = x_0 \in \Omega_{\hat{\rho}}$. If $x(t),\ \hat{x}(t) \in \Omega_{\hat{\rho}}$ for all $t \in [0, T]$, then the difference between $x(T)$ and $\hat{x}(T)$ is bounded by the function $f_w(\cdot)$:

$$|x(T) - \hat{x}(T)| \leq f_w(T) := \frac{L_w\theta + M_{err}}{L_x}\left(e^{L_x T} - 1\right) . \tag{2.25}$$

where M_{err} bounds the difference between right-hand sides of Eqs. 2.23-2.24 (with $w(t) \equiv 0$):

$$|f(x, u, 0) - (Ax + Bu)| \leq M_{err} \tag{2.26}$$

for all $x \in \Omega_{\hat{\rho}}$ and $u \in U$.

Proof 2.2 *Let $e(t)$ be the difference between the state trajectory of Eq. 2.23 and the state trajectory of Eq. 2.24 (i.e., $e(t) := x(t) - \hat{x}(t)$) with dynamics $\dot{e}(t) = \dot{x}(t) - \dot{\hat{x}}(t)$ and initial condition $e(0) = 0$). The error dynamics can be bounded by:*

$$\begin{aligned} |\dot{e}(t)| &= |f(x(t),u(t),w(t)) - (A\hat{x}(t) + Bu(t))| \\ &\leq |f(x(t),u(t),w(t)) - f(\hat{x}(t),u(t),0)| \\ &\quad + |f(\hat{x}(t),u(t),0) - (A\hat{x}(t) + Bu(t))| \,. \end{aligned} \tag{2.27}$$

For a given $\Omega_{\hat{\rho}}$, there exists a $M_{err} > 0$ such that:

$$|f(x,u,0) - (Ax + Bu)| \leq M_{err} \tag{2.28}$$

for all $x \in \Omega_{\hat{\rho}}$ and $u \in U$ owing to the Lipschitz property assumed for the vector function $f(\cdot,\cdot,\cdot)$ and the fact that x and u are bounded in compact sets. From Eq. 2.27 and Eq. 2.28 and the locally Lipschitz property for $f(\cdot,\cdot,\cdot)$ (Eq. 2.16), we have the following bound:

$$\begin{aligned} |\dot{e}(t)| &\leq L_x |x(t) - \hat{x}(t)| + L_w |w(t)| + M_{err} \\ &\leq L_x |e(t)| + L_w \theta + M_{err} \end{aligned} \tag{2.29}$$

for all $t \in [0,T]$ where the last inequality follows from the fact that $|w(t)| \leq \theta$. Integrating the bound of Eq. 2.29 from $t = 0$ to $t = T$ gives:

$$\int_0^T \frac{|\dot{e}(t)|}{L_x |e(t)| + L_w \theta + M_{err}} \, dt \leq T \tag{2.30}$$

and solving for $|e(T)|$:

$$|e(T)| = |x(T) - \hat{x}(T)| \leq \frac{L_w \theta + M_{err}}{L_x} \left(e^{L_x T} - 1 \right) \tag{2.31}$$

with $x(T)$, $\hat{x}(T) \in \Omega_{\hat{\rho}}$.

The next proposition bounds the difference of Lyapunov function values between any two points in $\Omega_{\hat{\rho}}$. The proof may be found in.[31]

Proposition 3 (c.f.[31]) *Consider the continuous differentiable Lyapunov function* $V(x)$ *that satisfies the inequalities of Eq. 2.2. There exists a quadratic function* $f_V(\cdot)$ *such that*

$$\hat{V}(x_1) \leq \hat{V}(x_2) + f_V(|x_1 - x_2|) \tag{2.32}$$

for all x_1, $x_2 \in \Omega_{\hat{\rho}}$ *where*

$$f_V(s) := \frac{c_4}{c_1}\hat{\rho}s + \beta s^2 \tag{2.33}$$

and β *is a positive constant.*

The state feedback controller $h_L(x)$ renders the origin of Eq. 2.3 asymptotically stable under continuous implementation. In general, the controller $h_L(x)$ implemented in a sample-and-hold fashion may only render the origin of the closed-loop system of Eq. 2.3 practically stable, that is the closed-loop state of Eq. 2.3 under the controller $h_L(x)$ implemented in a sample-and-hold is ultimately bounded in a small invariant set containing the origin in its interior. To guarantee a feasible solution to the optimization problem of Eq. 2.22 under mode 1 operation, the set $\Omega_{\hat{\rho}_e}$ must be larger than the set that closed-loop state is ultimately bounded in under the controller $h_L(x)$ implemented in a sample-and-hold fashion for a given sampling period $\Delta > 0$. The following proposition states sufficient conditions for that governs the minimum size of $\hat{\rho}_e$ for a given Δ needed to guarantee a feasible solution of Eq. 2.22e under mode 1 operation. To this end, let $\hat{x}(t)$ denote the solution of sampled-data system resulting from the system of Eq. 2.3 with the initial condition $\hat{x}(0) \in \Omega_{\hat{\rho}}$ and with the input trajectory obtained from the controller $h_L(x)$ implemented in a sample-and-hold fashion:

$$u(t) = h_L(\hat{x}(t_k)) \tag{2.34}$$

for $t \in [t_k, t_{k+1})$, $k = 0,\ 1,\ \ldots$ with $t_0 = 0$.

Proposition 4 *Consider the sampled-data system resulting from the system of Eq. 2.3 under the controller $h_L(x)$ that satisfies the inequalities of Eq. 2.6 implemented in a sample-and-hold fashion. Let $\Delta > 0$, $\hat{\varepsilon}_s > 0$, $\hat{\rho}_s > 0$, and $\hat{\rho}_e \geq \hat{\rho}_{\min} > 0$ satisfy:*

$$-\frac{c_3}{c_2}\hat{\rho}_s + L_L M_L \Delta \leq -\hat{\varepsilon}_s/\Delta \tag{2.35}$$

and

$$\hat{\rho}_{\min} := \max\left\{\hat{V}(\hat{x}(t+\Delta)) \ : \ \hat{V}(\hat{x}(t)) \leq \hat{\rho}_s\right\} \ . \tag{2.36}$$

If $\hat{x}(0) \in \Omega_{\hat{\rho}_e}$, then $\hat{x}(t) \in \Omega_{\hat{\rho}_e}$ for all $t \geq 0$ and

$$\hat{V}(\hat{x}(t_{k+1})) - \hat{V}(\hat{x}(t_k)) \leq -\hat{\varepsilon}_s \tag{2.37}$$

for $x(t_k) \in \Omega_{\hat{\rho}_e}$ and $\hat{x}(t)$ is ultimately bounded in $\Omega_{\hat{\rho}_{\min}}$.

Proof 2.3 *Consider the sampled-data system resulting from the system of Eq. 2.3 under the controller $h_L(x)$ applied in a sample-and-hold fashion. At each sampling period t_k, the input trajectory obtained from the controller $h_L(x)$ applied in a sample-and-hold fashion has the following property:*

$$\frac{\partial \hat{V}(\hat{x}(t_k))}{\partial x}\left(A\hat{x}(t_k) + Bh_L(\hat{x}(t_k))\right) \leq -c_3|\hat{x}(t_k)|^2 \tag{2.38}$$

from Eq. 2.6b. For simplicity of notation, let $\hat{u}(t_k) := h_L(\hat{x}(t_k))$. Consider the time-derivative of the Lyapunov function for the empirical model for $\tau \in [t_k, t_{k+1})$:

$$\begin{aligned}\frac{\partial \hat{V}(\hat{x}(\tau))}{\partial x}\left(A\hat{x}(\tau) + B\hat{u}(t_k)\right) &= \frac{\partial \hat{V}(\hat{x}(\tau))}{\partial x}\left(A\hat{x}(\tau) + B\hat{u}(t_k)\right) - \frac{\partial \hat{V}(\hat{x}(t_k))}{\partial x}\left(A\hat{x}(t_k) + B\hat{u}(t_k)\right) \\ &\quad + \frac{\partial \hat{V}(\hat{x}(t_k))}{\partial x}\left(A\hat{x}(t_k) + B\hat{u}(t_k)\right) \\ &\leq L_L\left|\hat{x}(\tau) - \hat{x}(t_k)\right| - c_3|\hat{x}(t_k)|^2 \end{aligned} \tag{2.39}$$

where the last inequality follows from Eq. 2.38 and Eq. 2.20. Owing to continuity of solutions in a

compact set and the bound of Eq. 2.19, the following bound holds:

$$|\hat{x}(\tau) - \hat{x}(t_k)| \leq M_L \Delta \tag{2.40}$$

for $\tau \in [t_k, t_{k+1}]$. *From Eq. 2.39 and Eq. 2.40, the time-derivative of the Lyapunov function is bounded by:*

$$\frac{\partial \hat{V}(\hat{x}(\tau))}{\partial x}\left(A\hat{x}(\tau) + B\hat{u}(t_k)\right) \leq -c_3|\hat{x}(t_k)|^2 + L_L M_L \Delta \tag{2.41}$$

for $\tau \in [t_k, t_{k+1})$.

If $\Delta > 0$ *is sufficiently small such that there exist* $\hat{\rho}_s > 0$, $\hat{\rho}_{\min} > 0$, *and* $\hat{\varepsilon}_s > 0$ *with* $\hat{\rho}_e \geq \hat{\rho}_{\min}$ *defined according to Eqs. 2.35-2.36, the state* $\hat{x}(t)$ *remains bounded in* $\Omega_{\hat{\rho}_e}$ *for* $t \geq 0$ *when* $\hat{x}(0) \in \Omega_{\hat{\rho}_e}$. *To show this, we need to consider two cases:* $\hat{x}(t_k) \in \Omega_{\hat{\rho}_e} \setminus \Omega_{\hat{\rho}_s}$ *and* $\hat{x}(t_k) \in \Omega_{\hat{\rho}_s}$. *When* $\hat{x}(t_k) \in \Omega_{\hat{\rho}_e} \setminus \Omega_{\hat{\rho}_s}$ *and* $\hat{x}(\tau) \in \Omega_{\hat{\rho}_e}$ *for* $\tau \in [t_k, t_{k+1})$, *the following bound on the time-derivative of the Lyapunov function can be written from the inequalities of Eq. 2.41 and Eq. 2.6a:*

$$\frac{\partial \hat{V}(\hat{x}(\tau)))}{\partial x}\left(A\hat{x}(\tau) + B\hat{u}(t_k)\right) \leq -\frac{c_3}{c_2}\hat{\rho}_s + L_L M_L \Delta \tag{2.42}$$

for $\tau \in [t_k, t_{k+1})$. *If the condition of Eq. 2.35 holds, there exists a* $\hat{\varepsilon}_s > 0$ *such that:*

$$\frac{\partial \hat{V}(\hat{x}(\tau)))}{\partial x}\left(A\hat{x}(\tau) + B\hat{u}(t_k)\right) \leq -\hat{\varepsilon}_s/\Delta \tag{2.43}$$

for $\tau \in [t_k, t_{k+1})$. *Integrating the bound for* $\tau \in [t_k, t_{k+1}]$, *we have:*

$$\begin{aligned} \hat{V}(\hat{x}(t_{k+1})) &\leq \hat{V}(\hat{x}(t_k)) - \hat{\varepsilon}_s, \\ \hat{V}(\hat{x}(\tau)) &\leq \hat{V}(\hat{x}(t_k)), \quad \forall\ \tau \in [t_k, t_{k+1}] \end{aligned} \tag{2.44}$$

for all $\hat{x}(t_k) \in \Omega_{\hat{\rho}_e} \setminus \Omega_{\hat{\rho}_s}$ *which shows the result of Eq. 2.37 and* $x(t) \in \Omega_{\hat{\rho}_e}$ *for all* $t \in [t_k, t_{k+1}]$.

For any $\hat{x}(t_k) \in \Omega_{\hat{\rho}_e} \setminus \Omega_{\hat{\rho}_s}$, *we showed that the Lyapunov function under the controller* $h_L(x)$ *applied in a sample-and-hold fashion will decrease at the next sampling period. When* $\hat{x}(t_k) \in \Omega_{\hat{\rho}_s}$

and there exists a $\hat{\rho}_{\min} \leq \hat{\rho}_e$ defined according to Eq. 2.36, the state is ultimately bounded in $\Omega_{\hat{\rho}_{\min}}$ under the Lyapunov-based controller applied in a sample-and-hold fashion owing to the definition of $\hat{\rho}_{\min}$. Thus, $\Omega_{\hat{\rho}_e}$ is forward invariant for the sampled-data system resulting from the system of Eq. 2.3 under the Lyapunov-based controller implemented in a sample-and-hold fashion (i.e., there exists a sample-and-hold trajectory with sampling period Δ that maintains $\hat{x}(t)$ in $\Omega_{\hat{\rho}_e}$).

The purpose of $\Omega_{\hat{\rho}_e}$ is to make $\Omega_{\hat{\rho}}$ invariant for the closed-loop system of Eq. 2.1 under the LEMPC of Eq. 2.22. The condition on $\hat{\rho}_e$ along with other sufficient conditions such that the closed-loop state trajectory of Eq. 2.1 under the LEMPC of Eq. 2.22 is always maintained in $\Omega_{\hat{\rho}}$ are given in the following theorem.

Theorem 1 *Consider the closed-loop system of Eq. 2.1 under the LEMPC of Eq. 2.22 based on the controller $h_L(x)$ that satisfies the inequalities of Eq. 2.6. Let $\varepsilon_w > 0$, $\Delta > 0$, $N \geq 1$, and $\hat{\rho} > \hat{\rho}_e > 0$ satisfy*

$$-\frac{\hat{c}_3}{c_2}\hat{\rho}_e + L_x' M\Delta + L_w'\theta \leq -\varepsilon_w/\Delta \,, \tag{2.45}$$

$$\hat{\rho}_e \leq \hat{\rho} - f_V(f_w(\Delta)) \,. \tag{2.46}$$

If $x(0) \in \Omega_{\hat{\rho}}$ and the conditions of Proposition 1 and Proposition 4 are satisfied, then the state trajectory $x(t)$ of the closed-loop system is always bounded in $\Omega_{\hat{\rho}}$ for $t \geq 0$.

Proof 2.4 *The proof is divide into two parts. In Part 1, feasibility of the LEMPC optimization problem is proved when the state is maintained in $\Omega_{\hat{\rho}}$. Subsequently, the closed-loop state under the LEMPC of Eq. 2.22 is shown to always bounded in $\Omega_{\hat{\rho}}$ in Part 2.*

Part 1: If mode 1 operation of the LEMPC of Eq. 2.22 is active ($x(t_k) \in \Omega_{\hat{\rho}_e}$) and the conditions of Proposition 4 are satisfied (i.e., there exist positive constants $\hat{\rho}_s$, $\hat{\rho}_{\min}$, and $\hat{\varepsilon}_s$ that satisfies Eqs. 2.35-2.35 for a given $\hat{\rho}_e$, Δ pair), the LEMPC (under mode 1 operation) is feasible because the sample-and-hold trajectory obtained from the controller $h_L(x)$ is a feasible solution to the LEMPC optimization problem which follows from Proposition 4. When the current state $x(t_k) \in \Omega_{\hat{\rho}} \setminus \Omega_{\hat{\rho}_e}$ and the LEMPC of Eq. 2.22e operates in mode 2 operation, the optimization problem is feasible

because the input trajectory $u(t) = h_L(x(t_k))$ for $t \in [t_k, t_{k+1})$ and any piecewise constant trajectory $u(t) \in U$ for $t \in [t_{k+1}, t_{k+N})$ will satisfy the input constraint of Eq. 2.22d and the mode 2 constraint of Eq. 2.22f. Thus, the LEMPC is recursively feasible if the closed-loop state is maintain in $\Omega_{\hat{\rho}}$.

Part 2: Consider the closed-loop state trajectory under the LEMPC of Eq. 2.22. If $x(t_k) \in \Omega_{\hat{\rho}} \setminus \Omega_{\hat{\rho}_e}$, the LEMPC operates in mode 2 (the constraint of Eq. 2.22f is active) and the computed input satisfies:

$$\frac{\partial \hat{V}(x(t_k))}{\partial x}\left(Ax(t_k) + Bu(t_k)\right) \leq \frac{\partial \hat{V}(x(t_k))}{\partial x}\left(Ax(t_k) + Bh_L(x(t_k))\right) \tag{2.47}$$

for all $x(t_k) \in \Omega_{\hat{\rho}} \setminus \Omega_{\hat{\rho}_e}$. From Proposition 1 (Eq. 2.15), for δ and $\hat{\rho}$ sufficiently small, there exists a $\hat{c}_3 > 0$ such that:

$$\frac{\partial \hat{V}(x(t_k))}{\partial x} f(x(t_k), h_L(x(t_k)), 0) \leq -\hat{c}_3 |x(t_k)|^2 \,. \tag{2.48}$$

The time-derivative of the Lyapunov function (of the closed-loop nonlinear system) over the sampling period is

$$\begin{aligned}
\dot{\hat{V}}(x(\tau)) = &\frac{\partial \hat{V}(x(\tau))}{\partial x} f(x(\tau), h_L(x(\tau)), w(\tau)) - \frac{\partial \hat{V}(x(t_k))}{\partial x} f(x(t_k), h_L(x(t_k)), 0) \\
&+ \frac{\partial \hat{V}(x(t_k))}{\partial x} f(x(t_k), h_L(x(t_k)), 0) \\
&\overset{(2.17),(2.47)}{\leq} L'_x |x(\tau) - x(t_k)| + L'_w |w(\tau)| - \hat{c}_3 |x(t_k)|^2 \\
&\leq -\frac{\hat{c}_3}{c_2}\hat{\rho}_e + L'_x |x(\tau) - x(t_k)| + L'_w |w(\tau)|
\end{aligned} \tag{2.49}$$

for $\tau \in [t_k, t_{k+1})$ where the last inequality follows from the fact that $x(t_k) \in \Omega_{\hat{\rho}} \setminus \Omega_{\hat{\rho}_e}$. From Eq. 2.18 and the continuity of solutions, the difference between $x(\tau)$ and $x(t_k)$ is bounded:

$$|x(\tau) - x(t_k)| \leq M\Delta \tag{2.50}$$

for all $\tau \in [t_k, t_{k+1})$. From Eqs. 2.49-2.50 and the fact that the disturbance vector is bounded

($|w(\tau)| \leq \theta$), we have:

$$\frac{\partial \hat{V}(x(\tau))}{\partial x} f(x(\tau), u(t_k), 0) \leq -\frac{\hat{c}_3}{c_2}\hat{\rho}_e + L_x' M\Delta + L_w'\theta \tag{2.51}$$

for all $\tau \in [t_k, t_{k+1})$. If the condition of Eq. 2.45 is satisfied, then the following can be derived:

$$\begin{aligned} \hat{V}(x(t_{k+1})) &\leq \hat{V}(x(t_k)) - \varepsilon_w, \\ \hat{V}(x(\tau)) &\leq \hat{V}(x(t_k)), \quad \forall\ \tau \in [t_k, t_{k+1}] \end{aligned} \tag{2.52}$$

for all $x(t_k) \in \Omega_{\hat{\rho}} \setminus \Omega_{\hat{\rho}_e}$ by employing the same steps used to derive the equations of Eq. 2.44. Thus, when the LEMPC operates in mode 2, the Lyapunov function value will decrease at the next sampling period and converge to the set $\Omega_{\hat{\rho}_e}$ in a finite number of sampling periods.

If $x(t_k) \in \Omega_{\hat{\rho}_e}$, the LEMPC will operate in mode 1. The predicted state at the next sampling period must be in $\Omega_{\hat{\rho}_e}$ ($\hat{x}(t_{k+1}) \in \Omega_{\hat{\rho}_e}$) which is enforced by the constraint of Eq. 2.22e. By Propositions 2 and 3, we have:

$$\begin{aligned} \hat{V}(x(t_{k+1})) &\leq \hat{V}(\hat{x}(t_{k+1})) + f_V(|x(t_{k+1}) - \hat{x}(t_{k+1})|) \\ &\leq \hat{\rho}_e + f_V(f_w(\Delta)) \end{aligned} \tag{2.53}$$

If the condition of Eq. 2.46 is satisfied, $x(t_{k+1}) \in \Omega_{\hat{\rho}}$. Thus, under mode 1 and mode 2 operation of the LEMPC, the closed-loop state is maintained in $\Omega_{\hat{\rho}}$ which completes the proof.

Remark 1 *Since the empirical model of Eq. 2.3 can only accurately predict the behavior of the system of Eq. 2.1 within a limited region in state-space, it may be difficult to find an empirical model that can adequately capture the dynamics of the system of Eq. 2.1 for use in EMPC. The accuracy of the model used in EMPC is critical because it affects both the closed-loop performance and stability. A strategy to improve the accuracy of the model of Eq. 2.3 is to use multiple empirical models for different regions of state-space to better capture the nonlinear dynamics of Eq. 2.1 and as a result of the increased accuracy, use a larger $\Omega_{\hat{\rho}}$ than what is possible (from a closed-loop*

stability perspective) with a single empirical model.

Remark 2 *The general heuristic is that the closed-loop economic performance improves with increasing prediction horizon when applying nonlinear EMPC (i.e., EMPC formulated with a nonlinear model). However, when using EMPC with an empirical model, the predicted behavior of the system obtained from the empirical model over a long horizon may be significantly different than the actual nonlinear behavior. Thus, increasing the prediction horizon of EMPC with an empirical model may not increase the performance. In other words, the accuracy of the prediction by the empirical model may affect the closed-loop performance and it be better from a closed-loop performance standpoint to restrict operation to a smaller region state-space where the empirical model can provide a sufficient degree of accuracy.*

Remark 3 *As a by-product of using an empirical model in LEMPC, the computational efficiency of LEMPC is improved in general compared to using a nonlinear model in LEMPC since the resulting the optimization problem has less nonlinearities and the empirical model of Eq. 2.3 can be converted to an exact discrete-time model with zeroth-order sample-and-hold inputs (i.e., no need to embed a numerical ordinary differential equation solver to solve the dynamic optimization problem of the LEMPC). Thus, one may consider to use an empirical model even when a nonlinear model is available owing to the improved computational efficiency. This point will be demonstrated in the "Application to a Chemical Process Example" section.*

Remark 4 *It is important to emphasize that at each sampling time the LEMPC of Eq. 2.22 is re-initialized with a state measurement. This incorporation of feedback allows for the LEMPC of Eq. 2.22 to maintain robustness to disturbances.*

2.4 Application to a Chemical Process Example

Consider a non-isothermal, well-mixed continuous stirred tank reactor (CSTR) where an irreversible, second-order, exothermic reaction occurs. The reaction converts the reactant A to the

Table 2.1: Parameter values of the CSTR.

$F = 5.0$	$\frac{m^3}{hr}$	$k_0 = 8.46 \times 10^6$	$\frac{m^3}{kmol\ hr}$
$T_0 = 300$	K	$\Delta H = -1.15 \times 10^4$	$\frac{kJ}{kmol}$
$V = 1.0$	m^3	$E = 5.0 \times 10^4$	$\frac{kJ}{kmol}$
$C_p = 0.231$	$\frac{kJ}{kg\ K}$	$\rho_L = 1000$	$\frac{kg}{m^3}$
$R = 8.314$	$\frac{kJ}{kmol\ K}$		

product B and is of the form $A \rightarrow B$. The feedstock of the reactor contains A in an inert solvent and the inlet concentration of A is C_{A0}, inlet temperature is T_0, and feed volumetric flow rate is F. A jacket is used to heat/cool the reactor at heat rate Q. The liquid density ρ_L, heat capacity C_p, and liquid hold-up V are assumed to be constant. The dynamic model equations describing the evolution of the CSTR, obtained by applying standard modeling assumptions and mass and energy balances to the reactor, are presented below:

$$\frac{dC_A}{dt} = \frac{F}{V}(C_{A0} - C_A) - k_0 e^{-E/RT} C_A^2 \tag{2.54a}$$

$$\frac{dT}{dt} = \frac{F}{V}(T_0 - T) - \frac{\Delta H k_0}{\rho_L C_p} e^{-E/RT} C_A^2 + \frac{Q}{\rho_L C_p V} \tag{2.54b}$$

where C_A and T are the reactant A concentration in the reactor and reactor temperature, respectively. The notation k_0, E, ΔH denotes the pre-exponential factor, activation energy of the reaction, and the enthalpy of the reaction, respectively. The values of the process parameters are given in Table 2.1. In the simulations below, the explicit Euler method with an integration time step of $h_c = 10^{-4}\ hr$ was used to integrate the dynamic model of Eq. 2.54.

The inlet concentration C_{A0} and the heat supply/removal Q are the two manipulated inputs of the CSTR. The manipulated inputs are bounded as follows: $0.5 \leq C_{A0} \leq 7.5\ kmol/m^3$ and $-5.0 \times 10^5 \leq Q \leq 5.0 \times 10^5\ kJ/hr$. The control objective is to maximize the time-averaged production rate of the product B by operating the CSTR in a compact state-space set around the operating steady-state of the CSTR. To this end, the operating steady-state vector of the CSTR is $[C_{As}\ T_s] = [1.2\ kmol/m^3\ 438.0\ K]$ and the corresponding steady-state input vector is

$[C_{A0s}\ Q_s] = [4.0\ kmol/m^3\ 0.0\ kJ/hr]$. The steady-state is open-loop asymptotically stable. The state and input vector of the CSTR are defined using deviation variables: $x^T = [C_A - C_{As}\ T - T_s]$ is the state vector and $u^T = [C_{A0} - C_{A0s}\ Q - Q_s]$ is the manipulated input vector. Given the control objective is to maximize the time-averaged production rate of B, the average production rate of B will be used in the LEMPC as the cost function and is given by:

$$L_e(x,u) = \frac{1}{(t_{k+N} - t_k)} \int_{t_k}^{t_{k+N}} k_0 e^{-E/RT(\tau)} C_A^2(\tau)\, d\tau\ . \tag{2.55}$$

In addition, we consider that there is a limitation on the amount of reactant material that may be fed to the CSTR during a given period of operation t_p. Therefore, the control input trajectory of u_1 should satisfy the following material constraint:

$$\frac{1}{t_p} \int_0^{t_p} u_1(\tau)\, d\tau = 0.0\, kmol/m^3. \tag{2.56}$$

where $t_p = 1.0\ hr$ is the operating period length to enforce the material constraint.

2.4.1 Model Identification and Validation

We assume that for the CSTR, the nonlinear model of Eq. 2.54 is not available and a model needs to be identified and validated. The model will be fit using standard input/output data-based techniques (recall that state feedback is assumed, so the output is the state) to identify a linear time invariant state-space model. A series of step inputs were used to generate the input/output data. An iterative process was employed to identify and validate the model. First, a step input sequence was generated and applied to the CSTR. From the input/output data, the ordinary multivariable output error state space (MOESP)[43] algorithm was used to regress a linear model of the CSTR of Eq. 2.54. Step, impulse, and sinusoidal input responses were used to validate the model. Additionally, a LEMPC scheme of the form described below in the subsequent subsection was designed using the empirical model. The LEMPC with the identified model was applied to the CSTR of Eq. 2.54. Extensive closed-loop simulations with the LEMPC were performed. From these vali-

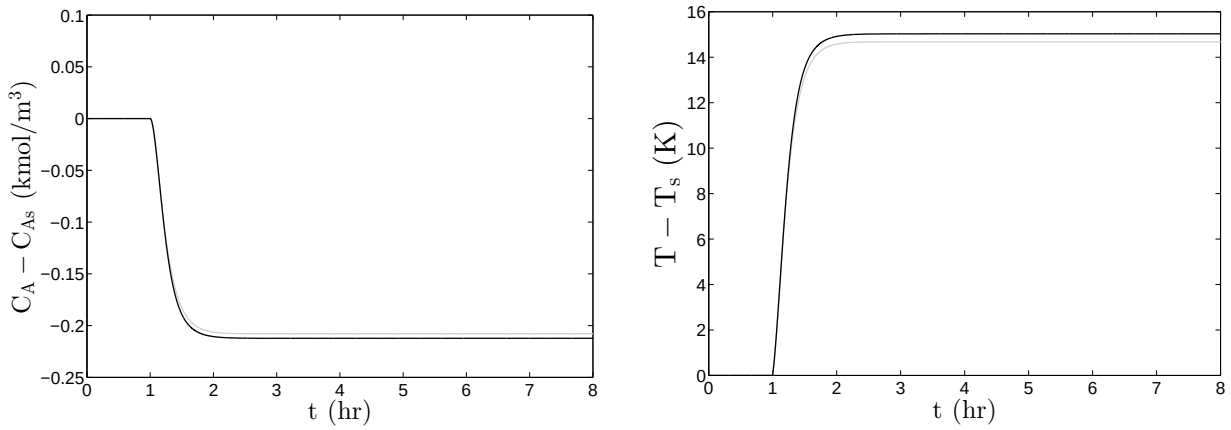

Figure 2.1: Response of the CSTR of Eq. 2.54 (black line) to a step input compared to the response predicted by the identified linear model of Eq. 2.57 (gray line). The step is in the heat rate input (u_2) starting at 1 hr with a magnitude of 5000 kJ/hr.

dation experiments (input response tests and the closed-loop simulations), a model was identified and validated.

The identified matrices for the linear model of the CSTR (in continuous-time) are:

$$A = \begin{bmatrix} -34.5 & -0.473 \\ 1430 & 18.1 \end{bmatrix}, \; B = \begin{bmatrix} 5.24 & -8.09 \times 10^{-6} \\ -11.6 & 4.57 \times 10^{-3} \end{bmatrix} \tag{2.57}$$

where the state-space coordinates correspond to the coordinates used in the nonlinear model of Eq. 2.54. The step, impulse, and sinusoidal input responses are shown in Figs. 2.1-2.3. From Figs. 2.1-2.3, the predicted response of the CSTR using the identified linear model is close to the response of the actual nonlinear system of Eq. 2.54.

2.4.2 Application of LEMPC based on an Empirical Model

Before an LEMPC may be designed, a Lyapunov-based controller is designed, a Lyapunov function under the Lyapunov-based controller is constructed, and the stability region of the CSTR under the Lyapunov-based controller is estimated. Since we assume that only the empirical model is available, we work with the empirical model to design the Lyapunov-based controller. The Lyapunov-based controller consists of two elements for each input: $h^T(x) = [h_1(x)\; h_2(x)]$, and

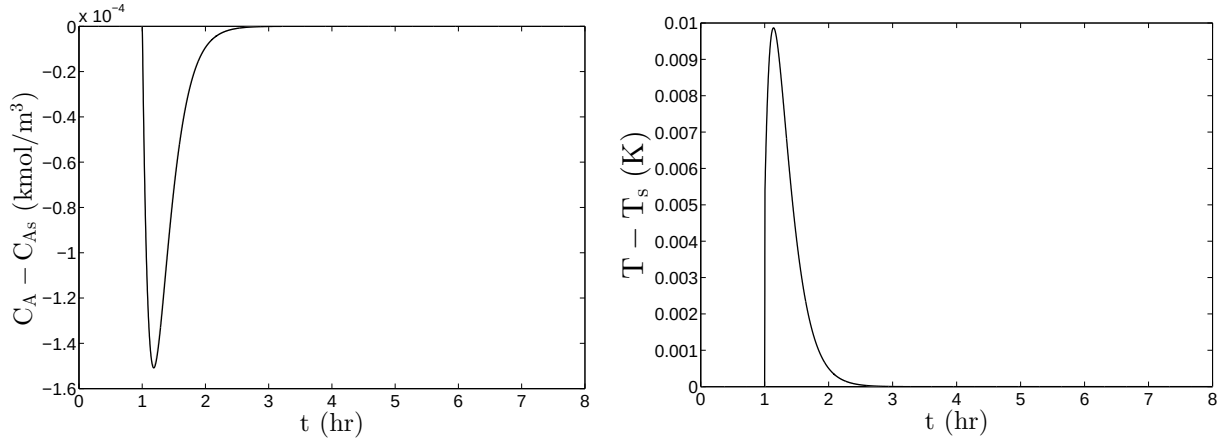

Figure 2.2: Response of the CSTR of Eq. 2.54 (black line) to an impulse input compared to the response predicted by the identified linear model of Eq. 2.57 (gray line) which are nearly overlapping. To numerically simulate the impulse, a rectangular pulse of magnitude $1,500$ kJ/hr in the heat rate input was applied for 36 *sec*.

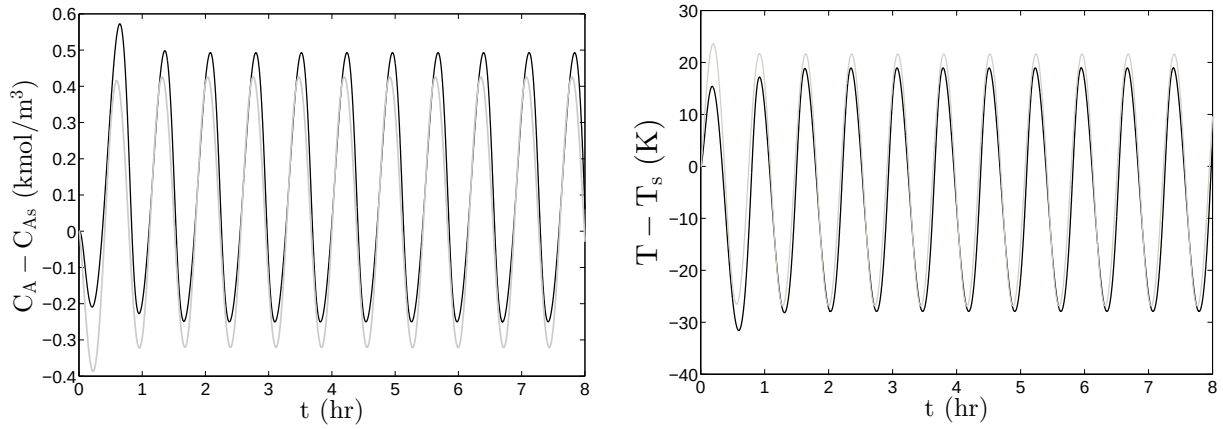

Figure 2.3: Response of the CSTR of Eq. 2.54 (black line) to a sinusoidal input response compared to the response predicted by the identified linear model of Eq. 2.57 (gray line). The amplitude of the heat rate input sinusoid is $30,000$ kJ/hr with a frequency of 8.72 rad/hr.

the inlet concentration input is fixed to 0.0 $kmol/m^3$ to satisfy the material constraint of Eq. 2.56 ($h_1(x) = 0$). Defining the vector and matrix functions $f : R^n \to R^n$ and $g : R^n \to R^n \times R^m$ as followed:

$$\dot{x} = \underbrace{Ax}_{=:f(x)} + \underbrace{B}_{=:g(x)} u \,, \tag{2.58}$$

the following control law is used for the heat rate input in the Lyapunov-based controller:[38]

$$h_2(x) = \begin{cases} -\dfrac{L_f V + \sqrt{L_f V^2 + L_{g_2} V^4}}{L_{g_2} V}, & \text{if } L_{g_2} V \neq 0 \\ 0, & \text{if } L_{g_2} V = 0 \end{cases} \tag{2.59}$$

where $L_f V$ is the Lie derivative of the Lyapunov function $V(x)$ with respect to the vector field $f(x)$ and the notation $g_2(x)$ denotes the second column of B. A quadratic Lyapunov function of the form: $V(x) = x^T P x$ where P is the following positive definite matrix:

$$P = \begin{bmatrix} 1060 & 22 \\ 22 & 0.52 \end{bmatrix} \tag{2.60}$$

was used. After extensive closed-loop simulations under the Lyapunov-based controller and under the LEMPC designed on the basis of the Lyapunov-based controller $h(x)$ and with the model of Eq. 2.57, the level sets $\Omega_{\hat{\rho}}$ and $\Omega_{\hat{\rho}_e}$, which will be used in the LEMPC, were estimated to be $\hat{\rho} = 64.3$ (i.e., $\Omega_{\hat{\rho}} = \{x \in R^n : V(x) \leq \hat{\rho}\}$), and $\hat{\rho}_e = 55.0$, respectively. The sampling period and prediction horizon of the LEMPC are $\Delta = 0.01$ hr and $N = 10$, respectively.

An LEMPC scheme of the form of Eq. 2.22 was designed utilizing the model of Eq. 2.57 for the CSTR with the cost function of Eq. 2.55 and the material constraint of Eq. 2.56. The material constraint of Eq. 2.56 is enforced over each 1.0 hr operating period using the strategy described in.[14] To solve the LEMPC optimization problem at each sampling period, the interior point solver IPOPT was employed.[45] To make the simulations more realistic, the solver was forced to terminate solving and return a solution by the end of the sampling period although instantaneous availability

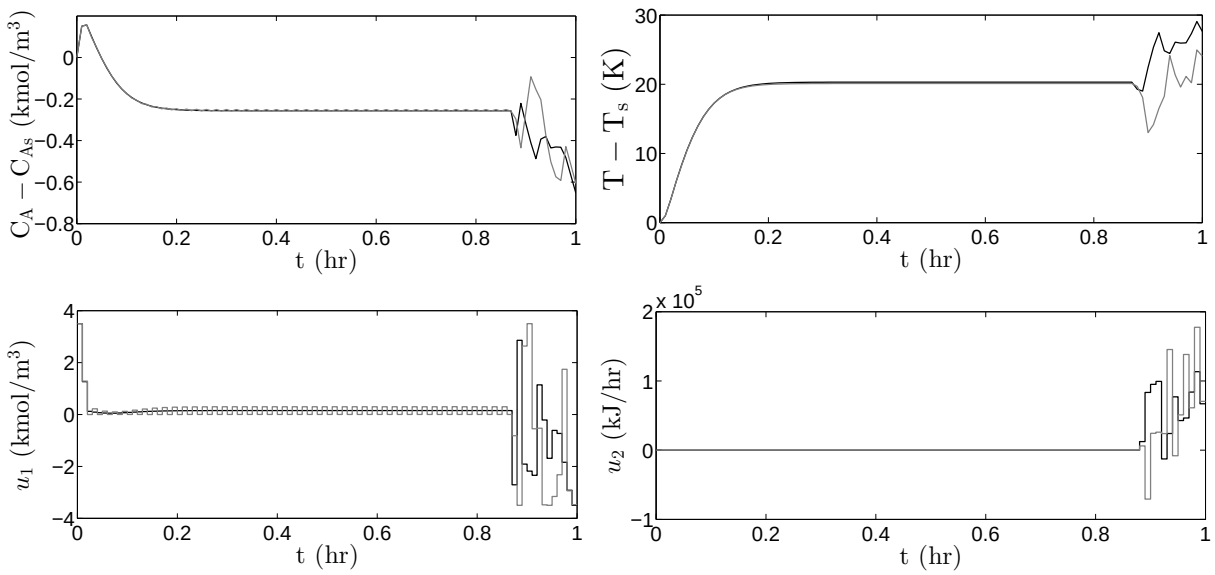

Figure 2.4: The state and input profiles of the closed-loop CSTR under the nonlinear LEMPC (black line) and under the linear LEMPC (gray line) for the initial condition: $C_A(0) = 1.2\ kmol/m^3$ and $T(0) = 438\ K$.

of the control action at the current sampling time is assumed in the closed-loop simulations. For the remainder, nonlinear LEMPC will refer to an LEMPC scheme formulated with the nonlinear dynamic model of Eq. 2.54, while linear LEMPC will refer to an LEMPC scheme formulated with the linear model of Eq. 2.57. In the following simulations, both nonlinear LEMPC and linear LEMPC were considered as a baseline comparison. While this comparison may be done through simulations, a nonlinear model may not be available and thus, this type of comparison may not be able to be completed in practice. For the nonlinear LEMPC simulations, only mode 1 operation of the controller was considered since the nonlinear LEMPC is able to maintain operation within $\Omega_{\hat{\rho}_e}$ under nominal operation. To solve the initial value problem embedded in the optimization problem, the explicit Euler method was used for the nonlinear LEMPC, and the discrete-time version of the model of Eq. 2.57 with a zero-order hold of the inputs with sampling period $\Delta = 0.01\ hr$ was used in the linear LEMPC.

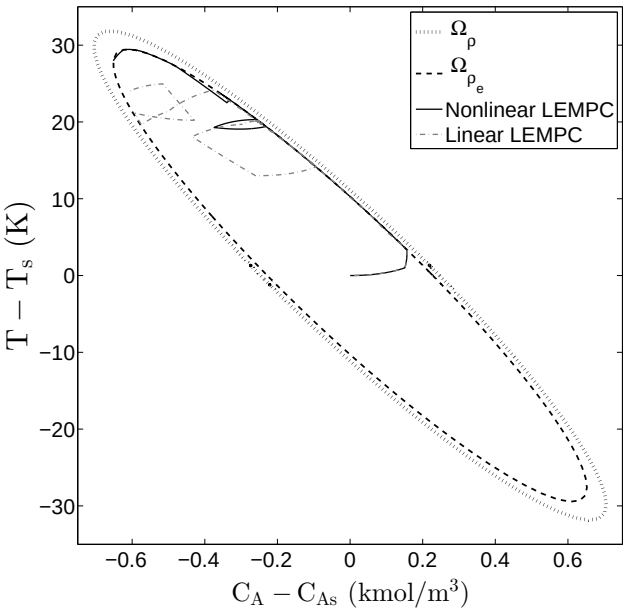

Figure 2.5: The state trajectories of the CSTR under: nonlinear LEMPC (solid line) and linear LEMPC (dashed-dotted line).

2.4.3 Linear LEMPC Compared with Nonlinear LEMPC

Both the nonlinear and linear LEMPC were applied to the CSTR of Eq. 2.54, and a closed-loop simulation over one operating period (1 hr) was completed for each case. The CSTR was initialized at the steady-state: $C_A(0) = 1.2\ kmol/m^3$ and $T(0) = 438.0\ K$. The closed-loop trajectories for the CSTR under both LEMPC schemes are shown in Fig. 2.4. The trajectories of the two cases demonstrate a similar behavior with three distinct phases. In the first phase, the LEMPC forces the CSTR from the initial condition to a greater temperature to increase the production rate of B. In the second phase, the trajectories settle on an equilibrium point located at the boundary of $\Omega_{\hat{\rho}_e}$ from approximately 0.2 hr to 0.8 hr. This steady-state has a greater temperature than the operating steady-state ($C_{As} = 1.2\ kmol/m^3$ and $T_s = 438.0\ K$). Finally, to achieve additional economic performance benefit at the end of the operating period and to satisfy the material constraint, the LEMPC forces the state away from the steady-state to a greater temperature. Perhaps, the two most noticeable differences in the closed-loop trajectories of Fig. 2.4, are the oscillations or chattering observed in the u_1 trajectory computed by the linear LEMPC and the differences in the trajectories

at the end of the operating period. The oscillations are caused by the linear LEMPC switching between mode 1 and mode 2 operations of the controller. Given the fact that the linear LEMPC uses an inexact model, it cannot compute a control action that exactly maintains the actual state at the boundary of $\Omega_{\hat{\rho}_e}$. A state starting in $\Omega_{\hat{\rho}_e}$ may leave $\Omega_{\hat{\rho}_e}$ under the linear LEMPC. However, it will still be contained in $\Omega_{\hat{\rho}}$ at the next sampling period by design of $\Omega_{\hat{\rho}_e}$. Once the state is in $\Omega_{\hat{\rho}} \setminus \Omega_{\hat{\rho}_e}$, the linear LEMPC switches to mode 2 operation to force the state back into $\Omega_{\hat{\rho}_e}$. The linear LEMPC operates in mode 1 operation after the state converges back to $\Omega_{\hat{\rho}_e}$. On the other hand, the nonlinear LEMPC is able to maintain the LEMPC at the boundary of $\Omega_{\hat{\rho}_e}$ since we are considering nominal operation (i.e., the LEMPC uses an exact model of the CSTR to compute its control action). Thus, the nonlinear LEMPC is able to maintain operation in $\Omega_{\hat{\rho}_e}$, so the controller always operates in mode 1 operation. To better observe the differences between the closed-loop state trajectories, the closed-loop trajectories for each of the two previous simulations are shown in state-space (Fig. 2.5). From Fig. 2.5, noticeable differences between the evolution of the two cases at the end of the operating period is observed. In the region of operation at the end of the operating period, the linear model is less accurate and hence, the linear LEMPC computes a different input trajectory than the nonlinear LEMPC.

The fact that a similar trend was observed between the closed-loop CSTR under the nonlinear LEMPC, which uses the exact dynamic model, and the linear LEMPC, which uses a linear model identified through input/output data, speaks positively on EMPC using an empirical model. It indicates that one may be able to use standard identification techniques to identify an empirical model for use within the context of EMPC when a nonlinear model is not available. However, it is also important to investigate the advantages and disadvantages and possible trade-offs of using nonlinear LEMPC (when a nonlinear model is available) and using linear LEMPC. To quantify the closed-loop performance of each case, we define the average economic cost index as:

$$J_e = \frac{1}{t_f} \int_0^{t_f} k_0 e^{-E/RT(t)} C_A^2(t)\, dt \tag{2.61}$$

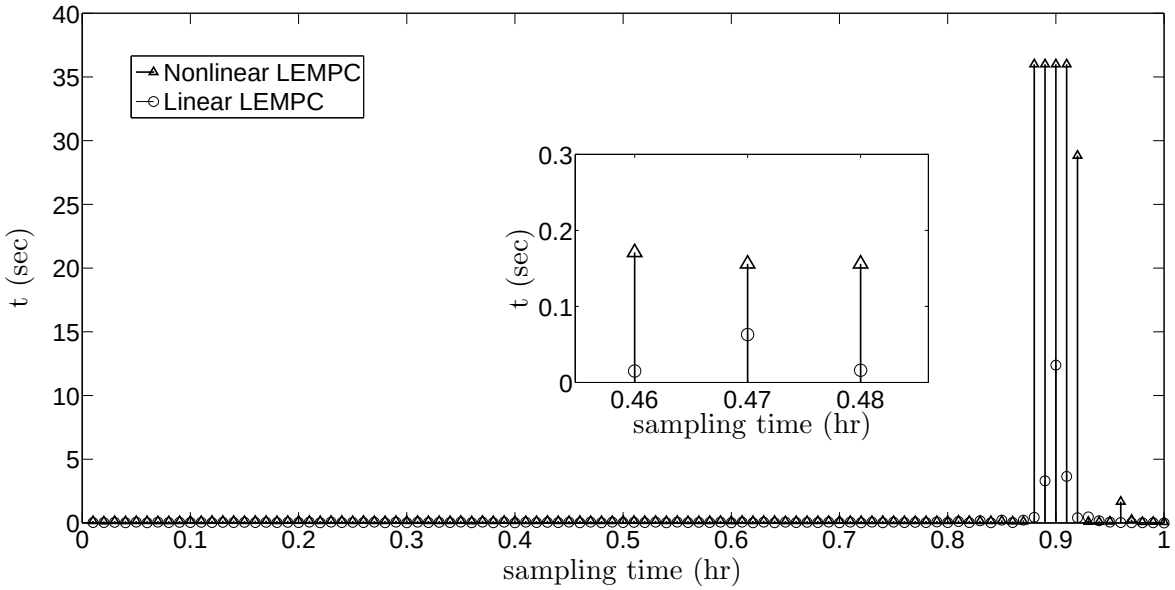

Figure 2.6: The computation time in seconds required to solve the nonlinear LEMPC (triangle markers) and the linear LEMPC (circle markers) optimization problem at each sampling period.

where t_f is the length of simulated closed-loop operation. For simplicity of presentation, the units on the average economic cost index, which are $kmol/m^3$, are omitted. For the linear LEMPC, the economic cost index is 15.70, while the economic cost index of the closed-loop CSTR under the nonlinear LEMPC is 15.77. For an 1 *hr* operating period, applying nonlinear LEMPC achieves less than a 0.5% improvement of the economic cost index compared to the economic cost under the linear LEMPC.

The computation time required to solve the LEMPC optimization problem at each sampling period was also considered for the nonlinear and linear LEMPCs. Fig. 2.6 shows the computation time required to solve the nonlinear and linear LEMPC at each sampling period, respectively. The higher computation time observed at the end of the operating period in each of the cases is associated with the fact that the constraints are active (the constraint to maintain operation in $\Omega_{\hat{\rho}_e}$ and the average input constraint). From Fig. 2.6, the optimization solver terminated early four times (recall that the solver was constrained to return a solution by the end of the current sampling period). For this case, the total amount of computation time required to solve the LEMPC optimization problem over all the sampling periods was 193 *sec*. For the linear LEMPC, early

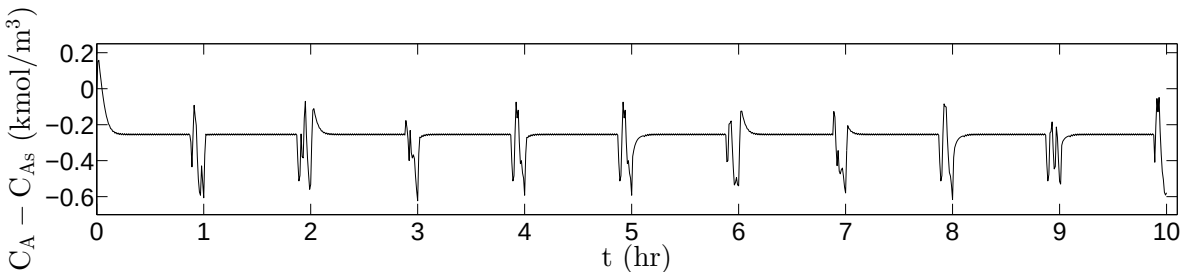

Figure 2.7: Closed-loop state trajectory ($x_1 = C_A - C_{As}$) of the CSTR under the linear LEMPC over ten hours.

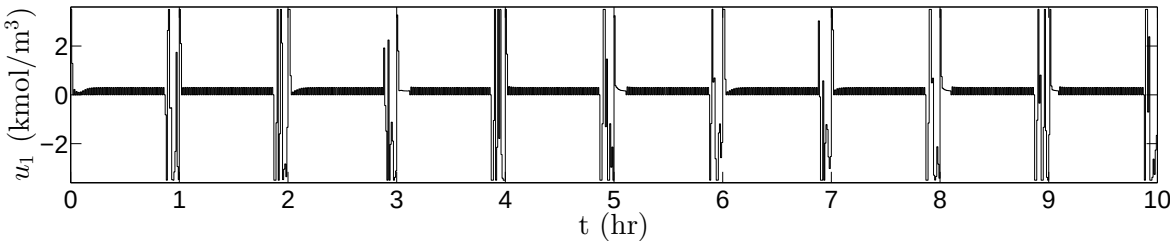

Figure 2.8: Input trajectory ($u_1 = C_{A0} - C_{A0s}$) under the linear LEMPC over ten hours.

termination of the optimization solver was never experienced and for most of the sampling periods, the solver converged in less than 0.1 *sec* (Fig. 2.6). The total computation time required to solve the LEMPC at each sampling period in the simulation was 22 seconds; the total time required to solve the nonlinear LEMPC at each sampling period is 777% greater than the computation time required to solve the linear LEMPC.

To demonstrate the application of the linear LEMPC to the CSTR of Eq. 2.54, a closed-loop simulation of ten hours was completed. The closed-loop trajectories are shown in Figs. 2.7-2.10. The closed-loop economic performance as measured by the average economic cost of Eq. 2.61

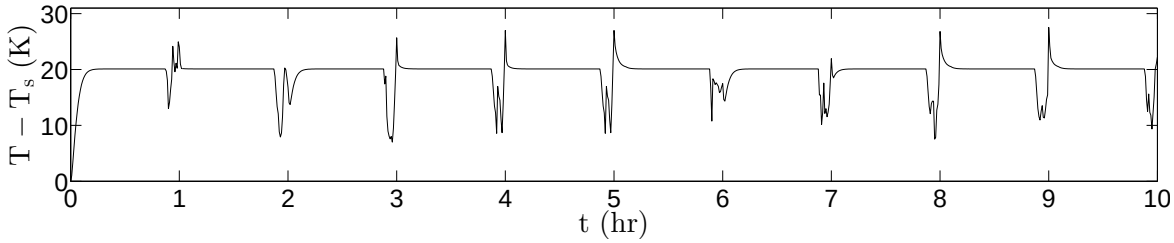

Figure 2.9: Closed-loop state trajectory ($x_2 = T - T_s$) of the CSTR under the linear LEMPC over ten hours.

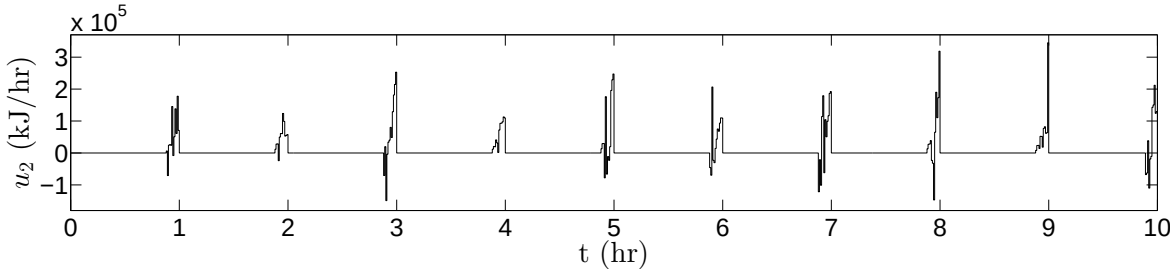

Figure 2.10: Input trajectory ($u_2 = Q - Q_s$) under the linear LEMPC over ten hours.

Table 2.2: Average economic cost (J_e) for one period of operation (1 hr) using various modeling methods.

Model	J_e
Nonlinear Model	15.77
Linear Model of Eq. 2.57	15.70
Least Squares Model	15.48
Jacobian Linearization of Nonlinear Model	15.39
Sinusoidal System ID	15.39
Impulse System ID	15.51

was 15.29. Maintaining the CSTR at the initial condition, which is the steady-state, has an average economic cost of 13.88 (the linear LEMPC dictates an operating policy that is 10% better than operating the CSTR at the operating steady-state). Another simulation was performed with the nonlinear LEMPC. The closed-loop trajectories of the CSTR under the nonlinear LEMPC were similar to that under the linear LEMPC except from a few differences: the closed-loop u_1 trajectory computed by the nonlinear LEMPC did not have chattering like the closed-loop u_1 trajectory computed by the linear LEMPC (Fig. 2.8) for reasons stated above and the other differences in the closed-loop trajectories noted above for the 1 *hr* simulations were also observed. The average economic cost of the closed-loop CSTR under the nonlinear LEMPC was 15.40. The closed-loop performance under the nonlinear LEMPC is 0.7% better than that achieved under linear LEMPC. However, the average total computation time required to solve the nonlinear LEMPC optimization problem over each operating period is 159 *sec*, while the average total computation time required to solve the linear LEMPC optimization problem is 23.6 *sec* (the nonlinear LEMPC average computation time is 560% more).

Other approaches to identify the empirical model could be used. To demonstrate this, several other methods were used to obtain a linear model of Eq. 2.54 and similar one operating period (1 *hr*) simulations were performed. Specifically, a model was obtained through the following methods: least squares parameter fit using the input/output data obtained through step tests, Jacobian linearization of the nonlinear model of Eq. 2.54 around the steady-state, applying the MOESP algorithm to input/output data generated from sinusoidal input response, and applying the MOESP algorithm to input/output data generated from impulse input response. The closed-loop average economic performance of these simulations are reported in Table 2.2. From Table 2.2, similar closed-loop performance was achieved in each case. The linear LEMPC using the model of Eq. 2.57 achieved the best performance by design (extensive closed-loop simulations under the LEMPC were employed to construct and validate the model of Eq. 2.57). In all cases, closed-loop stability (boundedness of the closed-loop state in $\Omega_{\hat{\rho}}$) was achieved.

2.4.4 Improved Accuracy with Empirical Models

Given that the CSTR exhibits nonlinear dynamic behavior (Eq. 2.54), the empirical model can only accurately predict the behavior within a limited region of state-space. In the previous simulations, the linear LEMPC computed a much different input trajectory compared to the nonlinear LEMPC at the end of each operating period owing to the fact that the linear model did not accurately predict the evolution within this region of operation. In this section, we consider two methods that improve the accuracy of the empirical model used in the LEMPC: employing on-line system identification and using multiple linear models to describe the process within different regions of operation.

The first method that is investigated is on-line system identification. In on-line system identification, the first model used in the linear LEMPC is the model of Eq. 2.57. The model is used for only one operating period. At the end of the operating period, the closed-loop input/output data of the first operating period is used to compute a new model from the MOESP algorithm. At the end of each subsequent operating period, a new model is generated via the input/output data of the previous operating period. Over the course of a ten hour simulation, the average economic cost with

on-line system identification was 15.41. Recall, for the ten hour simulation under linear LEMPC without on-line system identification (Figs. 2.7-2.10), the average economic cost was 15.29 and a less than 0.7% improvement in the closed-loop performance was realized with the on-line system identification. For this particular example, little benefit may be achieved when using on-line system identification.

The second method that was investigated is formulating and applying linear LEMPC with multiple linear models. In this method, multiple linear models are regressed off-line for different regions of operation. Given that employing multiple linear models can more accurately predict the behavior of the nonlinear CSTR, a larger estimate of the level sets used in the linear LEMPC can be used. For this set of simulations, the level sets used in the LEMPC design where $\hat{\rho} = 368.0$ and $\hat{\rho}_e = 340.0$. Operating the CSTR over a larger region in state-space is desirable from a process economics standpoint given that the (instantaneous) production rate scales with the exponential of $-1/T$ (i.e., the production rate is larger at higher temperatures). When multiple linear models were used within the linear LEMPC, the model used in the LEMPC optimization problem was selected on the basis of which region the initial condition was in. After extensive simulations, three models were identified for three regions in state-space. The first model is:

$$A = \begin{bmatrix} -34.5 & -0.473 \\ 1430 & 18.1 \end{bmatrix}, B = \begin{bmatrix} 5.24 & -8.09 \times 10^{-6} \\ -11.6 & 4.57 \times 10^{-3} \end{bmatrix} \tag{2.62}$$

and is most accurate for deviation temperatures less than 35.0 K (i.e., $x_2 \leq 35.0$). The second model is:

$$A = \begin{bmatrix} -48.6 & -0.657 \\ 1960 & 23.2 \end{bmatrix}, B = \begin{bmatrix} 6.22 & -1.13 \times 10^{-5} \\ 189 & 8.98 \times 10^{-3} \end{bmatrix}. \tag{2.63}$$

and is most accurate for deviation temperatures between 35.0 K to 43.0 K. The third model is:

$$A = \begin{bmatrix} 1.38 & 0.0894 \\ -476 & -10.7 \end{bmatrix}, B = \begin{bmatrix} 0.901 & -1.24 \times 10^{-4} \\ 504 & 9.98 \times 10^{-3} \end{bmatrix} \tag{2.64}$$

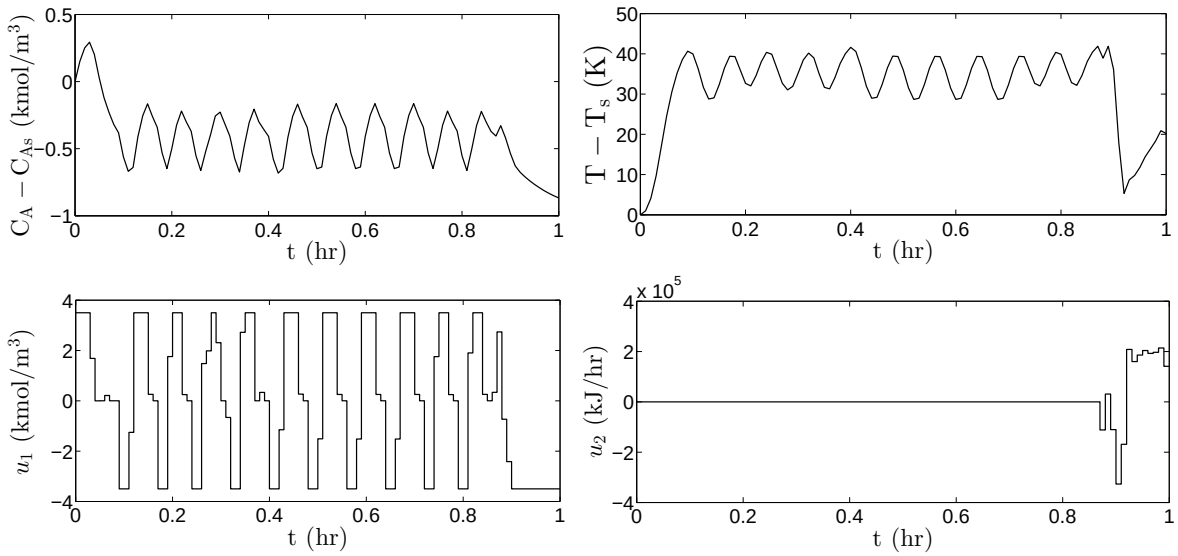

Figure 2.11: The closed-loop trajectories of the CSTR under the linear LEMPC (linear model of Eq. 2.62).

Table 2.3: Average economic cost for the CSTR under LEMPC formulated with multiple empirical models as well as with the nonlinear model for one period of operation (1 *hr*).

Method	J_e
One linear model	16.61
Two linear models	16.80
Three linear models	17.14
Nonlinear Model	17.22

and is most accurate for deviation temperatures greater than 43.0 *K*. The use of one, two, and three linear empirical models in the linear LEMPC was considered. Also, the nonlinear LEMPC was also considered for comparison purposes. The linear LEMPC based on one model uses the model of Eq. 2.62, the linear multiple-model LEMPC based on two models uses the models of Eqs. 2.62-2.63, and the linear multiple-model LEMPC based on three models uses the models of Eqs. 2.62-2.64.

One operating period simulations were completed with each LEMPC. The closed-loop trajectories for the CSTR: under the linear LEMPC with one model, under the linear multiple-model LEMPC with two models, and under the linear multiple-model LEMPC with three models and under the nonlinear LEMPC are shown in Fig. 2.11, Fig. 2.12, and Fig. 2.13, respectively. From these

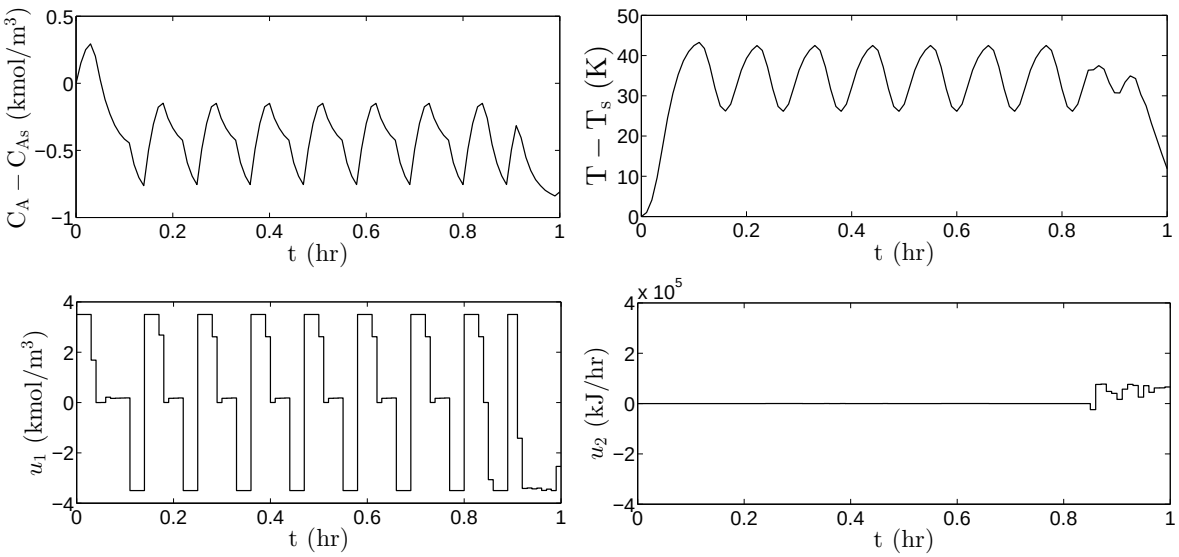

Figure 2.12: The closed-loop trajectories of the CSTR under the linear multiple-model LEMPC with two linear models.

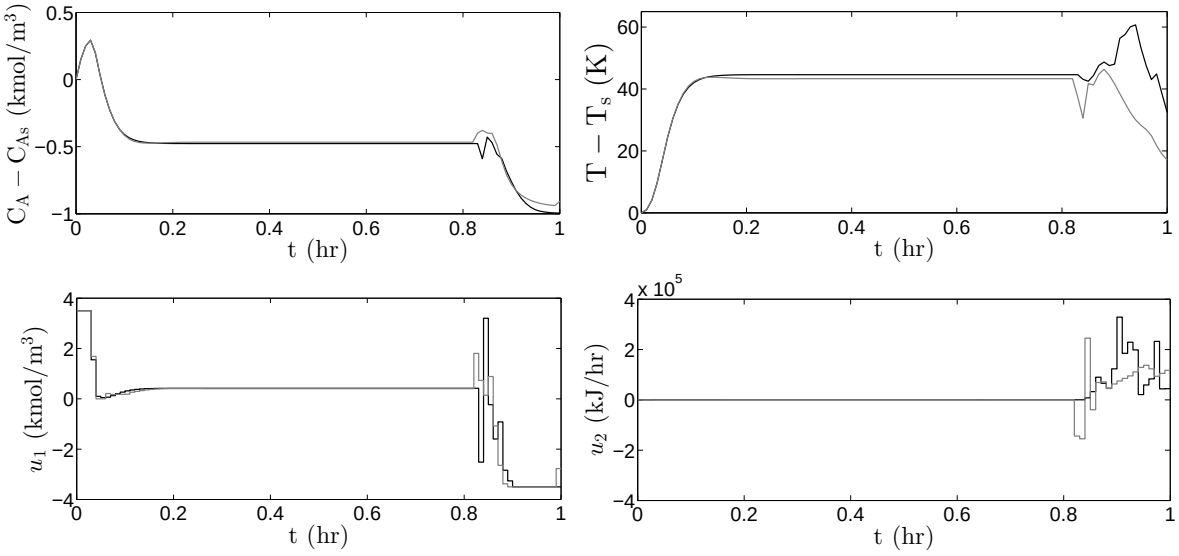

Figure 2.13: The closed-loop trajectories of the CSTR under the linear multiple-model LEMPC with three linear models (gray line) and under the nonlinear LEMPC (black line).

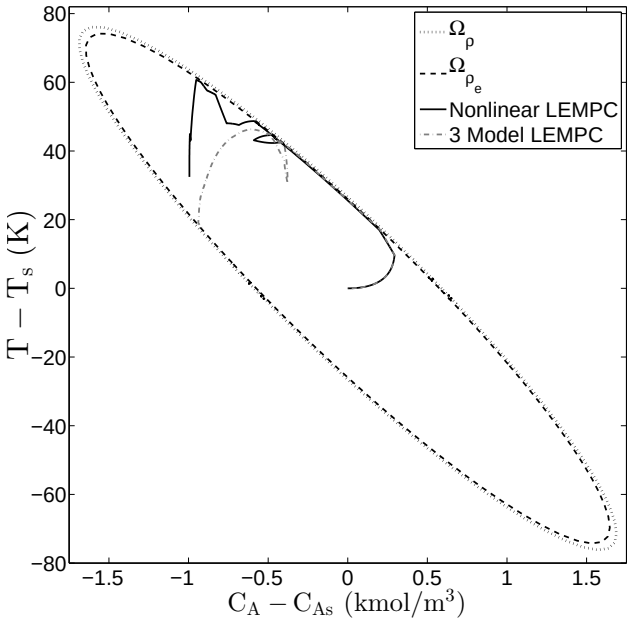

Figure 2.14: The closed-loop state trajectories of the CSTR under the linear multiple-model LEMPC with three linear models (dashed-dotted line) and under the nonlinear LEMPC (solid line).

figures, the closed-loop evolution of the CSTR under the linear LEMPC with one and two models is much different than that under the linear multiple-model LEMPC with three models and the nonlinear LEMPC because the CSTR under LEMPC is initially driven to and maintained in a region where the first and second models are not accurate. The closed-loop behavior of the CSTR under the linear multiple-model LEMPC with three models and the nonlinear LEMPC is similar with the most significant deviation being observed towards the end of the operation period (Fig. 2.14). The closed-loop average economic costs for these simulations are given in Table 2.3 and demonstrate that increasing the number of linear models used in the LEMPC improves the closed-loop performance and extends the region of time-varying operation (c.f., in Fig. 2.4 and Fig. 2.14). Over the one hour length of operation, the total computation time under the nonlinear LEMPC is 205.2 *sec* and under the linear LEMPC with three empirical models is 20.4 *sec* (the computation time for the nonlinear LEMPC is 906% greater than the computation time for the linear LEMPC with three empirical models).

2.5 Conclusions

In this chapter, an LEMPC method formulated with empirical models was considered for nonlinear process systems. Under the assumption that the error between the empirical linear model and the one of the linearization of the nonlinear model at the steady-state around which time-varying operation is considered, sufficient conditions such that the LEMPC formulated with the empirical linear model will guarantee closed-loop stability of the nonlinear system in the sense of boundedness of the closed-loop state in a compact set were derived. A chemical process example demonstrated the application of the proposed method and extensive simulation results were given. From these results, a similar closed-loop behavior between the chemical process under the LEMPC with the nonlinear model and under the LEMPC with an empirical model was observed with comparable closed-loop economic performance. However, a significant decrease in the computation time required to solve the LEMPC with a linear model compared to LEMPC with a nonlinear model was observed. In all of the simulations, the LEMPC with the linear model maintained closed-loop stability and obtained better closed-loop economic performance than that obtained at steady-state.

Chapter 3

On Identification of Well-Conditioned Nonlinear Systems: Application to Economic Model Predictive Control of Nonlinear Processes

3.1 Introduction

In the PNLSS approach, a linear state-space model is first obtained and it is then extended with polynomial nonlinear terms that are optimized to capture the system's nonlinear behavior.[52,64,67,77] The linear part can be obtained using the best linear fit or least-squares, or using subspace system identification.[64,67,68,75] This assures that the nonlinear model performs at least as well as the linear model locally.[68] PNLSS has shown superior results over linear models in various applications including control and modeling applications[67,77] and identifying the dynamics of electrical circuits.[55] The use of PNLSS in nonlinear model predictive control (NMPC) for an automotive clutch system has also been presented.[52] A crucial advantage of PNLSS is that it is very straightforward to apply for multivariable systems and has a very significant computation time benefit for

low-order polynomials (e.g., polynomial models with orders two or three).[68,75] A potential disadvantage of PNLSS is that it may lead to ill-conditioned models which may need a very small time step to be solved correctly with explicit numerical integration methods.

Motivated by the above, this chapter initially develops a nonlinear system identification technique for a broad class of nonlinear processes which leads to the construction of polynomial nonlinear state-space dynamic models which are well-conditioned over a broad region of process operation. This technique takes advantage of the framework of PNLSS models and utilizes additional constraints on the stiffness ratio of the Jacobian of the nonlinear identified models at various points in the region of process operation to ensure that the resulting models can be solved without using an unnecessarily small time step of integration when explicit temporal-integration methods are used. Subsequently, the design of LEMPC systems for nonlinear processes using the well-conditioned nonlinear models is addressed and sufficient conditions are derived for closed-loop stability. A classical chemical process example is used to illustrate the application and point out the advantages of the proposed system identification and LEMPC design techniques.

3.2 Class of systems

In this chapter, the class of systems to be considered are nonlinear, continuous-time systems with affine inputs, with dynamics described according to the system of differential equations:

$$\dot{x}(t) = f_p(x(t), w(t)) + \tilde{G}(x(t), w(t))u(t) \tag{3.1}$$

where the state vector is $x \in R^n$, the input vector is $u \in R^m$, the disturbance vector is $w \in R^l$, $f_p(x(t), w(t)) : R^n \times R^l \to R^n$ is a vector function, and $\tilde{G}(x(t), w(t)) : R^n \times R^l \to R^n \times R^m$ is a matrix of functions of x and w. It is assumed that the component functions of f_p and $\tilde{G}$ are analytic on $R^n \times R^l$ such that they are infinitely differentiable and locally expressed with a convergent power series.

We also assume that since all control actuators u have physical limits, the control actions are

bounded within a convex set $U := \{u \in R^m : u_i^{\min} \leq u_i \leq u_i^{\max},\ i = 1,\ \ldots,\ m\}$. In addition, all disturbances to the system are assumed to have a known bound of $\theta > 0$ (for all t, $|w(t)| \leq \theta$). The origin is assumed to be an equilibrium point of Eq. 3.1 ($f_p(0,0) = 0$ when $u = 0$).

Only nonlinear systems for which an explicit controller exists that can make the origin of Eq. 3.1 locally exponentially stable in the absence of disturbances ($w(t) \equiv 0$), while meeting the constraints on the control actions, will be considered. When such an explicit controller $h(x) \in U$ exists, converse Lyapunov theorems state that a positive definite, continuously differentiable, scalar-valued function $V(x)$ and positive constants c_1, c_2, c_3, and c_4 exist that result in the following inequalities:[30,111]

$$c_1|x|^2 \leq V(x) \leq c_2|x|^2, \tag{3.2a}$$

$$\frac{\partial V(x)}{\partial x}(f_p(x,0) + \tilde{G}(x,0)h(x)) \leq -c_3|x|^2, \tag{3.2b}$$

$$\left|\frac{\partial V(x)}{\partial x}\right| \leq c_4|x| \tag{3.2c}$$

for any x within the open connected set $D \subseteq R^n$ that includes the origin. Methods for developing $h(x)$ are available for various classes of systems (see, for example,[10,12,27,83]). The stability region Ω_ρ for the closed-loop system of Eq. 3.1 under the controller $h(x)$ is defined as a level set of V (a set within which $V(x) \leq \rho$) within D where $\dot{V}$ is negative.

3.3 System Identification

In this chapter, we use the PNLSS approach to obtain a model that is nonlinear in the states and affine in the inputs, with the following form:

$$\frac{dx}{dt} = \underbrace{Ax + P_z(x)}_{=:f(x)} + Bu \tag{3.3}$$

where $x \in R^n$ and $u \in R^m$ are the state vector and the input vector respectively, A is a constant square matrix of dimension n, and $B \in R^{n \times m}$ is a constant matrix. The notation $P_z(x)$ denotes a nonlinear

vector function that includes polynomial terms of order two and higher, with the subscript z used to indicate that the polynomial is a z^{th}-order polynomial. $P_z(x)$ is defined by the following equations:

$$P_z(x) = E\xi(x) \tag{3.4a}$$

$$\xi(x) = [x_1^2 \quad x_1x_2 \quad \ldots \quad x_n^z]^T \tag{3.4b}$$

where the vector $\xi(x)$ contains nonlinear monomials in x of order two and higher up to a chosen order z, and the constant matrix E contains the coefficients multiplying the nonlinear monomials in $\xi(x)$. The order z of the polynomial is chosen before data are fit to the model of Eq. 3.3. As an example, when $n = 2$ and $z = 3$, $\xi(x)$ has the following form:

$$\xi(x) = [x_1^2 \quad x_1x_2 \quad x_2^2 \quad x_1^3 \quad x_1^2x_2 \quad x_1x_2^2 \quad x_2^3]^T \tag{3.5}$$

3.3.1 PNLSS system identification methodology

The PNLSS identification problem is to find the terms A, B, and E in Eqs. 3.3-3.4 when the only available information is process input/output data. For the case when all states are available as measured outputs (full state feedback), an optimization problem can be used to find these terms that involves the following two steps:

1. A linear state-space model is obtained using a frequency domain subspace identification algorithm.

2. The linear model is used as an initial guess for a nonlinear optimization problem to identify a nonlinear model that captures the nonlinear behavior of the system.

To simplify the presentation in this chapter, we will consider that full state feedback is available and thus the measurements of the states can be used directly in order to obtain the PNLSS model. To implement the PNLSS method, one obtains $Z + 1$ state measurements of the system ($x_m(v)$,

$v = 0, ..., Z$, where $x_m(v)$ is the vector of measured states in deviation variable form at time $\tilde{t}_v = v\tilde{\Delta}$ and $\tilde{\Delta}$ is the time between measurements) with a known sequence of inputs. Then, using the same initial state $x_m(0)$ and the same sequence of inputs, Z modeled states (denoted as $x(v)$, $v = 1, ..., Z$, where $x(v)$ is the vector of modeled states in deviation variable form at time $\tilde{t}_v = v\tilde{\Delta}$) are obtained via numerical integration of the model to be identified (Eq. 3.3). The goal is then to minimize the difference between the measured and modeled states that correspond to the same times in the simulation by adjusting the model parameters A, B, and E in Eq. 3.3.

We denote the vector of measured states (in deviation form) that will be used in the PNLSS objective function in a vector form (the problem could be reformulated with the states in a matrix form if desired) as:

$$x_m = [x_m^T(1) \;\; x_m^T(2) \;\; ... \;\; x_m^T(Z)]^T \tag{3.6}$$

and the modeled states as:

$$x_p = [x^T(1) \;\; x^T(2) \;\; ... \;\; x^T(Z)]^T \tag{3.7}$$

where $x_m(0) = x(0)$ is the initial state ($x_m(0) = x(0) = 0$ if we start from the steady-state). Using this notation, the polynomial nonlinear state-space model is identified via a nonlinear optimization problem formulated as:

$$\min_{\eta} \quad \Phi(x_m - x_p) \tag{3.8a}$$

$$\text{s.t.} \quad \dot{x} \quad = Ax + P_z(x) + Bu \tag{3.8b}$$

where η signifies the optimization variables A, B, and E and Φ is a positive definite cost function to be minimized. Examples of commonly used functions include the vector 1-norm, vector 2-norm (also called least-squares), weighted least-squares, and a linear combination and/or a product of such functions (the induced matrix 1-norm, induced matrix 2-norm, or combinations/products of these norms are possible cost functions if this is reformulated for the matrix case).

If it is desired to identify a nonlinear model that minimizes the vector p-norm, the optimization problem is reduced to the following nonlinear optimization problem:

$$\min_{\eta} \quad | \, (x_m - x_p) \, |_p \tag{3.9a}$$

$$\text{s.t.} \quad \dot{x} \quad = Ax + P_z(x) + Bu \tag{3.9b}$$

After obtaining the model, this model is validated over a wide range of input/state data. However, the usefulness of the model depends on the purpose it serves. From a nonlinear model predictive control point of view, empirical models need to be well-conditioned so that they can be accurately solved with explicit integration schemes without employing very small time steps to predict the behavior of the nonlinear system in real-time. Numerical stability of an empirical model is not a central issue when performing linear system identification since the analytic solution of a linear system can be obtained. On the other hand, there is no general method for obtaining the analytic solution of highly coupled nonlinear ordinary differential equations and the numerical integration accuracy is sensitive to the numerical stability of the identified nonlinear model. The system identification procedure does not guarantee that a well-conditioned model will be obtained, so the identified model may be ill-conditioned requiring a very small numerical integration step size to be used.

Remark 1 *The existence of a numerical solution within the accuracy of the numerical integration method used is of concern when using explicit numerical integration methods (e.g., Explicit Euler or Runge-Kutta) as opposed to implicit numerical methods, especially for ill-conditioned nonlinear differential equations. This is because implicit methods are numerically stable for any integration step size, such that only the accuracy of the solution obtained depends on the step size, whereas explicit numerical methods are numerically stable only if the integration step size is sufficiently small, and the threshold at which a step size is sufficiently small is not generally possible to predict for a given system. Despite the relative time step advantage of using implicit methods for numerical integration over explicit ones, implicit methods are very complex to include in system identification*

and when modeling the outputs and states. Also, implicit methods are computationally expensive and from a predictive control point of view, it is preferred to use explicit methods with a suitable integration step size.

Remark 2 *It was noted that the modeled states $x(v)$, $v = 1,...,Z$ come from the numerical integration of Eq. 3.3. The numerical integration can be performed several different ways in system identification. One method is to perform numerical integration of the model of Eq. 3.3 as is typically done when integrating a differential equation with a given initial condition, and integrating the model between $\tilde{t}_0$ and $\tilde{t}_Z$ using only the initial state $x_m(0)$ and the known input sequence. This complete integration between the initial and final times makes the optimization substantially more burdensome and involved. Another numerical integration method used in practical implementation of system identification methods that is less computationally intensive involves using all of the measured states in the numerical integration used in modeling the states.*[76] *In this method, each measurement is used as an initial condition for numerical integration of Eq. 3.3 to obtain only the following modeled state (i.e., to obtain the value of $x(v)$, $v = 1,...,Z$, numerical integration over only one time interval $\tilde{\Delta}$ is performed with the initial condition for each $x(v)$ as $x_m(v-1)$, $v = 1,...,Z$). As the number of measured states increases, the number of numerical integration steps between $x_m(v-1)$ and $x(v)$ decreases. When the same number of measurements are used as the number of modeled states such that only one integration step is needed for each $x(v)$, the optimization problem is much easier to solve as will be demonstrated in the example.*

3.3.2 Motivating example: PNLSS application to a chemical process example

To illustrate the importance of considering model well-conditioning when deriving an empirical model for a process, a chemical process example is presented in this section.

Specifically, a second-order irreversible reaction that forms the product *B* from the reactant *A* occurs in a non-isothermal, well-mixed continuously stirred tank reactor (CSTR). The CSTR

is fed by an inlet stream containing A with molar concentration C_{A0} in an inert solvent at a feed volumetric flow rate F and feed temperature T_0. The reaction is exothermic, and the CSTR is operated non-isothermally with heat supplied/removed at heat rate Q. The liquid in the CSTR is assumed to have constant heat capacity C_p and constant liquid density ρ_L, and to be maintained at a constant volume V. The dynamic model equations for the CSTR are developed from standard mass and energy balances and have the form:

$$\frac{dC_A}{dt} = \frac{F}{V}(C_{A0} - C_A) - k_0 e^{-E/RT} C_A^2 \tag{3.10a}$$

$$\frac{dT}{dt} = \frac{F}{V}(T_0 - T) - \frac{\Delta H k_0}{\rho_L C_p} e^{-E/RT} C_A^2 + \frac{Q}{\rho_L C_p V} \tag{3.10b}$$

where C_A is the concentration of the reactant A inside the reactor and T is the reactor temperature. The reaction kinetics are modeled using the Arrhenius equation, with pre-exponential factor k_0, activation energy E, and enthalpy of reaction ΔH (see Table 3.1 for the values of the reactor parameters). The CSTR is operated at the steady-state $[C_{As}\ T_s] = [1.2\ kmol/m^3\ 438.0\ K]$, which is open-loop asymptotically stable and corresponds to a steady-state inlet concentration of $C_{A0s} = 4.0\ kmol/m^3$ and a heat rate of $Q_s = 0.0\ kJ/hr$.

Table 3.1: CSTR Parameters

$F = 5.0$	$\frac{m^3}{hr}$	$k_0 = 8.46 \times 10^6$	$\frac{m^3}{kmol\ hr}$
$T_0 = 300$	K	$\Delta H = -1.15 \times 10^4$	$\frac{kJ}{kmol}$
$V = 1.0$	m^3	$E = 5.0 \times 10^4$	$\frac{kJ}{kmol}$
$C_p = 0.231$	$\frac{kJ}{kg\ K}$	$\rho_L = 1000$	$\frac{kg}{m^3}$
$R = 8.314$	$\frac{kJ}{kmol\ K}$		

The dynamic model of Eq. 3.10 is of the following form (using the notation of Eq. 3.1):

$$\dot{x}(t) = f_p(x(t), 0) + \tilde{G}(x(t), 0)u(t) \tag{3.11}$$

where the vectors of states and inputs in Eq. 3.11 are defined in deviation form as

$$x = [x_1\ x_2]^T = [C_A - C_{As}\ T - T_s]^T \tag{3.12}$$

$$u = [u_1\ u_2]^T = [C_{A0} - C_{A0s}\ Q - Q_s]^T \tag{3.13}$$

The inlet concentration C_{A0} and the rate Q at which heat is supplied to or removed from the CSTR can be manipulated to affect the reactor state variables. These manipulated inputs are subject to the constraints:

$$0.5 \leq C_{A0} \leq 7.5\ kmol/m^3 \tag{3.14a}$$

$$-5.0 \times 10^5 \leq Q \leq 5.0 \times 10^5\ kJ/hr \tag{3.14b}$$

To show the influence of step size on the integration of an empirical model resulting from system identification of a process with the dynamics of Eq. 3.10, the PNLSS approach of Eq. 3.9 with $p = 2$ was applied to this chemical process. To generate the input/state data necessary to implement the PNLSS method, several steps in the inputs to the CSTR were simulated, and the input/state data was obtained from the integration of the dynamic model of Eq. 3.10 subject to the input changes. It was determined that the accuracy of the numerical integration of the CSTR model of Eq. 3.10 was sufficient with the Explicit Euler method using an integration step size of $h_c = 10^{-4}\ hr$, so this numerical integration procedure and step size were used for the first-principles process model of Eq. 3.10 throughout this chapter. From the input/state data, a polynomial nonlinear state-space model of the form of Eq. 3.3, where the vectors of states x and inputs u are as defined in Eqs. 3.12-3.13, was obtained. All PNLSS optimization problems in this chapter were solved using the open-source nonlinear interior point optimization solver Ipopt.[45] The states were modeled using both numerical integration methods discussed in Remark 2 (the states were modeled using only the initial state with the sequence of inputs, and also by using all of the measured states and the input sequence) and the resulting empirical models were almost identical. However,

solving the system identification optimization problem of Eq. 3.9 using the second method (using all measured states) was much less computationally intensive than using the first method (using only the initial measured state), so the second method will be used for all PNLSS optimization problems for this chemical process example throughout the rest of the chapter. The term $P_z(x)$ in Eq. 3.3 was chosen to be a second-order polynomial so $z = 2$ and $n = 2$. The identified nonlinear continuous-time model of the CSTR is:

$$\frac{dx_1}{dt} = -32.64x_1 - 0.479x_2 - 31.2x_1^2 - 1.0016x_1x_2 - 0.0075x_2^2 + 5.53u_1 - 0.000008u_2 \quad (3.15a)$$

$$\frac{dx_2}{dt} = 1398x_1 + 17.79x_2 - 30x_1^2 + 24.94x_1x_2 + 0.381x_2^2 - 1076u_1 + 0.00476u_2 \quad (3.15b)$$

This model is very sensitive to the numerical integration step. When the inputs are modeled as sinusoids and the process model is integrated with an integration step of $h_c = 10^{-4}\ hr$ with the Explicit Euler method and the resulting trajectories are compared to those of the first-principles CSTR process model of Eq. 3.10 using the same input and same step size, there are significant differences in the values of the states x_1 and x_2 between the two models, as shown in Fig. 3.1. However, when those same first-principles CSTR trajectories are compared with the trajectories resulting from using an integration step of $h_c = 10^{-6}\ hr$ in the model of Eq. 3.15 with the same sinusoidal input, the first-principles and PNLSS trajectories are very close, as shown in Fig 3.2.

Fig. 3.2 shows good agreement between the state trajectories using the first-principles CSTR model of Eq. 3.10 and the empirical nonlinear model of Eq. 3.15 when using the smaller step size. In order to quantify the difference between the two behaviors, the average squared error in the concentration and temperature over eight hours of operation, when a step size $h_c = 10^{-6}\ hr$ is used to integrate the empirical model, is calculated as follows:

$$\frac{1}{8}\int_0^8 (x_{1p}(t) - x_{1m}(t))^2\, dt = 1.6821 \times 10^{-4} \quad (3.16)$$

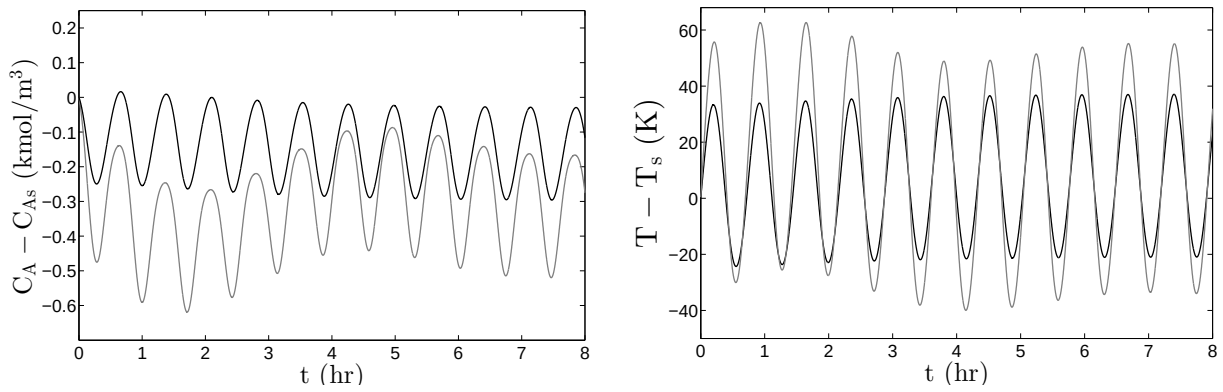

Figure 3.1: State trajectories of the first-principles CSTR model of Eq. 3.10 (black trajectory) and the identified PNLSS model of Eq. 3.15, $h_c = 10^{-4}$ *hr* (gray trajectory) when the heat rate and concentration inputs are varied sinusoidally with amplitudes $55,000$ kJ/hr and 0.25 $kmol/m^3$, respectively, and both with frequency 8.72 rad/hr.

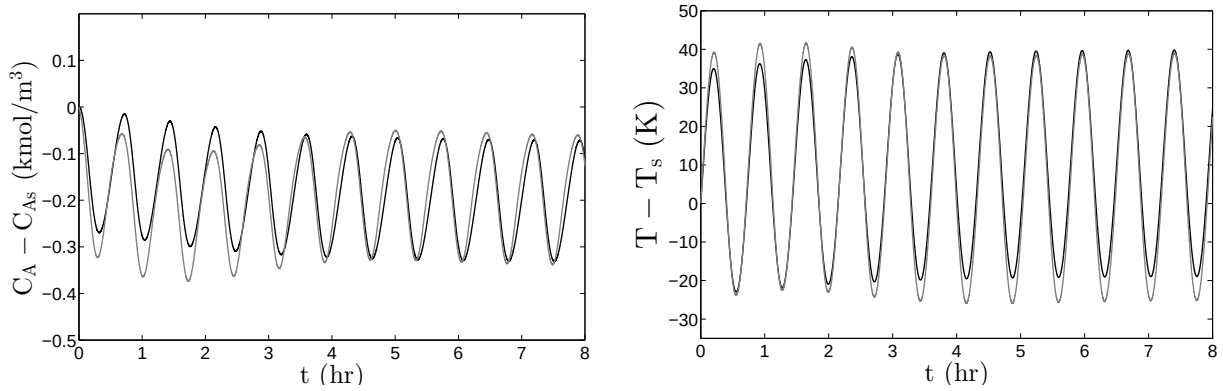

Figure 3.2: State trajectories of the first-principles CSTR model of Eq. 3.10 (black trajectory) and the identified PNLSS model of Eq. 3.15, $h_c = 10^{-6}$ *hr* (gray trajectory) when the heat rate and concentration inputs are varied sinusoidally with amplitudes $55,000$ kJ/hr and 0.25 $kmol/m^3$, respectively, and both with frequency 8.72 rad/hr.

$$\frac{1}{8}\int_0^8 (x_{2p}(t) - x_{2m}(t))^2 \, dt = 1.3059 \tag{3.17}$$

where x_{1p} and x_{1m} are the modeled and measured concentrations respectively, and x_{2p} and x_{2m} are the modeled and measured temperatures respectively.

3.3.3 Proposed approach for PNLSS system identification

Motivated by the effect of integration step size on the accuracy of the empirical model from the previous example, additional constraints on the PNLSS optimization are proposed. Adding extra constraints that assure well-conditioning of the nonlinear model is essential for effective control. The modified PNLSS optimization problem with the numerical stability constraints has the general form:

$$\min_{\eta \in C} \quad \Phi(x_m - x_p) \tag{3.18a}$$

$$\text{s.t.} \quad F(\eta) \quad = 0 \tag{3.18b}$$

$$R(\eta) \quad \leq 0 \tag{3.18c}$$

The optimization variable η represents the parameters A, B, and E of the polynomial nonlinear model of Eqs. 3.3-3.4. We allow that the values of these parameters belong to the bounded convex set C. $F(\eta)$ and $R(\eta)$ represent equality and inequality constraints that can be used to ensure well-conditioning of the nonlinear identified model. A major cause of ill-conditioning of a system of differential equations is system stiffness, meaning that the dynamics of some states are much faster than the dynamics of others with which they are coupled. As a result, though other numerical stability constraints could be conceived, we will explicitly derive numerical constraints based on stiffness for use in the PNLSS optimization problem.

The stiffness of a system can often be evaluated based on derivative information for the model in the region of operation. For example, the Jacobian of $f(x)$ in Eq. 3.3 evaluated at s points in the region of operation reveals information about the stiffness of the nonlinear model and its sensitivity to explicit forward numerical integration step sizes. The Jacobian of $f(x)$ evaluated at state-space point j is defined as the matrix of partial derivatives of the component functions f_i with respect to

the independent variables x_i, $i = 1, ..., n$:

$$J_j = \begin{bmatrix} \frac{\partial f_1}{\partial x_1}|_j & \frac{\partial f_1}{\partial x_2}|_j & \frac{\partial f_1}{\partial x_3}|_j & \cdots & \frac{\partial f_1}{\partial x_n}|_j \\ \frac{\partial f_2}{\partial x_1}|_j & \frac{\partial f_2}{\partial x_2}|_j & \frac{\partial f_2}{\partial x_3}|_j & \cdots & \frac{\partial f_2}{\partial x_n}|_j \\ \cdot & \cdot & \cdot & \cdot & \cdot \\ \cdot & \cdot & \cdot & \cdot & \cdot \\ \cdot & \cdot & \cdot & \cdot & \cdot \\ \frac{\partial f_n}{\partial x_1}|_j & \frac{\partial f_n}{\partial x_2}|_j & \frac{\partial f_n}{\partial x_3}|_j & \cdots & \frac{\partial f_n}{\partial x_n}|_j \end{bmatrix} \quad \text{where} \quad j = 1, ..., s \tag{3.19}$$

where j denotes the j^{th} state-space point.

The stiffness of the nonlinear model is often evaluated from its Jacobian using a measure such as the maximum singular value, maximum eigenvalue, condition number, or ratio of the absolute value of the eigenvalue with the greatest magnitude to the eigenvalue with the smallest magnitude (stiffness ratio) of the Jacobian. Therefore, the system identification problem can be improved to account for numerical stability of the model by adding constraints on the Jacobian of $f(x)$ in Eq. 3.3 evaluated at several points in the region of operation. As an example, for a system of n states, a constraint can be added on the maximum value of the stiffness ratio of the Jacobian of $f(x)$ evaluated at s points of interest in the region of operation, where the stiffness ratios are denoted as:

$$S_j = \frac{\lambda_{max_j}}{\lambda_{min_j}}, \quad j = 1, ..., s \tag{3.20}$$

with

$$\lambda_{max_j} = \max\{|\lambda_{1j}|, |\lambda_{2j}|, ..., |\lambda_{nj}|\}, \quad j = 1, ..., s \tag{3.21a}$$

$$\lambda_{min_j} = \min\{|\lambda_{1j}|, |\lambda_{2j}|, ..., |\lambda_{nj}|\}, \quad j = 1, ..., s \tag{3.21b}$$

where the notation λ_{ij} signifies the i^{th} ($i = 1, ..., n$) eigenvalue of the Jacobian matrix J_j, and λ_{max_j} and λ_{min_j} signify the maximum and minimum values of the magnitudes of the eigenvalues of J_j.

The numerical stability constraint to be incorporated in the PNLSS optimization problem of Eq. 3.18 is a bound on the maximum value of the stiffness ratio at all s points at which the Jacobian is evaluated, written as:

$$R(\eta) = \max\{S_1, S_2, ..., S_s\} \leq \hat{M} \tag{3.22}$$

where $\hat{M}$ is a number chosen to constrain the solutions to Eq. 3.18 to be models that are well-conditioned with respect to forward numerical integration in the region of interest.

The eigenvalues of the Jacobian matrices have to be evaluated numerically for an $n \times n$ Jacobian. To illustrate this point, we consider a two-input/two-output system with full state feedback. We define J_1, J_2,..., J_s as the Jacobians of the identified polynomial nonlinear model, evaluated at several points $j = 1, ..., s$ in the state-space region of interest. J_1 is the Jacobian evaluated at the steady-state and J_j is the Jacobian evaluated at the state-space point j where

$$J_j = \begin{bmatrix} a_j & b_j \\ c_j & d_j \end{bmatrix} \tag{3.23}$$

Thus, for a system with two inputs and two states, we can incorporate numerical stability constraints in the PNLSS optimization problem as follows:

$$\min_{\eta \in C} \quad | \, x_m - x_p \, |_2 \tag{3.24a}$$

$$\text{s.t.} \quad \dot{x} \quad = Ax + P_z(x) + Bu \tag{3.24b}$$

$$\frac{\lambda_{max_j}}{\lambda_{min_j}} \quad \leq \hat{M}, \quad j = 1, ..., s \tag{3.24c}$$

$$\lambda_{max_j} = \max\{|\lambda_{1j}|, |\lambda_{2j}|\}, \quad j = 1, ..., s \tag{3.24d}$$

$$\lambda_{min_j} = \min\{|\lambda_{1j}|, |\lambda_{2j}|\}, \quad j = 1, ..., s \tag{3.24e}$$

$$\lambda_{1j} = \frac{(a_j + d_j)}{2} + \left(\frac{(a_j + d_j)^2}{4} - (a_j d_j - b_j c_j) \right)^{1/2}, \quad j = 1, ..., s \tag{3.24f}$$

$$\lambda_{2j} = \frac{(a_j + d_j)}{2} - \left(\frac{(a_j + d_j)^2}{4} - (a_j d_j - b_j c_j) \right)^{1/2}, \quad j = 1, ..., s \tag{3.24g}$$

In this optimization problem, the cost function $\Phi(x_m - x_p)$ is taken to be the Euclidean norm of the difference between the vectors x_m and x_p.

For a 2×2 matrix, it is easy to obtain an explicit expression for the eigenvalues (e.g., Eqs. 3.24f-3.24g). However, for an $n \times n$ matrix, the calculation of eigenvalues is not as straightforward. The characteristic polynomial could be used as an equality constraint and solved by adding additional constraints that find the roots of the characteristic polynomial numerically through a method such as Newton's Method. For certain special classes of matrices, formulas are available that allow for the explicit solution of the eigenvalues, and these could be added as constraints if the Jacobians at the evaluated points have these special forms. For example, the eigenvalues of a 3×3 matrix or of a triangular matrix of any dimension can be written explicitly. For the general case when explicit expressions for the eigenvalues may not be available, the PNLSS optimization problem for a system with n states becomes:

$$\min_{\eta \in C} \quad | \, x_m - x_p \, |_2 \tag{3.25a}$$

$$\text{s.t.} \quad \dot{x} \quad = Ax + P_z(x) + Bu \tag{3.25b}$$

$$\frac{\lambda_{max_j}}{\lambda_{min_j}} \quad \leq \hat{M}, \quad j = 1, ..., s \tag{3.25c}$$

$$F(\eta) = 0 \tag{3.25d}$$

$$R(\eta) \leq 0 \tag{3.25e}$$

where $F(\eta)$ and $R(\eta)$ represent all constraints necessary to obtain the eigenvalues of the Jacobians J_j, $j = 1, ..., s$, and to assure numerical stability if additional constraints are desired beyond those of Eq. 3.25c.

3.3.4 Application of proposed method to the chemical process example

We now revisit the CSTR example described by Eq. 3.10 and apply the PNLSS model identification procedure once more, this time using the PNLSS approach accounting for numerical stability

(Eq. 3.24). The previously identified ill-conditioned model of Eq. 3.15 is used as an initial guess for the following nonlinear optimization problem:

$$\min_{\eta \in C} \quad | \, x_m - x_p \, |_2 \tag{3.26a}$$

$$\text{s.t.} \quad \dot{x} \quad = Ax + P_z(x) + Bu \tag{3.26b}$$

$$\frac{\lambda_{max_j}}{\lambda_{min_j}} \quad \leq 1000 \quad j = 1, ..., s \tag{3.26c}$$

$$\lambda_{max_j} = \max\{|\lambda_{1j}|, |\lambda_{2j}|\}, \quad j = 1, ..., s \tag{3.26d}$$

$$\lambda_{min_j} = \min\{|\lambda_{1j}|, |\lambda_{2j}|\}, \quad j = 1, ..., s \tag{3.26e}$$

$$\lambda_{1j} = \frac{(a_j + d_j)}{2} + \left(\frac{(a_j + d_j)^2}{4} - (a_j d_j - b_j c_j) \right)^{1/2} \quad j = 1, ..., s \tag{3.26f}$$

$$\lambda_{2j} = \frac{(a_j + d_j)}{2} - \left(\frac{(a_j + d_j)^2}{4} - (a_j d_j - b_j c_j) \right)^{1/2} \quad j = 1, ..., s \tag{3.26g}$$

where the modeled states in the vector x_p were determined by numerically integrating the model of Eq. 3.26b using Explicit Euler with a time step of $h_c = 10^{-4}$ *hr*. For this example, the ratios of the absolute value of the eigenvalue with the greatest magnitude to the eigenvalue with the smallest magnitude of the Jacobian were evaluated at ten different points (i.e., s = 10) in the region of interest and were constrained to be less than 1000 to obtain a well-conditioned model with respect to the integration step of $h_c = 10^{-4}$ *hr*. The nonlinear model of the CSTR (in continuous-time) that is identified by the optimization problem of Eq. 3.26 is:

$$\frac{dx_1}{dt} = -34.00x_1 - 0.495x_2 - 5.22x_1^2 - 0.902x_1x_2 - 0.0078x_2^2 - 4.6u_1 - 0.000008u_2 \tag{3.27a}$$

$$\frac{dx_2}{dt} = 1436x_1 + 18x_2 + 432x_1^2 + 43.6x_1x_2 + 0.376x_2^2 - 11u_1 + 0.00567u_2 \tag{3.27b}$$

We now compare the numerical stability of the model of Eq. 3.27 with that of the model of Eq. 3.15. We recall the results of Figs. 3.1-3.2, which showed that a step size of 10^{-4} *hr* was inadequate for sufficient model accuracy so that decreasing the step size was necessary to obtain a

more accurate integration. For the model of Eq. 3.27, however, a step size of 10^{-4} *hr* is sufficient. This is shown in Fig. 3.3, a plot of the state trajectories when the Explicit Euler method is use to numerically integrate the model of Eq. 3.27 with step size $h_c = 10^{-4}$ *hr* and a sinusoidal input to the system. Fig. 3.3 shows that the empirical model of Eq. 3.27 resulting from the PNLSS identification approach with numerical stability constraints is able to predict the nonlinear dynamics of the CSTR system of Eq. 3.10 accurately with a larger step size than was needed when using the model of Eq. 3.15. Examining the error in concentration and temperature defined according to Eqs. 3.16-3.17 for the model of Eq. 3.27 further illustrates this point. The average error in concentration for the model of Eq. 3.27 over eight hours of operation with an integration step size of 10^{-4} *hr* is 2.0276×10^{-4}, and the average error in the temperature is 0.2342. The concentration error with this larger step size for Eq. 3.27 is on the same order of magnitude as the concentration error using Eq. 3.15 with a step size of 10^{-6} *hr*, and the temperature error is almost an order of magnitude smaller.

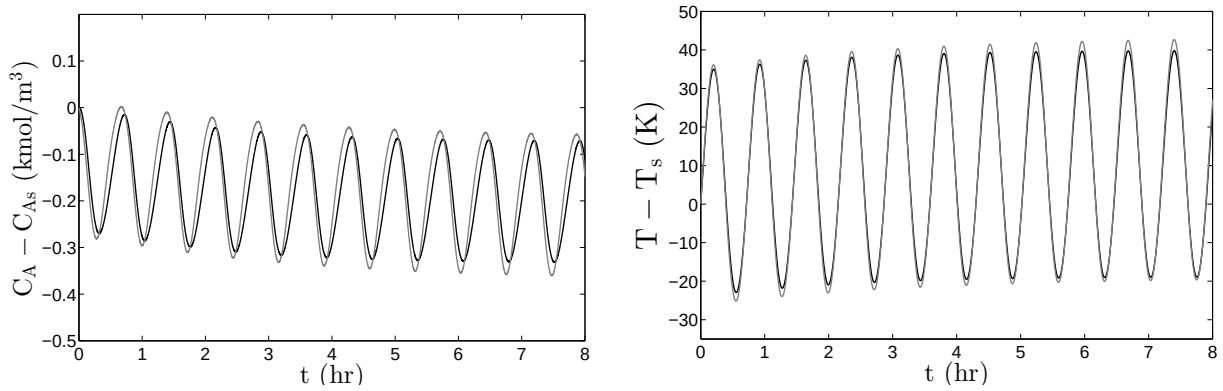

Figure 3.3: State trajectories of the first-principles CSTR model of Eq. 3.10 (black trajectory) and the identified PNLSS model of Eq. 3.27, $h_c = 10^{-4}$ *hr* (gray trajectory) when the heat rate and concentration inputs are varied sinusoidally with amplitudes $55,000$ kJ/hr and 0.25 $kmol/m^3$, respectively, and both with frequency 8.72 rad/hr.

The average computation time for each hour of simulation of the model of Eq. 3.27 with the 10^{-4} *hr* integration step is 0.986 CPU seconds which is more than 21 times faster than using Eq. 3.15 with the step size of $h_c = 10^{-6}$ *hr* for which each hour of simulation required 21.58 CPU

seconds. This shows that with a much larger integration time step, the model of Eq. 3.27 was able to accurately predict the nonlinear CSTR behavior.

A step input and impulse input were used to further validate the model of Eq. 3.27. The responses for the polynomial model of Eq. 3.27 and the first-principles model of Eq. 3.10 to a step change in u_2 and an impulse input of u_1 are very close, as is shown in Figs. 3.4-3.5.

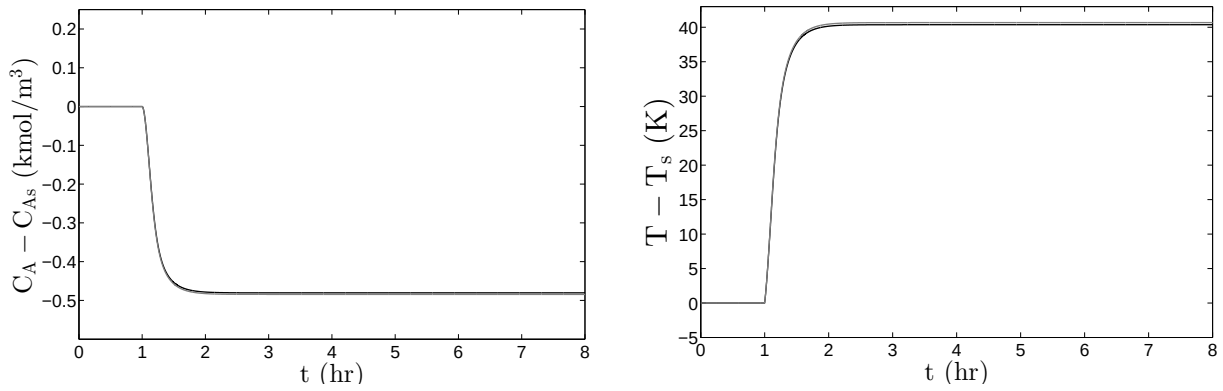

Figure 3.4: Step responses of the first-principles CSTR model of Eq. 3.10 (black trajectory) and of the identified PNLSS model of Eq. 3.27 (gray trajectory) when, after 1 hr of operation at the process steady-state, the heat rate (u_2) is suddenly increased by $20,000$ kJ/hr.

3.4 Economic Model Predictive Control Using Nonlinear Empirical Models

In this section, we first address the stability of the nonlinear process of Eq. 3.1 when a Lyapunov-based controller derived from the empirical PNLSS model of Eq. 3.3 is applied to it. We then develop the formulation of Lyapunov-based economic model predictive control (LEMPC) incorporating the PNLSS model and present a stability analysis for the nonlinear process in closed-loop with this LEMPC.

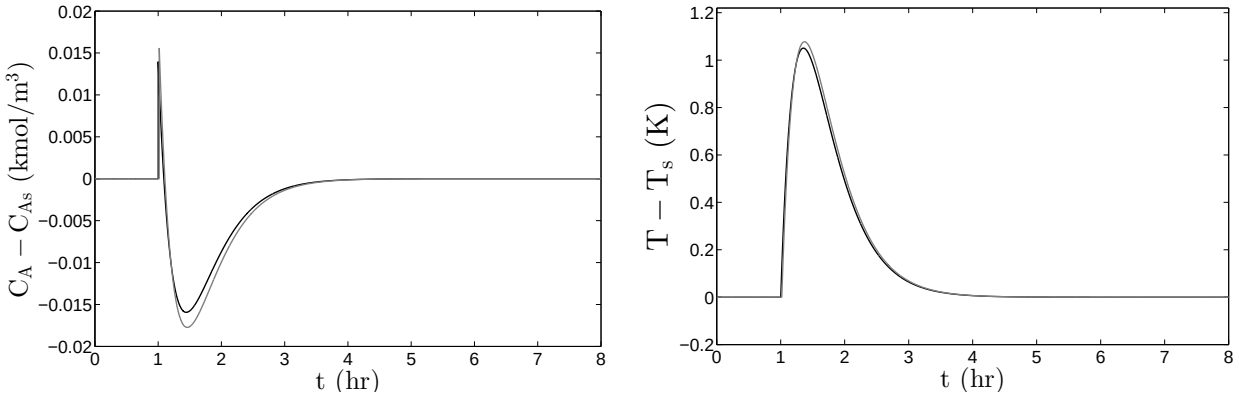

Figure 3.5: Impulse responses of the first-principles CSTR model of Eq. 3.10 (black trajectory) and of the identified PNLSS model of Eq. 3.27 (gray trajectory). The impulse was applied to the systems after 1 *hr* of operation at the process steady-state, and the impulse was numerically simulated as a rectangular pulse input in u_1 of magnitude 1 $kmol/m^3$ that was applied for 72 *sec*.

3.4.1 Lyapunov-based control using empirical models

The empirical nonlinear model of Eq. 3.3 is assumed to be stabilizable, which means that a state feedback controller $h_{NL}(x)$ exists that makes the closed-loop of the empirical nonlinear system of Eq. 3.3 exponentially stable for all $x \in D_{NL}$ where D_{NL} is an open connected region of state-space containing the origin. We will further assume that h_{NL} is locally Lipschitz on R^n such that one can find a constant $K > 0$ to bound the value of h_{NL} ($|h_{NL}(x)| < K|x|$ for all $x \in R^n$). When the controller $h_{NL}(x)$ that is designed based on the empirical model of Eq. 3.3 is applied to the nominal system of Eq. 3.1, closed-loop stability depends on whether the z^{th} order Taylor series expansion of the nominal model is sufficiently close to the polynomial empirical model expanded to the same order z. It also depends on the effect of the higher order terms (nonlinear terms of order $z+1$) on the trajectories of the system of Eq. 3.1. In the following, we introduce the Taylor series of the right-hand side of Eq. 3.1 in a compact form. To simplify the notation throughout this section, the right-hand side of Eq. 3.1 is denoted as follows:

$$\tilde{f}(x(t),w(t),u(t)) := f_p(x(t),w(t)) + \tilde{G}(x(t),w(t))u(t) \tag{3.28}$$

To obtain the Taylor series of the entire vector function $\tilde{f}(x(t),w(t),u(t)) : R^n \times R^l \times R^m \rightarrow R^n$, the Taylor series expansion of each function $\tilde{f}_i, i = 1,...,n$ is taken individually. The Taylor series expansion of the function $\tilde{f}_i$ of the nominal model ($w(t) = 0$) of Eq. 3.28 around an equilibrium point $x = 0$ with $u = 0$ is:

$$\tilde{f}_i(x,0,u) = \bar{a}_i x + \frac{1}{2!}\sum_{i=1}^{n}\sum_{q=1}^{n}\frac{\partial^2 \tilde{f}_i}{\partial x_i \partial x_q}(0,0,0)x_i x_q + ... + \bar{b}_i u + \frac{1}{2!}\sum_{\Gamma=1}^{m}\sum_{v=1}^{m}\frac{\partial^2 \tilde{f}_i}{\partial u_\Gamma \partial u_v}(0,0,0)u_\Gamma u_v + ... \tag{3.29}$$

where

$$\bar{a}_i = [\frac{\partial \tilde{f}_i}{\partial x_1}(0,0,0) \quad \frac{\partial \tilde{f}_i}{\partial x_2}(0,0,0) \quad \frac{\partial \tilde{f}_i}{\partial x_3}(0,0,0) \quad ... \quad \frac{\partial \tilde{f}_i}{\partial x_n}(0,0,0)] \tag{3.30}$$

$$\bar{b}_i = [\frac{\partial \tilde{f}_i}{\partial u_1}(0,0,0) \quad \frac{\partial \tilde{f}_i}{\partial u_2}(0,0,0) \quad \frac{\partial \tilde{f}_i}{\partial u_3}(0,0,0) \quad ... \quad \frac{\partial \tilde{f}_i}{\partial u_m}(0,0,0)] \tag{3.31}$$

Now, all terms in the Taylor series polynomial containing derivatives of $\tilde{f}_i$ of order $z+1$ and higher with respect to x are disregarded and only the linear terms with respect to the input u are kept because the model Eq. 3.28 is affine in u. In order to simplify notation of the remaining polynomial, we define $\tilde{g}_i(x)$ as:

$$\tilde{g}_i(x) \quad = \quad \hat{g}_i \Lambda(x) \tag{3.32a}$$

$$\Lambda(x) = [x_1^2 \quad x_1 x_2 \quad ... \quad x_n^z]^T \tag{3.32b}$$

where the vector $\Lambda(x)$ contains nonlinear monomials in x of order two and higher up to a chosen order z. The coefficients of these nonlinear terms in x are placed in the vector $\hat{g}_i$. As an example, when $n = 2$ and $z = 3$, $\Lambda(x)$ and $\hat{g}_1$ have the following form:

$$\hat{g_1} = [\frac{1}{2}\frac{\partial^2 \tilde{f}_1}{\partial x_1^2} \quad \frac{\partial^2 \tilde{f}_1}{\partial x_1 \partial x_2} \quad \frac{1}{2}\frac{\partial \tilde{f}_1}{\partial x_2^2} \quad \frac{1}{6}\frac{\partial^3 \tilde{f}_1}{\partial x_1^3} \quad \frac{1}{2}\frac{\partial^3 \tilde{f}_1}{\partial x_1^2 \partial x_2} \quad \frac{1}{2}\frac{\partial^3 \tilde{f}_1}{\partial x_1 \partial x_2^2} \quad \frac{1}{6}\frac{\partial^3 \tilde{f}_1}{\partial x_1^3}]_{(0,0,0)} \tag{3.33}$$

$$\Lambda(x) = [x_1^2 \quad x_1x_2 \quad x_2^2 \quad x_1^3 \quad x_1^2x_2 \quad x_1x_2^2 \quad x_2^3]^T \tag{3.34}$$

Repeating the same procedure to take the Taylor series for all $\tilde{f}_i$, $i = 1,...,n$ functions, and defining the matrices $\bar{A}$, $\bar{G}_z(x)$, and $\bar{B}$ as matrices with row vectors $\bar{a}_i$, $\tilde{g}_i(x)$, and $\bar{b}_i$, $i = 1,...,n$, respectively, the Taylor series approximation of the vector function $\tilde{f}$ can be represented in the following compact notation:

$$\tilde{f}(x,0,u) \approx \bar{A}x + \bar{G}_z(x) + \bar{B}u \tag{3.35}$$

where $\bar{A}$ and $\bar{B}$ represent the coefficients of the linear terms in x and u respectively and $\bar{G}_z(x)$ is a nonlinear vector function that includes terms of order two and higher. The subscript z is to indicate that $\bar{G}_z(x)$ is a z^{th} order polynomial vector function. We will now develop a proposition that shows that the state feedback controller $h_{NL}(x)$ is locally robust to the plant-model mismatch and the effect of nonlinearities (of order $z+1$ and higher) when the process model is close to the Taylor series expansion of the actual nonlinear model. To facilitate this development, we define the matrix of coefficients of the nonlinear terms in $\bar{G}_z(x)$ as $\hat{G}_z$ (the row vectors of $\hat{G}_z$ are $\hat{g}_i$, $i = 1,...,n$).

Proposition 5 *If the origin of the closed-loop system of Eq. 3.3 under the controller $h_{NL}(x)$ is exponentially stable and there exist $\hat{\rho} > 0$, $W > 0$, and $\delta > 0$ such that:*

$$\|(\bar{A} - A) + (\hat{G}_z - E)\|W + \|\bar{B} - B\|K \leq \delta \tag{3.36}$$

then the origin of the nominal closed-loop system of Eq. 3.1 under $h_{NL}(x)$ is exponentially stable for all $x \in \Omega_{\hat{\rho}} \subset D_{NL}$.

Proof 3.1 *To prove exponential stability of the origin of Eq. 3.1 for a sufficiently small $\hat{\rho}$ and δ, it is necessary to show that a Lyapunov function exists for that system in closed-loop with the controller h_{NL}. To derive the existence of such a function, we first note that the exponential stability of the origin of Eq. 3.3 under the controller h_{NL} guarantees that there is a continuously differentiable*

Lyapunov function $\hat{V} : R^n \to R_+$ that meets the following inequalities:[111]

$$c_1|x|^2 \leq \hat{V}(x) \leq c_2|x|^2, \tag{3.37a}$$

$$\frac{\partial \hat{V}(x)}{\partial x}\left(Ax + P_z(x) + Bh_{NL}(x)\right) \leq -c_3|x|^2, \tag{3.37b}$$

$$\left|\frac{\partial \hat{V}(x)}{\partial x}\right| \leq c_4|x| \tag{3.37c}$$

for all $x \in D_{NL}$ where c_i, $i = 1,\ 2,\ 3,\ 4$ are positive constants.

We next define

$$q(x) := \tilde{f}(x, h_{NL}(x), 0) - \bar{A}x - \bar{G}_z(x) - \bar{B}h_{NL}(x) \tag{3.38}$$

which contains terms of order $z+1$ and higher in x. Consider the following closed-loop system:

$$\dot{x} = Ax + P_z(x) + Bh_{NL}(x) + \tilde{f}(x, h_{NL}(x), 0) - Ax - P_z(x) - Bh_{NL}(x)\ . \tag{3.39}$$

The time-derivative of $\hat{V}$ along the trajectory of the closed-loop system of Eq. 3.39 is:

$$\begin{aligned}
\dot{\hat{V}} &= \frac{\partial \hat{V}(x)}{\partial x}\left(Ax + P_z(x) + Bh_{NL}(x)\right) + \frac{\partial \hat{V}(x)}{\partial x}\left(\tilde{f}(x, h_{NL}(x), 0) - Ax - P_z(x) - Bh_{NL}(x)\right) \\
&\overset{(3.37b)}{\leq} -c_3|x|^2 + \left|\frac{\partial \hat{V}(x)}{\partial x}\right| \left|\left(\bar{A} - A\right)x + \left(\bar{G}_z(x) - P_z(x)\right) + \left(\bar{B} - B\right)h_{NL}(x) + q(x)\right| \\
&\overset{(3.37c)}{\leq} -c_3|x|^2 + c_4|x|\left(\left|\left(\bar{A} - A\right)x + \left(\bar{G}_z(x) - P_z(x)\right) + \left(\bar{B} - B\right)h_{NL}(x)\right| + |q(x)|\right)
\end{aligned} \tag{3.40}$$

for all $x \in D_{NL}$. Using boundedness of vector fields and the fact that the $h_{NL}(x)$ controller is locally Lipschitz, there exist constants $W > 0$ and $K > 0$ such that:

$$\begin{aligned}
\dot{\hat{V}} &\leq -c_3|x|^2 + c_4|x|\left(\left(\left\|(\bar{A} - A) + (\hat{G}_z - E)\right\| W|x| + \|\bar{B} - B\|\,|h_{NL}(x)|\right) + |q(x)|\right) \\
&\leq -c_3|x|^2 + c_4|x|\left(\left(\left\|(\bar{A} - A) + (\hat{G}_z - E)\right\| W + \|\bar{B} - B\|K\right)|x| + |q(x)|\right)
\end{aligned} \tag{3.41}$$

for all $x \in B_{r'} = \{x \in R^n : |x| \leq r'\}$ where r' is any $r' > 0$ such that $B_{r'} \subset D_{NL}$. If the condition of

Eq. 3.36 is satisfied, there exits a $\delta > 0$ *such that:*

$$\dot{\hat{V}} \leq -c_3|x|^2 + c_4\delta|x|^2 + c_4|x||q(x)| \tag{3.42}$$

for all $x \in B_{r'}$*. Since* $q(x)$ *contains terms of order* $z+1$ *and higher in* x *and vanishes near the origin, there exists a* $\gamma > 0$ *such that:*

$$|q(x)| < \gamma|x|^{z+1} \tag{3.43}$$

for all $x \in B_{r'}$*. Thus,*

$$\dot{\hat{V}} \leq -c_3|x|^2 + c_4\delta|x|^2 + c_4\gamma|x|^{z+2} \tag{3.44}$$

for all $x \in B_{r'}$*. For any* $B_r \subset B_{r'}$*, the time-derivative of* $\hat{V}$ *can be bounded by:*

$$\dot{\hat{V}} \leq -c_3|x|^2 + c_4(\delta + \gamma r^z)|x|^2 \tag{3.45}$$

for all $x \in B_r$ *where* $r < r'$*. If* $\delta > 0$ *and* $r > 0$ *are chosen to satisfy* $c_3/c_4 > (\delta + \gamma r^z)$*, then there exists a* $\hat{c}_3 > 0$ *such that:*

$$\dot{\hat{V}} = \frac{\partial \hat{V}(x)}{\partial x}\left(\tilde{f}(x, h_{NL}(x), 0)\right) \leq -\hat{c}_3|x|^2 \tag{3.46}$$

for all $|x| \leq r$*. Let* $\hat{\rho} > 0$ *be the forward invariant set such that* $\hat{\rho} \leq \min\{\hat{V}(x) : |x| = r\}$ *and this ends the proof.*

Remark 3 *Even though this conservative result holds locally, when higher order terms are used to better capture the nonlinear behavior in a practical setting, the region* $\Omega_{\hat{\rho}}$ *could be expanded as will be demonstrated in the example.*

3.4.2 Lyapunov-based EMPC formulation with empirical models

The formulation of EMPC to be used in this chapter is Lyapunov-based EMPC (LEMPC),[20] a receding horizon EMPC strategy that includes constraints based on the stability region of the stabilizing controller $h_{NL}(x)$ and the Lyapunov function $\hat{V}(x)$ for the closed-loop system of Eq. 3.3 under this controller. LEMPC uses a model of the process dynamics to predict the evolution of the process states with time. In this chapter, We incorporate the nonlinear PNLSS empirical model in LEMPC, and the LEMPC formulation is similar to that derived in chapter 2 using an empirical model. The LEMPC optimization problem incorporating the PNLSS empirical model is

$$\min_{u\in S(\Delta)} \quad \int_{t_k}^{t_{k+N}} L_e(\tilde{x}(\tau),u(\tau))\,d\tau \tag{3.47a}$$

$$\text{s.t.} \quad \dot{\tilde{x}}(t) = A\tilde{x} + P_z(\tilde{x}) + Bu \tag{3.47b}$$

$$\tilde{x}(t_k) = x(t_k) \tag{3.47c}$$

$$u(t) \in U,\ \forall\, t \in [t_k, t_{k+N}) \tag{3.47d}$$

$$\hat{V}(\tilde{x}(t)) \leq \hat{\rho}_e,\ \forall\, t \in [t_k, t_{k+N}), \quad \text{if } x(t_k) \in \Omega_{\hat{\rho}_e} \tag{3.47e}$$

$$\begin{aligned} &\frac{\partial \hat{V}(x(t_k))}{\partial x}\left(Ax(t_k) + P_z(x(t_k)) + Bu\right) \\ &\quad \leq \frac{\partial \hat{V}(x(t_k))}{\partial x}\left(Ax(t_k) + P_z(x(t_k)) + Bh_{NL}(x(t_k))\right), \quad \text{if } x(t_k) \notin \Omega_{\hat{\rho}_e} \end{aligned} \tag{3.47f}$$

where the optimization variable is the process input vector u for every sampling period of length Δ in the prediction horizon (denoted by $u \in S(\Delta)$ where $S(\Delta)$ represents the family of piecewise constant functions with period Δ). To solve for this optimization variable, the LEMPC minimizes a cost function representing the process economics (Eq. 3.47a, where $L_e(x,u)$ is the stage cost) and ensures that the calculated values of u are maintained within the specified limits on the available control action (Eq. 3.47d). The LEMPC receives a measurement of the process states at time t_k (the time at the beginning of a sampling period) and incorporates this through Eq. 3.47c as the initial condition in the PNLSS process model of Eq. 3.47b. The prediction of the process state from Eq. 3.47b is denoted as $\tilde{x}$. The PNLSS process model is used to predict future states of the

process system to ensure that they are constrained by the mode 1 and mode 2 Lyapunov-based constraints of Eqs. 3.47e and 3.47f respectively.

The mode 1 constraint is used to promote dynamic off-steady-state operation of the process to achieve the greatest profit possible, and is active when the states are maintained within a subset of the stability region $\Omega_{\hat{\rho}}$ that is referred to as $\Omega_{\hat{\rho}_e}$ for which states starting within this subset are guaranteed to be maintained in the stability region $\Omega_{\hat{\rho}}$ for all time. Process disturbances or plant-model mismatch may cause the actual process trajectories to enter the region $\Omega_{\hat{\rho}} \setminus \Omega_{\hat{\rho}_e}$, in which case the mode 2 LEMPC constraint becomes active to drive the process states back into $\Omega_{\hat{\rho}_e}$ within a finite number of sampling periods. LEMPC is implemented as a receding horizon strategy with sampling period Δ and prediction horizon N.

3.4.3 Stability analysis

In this section, we examine stability of the closed-loop process of Eq. 3.1 under LEMPC incorporating the empirical model derived from PNLSS with numerical stability constraints. We begin by noting several bounds on the process models of Eqs. 3.1 and 3.3 and of the derivatives of Lyapunov functions along the closed-loop trajectories of these systems. Because it is assumed that $\tilde{f}(\cdot,\cdot,\cdot)$ in Eq. 3.1 is locally Lipschitz and that the Lyapunov function $\hat{V}$ is continuously differentiable, the following inequalities hold for all $x_1, x_2 \in \Omega_{\hat{\rho}}$, $u \in U$ and $|w| \leq \theta$:

$$\left|\tilde{f}(x_1,u,w) - \tilde{f}(x_2,u,0)\right| \leq L_x |x_1 - x_2| + L_w |w|, \tag{3.48}$$

$$\left|\frac{\partial \hat{V}(x_1)}{\partial x}\tilde{f}(x_1,u,w) - \frac{\partial \hat{V}(x_2)}{\partial x}\tilde{f}(x_2,u,0)\right| \leq L'_x |x_1 - x_2| + L'_w |w| \tag{3.49}$$

where L_x, L_w, L'_x, and L'_w are positive constants. The Lipschitz property of $\tilde{f}$, combined with the bounds on u and w, establishes the existence of a constant $M > 0$ such that:

$$\left|\tilde{f}(x,u,w)\right| \leq M \tag{3.50}$$

for all $x \in \Omega_{\hat{\rho}}$, $u \in U$ and $|w| \leq \theta$ since $\Omega_{\hat{\rho}}$ and U are compact sets.

The polynomial model of Eq. 3.3 and its Lyapunov function are similarly bounded by $M_{NL} > 0$ and $L_{NL} > 0$:

$$|Ax_1 + P_z(x_1) + Bu| \leq M_{NL} \tag{3.51}$$

$$\left| \frac{\partial \hat{V}(x_1)}{\partial x} (Ax_1 + P_z(x_1) + Bu) - \frac{\partial \hat{V}(x_2)}{\partial x} (Ax_2 + P_z(x_2) + Bu) \right| \leq L_{NL} |x_1 - x_2| \tag{3.52}$$

for all $x_1, x_2 \in \Omega_{\hat{\rho}}$ and $u \in U$.

The following proposition and its proof closely follow that for Proposition 2 from chapter 2. This proposition bounds the difference between the actual process state trajectory of Eq. 3.1 in the presence of disturbances $w(t)$ and the process state trajectory predicted from the empirically derived PNLSS model of Eq. 3.3 over a time interval of length T.

Proposition 6 *Consider the solutions, denoted as $x(t)$ and $\hat{x}(t)$, respectively, of the following dynamic equations:*

$$\dot{x}(t) = \tilde{f}(x(t), u(t), w(t)), \quad x(0) = x_0, \tag{3.53}$$

$$\dot{\hat{x}}(t) = A\hat{x}(t) + P_z(\hat{x}(t)) + Bu(t), \quad \hat{x}(0) = x_0, \tag{3.54}$$

where $u(t) \in U$ and $|w(t)| \leq \theta$ for all $t \in [0, T]$ and initial condition $x(0) = \hat{x}(0) = x_0 \in \Omega_{\hat{\rho}}$. If $x(t),\ \hat{x}(t) \in \Omega_{\hat{\rho}}$ for all $t \in [0, T]$, then the difference between $x(T)$ and $\hat{x}(T)$ is bounded by the function $f_w(\cdot)$:

$$|x(T) - \hat{x}(T)| \leq f_w(T) := \frac{L_w \theta + M_{err}}{L_x} \left(e^{L_x T} - 1 \right) \tag{3.55}$$

where M_{err} bounds the difference between right-hand sides of Eqs. 3.53-3.54 (with $w(t) \equiv 0$):

$$\left| \tilde{f}(\hat{x}, u, 0) - (A\hat{x} + P_z(\hat{x}) + Bu) \right| \leq M_{err} \tag{3.56}$$

for all $\hat{x} \in \Omega_{\hat{\rho}}$ and $u \in U$.

Proof 3.2 *We will first define $e(t)$ to be the difference $x(t)-\hat{x}(t)$, such that its time derivative is $\dot{e}(t)=\dot{x}(t)-\dot{\hat{x}}(t)$. Per Eqs. 3.53 and 3.54, the initial condition for this differential equation is $e(0)=0$. Substituting the definitions of $\dot{x}(t)$ and $\dot{\hat{x}}(t)$ from Eqs. 3.53 and 3.54 and adding and subtracting $\tilde{f}(\hat{x}(t),u(t),0)$ in the definition of $\dot{e}(t)$ produces the following inequality:*

$$\begin{aligned}|\dot{e}(t)| &= \left|\tilde{f}(x(t),u(t),w(t))-(A\hat{x}(t)+P_z(\hat{x}(t))+Bu(t))\right| \\ &\leq |\tilde{f}(x(t),u(t),w(t))-\tilde{f}(\hat{x}(t),u(t),0)| \\ &\quad +|\tilde{f}(\hat{x}(t),u(t),0)-(A\hat{x}(t)+P_z(\hat{x}(t))+Bu(t))| \end{aligned} \tag{3.57}$$

for all x, $\hat{x}$ contained in $\Omega_{\hat{\rho}}$. From the bounds in Eqs. 3.50 and 3.51 above and the fact that x and u are in compact sets, a constant $M_{err}>0$ exists such that:

$$\left|\tilde{f}(\hat{x},u,0)-(A\hat{x}+P_z(\hat{x})+Bu)\right| \leq M_{err} \tag{3.58}$$

for all $\hat{x}\in\Omega_{\hat{\rho}}$ and all $u\in U$. Using this bound in Eq. 3.57 along with the bound from Eq. 3.48 and $|w(t)|\leq\theta$, the following is derived for all $t\in[0,T]$:

$$\begin{aligned}|\dot{e}(t)| &\leq L_x|x(t)-\hat{x}(t)|+L_w|w(t)|+M_{err} \\ &\leq L_x|e(t)|+L_w\theta+M_{err}\end{aligned} \tag{3.59}$$

Integration is then performed on the differential equation in Eq. 3.59 between $t=0$ and $t=T$:

$$\int_0^T \frac{|\dot{e}(t)|}{L_x|e(t)|+L_w\theta+M_{err}}\,dt \leq T \tag{3.60}$$

which gives the following equation for $|e(T)|$, with $x(T)$, $\hat{x}(T)\in\Omega_{\hat{\rho}}$:

$$|e(T)|=|x(T)-\hat{x}(T)| \leq \frac{L_w\theta+M_{err}}{L_x}\left(e^{L_xT}-1\right) \tag{3.61}$$

This completes the proof of Proposition 6.

The following proposition is proved in[31] and states that the difference between the values of a Lyapunov function evaluated at any two different points in $\Omega_{\hat{\rho}}$ is bounded.

Proposition 7 (c.f.[31]) *Consider the continuously differentiable Lyapunov function $\hat{V}(x)$ that satisfies the inequalities of Eq. 3.37. There exists a quadratic function $f_V(\cdot)$ such that*

$$\hat{V}(x_1) \leq \hat{V}(x_2) + f_V(|x_1 - x_2|) \tag{3.62}$$

for all x_1, $x_2 \in \Omega_{\hat{\rho}}$ where

$$f_V(s) := \frac{c_4\sqrt{\hat{\rho}}}{\sqrt{c_1}}s + \beta s^2 \tag{3.63}$$

and β is a positive constant.

The above propositions will now be used to show that firstly, there exists a feedback control law h_{NL} that meets the requirements of Eq. 3.37 that can stabilize the closed-loop system of Eq. 3.1, and secondly, that this has implications for the stability properties of an LEMPC based on the stability region derived from the use of this feedback control law. To develop the type of stability that the feedback control law can provide, we first note that when h_{NL} meeting Eq. 3.37 is applied continuously to the system of Eq. 3.3, it exponentially stabilizes the origin of the closed-loop system. However, for the LEMPC control problem at hand, the control laws will be implemented in sample-and-hold. When using a sufficiently small sampling period $\Delta > 0$, the control law h_{NL} implemented in sample-and-hold can practically stabilize the origin, meaning that it can drive the state trajectories to a small neighborhood of the origin $\Omega_{\hat{\rho}_{\min}}$ and maintain them there.[31] It has previously been stated that the Lyapunov-based constraints in LEMPC are able to ensure that the closed-loop state trajectories using mode 1 operation are maintained in the stability region $\Omega_{\hat{\rho}}$ and that the origin is practically stable in mode 2; this, however, implies that feasible solutions to the LEMPC exist, which is only the case for mode 1 operation when $\hat{\rho}_e \geq \hat{\rho}_{\min}$. The following proposition states that when $\hat{\rho}_e$ is restricted in this manner, the state trajectories $\hat{x}(t)$ for the closed-

loop system of Eq. 3.54 under the control law h_{NL} in sample-and-hold are always bounded in $\Omega_{\hat{\rho}_e}$, which is necessary for feasibility of mode 1 operation of LEMPC, and are ultimately bounded in $\Omega_{\hat{\rho}_{\min}}$. It closely follows Proposition 4 in chapter 2.

Proposition 8 *Consider the sampled-data system resulting from the system of Eq. 3.54 under the controller $h_{NL}(\hat{x})$ that satisfies the inequalities of Eq. 3.37 implemented in a sample-and-hold fashion. Let $\Delta > 0$, $\hat{\varepsilon}_s > 0$, $\hat{\rho}_s > 0$, and $\hat{\rho}_e \geq \hat{\rho}_{\min} > 0$ satisfy:*

$$-\frac{c_3}{c_2}\hat{\rho}_s + L_{NL}M_{NL}\Delta \leq -\hat{\varepsilon}_s/\Delta \tag{3.64}$$

and

$$\hat{\rho}_{\min} := \max\left\{\hat{V}(\hat{x}(t+\Delta)) \ : \ \hat{V}(\hat{x}(t)) \leq \hat{\rho}_s\right\} . \tag{3.65}$$

If $\hat{x}(0) \in \Omega_{\hat{\rho}_e}$, then $\hat{x}(t) \in \Omega_{\hat{\rho}_e}$ for all $t \geq 0$ and

$$\hat{V}(\hat{x}(t_{k+1})) - \hat{V}(\hat{x}(t_k)) \leq -\hat{\varepsilon}_s \tag{3.66}$$

for $\hat{x}(t_k) \in \Omega_{\hat{\rho}_e} \setminus \Omega_{\hat{\rho}_s}$ and $\hat{x}(t)$ is ultimately bounded in $\Omega_{\hat{\rho}_{\min}}$.

Proof 3.3 *The proposition considers the state trajectories of the system of Eq. 3.54, starting from $\hat{x}(0) \in \Omega_{\hat{\rho}}$, when the control law $h_{NL}(\hat{x})$ is implemented in sample-and-hold. This sample-and-hold implementation will be denoted as $h_{NL}(\hat{x}(t_k))$, with $t \in [t_k, t_{k+1})$, $k = 0,\ 1,\ \ldots$ with $t_0 = 0$, to represent the value of h_{NL} held for a time period of length Δ based on a measurement of the state $\hat{x}$ at time t_k. Using this notation and the inequality of Eq. 3.37b that holds at each sampling time, the following holds:*

$$\frac{\partial \hat{V}(\hat{x}(t_k))}{\partial \hat{x}}\left(A\hat{x}(t_k) + P_z(\hat{x}(t_k)) + Bh_{NL}(\hat{x}(t_k))\right) \leq -c_3|\hat{x}(t_k)|^2 \tag{3.67}$$

The inequality of Eq. 3.67 can be used with the inequality of Eq. 3.52 to bound the time-derivative of the Lypaunov function for all $\tau \in [t_k, t_{k+1})$ as follows (the notation for the input is abbreviated

as $\hat{u}(t_k) := h_{NL}(\hat{x}(t_k))$*):*

$$\begin{aligned}\frac{\partial \hat{V}(\hat{x}(\tau))}{\partial \hat{x}}\left(A\hat{x}(\tau)+P_z(\hat{x}(\tau))+B\hat{u}(t_k)\right) &= \frac{\partial \hat{V}(\hat{x}(\tau))}{\partial \hat{x}}\left(A\hat{x}(\tau)+P_z(\hat{x}(\tau))+B\hat{u}(t_k)\right)\\ &\quad - \frac{\partial \hat{V}(\hat{x}(t_k))}{\partial \hat{x}}\left(A\hat{x}(t_k)+P_z(\hat{x}(t_k))+B\hat{u}(t_k)\right)\\ &\quad + \frac{\partial \hat{V}(\hat{x}(t_k))}{\partial \hat{x}}\left(A\hat{x}(t_k)+P_z(\hat{x}(t_k))+B\hat{u}(t_k)\right)\\ &\leq L_{NL}\left|\hat{x}(\tau)-\hat{x}(t_k)\right| - c_3|\hat{x}(t_k)|^2 \end{aligned} \tag{3.68}$$

Because the solutions of Eq. 3.54 are continuous in the compact set $\Omega_{\hat{\rho}_e}$*, a discretization of the time-derivative of* $\hat{x}$ *defined according to Eq. 3.54 for a sufficiently small time* Δ*, combined with the inequality in Eq. 3.51, yields the following bound for* $\tau \in [t_k, t_{k+1})$*:*

$$\left|\hat{x}(\tau)-\hat{x}(t_k)\right| \leq M_{NL}\Delta \tag{3.69}$$

Substituting Eq. 3.69 into Eq. 3.68 gives for $\tau \in [t_k, t_{k+1})$*:*

$$\frac{\partial \hat{V}(\hat{x}(\tau))}{\partial \hat{x}}\left(A\hat{x}(\tau)+P_z(\hat{x}(\tau))+B\hat{u}(t_k)\right) \leq -c_3|\hat{x}(t_k)|^2 + L_{NL}M_{NL}\Delta \tag{3.70}$$

We now use these results to show that $\hat{x}(t) \in \Omega_{\hat{\rho}_e}$ *for all* $t \geq 0$ *when* $\hat{x}(0) \in \Omega_{\hat{\rho}_e}$*,* $\hat{\rho}_s > 0$*,* $\hat{\rho}_{\min} > 0$*,* $\hat{\varepsilon}_s > 0$*, and* $\hat{\rho}_e \geq \hat{\rho}_{\min}$ *satisfy Eqs. 3.64-3.65 with a sufficiently small* $\Delta > 0$*. We first examine the case when* $\hat{x}(t_k) \in \Omega_{\hat{\rho}_e} \setminus \Omega_{\hat{\rho}_s}$ *(and* $\hat{x}(\tau) \in \Omega_{\hat{\rho}_e}$ *for* $\tau \in [t_k, t_{k+1})$*). In this case, Eq. 3.70, Eq. 3.37b, and Eq. 3.65 are combined to give:*

$$\frac{\partial \hat{V}(\hat{x}(\tau))}{\partial \hat{x}}\left(A\hat{x}(\tau)+P_z(\hat{x}(\tau))+B\hat{u}(t_k)\right) \leq -\frac{c_3}{c_2}\hat{\rho}_s + L_{NL}M_{NL}\Delta \tag{3.71}$$

for $\tau \in [t_k, t_{k+1})$*. Since we assume that Eq. 3.64 is met:*

$$\frac{\partial \hat{V}(\hat{x}(\tau))}{\partial \hat{x}}\left(A\hat{x}(\tau)+P_z(\hat{x}(\tau))+B\hat{u}(t_k)\right) \leq -\hat{\varepsilon}_s/\Delta \tag{3.72}$$

for $\tau \in [t_k, t_{k+1})$. Integration of this equation proves that the bound of Eq. 3.66 holds and further shows that the Lyapunov function is decreasing for $\tau \in [t_k, t_{k+1})$, which proves that $\hat{x}(t)$ is maintained in $\Omega_{\hat{\rho}_e}$ during this time period as guaranteed by the proposition:

$$\begin{aligned} \hat{V}(\hat{x}(t_{k+1})) &\leq \hat{V}(\hat{x}(t_k)) - \hat{\varepsilon}_s, \\ \hat{V}(\hat{x}(\tau)) &\leq \hat{V}(\hat{x}(t_k)), \quad \forall\, \tau \in [t_k, t_{k+1}) \end{aligned} \tag{3.73}$$

We now prove ultimate boundedness of the state trajectories in $\Omega_{\hat{\rho}_{\min}}$ by considering $\hat{x}(t_k) \in \Omega_{\hat{\rho}_s}$. Because the proof for $\hat{x}(t_k) \in \Omega_{\hat{\rho}_e} \setminus \Omega_{\hat{\rho}_s}$ shows that the Lyapunov function continues to decrease with time in that set, the trajectories eventually enter $\Omega_{\hat{\rho}_s}$. From the definition of $\Omega_{\hat{\rho}_{\min}}$ in Eq. 3.65, once the state trajectories enter $\Omega_{\hat{\rho}_{\min}}$, they are ultimately bounded in this set. This completes the proof of Proposition 8 and shows that for appropriately chosen parameters $\hat{\rho}_s$, $\hat{\varepsilon}_s$, $\hat{\rho}_e$, and Δ, an explicit stabilizing controller exists for the system of Eq. 3.54 that, when implemented in sample-and-hold, can render the set $\Omega_{\hat{\rho}_e}$ forward invariant for any initial state in $\Omega_{\hat{\rho}_e}$.

Propositions 6-8 are now combined to give a theorem that shows that the LEMPC applied to the system of Eq. 3.1 using the empirical PNLSS model of Eq. 3.3 requests control actions that maintain boundedness of the closed-loop state within $\Omega_{\hat{\rho}}$ under appropriate conditions. This theorem and its proof follow that of Theorem 1 in chapter 2.

Theorem 2 *Consider the closed-loop system of Eq. 3.1 under the LEMPC of Eq. 3.47 based on the controller $h_{NL}(x)$ that satisfies the inequalities of Eq. 3.37. Let $\varepsilon_w > 0$, $\Delta > 0$, $N \geq 1$, and $\hat{\rho} > \hat{\rho}_e > 0$ satisfy*

$$-\frac{\hat{c}_3}{c_2}\hat{\rho}_e + L_x' M \Delta + L_w' \theta \leq -\varepsilon_w/\Delta\,, \tag{3.74}$$

$$\hat{\rho}_e \leq \hat{\rho} - f_V(f_w(\Delta))\,. \tag{3.75}$$

If $x(0) \in \Omega_{\hat{\rho}}$ and the conditions of Proposition 5 and Proposition 8 are satisfied, then the state trajectory $x(t)$ of the closed-loop system is always bounded in $\Omega_{\hat{\rho}}$ for $t \geq 0$.

Proof 3.4 *In Part 1 of this proof, we show that the LEMPC optimization problem is recursively*

feasible for any initial state within $\Omega_{\hat{\rho}}$, and in Part 2, we prove boundedness of the states of the closed-loop system in $\Omega_{\hat{\rho}}$.

Part 1: For all $x(t_k) \in \Omega_{\hat{\rho}_e}$ when all conditions in Proposition 8 are met, the optimization problem is feasible since the control action $h_{NL}(x(t_k))$ that maintains the process states within $\Omega_{\hat{\rho}_e}$ meets the input constraints and Lyapunov-based constraints of Eqs. 3.47d-3.47e. For all $x(t_k) \in \Omega_{\hat{\rho}} \setminus \Omega_{\hat{\rho}_e}$, the controller $h_{NL}(x(t_k))$ is feasible by design since it is stabilizing in sample-and-hold with a sufficiently small sampling period and meets the constraints of Eqs. 3.47d and 3.47f. This shows that for all $x(0) \in \Omega_{\hat{\rho}}$, the LEMPC optimization problem of Eq. 3.47 will be recursively feasible.

Part 2: If $x(t_k) \in \Omega_{\hat{\rho}} \setminus \Omega_{\hat{\rho}_e}$, the LEMPC requires that the mode 2 constraint of Eq. 3.47f be satisfied, which leads to the following requirement for any solution requested by the LEMPC at time t_k:

$$\frac{\partial \hat{V}(x(t_k))}{\partial x}\left(Ax(t_k)+P_z(x(t_k))+Bu(t_k)\right) \leq \frac{\partial \hat{V}(x(t_k))}{\partial x}\left(Ax(t_k)+P_z(x(t_k))+Bh_{NL}(x(t_k))\right) \quad (3.76)$$

Since Theorem 2 requires that Proposition 5 be met, Eq. 3.46 holds and:

$$\frac{\partial \hat{V}(x(t_k))}{\partial x}\tilde{f}(x(t_k),h_{NL}(x(t_k)),0) \leq -\hat{c}_3|x(t_k)|^2 \, . \quad (3.77)$$

Eq. 3.77 can be used to bound the time-derivative of the Lyapunov function of the closed-loop system using the empirical model for all $\tau \in [t_k, t_{k+1})$:

$$\begin{aligned}
\dot{\hat{V}}(x(\tau)) &= \frac{\partial \hat{V}(x(\tau))}{\partial x}\tilde{f}(x(\tau),h_{NL}(x(t_k)),w(\tau)) - \frac{\partial \hat{V}(x(t_k))}{\partial x}\tilde{f}(x(t_k),h_{NL}(x(t_k)),0) \\
&\quad + \frac{\partial \hat{V}(x(t_k))}{\partial x}\tilde{f}(x(t_k),h_{NL}(x(t_k)),0) \\
&\overset{(3.49),(3.77)}{\leq} L_x'|x(\tau)-x(t_k)| + L_w'|w(\tau)| - \hat{c}_3|x(t_k)|^2 \\
&\leq -\frac{\hat{c}_3}{c_2}\hat{\rho}_e + L_x'|x(\tau)-x(t_k)| + L_w'|w(\tau)| \quad (3.78)
\end{aligned}$$

where the final inequality results from the definition of the value of $\hat{V}(x)$ *when* $x(t_k) \in \Omega_{\hat{\rho}} \setminus \Omega_{\hat{\rho}_e}$. *Using Eq. 3.50 and a derivation similar to that used to arrive at Eq. 3.69:*

$$|x(\tau) - x(t_k)| \leq M\Delta \tag{3.79}$$

for all $\tau \in [t_k, t_{k+1})$. *Substituting this inequality and the bound* θ *on w into Eq. 3.78:*

$$\frac{\partial \hat{V}(x(\tau))}{\partial x} \tilde{f}(x(\tau), u(t_k), 0) \leq -\frac{\hat{c}_3}{c_2}\hat{\rho}_e + L_x' M\Delta + L_w'\theta \tag{3.80}$$

for all $\tau \in [t_k, t_{k+1})$. *Substituting Eq. 3.74 and integrating as was performed to arrive at Eq. 3.73:*

$$\begin{aligned} \hat{V}(x(t_{k+1})) &\leq \hat{V}(x(t_k)) - \varepsilon_w, \\ \hat{V}(x(\tau)) &\leq \hat{V}(x(t_k)), \quad \forall\ \tau \in [t_k, t_{k+1}) \end{aligned} \tag{3.81}$$

This result shows that for all $x(t_k) \in \Omega_{\hat{\rho}} \setminus \Omega_{\hat{\rho}_e}$, *the Lyapunov function of the closed-loop system decreases throughout a sampling period, which means that the state will be driven back into* $\Omega_{\hat{\rho}_e}$ *in finite time.*

When $x(t_k) \in \Omega_{\hat{\rho}_e}$, *the predicted trajectory* $\tilde{x}(t_{k+1}) \in \Omega_{\hat{\rho}_e}$ *by Eq. 3.47e. By Propositions 6 and 7, the actual state* $x(t_{k+1})$ *is within a bound of the predicted state and the following hold:*

$$\begin{aligned} \hat{V}(x(t_{k+1})) &\leq \hat{V}(\tilde{x}(t_{k+1})) + f_V(|x(t_{k+1}) - \tilde{x}(t_{k+1})|) \\ &\leq \hat{\rho}_e + f_V(f_w(\Delta)) \end{aligned} \tag{3.82}$$

Since Eq. 3.75 holds, $x(t_{k+1}) \in \Omega_{\hat{\rho}}$. *This completes the proof of Theorem 2 by showing that for any* $x(0) \in \Omega_{\hat{\rho}}$, *the closed-loop state trajectories of the actual process are maintained in* $\Omega_{\hat{\rho}}$ *provided that the assumptions of Theorem 2 are met.*

Remark 4 *The stability discussion above shows that disturbances, which include plant-model mismatch, are required to be sufficiently small if closed-loop stability is to be maintained under*

LEMPC. It may in general be difficult to find an empirical model for use in LEMPC for which the plant-model mismatch is low over a large enough operating range that the stability region for use in LEMPC is not restrictively small, since a small stability region would likely not perform much differently than steady-state operation. One method for improving the range over which an empirical model is applicable (and thus possibly increasing the size of $\Omega_{\hat{\rho}}$) is to use higher-order polynomials in the PNLSS identification. This concept is demonstrated in the chemical process example of this chapter.

Remark 5 *For the reasons noted in Remark 3 of chapter 2, a longer prediction horizon may not be able to improve the closed-loop performance of an EMPC formulated with an empirical model, especially if there are significant differences between the actual process behavior and that predicted by the model.*

Remark 6 *For systems that can be approximated over the region of interest with low-order polynomials (e.g., second or third order), a significant benefit in terms of computation time may be observed when using the low-order empirical model as compared to using the full nonlinear first-principles process model. An example is given for which this is the case in the "Application of LEMPC Based on the Well-Conditioned PNLSS Model to the Chemical Process" section of this chapter. If computation time is a significant consideration for an actual process control system, an empirical model may be considered even if a first-principles model can be derived for a given process.*

Remark 7 *One major factor in the stability of the LEMPC of Eq. 3.47 is that it is a feedback control strategy, incorporating a measurement of the actual process state at every sampling period so that it is able to tolerate some level of process disturbances and plant-model mismatch.*

3.5 LEMPC Application of to the Chemical Process Example

In the following sections, we return to the CSTR example described above and compare the closed-loop state and input trajectories for the CSTR under the LEMPC utilizing the first-principles model

of Eq. 3.10 and the LEMPC utilizing the empirical model of Eq. 3.27 developed using PNLSS with numerical stability constraints. In addition, comparisons will be made between the results of using the nonlinear empirical model of Eq. 3.27 in LEMPC with the results of using the linear empirical models described in chapter 2 with LEMPC. The process model used here is the same as that in chapter 2 to facilitate direct comparison.

As noted previously, it is assumed that the dynamics of the CSTR are perfectly modeled by Eq. 3.10, and that the available control actions are constrained by the actuators to the sets in Eq. 3.14. Simulations assuming full state feedback were used to perform system identification using PNLSS per the optimization problem of Eq. 3.26 to develop the nonlinear empirical model of Eq. 3.27, where u and x are written in terms of deviation variables as defined in Eqs. 3.12-3.13. It is desired to maximize the time-average production rate of B while maintaining the states within a compact state-space set around the steady-state $[C_{As}\ T_s] = [1.2\ kmol/m^3\ 438.0\ K]$. Thus, the cost function to be used in the LEMPC of Eq. 3.47a is the negative of the time-average of the total amount of B produced per the Arrhenius rate law throughout a time period (it is the negative since Eq. 3.47 is a minimization problem and our goal is to maximize the production of B):

$$L_e(x,u) = -\frac{1}{(t_{k+N}-t_k)}\int_{t_k}^{t_{k+N}} k_0 e^{-E/RT(\tau)} C_A^2(\tau)\, d\tau\ . \tag{3.83}$$

In addition to the bounds on the control actions caused by the actuators, we assume that the amount of reactant that is available to be fed to the reactor is limited in a given time period $t_p = 1.0\ hr$ by the following constraint:

$$\frac{1}{t_p}\int_0^{t_p} u_1(\tau)\, d\tau = 0.0\ kmol/m^3. \tag{3.84}$$

To maintain process stability when the empirical process model of Eq. 3.27 is used, the Lyapunov stability region constraints for LEMPC must be defined. The stability region is defined using a Lyapunov-based controller $h(x) = [h_1(x)\ h_2(x)]^T$ for the process that meets the requirements of Eq. 3.2. The Lyapunov-based controller is developed here by considering h_1 and h_2

separately. To ensure that the material constraint of Eq. 3.84 is satisfied by the closed-loop process under controller $h(x)$, the value of h_1 is set to 0.0 $kmol/m^3$. The value of h_2 is determined using a Lyapunov-based control law calculated based on the process model. It is assumed here, as would be the case in practice, that the only process model available from which to determine $h_2(x)$ is the empirical model of Eq. 3.27. To develop the control law, terms in the empirical model of Eq. 3.3 are denoted as functions $f : R^n \to R^n$ and $g : R^n \to R^n \times R^m$ as follows:

$$\dot{x} = \underbrace{Ax + P_z(x)}_{=:f(x)} + \underbrace{B}_{=:g(x)} u \,, \tag{3.85}$$

Since there are two inputs for this chemical process example, $g(x) = [g_1 \; g_2]$ where $g_1, g_2 \in R^n$. The control law for h_2 is then determined from the Lyapunov-based control law in:[38]

$$h_2(x) = \begin{cases} -\dfrac{L_f\hat{V} + \sqrt{L_f\hat{V}^2 + L_{g_2}\hat{V}^4}}{L_{g_2}\hat{V}}, & \text{if } L_{g_2}\hat{V} \neq 0 \\ 0, & \text{if } L_{g_2}\hat{V} = 0 \end{cases} \tag{3.86}$$

where $L_f\hat{V}$ and $L_{g_2}\hat{V}$ denote the Lie derivatives of the Lyapunov function $\hat{V}(x)$ with respect to the vector fields $f(x)$ and $g_2(x)$. The Lyapunov function $\hat{V}$ was chosen as $\hat{V}(x) = x^T P x$ with P being the following positive definite matrix:

$$P = \begin{bmatrix} 1030 & 20 \\ 20 & 0.6 \end{bmatrix} \tag{3.87}$$

Extensive simulations were performed using the controller $h(x)$ in closed-loop with the empirical model of Eq. 3.27 to obtain an estimate of the stability region of the actual process. Because an estimate of the process model was used to determine the stability region, a conservative subset of this stability region was chosen for the LEMPC design. This subset was chosen based on simulations that showed it was a region within which the first-principles and empirical models show good agreement of the state trajectories, but was large enough that there was a significant benefit

with LEMPC operation compared with steady-state operation. The stability regions for use in the Lyapunov-based constraints of Eqs. 3.47e-3.47f were taken to be $\Omega_{\hat{\rho}}$ with $\hat{\rho} = 370$ and $\Omega_{\hat{\rho}_e}$ with $\hat{\rho}_e = 350$.

Using the above constraints, two different LEMPCs will be compared, each with the general form of Eq. 3.47 and formulated for use in closed-loop with the process model of Eq. 3.10. Both LEMPCs use the cost function of Eq. 3.83, the input constraints of Eq. 3.14 and Eq. 3.84, $\hat{\rho}_e = 350$, an integration step size of 10^{-4} hr with the Explicit Euler numerical integration method, a sampling period $\Delta = 0.01$ hr, and a prediction horizon $N = 10$. The first of the LEMPCs, which will henceforth be designated as the second-order empirical LEMPC, uses the PNLSS dynamic model of Eq. 3.27. The second of the LEMPCs, which will henceforth be designated as the first-principles LEMPC, uses the nonlinear dynamic model of Eq. 3.10. Because it is assumed that the nominal model of Eq. 3.10 perfectly represents the process dynamics, the mode 2 constraint of Eq. 3.47f was not used in this first-principles LEMPC since there is no measurement noise or plant-model mismatch to drive the state outside of $\Omega_{\hat{\rho}_e}$. For both LEMPCs, the material constraint of Eq. 3.84 is applied in the manner outlined in.[14] The first-principles and second-order empirical LEMPC optimization problems were solved at each sampling time using Ipopt. To account for practical implementation considerations, the optimizations were terminated and the current estimate of the optimization variable u was returned if they were not complete at the end of a sampling period. The actuator dynamics were considered to be sufficiently fast such that the returned solutions were directly implemented on the process of Eq. 3.10 with a zero-order hold of length Δ.

3.5.1 Empirical LEMPC compared with first-principles LEMPC

The process of Eq. 3.10 was simulated in closed-loop with both the second-order empirical and the first-principles LEMPCs for one operating period of length $t_p = 1$ hr. The resulting state and input trajectories are shown in Fig. 3.6. These trajectories exhibit behavior similar to that reported in chapter 2. The state trajectories are initiated from the steady-state $[C_A(0)\ T(0)] = [1.2\ kmol/m^3\ 438.0\ K]$, and they subsequently level off at a new steady-state with a temperature

greater than that at the initial steady-state to maximize the reaction rate of B within the stability region. At the end of the operating period, the concentration of A in the reactor decreases as the inlet concentration of A is reduced to meet the material constraint of Eq. 3.84. The decrease in C_A allows the reactor temperature to increase to improve the production rate of B without leaving the stability region. Fig. 3.6 shows that the state and input trajectories using the second-order empirical LEMPC closely track those of the first-principles LEMPC until approximately 0.8 hr, at which time the first-principles and second-order empirical LEMPCs request significantly different control actions because they require that the material constraint be met in the short remainder of the simulation interval though different process models are being used in the LEMPCs to ensure that the predicted trajectories meet this constraint. The differences in the requested control actions cause the process states under the second-order empirical LEMPC to leave $\Omega_{\hat{\rho}_e}$ six times at the end of the operating period, starting at approximately 0.85 hr, while the first-principles LEMPC never leaves $\Omega_{\hat{\rho}_e}$. This means that in addition to the differences in the process state trajectories that result from using different model equations to satisfy constraints, there are added differences that result because the second-order empirical LEMPC switches to mode 2 operation though the first-principles LEMPC remains operating in mode 1. Fig. 3.7 illustrates the state-space behavior of the first-principles and second-order empirical LEMPCs, including their initial close agreement, their evolution along the edge of the stability region between approximately $t = 0.1$ and 0.8 hr, and their subsequent deviation from one another. Despite the differences at the end of the interval, the overall closeness of the state and input trajectories using both the second-order empirical and first-principles LEMPCs shows that the second-order empirical LEMPC using the model derived from PNLSS with numerical stability constraints may be suitable for the process in this example and has the potential to produce similarly good results for other processes.

The main reason for considering the first-principles LEMPC over the second-order empirical LEMPC, since both maintain process stability within the stability region, would be related to the economic benefit of using the first-principles LEMPC. Since the first-principles LEMPC represents the ideal case in which the full nonlinear process model is known so that the profit of the actual

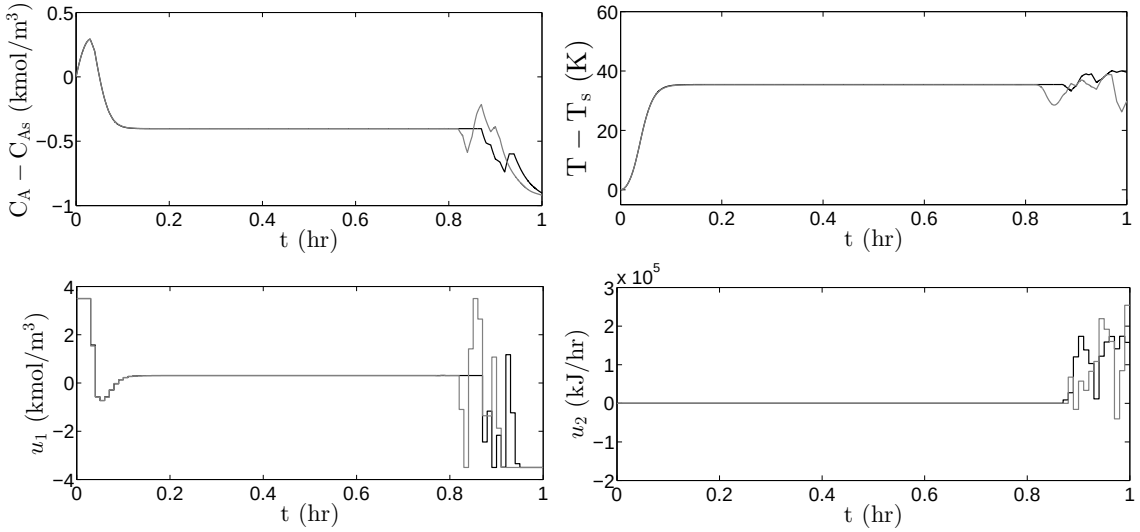

Figure 3.6: Closed-loop state and input trajectories for one operating period $t_p = 1$ *hr* for the CSTR model of Eq. 3.10 under the first-principles LEMPC (black line) and the second-order empirical LEMPC (gray line) starting from $C_A(0) = 1.2$ $kmol/m^3$, $T(0) = 438$ K.

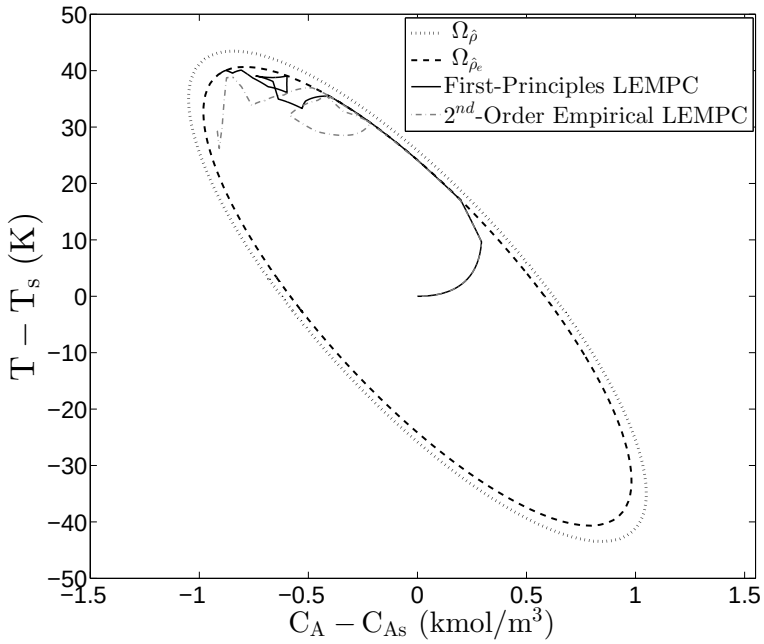

Figure 3.7: Closed-loop state trajectories in state-space for one operating period $t_p = 1$ *hr* for the CSTR model of Eq. 3.10 under the first-principles LEMPC (solid line) and the second-order empirical LEMPC (dashed-dotted line) starting from $C_A(0) = 1.2$ $kmol/m^3$, $T(0) = 438$ K.

process is being maximized, it would be expected to have a higher profit than any variants of that LEMPC. In order to quantify the closed-loop performance of the first-principles LEMPC and

compare it with that of the second-order empirical LEMPC, the following average economic cost index is used (which has units $kmol/m^3$):

$$J_e = \frac{1}{t_f}\int_0^{t_f} k_0 e^{-E/RT(t)} C_A^2(t)\, dt \tag{3.88}$$

where t_f is the length of time for which the closed-loop process is simulated. The value of the economic cost index for the closed-loop CSTR under the second-order empirical LEMPC is 16.1227 and for the first-principles LEMPC it is 16.1626. This shows that for an operating period of 1 *hr*, an improvement of less than 0.3% is achieved when using the first-principles LEMPC instead of the second-order empirical LEMPC.

One major benefit of using the second-order empirical state-space model of Eq. 3.27 compared to the full process model of Eq. 3.10 is the reduction in computation time required by the LEMPC with the simpler empirical model. Fig. 3.8 shows the amount of time in CPU seconds to find a solution to the first-principles and second-order empirical LEMPCs for each sampling period. The time required to solve the optimization problems is greatest for both LEMPCs at the end of the operating period due to the increased number of function evaluations required to ensure that the material constraint is satisfied in the small remaining period of operation while the other input and stability region constraints remain satisfied (the computation time is increased as there are less degrees of freedom when finding a solution). As demonstrated in Fig. 3.8, the first-principles LEMPC optimization problem terminated early two times in the operating period because it reached the end of the 0.01 *hr* (36 *sec*) sampling period before finding a solution (and thus returned a sub-optimal solution). The second-order empirical LEMPC, however, never came close to the 36 *sec* computation time constraint, and the optimal solutions were obtained in less than 0.15 *sec* in most of the sampling periods. The sum of the computation times for all sampling periods in the operating window (total computation time) was 206.317 *sec* for the first-principles LEMPC, but only 30.108 *sec* for the second-order empirical LEMPC. The first-principles LEMPC is much more computationally expensive than the second-order empirical LEMPC, with a total computation time that is 580%

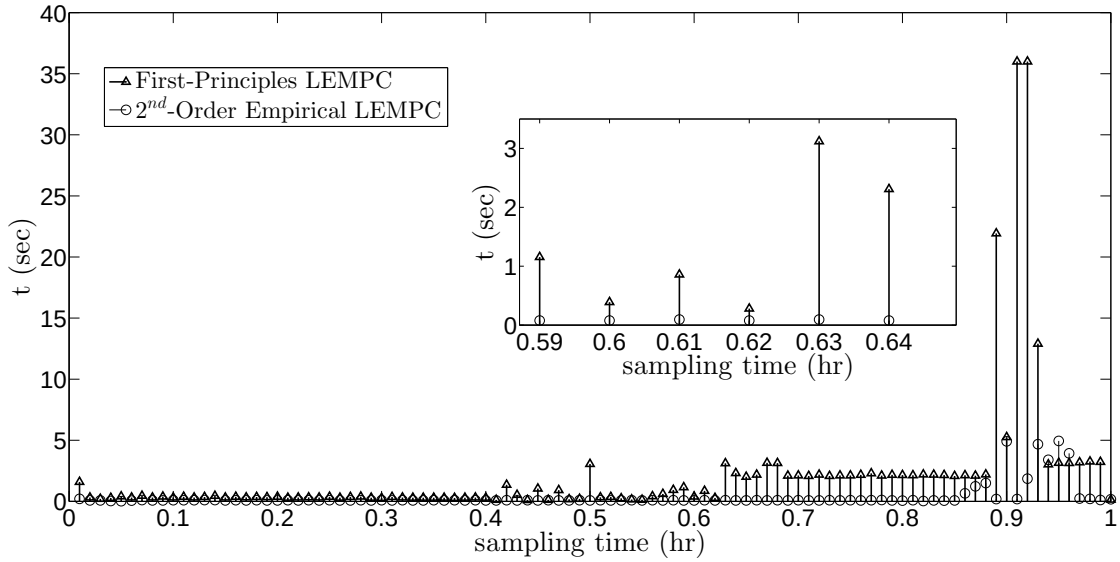

Figure 3.8: Computation time in seconds used in each sampling period to solve the optimization problems of the first-principles LEMPC (triangle markers) and the second-order empirical LEMPC (circle markers) during one operating period.

higher than for the second-order empirical LEMPC.

To investigate the long-term performance and computation time differences between the first-principles and second-order empirical LEMPCs, a ten-hour simulation was conducted for the CSTR of Eq. 3.10, and the results are shown in Figs. 3.9-3.12. The average economic cost per Eq. 3.88 was 15.91 for the second-order empirical LEMPC and 15.96 for the first-principles LEMPC; less than 0.4% performance improvement is observed when using the first-principles LEMPC. Both the first-principles and the second-order empirical LEMPCs significantly out-perform steady-state operation; the average economic cost at the end of the ten hours is 13.88 for steady-state operation at $[C_{As}\ T_s\ C_{A0s}\ Q_s] = [1.2\ kmol/m^3\ 438.0\ K\ 4.0\ kmol/m^3\ 0.0\ kJ/hr]$. Thus, the average economic cost for the second-order empirical LEMPC is 14.6% greater than that for steady-state operation.

The computation times for the first-principles and second-order empirical LEMPCs were also compared for the ten-hour simulation. The average total computation time for each 1 *hr* operating period of the ten-hour simulation is 197.682 *sec* for the first-principles LEMPC and 26.229 *sec* for the second-order empirical LEMPC. The first-principles LEMPC average computation time is

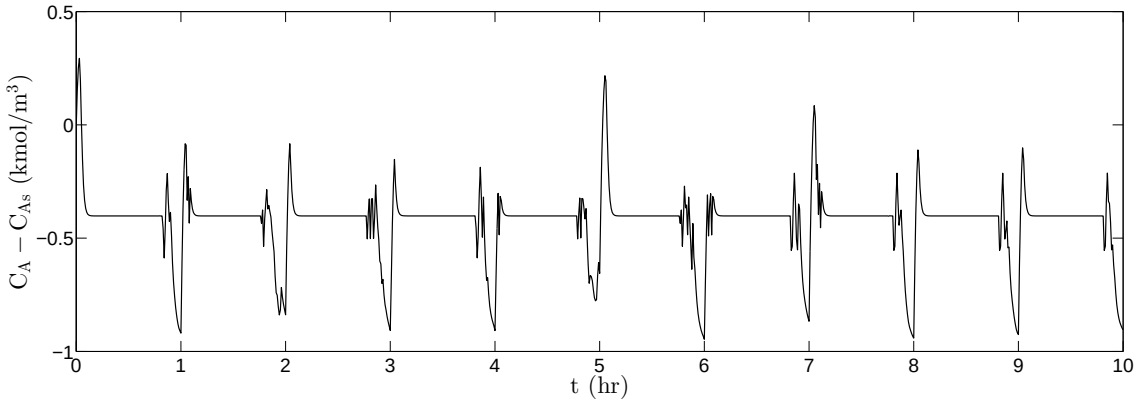

Figure 3.9: Trajectory of the CSTR concentration over ten hours for the CSTR model of Eq. 3.10 under the second-order empirical LEMPC.

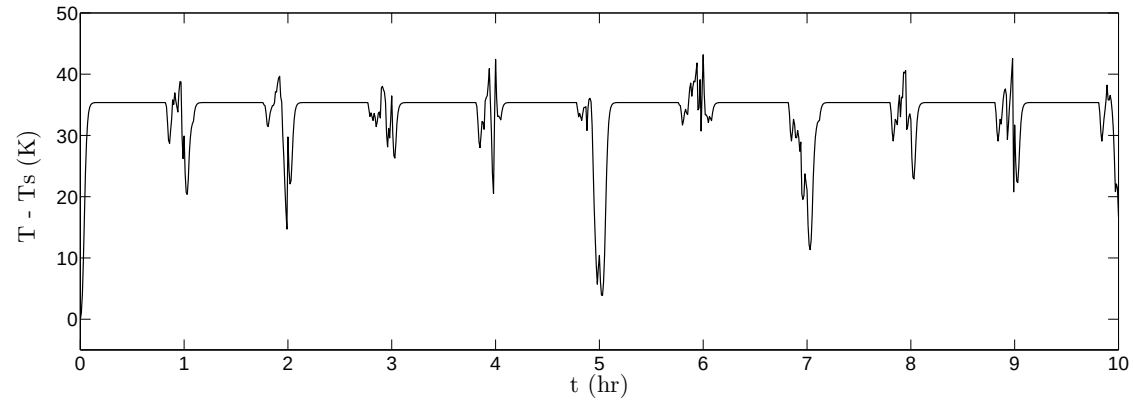

Figure 3.10: Trajectory of the CSTR temperature over ten hours for the CSTR model of Eq. 3.10 under the second-order empirical LEMPC.

650% higher than that of the second-order empirical LEMPC.

The results using the second-order empirical LEMPC above can be compared to the results presented for the linear empirical model in the chemical process example in chapter 2. The linear empirical model of Eqs. 57-58 in chapter 2 is henceforth referred to as the linear model. Because the second-order empirical model of Eq. 3.27 is a better approximation of the actual system than a linear model, the LEMPC using the second-order empirical model calculates inputs that do not cause the closed-loop state trajectories to leave the set $\Omega_{\hat{\rho}_e}$ as often as do the trajectories from using the linear model. A comparison of Fig. 4 of chapter 2 for the linear model with Fig. 3.6 for the second-order empirical model demonstrates this. From these figures, it is seen that the u_1 and hence C_A trajectories for the linear model exhibit extensive chattering caused by frequent switching

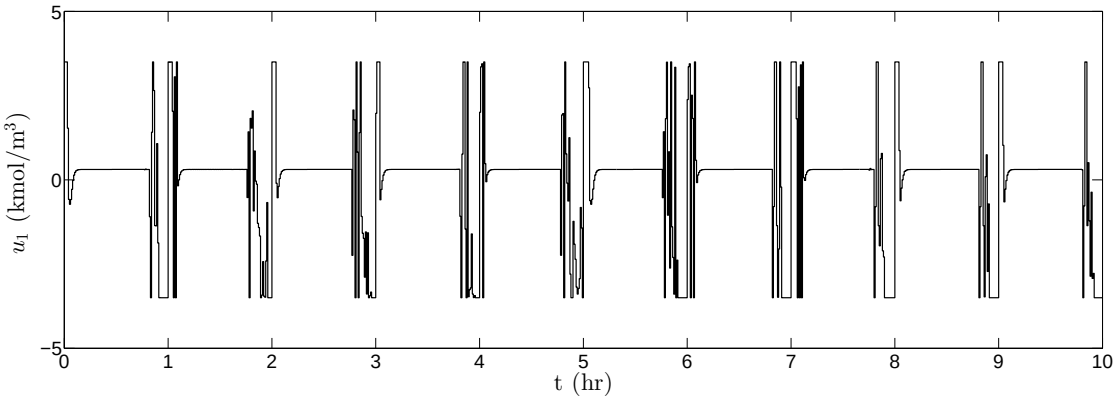

Figure 3.11: Trajectory of the feed concentration input to the CSTR over ten hours for the CSTR model of Eq. 3.10 under the second-order empirical LEMPC.

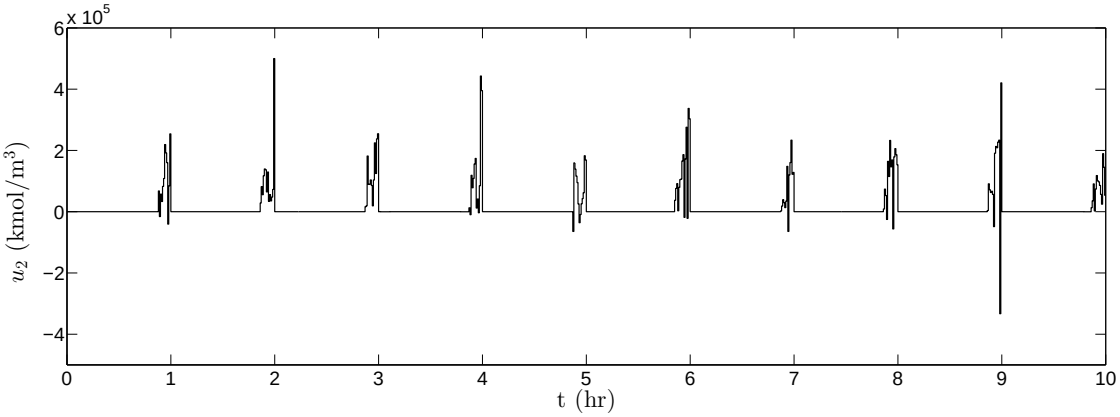

Figure 3.12: Trajectory of the heat input to the CSTR over ten hours for the CSTR model of Eq. 3.10 under the second-order empirical LEMPC.

of the LEMPC between mode 1 and 2 operation; this chattering is not exhibited in the trajectories resulting from the use of the second-order empirical model, and as previously noted, the second-order empirical model only switched between mode 1 and mode 2 operation six times. Another result of using the second-order empirical model as a better approximation of the actual process system is that the stability region used with the second-order empirical model is significantly larger than with the linear empirical model (for the linear model, $\hat{\rho}_e$ is 55.0, while for the second-order empirical model, it is 350). The more restricted stability region results in a lesser value of the average economic cost index at the end of an operating period for the linear model than for the second-order empirical model, since the state variables cannot extend as far to maximize the profit during the part of the trajectory when they remain on the edge of the stability region (compare,

for example, the temperature of approximately 20 K in the time period from 0.2 to 0.8 hr in Fig. 4 of chapter 2 with the temperature of approximately 35 K in Fig. 3.6 above). Over one operating period of 1 hr, the average economic cost index of the second-order empirical LEMPC is approximately 2.7% greater using the second-order empirical model than the linear model, and for the ten-hour simulation, the average economic cost index for one operating period is approximately 4.1% greater using the second-order empirical model than the linear model. The computation time for the linear LEMPC is less than that for the second-order empirical LEMPC, however. The total computation time for one operating period is 36.9% greater for the second-order empirical LEMPC than for the linear LEMPC, and the average total computation time for a one-hour operating period from the ten-hour simulation is 11.1% greater for the second-order empirical LEMPC than for the linear LEMPC. Both the second-order empirical and linear LEMPCs have profits close to those of the LEMPCs for the actual process with the corresponding stability region (the profit from the second-order empirical LEMPC is close to that of the first-principles LEMPC, and the profit from the linear LEMPC is close to that of the actual process with which it is compared in chapter 2), and both have computation times much lower than those for the actual process with the corresponding stability region. Thus, the decision to use the linear, second-order empirical, or first-principles LEMPC for this process would depend on the practical significance of a percentage change in profit compared to a percentage change in computation time.

3.5.2 Improved accuracy with higher-order empirical models

In the comparison between the second-order empirical and first-principles LEMPCs above, it was noted that the first-principles LEMPC had a greater profit than the second-order empirical LEMPC, since the first-principles LEMPC was taken to represent the actual process and the second-order empirical LEMPC was only an approximation. It would thus be expected that as the accuracy of the model derived from the PNLSS model identification procedure is increased (additional nonlinear terms are kept in the function $P_z(x)$ of Eq. 3.3) that the resulting model would more accurately represent the actual process dynamics over a larger region and thus allow a greater profit for the

process, closer to that which could be achieved with the LEMPC using the actual first-principles process model of Eq. 3.10. This motivated the identification of an empirical model using higher-order terms for use in LEMPC, which will be described in this section.

To determine the effect of using an empirical model using higher-order nonlinear terms on the performance and computation time of an LEMPC, the PNLSS model identification procedure of Eq. 3.26 was used to find empirical process models with both a third-order polynomial and a fourth-order polynomial for $P_z(x)$ that satisfy the numerical stability constraints. Extensive simulations were used to validate the third and fourth-order models obtained. Because all coefficients of the fourth-order terms from the verified fourth-order model were very small (on the order of 10^{-13}), the third-order model was considered to be sufficient to demonstrate the impact of the higher-order terms on the LEMPC output, so that was the only model for which closed-loop LEMPC simulations were conducted. The validated third-order model is:

$$\begin{aligned}\frac{dx_1}{dt} = &-34x_1 - 0.495x_2 + 48x_1^2 + 1.95x_1x_2 \quad + 18x_2^2 \quad - 92x_1^3 - \quad 0.000707x_1^2x_2 \\ &-0.000016x_1x_2^2 - 0.0005x_2^3 - 4.6u_1 - 0.000008u_2 \end{aligned} \tag{3.89a}$$

$$\begin{aligned}\frac{dx_2}{dt} = &1436x_1 + 18x_2T - 1475x_1^2 - 51x_1x_2 - 0.00509x_2^2 - 0.0005x_1^3 - 0.0233x_1^2x_2 \\ &-0.000526x_1x_2^2 - 0.000024x_2^3 - 11u_1 + 0.00567u_2 \end{aligned} \tag{3.89b}$$

To use this third-order model in the LEMPC of Eq. 3.47, it is necessary to first specify the stability region for the Lyapunov-based constraints of Eqs. 3.47e-3.47f. The Lyapunov function for this third-order process model, in closed-loop with a Lyapunov-based controller $h(x)$ designed similarly to that used for the second-order empirical LEMPC ($h(x) = [0\ h_2(x)]^T$ where $h_2(x)$ is designed using Eq. 3.86 with the third-order model), was again taken to have the form $\hat{V}(x) = x^T Px$, but with P as:

$$P = \begin{bmatrix} 1170 & 24 \\ 24 & 0.56 \end{bmatrix} \tag{3.90}$$

After extensive closed-loop simulations, the stability region for LEMPC including the third-

order empirical model was taken to be $\Omega_{\hat{\rho}}$ with $\hat{\rho} = 485$ and $\Omega_{\hat{\rho}_e}$ with $\hat{\rho}_e = 285$.

As was done for the second-order empirical LEMPC, two different LEMPCs will now be compared. Each has the general form of Eq. 3.47 and is formulated for use in closed-loop with the process of Eq. 3.10; however, the first LEMPC (which will be referred to as the third-order empirical LEMPC) uses the third-order PNLSS model of Eq. 3.89 while the second LEMPC (which will be referred to as the first-principles LEMPC) uses the dynamic model of Eq. 3.10. Both LEMPCs define the stability region using $\hat{\rho}_e = 285$; the first-principles LEMPC does not require mode 2 operation, though the third-order empirical LEMPC requires both mode 1 and mode 2 operation. As in the example presented above, these LEMPCs use the cost function of Eq. 3.83, the input constraints of Eq. 3.14 and Eq. 3.84, an Explicit Euler integration step size of $h_c = 10^{-4}$ *hr*, $\Delta = 0.01$ *hr*, $t_p = 1$ *hr*, and $N = 10$, and also terminate the optimization problem after 0.01 *hr* has elapsed. The closed-loop state and input trajectories for one hour of operation for these two LEMPCs are presented in Fig. 3.13, with the state-space representation of these trajectories in Fig. 3.14.

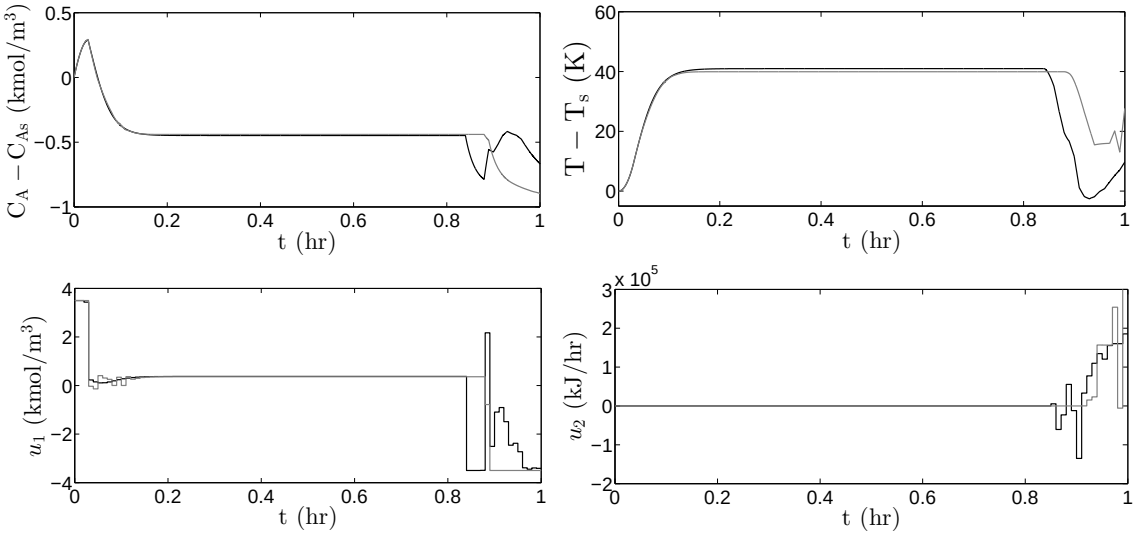

Figure 3.13: Closed-loop state and input trajectories for one operating period $t_p = 1$ *hr* for the CSTR model of Eq. 3.10 under the first-principles LEMPC (black line) and the third-order empirical LEMPC (gray line) starting from $C_A(0) = 1.2$ $kmol/m^3$, $T(0) = 438$ K.

The trajectories in Fig. 3.13 show similar behavior to those in Fig. 3.6, with a notable dif-

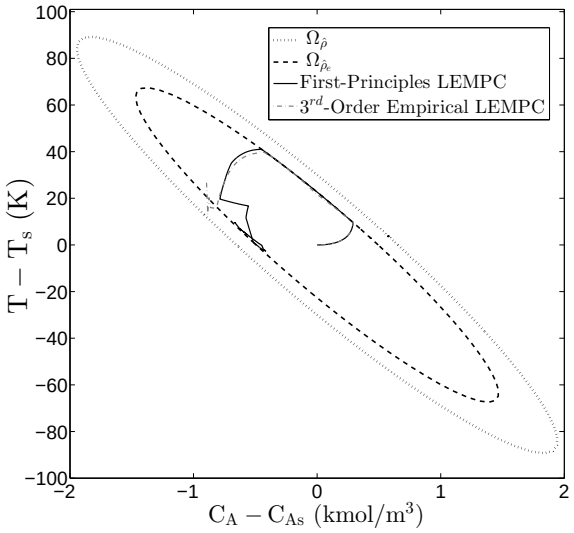

Figure 3.14: Closed-loop state trajectories in state-space for one operating period $t_p = 1$ *hr* for the CSTR model of Eq. 3.10 under the first-principles LEMPC (solid line) and the third-order empirical LEMPC (dashed-dotted line) starting from $C_A(0) = 1.2$ $kmol/m^3$, $T(0) = 438$ K.

ference being that the temperature is able to reach a higher value during the period of time from approximately $t = 0.1$ to 0.8 *hr* in the third-order case of Fig. 3.13 due to the different stability region calculated for the more accurate third-order model. In addition, the stability region difference causes both the third-order empirical and first-principles LEMPCs to produce a drop in reactor temperature at the end of the one hour operating period where the material constraints come in to play, whereas the temperatures increase at the end of this period for the second-order case.

A ten-hour simulation was also conducted for the third-order empirical LEMPC, and the resulting state and input trajectories are shown in Figs. 3.15-3.18. The average value of the economic cost index in one operating period throughout this ten-hour simulation was 16.26, which is 17% greater than steady-state operation (for which the average economic cost index for one operating period is 13.88). This is a greater performance enhancement over steady-state operation than was attained with the second-order empirical LEMPC of the previous section.

To facilitate a comparison between the third-order empirical and first-principles LEMPCs from this section with the second-order empirical and first-principles LEMPCs from the previous section, we will identify the first-principles LEMPC from the previous section as the "First-Principles

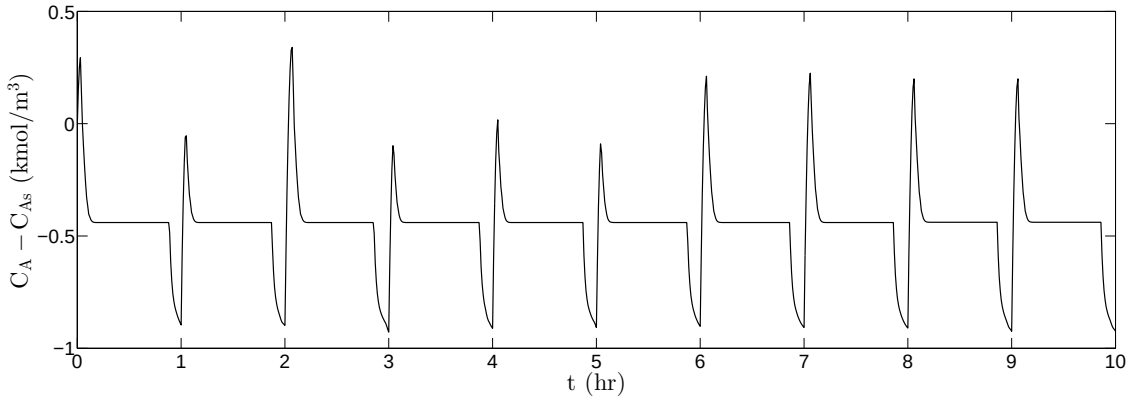

Figure 3.15: Trajectory of the CSTR concentration over ten hours for the CSTR model of Eq. 3.10 under the third-order empirical LEMPC.

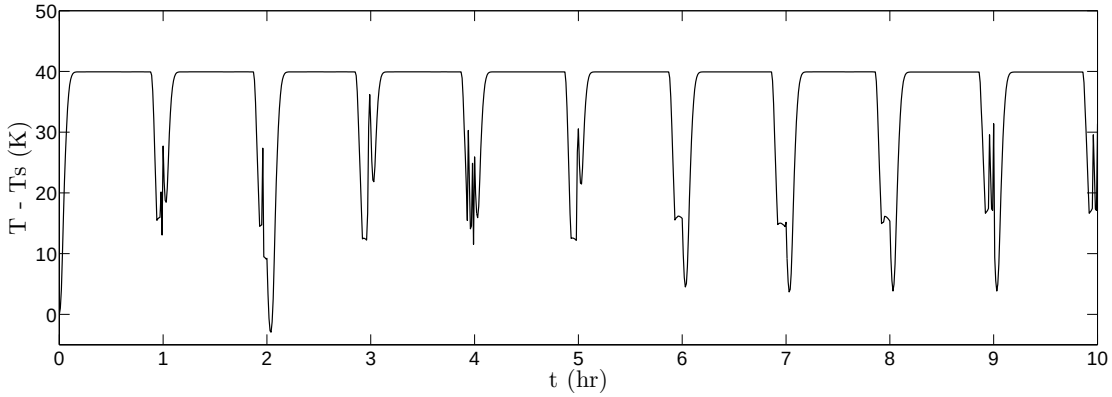

Figure 3.16: Trajectory of the CSTR temperature over ten hours for the CSTR model of Eq. 3.10 under the third-order empirical LEMPC.

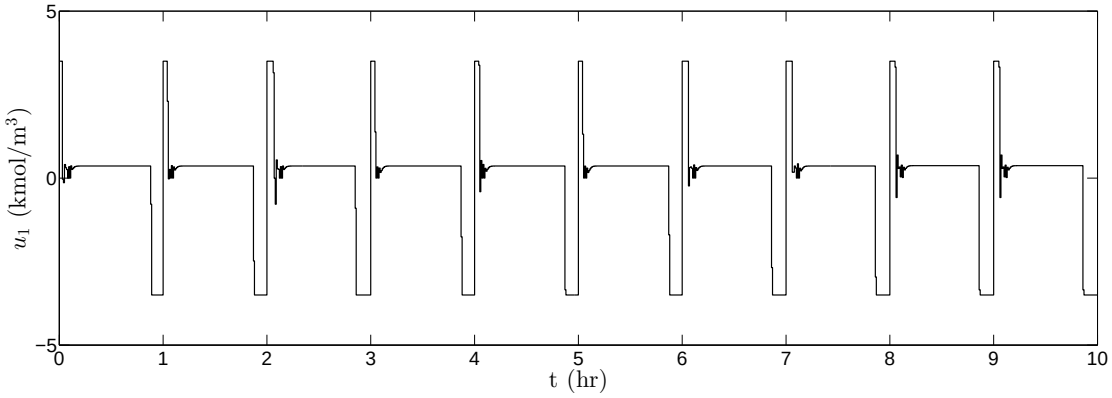

Figure 3.17: Trajectory of the feed concentration input to the CSTR over ten hours for the CSTR model of Eq. 3.10 under the third-order empirical LEMPC.

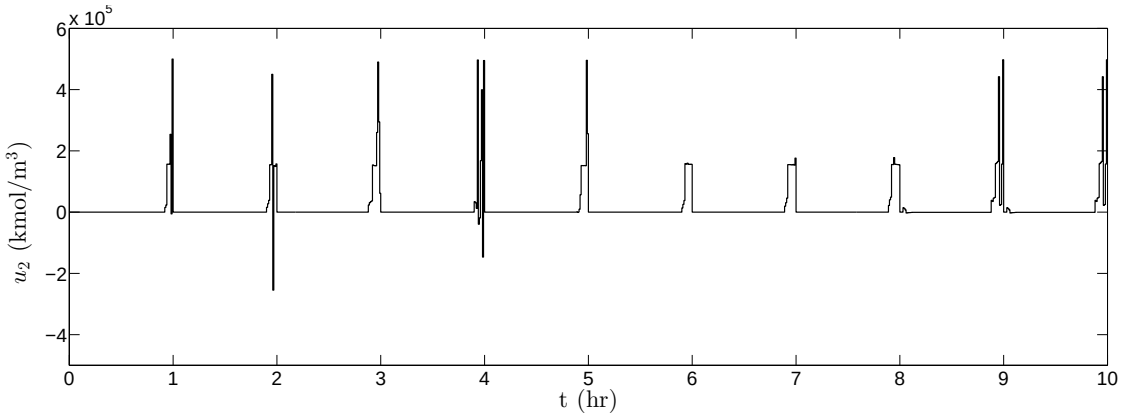

Figure 3.18: Trajectory of the heat input to the CSTR over ten hours for the CSTR model of Eq. 3.10 under the third-order empirical LEMPC.

1" LEMPC and the first-principles LEMPC from this section as the "First-Principles 2" LEMPC. The average economic cost index of Eq. 3.88 over one hour of operation and the total computation time for one hour of operation are shown in Table 3.2 for the empirical and first-principles models of this section and of the previous section. It is notable that the average economic cost index for the third-order empirical LEMPC and the First-Principles 2 LEMPC are higher than for the two LEMPCs of the previous section due to the different stability region chosen for the more accurate third-order empirical model. It is also notable that the performance gap between the third-order empirical LEMPC and the First-Principles 2 LEMPC is less than that between the second-order empirical LEMPC and the First-Principles 1 LEMPC since the third-order empirical model more accurately captures the dynamics of the first-principles model (the performance of the First-Principles 2 LEMPC is only 0.09% higher than that of the third-order empirical LEMPC, while the performance of the First-Principles 1 LEMPC was 0.3% higher). It would be expected, however, that the computation time would increase as the polynomial approximation of the process dynamics contains more terms to evaluate; Table 3.2 that the total computation time for the third-order empirical LEMPC for one operating period is 116% greater than that of the second-order empirical LEMPC.

Table 3.2: Comparison of average economic cost (J_e) and total computation time for one period of operation (1 *hr*) using various LEMPCs.

Model	J_e	Computation Time (*sec*)
Second-Order Empirical	16.1227	30.108
Third-Order Empirical	16.7569	65.156
First-Principles 1	16.1626	206.317
First-Principles 2	16.7712	201.428

3.6 Conclusions

In this chapter, a nonlinear system identification technique was developed for general nonlinear systems with affine inputs using a polynomial nonlinear state-space (PNLSS) model with additional constraints on the numerical stability of the identified model so that the identification process would produce empirical models that could be numerically integrated with explicit methods without using a very small integration step size. The motivation for this is that such models have an advantage in model predictive control applications, in contrast to the models identified with standard techniques that may require a step size too small for real-time use. This chapter demonstrates the benefits of the proposed system identification method in model predictive control by developing the formulation of an LEMPC scheme that uses an empirical model derived from the PNLSS method accounting for model well-conditioning to predict the process dynamics. A stability analysis of the closed-loop system under this controller provided sufficient conditions such that closed-loop stability in the sense of boundedness of the closed-loop state in a compact set is established. A chemical process example demonstrated that incorporating the well-conditioned empirical model in place of a first-principles model in LEMPC has significant computational advantages such that the LEMPC with the empirical model can be used for real-time control, with minimal reduction in profit compared to using the first-principles model.

Chapter 4

Error-Triggered On-line Model Identification for Model-Based Feedback Control

4.1 Introduction

The operational excellence and energy management of chemical and petrochemical processes rely on finding industrial solutions for the global energy demand, which led engineers to develop technologies that promote optimal process operation. To achieve improvements in process control, model-based control strategies, such as Lyapunov-based control and model predictive control (MPC), have been introduced. These types of controllers can improve process operation and thus may increase profit. A fairly recent model-based control strategy termed economic model predictive control (EMPC), for example, performs dynamic economic optimization incorporating predictions of future process states and state or output feedback to establish optimal time-varying operation under constraints.[14,20,22,49] The potential of model-based control strategies to improve process efficiency and to obtain desired closed-loop response characteristics makes these strategies desirable for use in industry.

A dynamic process model is required for any process for which model-based control is proposed and such models can be established through first-principles or empirical modeling.[79] First-principles models mathematically describe observed phenomena; the development of such models is difficult for processes that are complex and/or poorly understood. Numerous research efforts have been dedicated to the development of highly reliable model identification methods that require only input and output data to develop linear and nonlinear empirical models that can be used when first-principles models are undeveloped or impractical for on-line process control computations.[1,76,79]

A well-known class of empirical models are those designed using subspace model identification (SMI) methods, which are state-space model identification techniques for multiple-input multiple-output (MIMO) systems.[16,43,44,56,76] SMI methods are non-iterative robust methods that take into account multivariable interactions and result in highly reliable models.[39,76] Linear subspace identification algorithms include the Canonical Variate Algorithm (CVA),[59] the multivariable output error state-space (MOESP) algorithm,[43,44] and numerical algorithms for subspace state-space system identification (N4SID).[39] These methods have been successful in industrial applications and they result in numerically stable models.[1,16,29,43] SMI methods have also been considered for use in model predictive control (MPC) and EMPC.[48,56,89] Recursive subspace identification, in which the identified model is updated in order to correct for disturbances and nonlinearities, has also been an active area of research.[80] Most of this research has focused on the mathematical analysis of the methods used to update the identified models, including recursive least-squares, least mean squares, and recursively updating the singular value decomposition.[80–82] However, such methods have not focused on determining an approach for triggering the re-identification of a model when necessary.

In this chapter, an error-triggered on-line model identification approach is introduced for model-based control strategies. The re-identification of the model is conducted on-line to reduce plant-model mismatch that occurs very often in the chemical industry due to various reasons such as significant disturbances, catalyst deactivation in reactors, and upsets in feed streams, to name a

few. Also, the on-line model identification method can be used to update an empirical model when significant plant-model mismatch is detected because the region of operation shifts and the current model no longer captures the nonlinear dynamics. A moving horizon error detector monitors the prediction error between the states predicted by the empirical model and the measured states of the process. When the error exceeds a pre-specified threshold, the detector triggers an on-line model re-identification which is performed using the most recently generated input/output data. The approach is applied in the context of Lyapunov-based economic model predictive control (LEMPC) for nonlinear process systems through two chemical process examples. The first example demonstrates the ability of the proposed approach to improve the accuracy of the predicted states when significant plant-model mismatch occurs due to variations in the plant (catalyst deactivation). In the second example, the operating region is expanded gradually to allow the process to operate in a larger region for improved profit, and the proposed approach improves the accuracy of states predicted by the LEMPC over a larger region of state-space.

4.2 Preliminaries

4.2.1 Notation

The symbol x^T is used to denote the transpose of the vector x. The operator $|\cdot|$ designates the 2-norm of a vector. A continuous function $\alpha : [0,a) \to [0,\infty)$ is said to belong to class $\mathscr{K}$ if it is strictly increasing and equal to zero only when evaluated at zero. The symbol Ω_ρ is used to denote a level set of a sufficiently smooth scalar function $V(x)$ ($\Omega_\rho := \{x \in R^n : V(x) \leq \rho\}$). A square diagonal matrix is designated as diag(v) where the diagonal elements equal the components of the vector v. The symbol $\Delta > 0$ denotes the sampling period. The notation $S(\Delta)$ signifies the set of piecewise-constant vector functions with period Δ.

4.2.2 Class of Systems

The class of nonlinear systems considered in this chapter is of the following form:

$$\frac{dx(t)}{dt} = f(x(t), u(t), w(t)) \tag{4.1}$$

where $x \in R^n$, $u \in R^m$, and $w \in R^l$ are the system state vector, the manipulated input vector, and the disturbance vector respectively. Physical limitations on the available control energy set by actuator constraints are considered by restricting the control actions to the convex set $U := \{u \in R^m : u_i^{\min} \leq u_i \leq u_i^{\max},\ i = 1, \ldots, m\}$. We consider a bounded disturbance vector in this chapter (i.e., $w \in W := \{w\ :\ |w(t)| \leq \theta\ \forall\ t\}$). Measurements of the entire state vector $x(t_k)$ are assumed to be available at each sampling time $t_k = k\Delta$, $k = 0, 1, \ldots$.

We restrict our discussion to the class of stabilizable nonlinear systems for which there exists a controller $h(x) \in U$ that can render the origin of the nominal ($w(t) \equiv 0$) closed-loop system of Eq. 4.1 asymptotically stable in the sense that there exists a sufficiently smooth Lyapunov function $V : R^n \to R_+$ that satisfies the following inequalities:[30,111]

$$\alpha_1(|x|) \leq V(x) \leq \alpha_2(|x|), \tag{4.2a}$$

$$\frac{\partial V(x)}{\partial x} f(x, h(x), 0) \leq -\alpha_3(|x|), \tag{4.2b}$$

$$\left| \frac{\partial V(x)}{\partial x} \right| \leq \alpha_4(|x|) \tag{4.2c}$$

for all x in an open neighborhood $D \subseteq R^n$ that includes the origin and $\alpha_j(\cdot)$, $j = 1,\ 2,\ 3,\ 4$, are class $\mathscr{K}$ functions. Various stabilizing controllers that take into account input constraints have been developed for several classes of nonlinear systems.[10,12,27] The stability region of the closed-loop system is taken to be a level set $\Omega_\rho \subset D$ where the time derivative of the Lyapunov function is strictly negative ($(dV/dt) < 0$). In addition, the origin of the system of Eq. 4.1 is rendered practically stable[31] when the controller $h(x)$ is applied in a sample-and-hold fashion for a

sufficiently small sampling period. The function f is assumed to be locally Lipschitz on $\Omega_\rho \times U \times W$ and the origin is taken to be an equilibrium of the unforced system of Eq. 4.1 (i.e., $f(0,0,0) = 0$).

The proposed on-line model identification approach develops linear empirical models to predict the evolution of the state of the system of Eq. 4.1. Although the method discussed in this chapter extends to a wide range of linear empirical models such as input/output models, we will demonstrate the scheme where the empirical models obtained on-line are state-space linear time-invariant (LTI) models of the form:

$$\frac{dx(t)}{dt} = A_i x(t) + B_i u(t) \tag{4.3}$$

where A_i and B_i are constant matrices of appropriate dimensions corresponding to the $i-th$ model identification performed ($i = 1,\ \ldots,\ \tilde{M}$).

We assume that a set of stabilizing controllers $h_{L1}(x)$, $h_{L2}(x)$, ..., $h_{L\tilde{M}}(x)$ designed based on the empirical models exists such that each controller renders the origin of the closed-loop system of Eq. 4.1 asymptotically stable and yields a sufficiently smooth Lyapunov function $\hat{V} : R^n \to R_+$ with the following properties:[111]

$$\hat{\alpha}_1(|x|) \leq \hat{V}(x) \leq \hat{\alpha}_2(|x|), \tag{4.4a}$$

$$\frac{\partial \hat{V}(x)}{\partial x} f(x, h_{Li}(x), 0) \leq -\hat{\alpha}_{3_i}(|x|),\ i = 1,\ \ldots,\ \tilde{M} \tag{4.4b}$$

$$\left| \frac{\partial \hat{V}(x)}{\partial x} \right| \leq \hat{\alpha}_4(|x|) \tag{4.4c}$$

for all $x \in D_{Li} \subseteq R^n$ where D_{Li} is an open neighborhood that includes the origin and the functions $\hat{\alpha}_j(\cdot)$, $j = 1,\ 2,\ 4$, and $\hat{\alpha}_{3_i}$, $i = 1,\ \ldots,\ \tilde{M}$, are class $\mathscr{K}$ functions. The system of Eq. 4.1 under the controller $h_{Li}(x)$ has the stability region $\Omega_{\hat{\rho}_i} \subset D_{Li}$, $i = 1,\ \ldots,\ \tilde{M}$.

4.2.3 Lyapunov-Based Economic Model Predictive Control

The model-based controller that will be used in the chemical process examples presented in this chapter is Lyapunov-based economic model predictive control (LEMPC).[20] LEMPC uses a reced-

ing horizon control strategy that minimizes a cost function while incorporating stability constraints based on the explicit stabilizing controller $h(x)$ in its design. The formulation of LEMPC is:

$$\min_{u\in S(\Delta)} \quad \int_{t_k}^{t_{k+N}} L_e(\tilde{x}(\tau),u(\tau))\,d\tau \tag{4.5a}$$

$$\text{s.t.} \quad \dot{\tilde{x}}(t) = f(\tilde{x}(t),u(t),0) \tag{4.5b}$$

$$\tilde{x}(t_k) = x(t_k) \tag{4.5c}$$

$$u(t) \in U,\ \forall\, t \in [t_k,t_{k+N}) \tag{4.5d}$$

$$V(\tilde{x}(t)) \leq \rho_e,\ \forall\, t \in [t_k,t_{k+N})$$

$$\text{if } x(t_k) \in \Omega_{\rho_e} \tag{4.5e}$$

$$\frac{\partial V(x(t_k))}{\partial x} f(x(t_k),u(t_k),0)$$

$$\leq \frac{\partial V(x(t_k))}{\partial x} f(x(t_k),h(x(t_k)),0)$$

$$\text{if } x(t_k) \notin \Omega_{\rho_e} \tag{4.5f}$$

where the optimization variable is the control input trajectory over the prediction horizon $N\Delta$. LEMPC uses the process dynamic model (Eq. 4.5b) to predict the state trajectory $\tilde{x}(t)$ over time starting from the initial condition in Eq. 4.5c which is obtained from the state measurement at time t_k. The LEMPC design takes into account constraints on the manipulated inputs in Eq. 4.5d. The stage cost L_e (Eq. 4.5a) is formulated to represent the process economics.

Based on the state measurement of Eq. 4.5c, either the Mode 1 (Eq. 4.5e) or the Mode 2 (Eq. 4.5f) stability constraint is active. In Mode 1, time-varying operation is promoted to maximize profit while maintaining the state in a region $\Omega_{\rho_e} \subset \Omega_\rho$ chosen to make Ω_ρ invariant in the presence of disturbances. If the measured process state is outside of Ω_{ρ_e}, Mode 2 is activated to compute control actions that decrease the Lyapunov function value and force the state back into Ω_{ρ_e}. The solution of the LEMPC optimization problem is denoted as $u^*(t|t_k)$, $t \in [t_k,t_{k+N})$, but only $u^*(t_k|t_k)$ is implemented at each sampling time.

4.2.4 Lyapunov-Based Economic Model Predictive Control with Empirical Models

The plant model of Eq. 4.5b may be unavailable, in which case it can be replaced by an empirical model. In this chapter, we will replace the nonlinear plant model of Eq. 4.5b with the $i-th$ linear empirical model, $i = 1, \ldots, \tilde{M}$ (which is the model last identified by the error-triggered on-line model identification procedure prior to the sampling time t_k). The empirical model is also used to design $h_{Li}(x)$ and $\hat{V}(x)$ for the Lyapunov-based constraints in Eq. 4.5. The level set $\Omega_{\hat{\rho}_{ei}} \subset \Omega_{\hat{\rho}_i}$ that prompts the switch between Mode 1 and Mode 2 is chosen such that the controller maintains operation of the process of Eq. 4.1 within $\Omega_{\hat{\rho}_i}$ in the presence of bounded disturbances. The formulation of LEMPC using the $i-th$ linear empirical model is:[48]

$$\min_{u\in S(\Delta)} \quad \int_{t_k}^{t_{k+N}} L_e(\hat{x}(\tau), u(\tau))\, d\tau \tag{4.6a}$$

$$\text{s.t.} \quad \dot{\hat{x}}(t) = A_i\hat{x}(t) + B_i u(t) \tag{4.6b}$$

$$\hat{x}(t_k) = x(t_k) \tag{4.6c}$$

$$u(t) \in U,\ \forall\, t \in [t_k, t_{k+N}) \tag{4.6d}$$

$$\hat{V}(\hat{x}(t)) \leq \hat{\rho}_{ei},\ \forall\, t \in [t_k, t_{k+N}) \quad \text{if } x(t_k) \in \Omega_{\hat{\rho}_{ei}}, \tag{4.6e}$$

$$\frac{\partial \hat{V}(x(t_k))}{\partial x}\left(A_i x(t_k) + B_i u(t_k)\right) \leq \frac{\partial \hat{V}(x(t_k))}{\partial x}\left(A_i x(t_k) + B_i h_{Li}(x(t_k))\right) \quad \text{if } x(t_k) \notin \Omega_{\hat{\rho}_{ei}} \tag{4.6f}$$

where the notation follows that in Eq. 4.5 except that $\hat{x}(t)$ is the predicted state of the system using the linear empirical model (Eq. 4.6b), starting from a measurement of the actual process state (Eq. 4.6c) to predict the evolution of the system of Eq. 4.1.

Remark 5 *In the formulation of Eq. 4.6, $\hat{V}$ is not updated when the model of Eq. 4.6b is updated.*

Though it may be replaced with $\hat{V}_i$, this is not required if the stability region of an updated model can be found to be a level set of the same Lyapunov function as was used for the prior model.

Remark 6 *A key feature of the LEMPCs in Eqs. 4.5 and 4.6 is that they may not drive the process to a steady-state, but rather operate it in a time-varying fashion within a stability region, when the cost function does not have its minimum at a steady-state. When such dynamic operation is achieved, the time-varying nature of the input trajectories generated using LEMPC can result in persistent excitation of the process states, which makes the inputs ideal for on-line model identification. The chemical process examples in this chapter demonstrate the time-varying nature of inputs that may be calculated by an LEMPC.*

4.3 Error-Triggered On-Line Model Identification

This section discusses the proposed error-triggered on-line model identification method.

4.3.1 Error-Triggering Mechanism for On-Line Model Identification

In this section, we describe an error-triggering mechanism that can trigger on-line updates of the model utilized in the design and implementation of a model-based controller. A major advantage of this mechanism is that it can prevent constant updating of the process model, which may be computationally expensive and result in frequent changes to the control law that are undesirable. It also prevents the use of an inaccurate model when there is significant plant-model mismatch.

In the proposed method, a moving horizon error detector quantifies the accuracy of an empirical model by calculating the following moving horizon error metric e_d at times t_k:

$$e_d(t_k) = \sum_{r=0}^{M} \sum_{j=1}^{n} \frac{|x_{p,j}(t_{k-r}) - x_j(t_{k-r})|}{|x_j(t_{k-r})|} \tag{4.7}$$

where M is the number of sampling periods before t_k that contribute to the quantification of the prediction error, $x_j(t_{k-r})$, $r = 0, \ldots, M$, are the past measurements of the process states at sampling

periods between t_{k-M} and t_k, and $x_{p,j}(t_{k-r})$, $r = 0, \ \ldots, \ M$, are the predictions of the past states of the system from a linear empirical model. A threshold value $e_{d,T}$ is set for the error metric, and when the moving horizon error detector determines that this threshold has been exceeded, it triggers model re-identification. There are several parameters that need to be defined to carry out this error-triggered approach: the number of input and output data points N_d that must be kept for model identification when it is triggered, the length M of the moving horizon used in the calculation of e_d, and the threshold $e_{d,T}$ of the error above which model re-identification is triggered. To determine these parameters initially, the following strategy is proposed:

Step 1. When no initial linear model is available (e.g., through the linearization of a first-principles model), the process is initially excited off-line in open-loop using long sequences of standard input types (e.g., impulse or step inputs) to excite the important dynamics. The corresponding output data is collected. System identification is carried out on the (open-loop) input/output data using standard techniques (e.g., determination of a large order model followed by model order reduction[76]) to determine an $i = 1$ empirical model that captures the dominant process dynamics. The number of input/output data points N_d that need to be stored for a possible future system identification can be set to the number of input/output data points required to identify the $i = 1$ empirical model.[39,76]

Step 2. The value of M to be used in the calculation of e_d must be long enough such that disturbances common during normal operation do not significantly affect e_d (which could lead to unnecessary error-triggering) but are smoothed out. However, M also should not be longer than necessary because this would require unnecessary data storage and processing. One method for determining M is by calculating the value of $e_d(t_k)$, $t_k > t_M$, at every sampling period for a set of input/output data collected during normal process operation (in closed-loop under the model-based controller) in the region of operation for which the $i = 1$ empirical model was developed and validated. This calculation is then repeated for various values of M. The minimum and maximum values of e_d for a given value of M may be significantly different if M is small, since then any disturbance or measurement noise within the moving horizon contributes significantly to the value

of e_d. As M is increased, however, the effect of disturbances and measurement noise will become less significant. At some point, it would be expected that the minimum and maximum values of e_d will not change much when M is further increased; in this case, the smallest value of M for which the minimum and maximum values of e_d seem to have reached their approximate final value could be chosen to be used in Eq. 4.7. From this, it is seen that the statistical properties of $w(t)$ will affect the value of M for a given process.

Step 3. The value of $e_{d,T}$ is determined off-line, based on the chosen value of M, such that measurement noise, small constant disturbances, and time-varying disturbances that cause reasonably accurate predictions with the current model do not trigger model re-identification. One method for achieving this is by analyzing the statistical properties of e_d for a set of closed-loop input/output data corresponding to normal process operation in the region within which the linear empirical model was developed and validated. For example, the maximum value of e_d for such data could be determined with the selected value of M, and then the threshold could be chosen to be a reasonable percentage greater than the maximum value of e_d observed for this normal operating data (which should include the disturbances and measurement noise that regularly affect the system). Other statistical measures (e.g., choosing the value of $e_{d,T}$ to be several standard deviations above its mean value from the normal operating data) could also be used, and the appropriate measure to use will depend on the system analyzed. It is noted that even if there were no disturbances or measurement noise, e_d would be expected to have a value because the linear empirical model identified is unlikely to fully capture the nonlinear dynamics of a given process.

The lack of a formula for obtaining N_d, M, and $e_{d,T}$ does not pose practical limitations because, as will be discussed further in later sections, the on-line, data-based methodology employed allows for constant monitoring of the process performance under a controller based on the current linear empirical model such that "poor" choices of the parameters can be detected and the parameters adjusted.

Remark 7 *For consistency with Step 1 as presented above, in the remainder of the manuscript we will assume that no first-principles process model is available and we will call the linear models*

developed before the initiation of error-triggered on-line model identification the initial linear empirical models. However, it is not required that these models be empirical. The initial linear model obtained in Step 1 of the above procedure may be obtained using a linearization of a nonlinear first-principles model if such a model is available. In this case, the utility of on-line updating of the linear model using the error-triggered model identification method is that it prevents the need for using a nonlinear model and may aid in capturing the process dynamics better than a first-principles model as the process dynamics change in time.

Remark 8 *The value of $x_{p,j}(t_{k-r})$ may be calculated in multiple ways. For example, one method is to calculate each value of $x_{p,j}(t_{k-r})$ by numerically integrating the linear empirical model of Eq. 4.3, starting from the measured state $x(t_{k-r-1})$ at the previous sampling time, and using the input applied for $t \in [t_{k-r-1}, t_{k-r})$ in the integration. Another method is to determine the value of each $x_{p,j}(t_{k-r})$ by integrating the linear model, starting from the measurement of the state $x(t_{k-M-1})$ and applying the sequence of control actions implemented on the process throughout time. If more than one model has been used between t_{k-M-1} and t_k, the applicable model should be used for the integration corresponding to its period of use.*

Remark 9 *Practically, when the model-based controller is updated due to the identification of a new model, it may be necessary to include additional precautions in the control system design. For example, a constraint or saturation could be imposed when the controller is initially updated that prevents the inputs calculated from the new controller from differing more than a certain amount from the control actions calculated most recently by the prior controller. If this is used, the closed-loop stability properties of the resulting controller should be considered.*

Remark 10 *In model-based controllers such as standard tracking model predictive control (MPC), the replacement of a prior linear empirical model in the MPC with a newer model obtained from the error-triggered on-line model identification strategy may be sufficient for keeping the control law up-to-date. Some model-based control laws may require further computation to determine the new control law after an updated linear empirical model is developed (e.g., Sontag's control law*

will need to be re-calculated based on the new model[27]). Other control laws may have additional aspects that require them to be further adjusted as the linear empirical models are updated. For example, LEMPC may require that the process model be updated and also that other components of the control law in Eq. 4.6 be updated (e.g., h_{Li}).

4.3.2 Implementation Strategy for Error-Triggered On-Line Model Identification

Once the values of N_d, M and $e_{d,T}$ are set according to the methodology of the prior section, the proposed error-triggered on-line model identification strategy can be executed with the following implementation strategy:

Step 1. An initial linear empirical model of the plant (A_1 and B_1) is developed (this becomes the "current model" for the process). This model is used to design the model-based controller.

Step 2. The process is operated under the model-based controller designed based on the current linear empirical model, and input/output data (up to N_d values of each) are collected and stored for possible future model identification. The moving horizon error detector is initiated at t_M to calculate $e_d(t_k)$.

Step 3. As the current linear model begins to fail to describe the process dynamics (due to, for example, variations in the plant or changes in the region of operation), $e_d(t_k)$ will increase and when $e_d(t_k)$ exceeds $e_{d,T}$, the most recent set of N_d values of input and output data (collected up to time t_k) are used to identify a new model on-line to become the current model for use in updating the model-based controller formulation.

Step 4. Steps 2-3 are repeated as process operation continues.

4.4 Applications of Error-Triggered On-Line Model Identification

In this section, we present two applications of the error-triggered on-line model identification methodology (Steps 1-4 of the prior section) to demonstrate the flexibility of the approach and its utility in a variety of circumstances.

4.4.1 Application of Error-Triggered On-Line Model Identification to Plant Variations

The first application to be discussed is that in which the plant model changes in time. This may occur, for example, due to catalyst deactivation that affects the reaction rates in the process, due to heat exchanger fouling that affects the rate of heat transfer, or due to changes in the valve dynamics with time as dynamic valve nonlinearities such as stiction worsen in time due to valve degradation. For this application, it is possible that as the plant model changes in time, the values of N_d, M, and $e_{d,T}$ originally determined may no longer be the appropriate values. For example, N_d may need to be increased to obtain a more accurate model, and the combination of M and $e_{d,T}$ may cause the linear empirical model to be updated more or less frequently than necessary. This can be handled on-line by varying the parameters in small increments until better performance is obtained. For example, N_d may be lengthened until the linear empirical models are shown to better capture the nonlinear dynamics in the current region of state-space. M and $e_{d,T}$ may be increased if the on-line model updates are triggered too frequently even when the linear empirical models being identified do not result in poor closed-loop performance, or they may be decreased if the model updates are not triggered frequently enough and process and controller performance degrades. Alternatively, experiments can be performed to determine new values of these parameters.

Remark 11 *If the values of N_d, M, and $e_{d,T}$ are picked appropriately such that the model-based controller used at any given time is based on a reasonably accurate empirical model, this controller*

may often be stabilizing if the computation time required by the moving horizon error detector and for model updates is short compared to the process dynamics (this prevents the process state from changing significantly before errors are detected and the model is updated). To develop a rigorous proof of closed-loop stability of a process under the error-triggered on-line model identification procedure as plant variations occur in time, however, a number of mathematical assumptions would need to be made that are specific to each model-based controller type. Proofs of closed-loop stability of processes under various model-based controllers and feasibility of such controllers as applicable are addressed in many works (e.g.,[20,48,83,84,111] *and the references therein), and similar methods could be investigated for nonlinear processes under model-based controllers designed based on linear empirical models developed from the error-based triggering approach. An example of an assumption that may be considered in the proofs of feasibility and closed-loop stability of a process under the LEMPC of Eq. 4.6 is that the closed-loop state is within both* $\Omega_{\hat{\rho}_{i-1}}$ *and* $\Omega_{\hat{\rho}_i}$ *at the time that the model used in the design of the LEMPC of Eq. 4.6 changes from the* $(i-1)-th$ *to the* $i-th$ *linear empirical model. The primary purpose of the present chapter is not for providing rigorous closed-loop stability proofs (though the more accurate empirical models may aid closed-loop system stabilizability), but is for providing more accurate models for model-based control strategies so that more desirable control actions (e.g., more economically beneficial or more capable of meeting process constraints) can be calculated.*

Application of Error-Triggered On-Line Model Identification to Plant Variations: Application to a Chemical Process Example

In this section, we demonstrate the proposed error-triggered on-line model identification procedure for the control of a benchmark chemical reactor for which plant model changes occur, specifically catalyst deactivation. The catalytic oxidation of ethylene (C_2H_4) in a non-isothermal continuous stirred tank reactor (CSTR) is considered. The ethylene is oxidized with air to produce the desired ethylene oxide (C_2H_4O) product. Two combustion reactions that consume ethylene oxide and

ethylene occur concurrently in the reactor as presented in the following chemical reactions:

$$C_2H_4 + \frac{1}{2}O_2 \xrightarrow{R_1} C_2H_4O \tag{R1}$$

$$C_2H_4 + 3O_2 \xrightarrow{R_2} 2CO_2 + 2H_2O \tag{R2}$$

$$C_2H_4O + \frac{5}{2}O_2 \xrightarrow{R_3} 2CO_2 + 2H_2O \tag{R3}$$

The rates of the reactions R_1, R_2, and R_3 are given by the following rate laws:[85]

$$R_1 = k_1 \exp\left(\frac{-E_1}{RT}\right) P_E^{0.5} \tag{4.8a}$$

$$R_2 = k_2 \exp\left(\frac{-E_2}{RT}\right) P_E^{0.25} \tag{4.8b}$$

$$R_3 = k_3 \exp\left(\frac{-E_3}{RT}\right) P_{EO}^{0.5} \tag{4.8c}$$

where the pre-exponential factors are k_1, k_2, and k_3 and the activation energies are E_1, E_2, and E_3. T is the temperature and R is the gas constant. P_E and P_{EO} are the partial pressures of ethylene (P_E) and of ethylene oxide (P_{EO}) and it is assumed that the gas mixture in the reactor is an ideal gas, and thus, the partial pressures can be written in terms of the molar concentrations. The dimensionless first-principles dynamic model which is derived from mass and energy balances for this process from[86] is of the following form:

$$\frac{dx_1(t)}{dt} = u_1(1 - x_1x_4) \tag{4.9a}$$

$$\frac{dx_2(t)}{dt} = u_1(u_2 - x_2x_4) - A_1 e^{\frac{\gamma_1}{x_4}} (x_2x_4)^{0.5} - A_2 e^{\frac{\gamma_2}{x_4}} (x_2x_4)^{0.25} \tag{4.9b}$$

$$\frac{dx_3(t)}{dt} = -u_1x_3x_4 + A_1 e^{\frac{\gamma_1}{x_4}} (x_2x_4)^{0.5} - A_3 e^{\frac{\gamma_3}{x_4}} (x_3x_4)^{0.5} \tag{4.9c}$$

$$\frac{dx_4(t)}{dt} = \frac{u_1}{x_1}(1 - x_4) + \frac{B_1}{x_1} e^{\frac{\gamma_1}{x_4}} (x_2x_4)^{0.5} + \frac{B_2}{x_1} e^{\frac{\gamma_2}{x_4}} (x_2x_4)^{0.25} + \frac{B_3}{x_1} e^{\frac{\gamma_3}{x_4}} (x_3x_4)^{0.5} - \frac{B_4}{x_1}(x_4 - u_3)$$

where the dimensionless variables x_1, x_2, x_3, and x_4 correspond to the gas density in the reactor, ethylene concentration, ethylene oxide concentration, and reactor temperature, respectively. The

manipulated inputs u_1 u_2, and u_3 are the dimensionless feed volumetric flow rate, ethylene concentration of the reactor feed, and coolant temperature, respectively. The manipulated inputs are bounded by physical limitations on actuators and hence, the inputs are constrained to belong to the following convex sets: $0.0704 \leq u_1 \leq 0.7042$, $0.2465 \leq u_2 \leq 2.4648$, $0.6 \leq u_3 \leq 1.1$. The values of the parameters of this model are presented in Table 4.1. The CSTR has an asymptotically stable steady-state that occurs at $x_s^T = [x_{1s}\ x_{2s}\ x_{3s}\ x_{4s}] = [0.998\ 0.424\ 0.032\ 1.002]$ when $[u_{1s}\ u_{2s}\ u_{3s}] = [0.35\ 0.5\ 1.0]$.

Table 4.1: Dimensionless Parameters of the Ethylene Oxidation CSTR.

$A_1 = 92.8$	$B_2 = 10.39$	$\gamma_2 = -7.12$
$A_2 = 12.66$	$B_3 = 2170.57$	$\gamma_3 = -11.07$
$A_3 = 2412.71$	$B_4 = 7.02$	
$B_1 = 7.32$	$\gamma_1 = -8.13$	

The CSTR is controlled by an LEMPC with the goal of feeding the ethylene to the reactor in a manner that maximizes the average yield of ethylene oxide. The average yield of ethylene oxide, which quantifies the amount of ethylene oxide produced compared to the amount of ethylene fed to the reactor, over a time period from t_0 to t_e, is given by:

$$Y(t_e) = \frac{\int_{t_0}^{t_e} u_1(\tau)x_3(\tau)x_4(\tau)\, d\tau}{\int_{t_0}^{t_e} u_1(\tau)u_2(\tau)\, d\tau} \tag{4.10}$$

where t_e is an integer multiple of the length t_f of an operating period. Because the amount of reactant material available is fixed, the time-averaged molar flow rate of ethylene that can be fed to the reactor in an operating period is limited by the following constraint:

$$\frac{1}{t_f}\int_{(j-1)t_f}^{jt_f} u_1(\tau)u_2(\tau)\, d\tau = u_{1s}u_{2s} = 0.175 \tag{4.11}$$

where j is the operating period number ($j = 1, 2, \ldots$). This constraint ensures that in each operating period, the amount of ethylene fed to the reactor is the same as that which would have been fed

under steady-state operation. Because the integral input constraint of Eq. 4.11 fixes the value of the denominator in Eq. 4.10, the LEMPC seeks to maximize the following function:

$$\int_{t_0}^{t_e} L_e(x,u) = \int_{t_0}^{t_e} u_1(\tau)x_3(\tau)x_4(\tau)d\tau \tag{4.12}$$

By maximizing this objective, the ethylene oxide yield is maximized subject to the integral material constraint that is enforced due to restrictions on the available feedstock.

The first-principles nonlinear process model in Eq. 4.9 is assumed to be unavailable from a controller design point of view such that an empirical model must be obtained to formulate an LEMPC that meets the above objective and constraints. To construct such an empirical model that captures the dynamics within a region around the CSTR steady-state, a large number of input step changes of varying magnitudes were applied to the CSTR from the steady-state and the corresponding output data was collected. The ordinary multivariable output error state-space (MOESP)[43] algorithm was applied to this data to obtain the initial ($i = 1$) linear state-space empirical model for the CSTR of Eq. 4.9. This model was validated using a wide range of step, impulse, and sinusoidal input responses and is expressed by the following matrices:

$$\begin{aligned} A_1 &= \begin{bmatrix} -0.349 & 0.00051 & 0.00825 & -0.349 \\ -0.00488 & -0.374 & 0.0374 & -0.369 \\ 0.00109 & 0.0213 & -0.452 & 0.0653 \\ -0.0078 & 0.0259 & 0.0204 & -7.24 \end{bmatrix} \\ B_1 &= \begin{bmatrix} -0.00011 & -0.000149 & -0.0239 \\ 0.0757 & 0.349 & -0.0194 \\ -0.0315 & 0.000208 & 0.00426 \\ -0.0173 & -0.00264 & 6.529 \end{bmatrix} \end{aligned} \tag{4.13}$$

Since it is assumed that the only model available for controller design is the empirical model, the model of Eq. 4.13 is used to design the Lyapunov-based controller used in LEMPC. The con-

troller can be represented as a vector with three components: $h_{L1}^T(x) = [h_{L1,1}(x)\ h_{L1,2}(x)\ h_{L1,3}(x)]$, where $h_{L1}(x_s) = 0$. The control laws $h_{L1,1}(x)$ and $h_{L1,2}(x)$ were set to the steady-state values of u_1 and u_2 to meet the material constraint of Eq. 4.11. The control law $h_{L1,3}(x)$ was designed using the standard linear quadratic regulator (LQR) with a quadratic objective defined using the A_1 matrix and the third column of the B_1 matrix (Eq. 4.13) and taking both the Q and R weighting matrices to be the identity matrix. This results in the control law $u_3 = h_{L1,3}(x) = -K(x-x_s)+u_{3s}$, with K equal to [-0.287 -0.276 0.023 0.405]. A quadratic Lyapunov function of the form $\hat{V}(x) = (x-x_s)^T P(x-x_s)$ was utilized to characterize the stability region of the closed-loop system of Eq. 4.9 under the stabilizing controller h_{L1} with the positive definite matrix P defined as P=diag[20 30 40 10]. Extensive simulations of the closed-loop system under the Lyapunov-based controller $h_{L1}(x)$ were conducted to define the level set $\Omega_{\hat{\rho}_{e1}}$ with $\hat{\rho}_{e1} = 87.4$. This is a region within which the nonlinear dynamics of Eq. 4.9 are well-captured by the linear model of Eq. 4.13.

Though this chemical process example will be used to illustrate the error-triggered on-line model identification procedure in the presence of plant variations, we will first demonstrate that the initial linear empirical model performs well in the time period before any catalyst deactivation (plant variation) occurs. To demonstrate this, two LEMPC schemes, one of the form of Eq. 4.6 and the other of the form of Eq. 4.5, both with the additional material constraint of Eq. 4.11, were designed to compare closed-loop behavior. Both used the cost function of Eq. 4.12, the upper and lower bounds on u_1, u_2, and u_3 described above, and the same Lyapunov-based controller and stability region. The process model utilized in the first LEMPC was the empirical model of Eq. 4.13, while the second LEMPC utilized the first-principles model of Eq. 4.9. In all simulations for this example, the LEMPC designs had prediction horizons of $N = 10$, sampling periods of $\Delta = 0.1$, and operating periods of 100 sampling periods ($t_f = 10$). The interior point solver IPOPT[119] was used to solve the LEMPC optimization problems. The empirical LEMPC and the first-principles LEMPC were both applied to the CSTR model of Eq. 4.9. The reactor was initialized off steady-state at $x_I^T = [x_{1I}\ x_{2I}\ x_{3I}\ x_{4I}] = [0.997\ 1.264\ 0.209\ 1.004]$ and closed-loop simulations over ten operating periods for each case were completed. The explicit Euler numerical integration method was

used in all simulations for this example with an integration step size of $h = 10^{-4}$. The closed-loop trajectories for the CSTR under both LEMPC schemes are shown in Figs. 4.1-4.2 which demonstrate very similar behavior. The average yield of the first-principles LEMPC over ten operating periods was 8.98, compared to 8.93 for the empirical LEMPC. The agreement between the trajectories and yields of the process under the first-principles and empirical LEMPCs demonstrates that the initial linear empirical model is capable of adequately describing the process behavior before plant variation occurs. It is noted that the periodic nature of the trajectories is consistent with prior literature for this example (e.g.,[86] and[53]) which demonstrated that time-varying operation can be economically beneficial for the ethylene oxide production process, and also other literature on optimal periodic operation (e.g.,[87] and[88]).

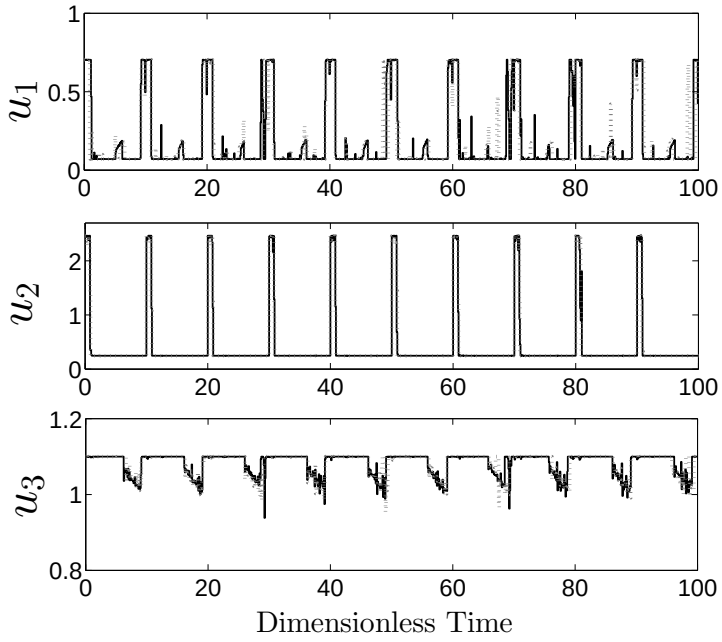

Figure 4.1: Input profiles of the closed-loop CSTR under the LEMPC using the first-principles model (solid black trajectories) and the LEMPC using the empirical model in Eq. 4.13 (dotted gray trajectories) for 10 operating periods starting from $x_I^T = [x_{1I}\ x_{2I}\ x_{3I}\ x_{4I}] = [0.997\ 1.264\ 0.209\ 1.004]$.

After the 10 operating periods, plant variations begin to occur (a reduction in the reaction pre-exponential factor is assumed to occur due to catalyst deactivation). Specifically, the pre-exponential factor values for reactions R_1, R_2, and R_3 are decreased by 40 percent gradually

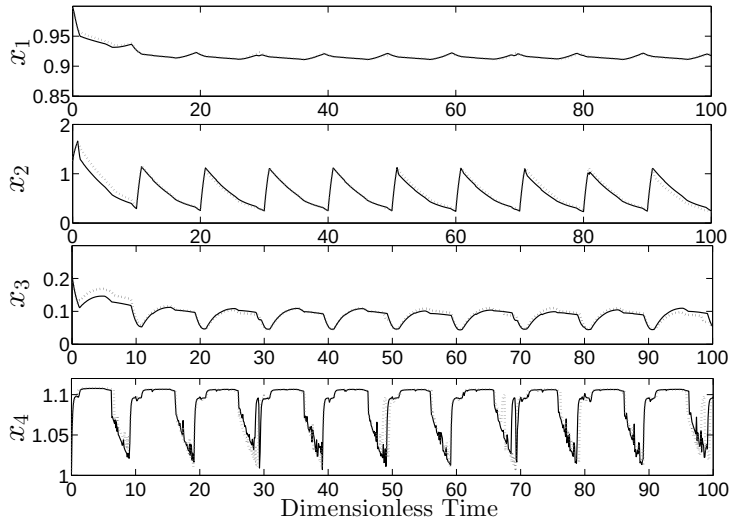

Figure 4.2: State profiles of the closed-loop CSTR under the LEMPC using the first-principles model (solid black trajectories) and the LEMPC using the empirical model in Eq. 4.13 (dotted gray trajectories) for 10 operating periods starting from $x_I^T = [x_{1I}\ x_{2I}\ x_{3I}\ x_{4I}] = [0.997\ 1.264\ 0.209\ 1.004]$.

throughout 9 operating periods. The pre-exponential factors are decreased by 10 percent of their original values at the beginning of the eleventh and twelfth operating periods, reaching the values $0.8k_1, 0.8k_2$, and $0.8k_3$. The pre-exponential factors then stay at those values for three operating periods and are subsequently decreased by 5 percent of their original values at the beginning of the fifteenth and sixteenth operating periods to $0.7k_1, 0.7k_2$, and $0.7k_3$. After that, the pre-exponential factor values stay at $0.7k_1, 0.7k_2$, and $0.7k_3$ for three operating periods and then are decreased by 5 percent of their original values at the beginning of the nineteenth and twentieth operating periods, reaching the final values $0.6k_1, 0.6k_2$, and $0.6k_3$.

To monitor the prediction error for the linear empirical model when catalyst deactivation occurs, a moving horizon error detector was initiated early in process operation (after M prior input/output data points were available) to calculate the value of e_d at each sampling time to determine when it is necessary to trigger re-identification of the empirical process model. Simulations of the CSTR before catalyst deactivation occurs suggest that significant plant-model mismatch under the original linear empirical model is indicated when the value of e_d exceeds 2.5 (i.e., $e_{d,T} = 2.5$) and thus, this value was chosen as the threshold to trigger model re-identification. When on-line

model identification is triggered, input/output data from the previous 200 sampling times (i.e., $N_d = 200$) is used to identify a new model. The moving horizon error detector calculates the relative prediction error in the gas density in the reactor, ethylene concentration, ethylene oxide concentration, and the reactor temperature throughout the past 40 sampling periods (i.e., $M = 40$) and the current sampling time as follows:

$$\begin{aligned} e_d(t_k) = \sum_{r=0}^{40} \frac{|x_{p,1}(t_{k-r}) - x_1(t_{k-r})|}{|x_1(t_{k-r})|} + \\ \frac{|x_{p,2}(t_{k-r}) - x_2(t_{k-r})|}{|x_2(t_{k-r})|} + \frac{|x_{p,3}(t_{k-r}) - x_3(t_{k-r})|}{|x_3(t_{k-r})|} \\ + \frac{|x_{p,4}(t_{k-r}) - x_4(t_{k-r})|}{|x_4(t_{k-r})|} \end{aligned} \tag{4.14}$$

The first approach from Remark 8 was used to calculate each $x_{p,i}$, $i = 1,2,3,4$, in Eq. 4.14 above.

Model re-identification was triggered four times by the moving horizon error detector throughout the gradual decrease in the pre-exponential factors from k_1, k_2, k_3 to $0.6k_1, 0.6k_2, 0.6k_3$, resulting in the identification of four models as follows:

$$\begin{aligned} A_2 &= \begin{bmatrix} -0.341 & -0.00281 & 0.00482 & -0.347 \\ -0.00481 & -0.403 & -0.223 & -0.235 \\ -0.00431 & 0.0265 & -0.314 & 0.0220 \\ 0.111 & -0.0137 & 0.424 & -7.31 \end{bmatrix} \\ B_2 &= \begin{bmatrix} -0.00073 & -0.000851 & -0.0243 \\ 0.0891 & 0.381 & -0.0426 \\ -0.0358 & 0.00983 & 0.0131 \\ -0.00043 & -0.00758 & 6.56 \end{bmatrix} \end{aligned} \tag{4.15}$$

$$
\begin{aligned}
A_3 &= \begin{bmatrix} -0.369 & 0.00284 & 0.0665 & -0.350 \\ -0.174 & -0.367 & 0.590 & -0.383 \\ -0.125 & 0.0212 & -0.888 & 0.0774 \\ -0.443 & 0.0613 & -1.614 & -7.27 \end{bmatrix} \\
B_3 &= \begin{bmatrix} -0.00166 & -0.000408 & -0.0240 \\ 0.0378 & 0.318 & -0.00252 \\ -0.0205 & 0.00908 & -0.00474 \\ -0.0172 & 0.0126 & 6.517 \end{bmatrix}
\end{aligned} \tag{4.16}
$$

$$
\begin{aligned}
A_4 &= \begin{bmatrix} -0.354 & 0.00238 & 0.00646 & -0.346 \\ -0.191 & -0.263 & -0.812 & -0.226 \\ 0.0737 & 0.0223 & -0.0639 & 0.0202 \\ -0.0539 & -0.0172 & 0.616 & -7.25 \end{bmatrix} \\
B_4 &= \begin{bmatrix} -0.00762 & -0.00367 & -0.0272 \\ -0.203 & 0.238 & -0.118 \\ 0.0599 & 0.00373 & 0.00372 \\ -0.00439 & 0.00381 & 6.516 \end{bmatrix}
\end{aligned} \tag{4.17}
$$

$$
\begin{aligned}
A_5 &= \begin{bmatrix} -0.345 & 0.0045 & 0.0147 & -0.343 \\ 0.0416 & -0.271 & -0.830 & -0.0905 \\ -0.00380 & -0.0106 & -0.0335 & -0.0239 \\ 0.0515 & 0.00891 & 0.683 & -7.34 \end{bmatrix} \\
B_5 &= \begin{bmatrix} 0.00172 & 0.00154 & -0.0333 \\ 0.1025 & 0.388 & -0.377 \\ -0.0346 & -0.0194 & 0.124 \\ -0.00951 & -0.00052 & 6.548 \end{bmatrix}
\end{aligned} \tag{4.18}
$$

All linear empirical models used in this example had their origin at x_s. As the models were updated,

$h_{Li,3}$, $i = 2,3,4,5$, was updated to be a new linear quadratic regulator, but $\hat{V}$ was not changed in the LEMPC because it was sufficient for identifying the stability region of the nonlinear process under h_{Li}. The same stability region was used for the nonlinear process under all h_{Li} because for the simulations performed, these controllers were stabilizing within this region.

Fig. 4.3 presents the decrease of the pre-exponential factor values with time and indicates the four times at which the model re-identification was triggered (in all figures throughout the rest of this example, the zero on the time axis corresponds to the time at which the pre-exponential factor values first began to decrease). After the pre-exponential factor values reached their final values at the beginning of the twentieth operating period, the process was simulated for three additional operating periods, and no further model identification was triggered after the model update at the end of the twentieth operating period. This indicates that the proposed approach was effective at updating the empirical model of the process to account for variations in the plant, with each empirical model giving low plant-model mismatch during the duration of its use. The figure also shows that the error-triggering is successful at deciding the necessity of model updates, because even though the pre-exponential factors did decrease at the beginning of the eleventh, fifteenth, and nineteenth operating periods, no re-identification was required since the error did not exceed the pre-specified threshold. In addition, Fig. 4.4 presents the values of e_d with respect to time and shows the rise of the e_d values that triggered the model re-identification. At each time that $e_d(t_k)$ exceeded the value of 2.5 and the model was re-identified using the most recent input/output data, the value of $e_d(t_k)$ rapidly decreased. The input and state trajectories of the reactor process under the LEMPC of Eq. 4.6 with the empirical models of Eq. 4.13 and Eqs. 4.15-4.18 throughout the 12 operating periods after the pre-exponential factor values first began to decrease are presented in Figs. 4.5-4.6.

The on-line model identification not only decreases the plant-model mismatch, but also has a significant impact on the process economic performance. This is shown in Table 4.2, which presents the average yield and the maximum value of $e_d(t_k)$ for the two operating periods after the first on-line model re-identification (when the pre-exponential factors have the values $0.8k_1, 0.8k_2$,

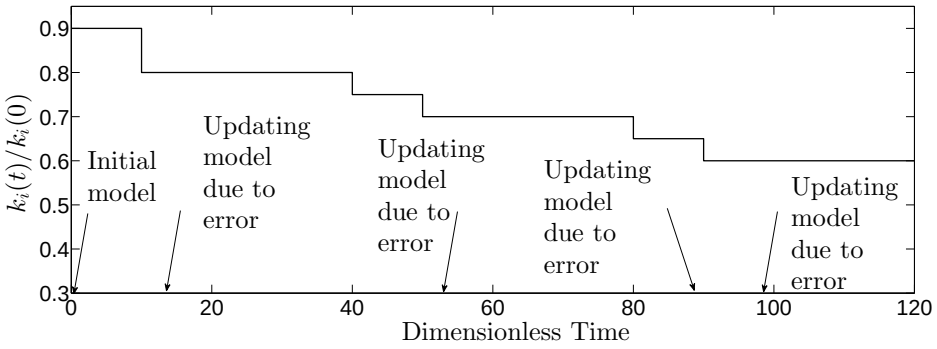

Figure 4.3: Plot presenting the decrease in the pre-exponential factor values and the times at which the model re-identification procedure was conducted over 12 operating periods (the zero on the time axis corresponds to the time at which the pre-exponential factor values first began to decrease).

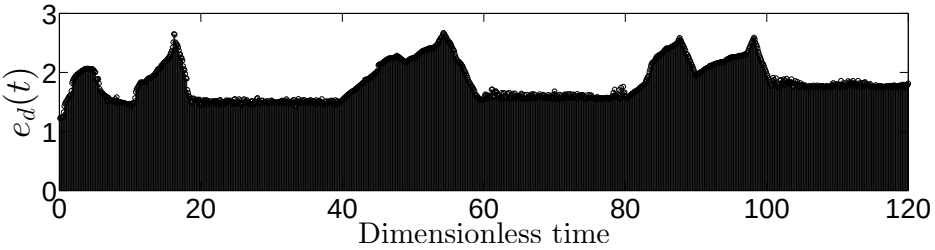

Figure 4.4: Value of error metric e_d using the detector of Eq. 4.14 and the integrated LEMPC design with error-triggered on-line model identification at each sampling time (the zero on the time axis corresponds to the time at which the pre-exponential factor values first began to decrease).

and $0.8k_3$) and also for the two operating periods after the final model identification (when the pre-exponential factors have the values $0.6k_1, 0.6k_2$, and $0.6k_3$). The data is presented for three approaches: the "1 Empirical Model" approach, in which the model is not re-identified and the initial empirical model (A_1 and B_1) is used throughout the entirety of process operation, the "On-line Model ID" approach, in which the proposed on-line model re-identification methodology is applied, and the "Nonlinear Model" approach, in which the nonlinear model of Eq. 4.9 is used in the LEMPC including the changes in the pre-exponential factor. This table shows that the use of on-line model identification significantly improves the process yield compared to using one empirical model throughout process operation, both when the pre-exponential factor changes slightly and, even more, when it changes significantly. In addition, it shows that though no study was performed to determine whether N_d, M, or $e_{d,T}$ should be updated as the process model changed in time due to the catalyst deactivation, the use of the on-line model updates still provided meaningful economic

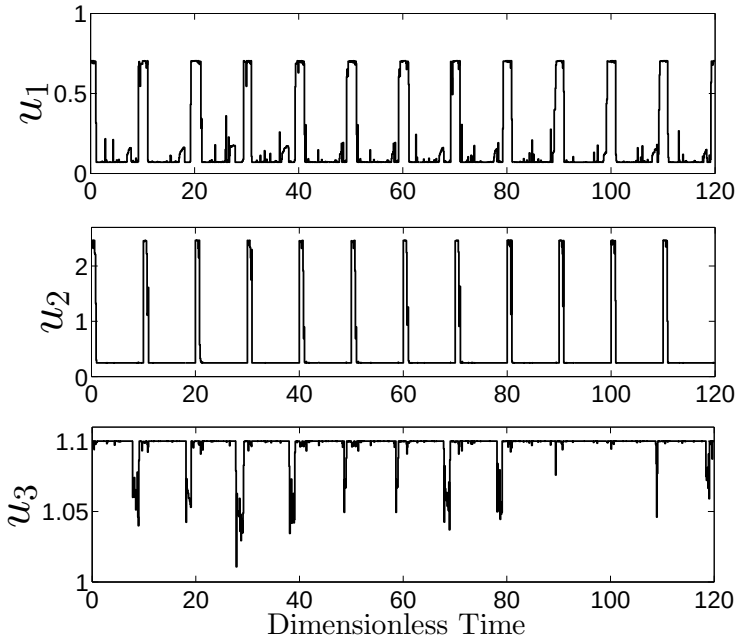

Figure 4.5: Input profiles of the closed-loop CSTR under the LEMPC using the error-triggered on-line model identification scheme starting from the final state reached in Fig. 4.2 (the zero on the time axis corresponds to the time at which the pre-exponential factor values first began to decrease).

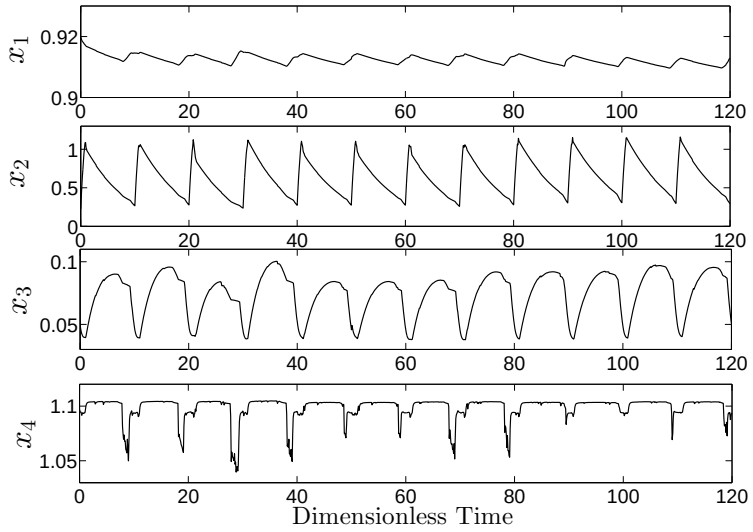

Figure 4.6: State profiles of the closed-loop CSTR under the LEMPC using the error-triggered on-line model identification scheme starting from the final state reached in Fig. 4.2 (the zero on the time axis corresponds to the time at which the pre-exponential factor values first began to decrease).

benefit.

Table 4.2: Relative prediction error and average yield for the CSTR under LEMPC.

	After 1^{st} on-line model ID		At final conditions	
Approach	Y	Max $e_d(t_k)$	Y	Max $e_d(t_k)$
1 Empirical Model	8.46	3.41	6.89	9.75
On-line Model ID	8.71	1.65	7.91	1.86
Nonlinear Model	8.80	-	8.02	-

4.4.2 Application of Error-Triggered On-Line Model Identification to Operating Region Changes

A second application of the error-triggered on-line model identification strategy is for shifts in the region of process operation such that the initial linear model does not capture the nonlinear process dynamics as well as desirable after the shift. This may occur, for example, if the model identified around a desired steady-state does not capture the nonlinear dynamics in the entire region of state-space around this steady-state that is accessed by the process states in the presence of disturbances. It may also occur if the initial linear model is identified for a certain steady-state but it is desirable to switch the steady-state of process operation at a time t'. In addition, it may occur if a control strategy that promotes time-varying operation within a region of state-space for economic reasons, such as LEMPC, is used and it is desirable to expand, shrink, or otherwise adjust the operating region in time for economic or safety reasons. In each case, the steps of the implementation strategy discussed in the section "Implementation Strategy for Error-Triggered On-Line Model Identification" are followed, but the procedure may be re-initialized at Step 1 at certain points during process operation or the operating region may be adjusted independently of the linear empirical model during Step 2 (which will be discussed further below).

We will first address the case (Case 1) that the initial linear empirical model does not capture the nonlinear process dynamics in the full region of state-space that is accessed by the process when disturbances occur, and it is desired to track a given steady-state. Consider the case that the process

is originally operated in a region of state-space around the initial steady-state, and the initial linear empirical model captures the nonlinear process dynamics well in this region. Then, a disturbance moves the process state away from the steady-state to a new region where the initial linear empirical model does not capture the nonlinear process dynamics well. If the process is operated under the error-triggered on-line model identification procedure, the increase in prediction error would be expected to eventually trigger model re-identification. However, it may take some time for the triggering to occur, or if it is triggered quickly, the model identified may not capture the nonlinear dynamics as well as desirable if there is not yet sufficient input/output data in the new region of operation (particularly if the disturbance moves the state away from its original operating region quickly). To overcome such issues, multiple linear empirical models may be identified at a number of locations throughout the region of state-space which the process states are expected to access before initiating the error-triggered on-line model identification process. Then, when the error-triggered on-line model identification process is initiated, the initial empirical model used in Step 1 of the implementation strategy can be taken to be that which was developed using process data from the state-space region closest to the initial state-space point. This may lead to an initial linear empirical model that better captures the nonlinear dynamics at the initial state-space location and may lead to better model-based controller design. The monitoring and control system could also re-initialize the implementation strategy at Step 1 when the process state moves away significantly from the region where Step 1 was last implemented, with the initial linear empirical model used in Step 1 as that developed from data in state-space closest to the current state-space point. As the controller then drives the process state toward the desired steady-state, the error-triggering procedure would allow more accurate models to be determined.

A second case (Case 2) in which error-triggered on-line model identification may be applied to changes in the region of process operation is the case that it is desired to change the operating steady-state. In this case, before initializing the error-triggered on-line model identification strategy, it may be desirable to obtain initial linear empirical models with respect to both steady-states. The error-triggered on-line model identification implementation strategy would be started from

Step 1 at $t = 0$ with the linear empirical model around the first steady-state and would be re-started from Step 1 at t' with the linear empirical model around the second steady-state.

The final case (Case 3) mentioned above for the application of error-triggered on-line model identification to changes in the operating region is the case that the region of operation is adjusted on-line for the process under LEMPC. As shown in Eq. 4.6, LEMPC searches for economically optimal control actions that maintain the predicted state within the level set $\Omega_{\hat{\rho}_{ei}}$, subject to the other constraints. It may be desirable to expand, shrink, or change the size or orientation of the level set on-line for a variety of reasons. It may be desirable to expand the level set because the expansion of the level sets can allow the LEMPC to search for economically optimal control actions throughout a larger region of state-space, and thus the controller may find a more profitable manner of operating the process than if it could only search in a smaller region. Alternatively, it may be desirable to shrink the level set to prevent the process from operating in as large a region of state-space for safety reasons. It may also be desirable to adjust the size or orientation of the level set on-line if the state of the closed-loop system under EMPC moves toward a boundary of the initial level set to increase profit. Then, the adjustment of the size or orientation of the level set may allow the state to move into areas beyond this boundary in which the profit can be further increased for the closed-loop system.

The aforementioned level set adjustments can be implemented in Step 2 of the error-triggered on-line model identification procedure by changing the level set of the linear empirical model used in the LEMPC of Eq. 4.6 at a desired rate while the process is operated under the LEMPC with an empirical model. These level set changes (accompanied by changes to the Lyapunov function and Lyapunov-based controller when necessary, e.g., when the level set orientation is adjusted) occur at the determined rate independently of model re-identifications, which occur only when e_d exceeds $e_{d,T}$. The rate at which the level sets are changed should allow for the collection of a sufficient amount of input/output data in the new state-space regions accessed during the level set adjustment for the calculation of $e_d(t_k)$ and for future possible model re-identification. This rate can be set before initiation of the error-triggered on-line model identification procedure, or

can be deduced on-line by trying different rates and seeing whether the process state begins to traverse the new regions of state-space too quickly for collection of sufficient input/output data, or too slowly for the desired economic or safety considerations. The level set changes continue until the final desired level set is reached. The final desired level set should be one in which process closed-loop stability can be maintained (e.g., for the case of expanding level sets, it cannot be larger than the region within which closed-loop stability of the system of Eq. 4.1 is maintained under the LEMPC with an empirical model) and which is feasible (i.e., a solution exists in this region in which all process constraints can be met), but it also should be a level set that allows profit to be appropriately maximized (e.g., for the case of expanding level sets, it should be as large as possible since restrictions to the region of operation may reduce process profit compared to that which could be obtained if there were less restrictions). Fig. 4.7 illustrates the concepts presented specifically for the expansion of level sets. Because for this changing level set case, the level set in Eqs. 4.6e-4.6f can change even when the $i-th$ model is retained, the level set in these equations will be denoted by $\Omega_{\hat{\rho}_{e,q}}$ in the remainder of the discussion of LEMPC with changing level sets.

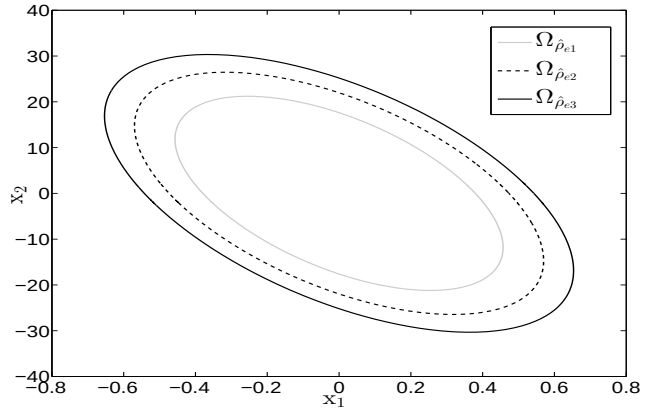

Figure 4.7: Example of level set expansion from $\Omega_{\hat{\rho}_{e1}}$ to $\Omega_{\hat{\rho}_{e2}}$ and to $\Omega_{\hat{\rho}_{e3}}$.

It is notable that the use of the error-triggered on-line model identification procedure for model-based control design with operating region changes provides significant practical advantages compared to using multiple linear models identified *a priori*. The *a priori* models may indeed be used for low-dimensional systems (i.e., processes whose state-space is of dimension two or three) for

which assessing all areas throughout the region of operation in which new linear empirical models should be identified *a priori* is computationally attractive (e.g., multiple linear empirical models in the context of LEMPC has been investigated in[89]). However, as the dimension of the system increases, it is very time-consuming computationally to search the region of operation to determine all possible areas in which a new linear empirical model should be identified *a priori*. A benefit of the proposed error-triggered approach is that it identifies models only in the regions of state-space that are accessed by the process and there is no need to obtain large amounts of input-output data in regions that the states do not actually access. This is a significant practical advantage of the proposed method, particularly since many models used in the chemical industry have tens or hundreds of states for which it would not be possible to *a priori* investigate the entire state-space to develop multiple linear models. In addition, the multiple linear empirical models approach implicitly assumes that the plant dynamics do not change in time so that any models identified *a priori* remain valid throughout time. The error-triggered on-line model identification approach, however, can handle changes in the plant dynamics in time (even concurrently with operating region changes). However, part of the theoretical challenge of proving closed-loop stability of a nonlinear process under the error-triggered on-line model identification method is that it is not known *a priori* when the moving horizon error detector will trigger an on-line model identification or what new model will be obtained in this case, though all models are known *a priori* in the multiple linear empirical models case.

Remark 12 *In Case 1, multiple initial empirical models were developed before initiating the on-line model identification strategy, but all with their origin at the desired steady-state. However, it is possible that if the state moves far from the desired steady-state, it may be difficult to identify an empirical model with the origin at the desired steady-state that will be sufficiently accurate for use in model-based control design. Thus, an alternative to developing multiple initial empirical models with origins at the desired steady-state before initiating the on-line model identification strategy is to develop multiple initial linear empirical models with their origins at state-space points that are not the desired steady-state. Then, when the state is driven far from the operating steady-*

state, a path can be designed to drive the process state through a number of these intermediate state-space points to the origin. Whenever one of the selected points in the path to the steady-state is approached sufficiently closely, the error-triggered on-line model identification strategy can be re-initiated at Step 1 using the initial linear empirical model corresponding to the next desired steady-state in the path. Error-triggering is used to improve the models as the process state transitions between the selected steady-states on its way to the desired operating steady-state. A similar method could be used in Case 2 of this section to guide the state between two steady-states if desired.

Remark 13 *For the LEMPC with expanding level sets, or with level sets that change orientation or size in time, it may be possible to set* $\Omega_{\hat{\rho}_{e,1}}$ *to the desired final level set of operation and to use the error-triggered on-line model identification procedure to change the linear empirical model as the process state moves throughout* $\Omega_{\hat{\rho}_{e,1}}$ *instead of following a level set adjustment procedure. However, the region* $\Omega_{\hat{\rho}_{e,1}}$ *may be large enough such that the linear empirical model developed for the initial state-space point cannot capture the nonlinear dynamics of the process as well as desired in the most economically optimal location of state-space. If the LEMPC calculates control actions that cause the state to quickly move toward the economically optimal location and leave the state-space region where the initial linear empirical model captures the nonlinear process dynamics well, the moving horizon error detector may trigger model re-identification, but there may be insufficient input/output data stored in the new region of operation for an appropriate linear empirical model to be identified when the error-triggering occurs. This shows that one advantage of the level set adjustment procedure described is that it can allow the rate at which level sets are changed to be slow enough for sufficient input/output data to be collected in the new regions of operation that are accessed as the level sets change. The effect of the rate at which the level sets are adjusted is illustrated in the chemical process example of the following section. In addition, when the level set orientation or size is adjusted on-line (instead of only expanded), the opportunity is available to move the state throughout regions which cannot be captured within one level set alone. If* $\Omega_{\hat{\rho}_{e,1}}$ *is set to the final level set of operation, several initial linear empirical*

models within $\Omega_{\hat{\rho}_{e,1}}$ may be developed and used to re-initiate Step 1 of the error-triggered on-line model identification procedure, as discussed in Remark 12, to improve the model predictions throughout $\Omega_{\hat{\rho}_{e,1}}$.

Remark 14 *Feasibility and closed-loop stability of model-based controllers under the on-line model identification strategy when changes in the region of operation occur will depend on many factors including the type of controller, the extent of the change in the operating region, and the manner in which the change occurs (e.g., whether several pre-identified linear empirical models are used to define a path to a steady-state as described above). As noted in Remark 11, controller feasibility and closed-loop stability of a process under a model-based controller based on the linear empirical models with operating region changes is outside the scope of this chapter, but the factors mentioned in that remark (e.g., the values of N_d, M, and $e_{d,T}$, computation time, and assumptions on the process and controller) could be considered for such proofs. For the LEMPC with expanding level sets, for example, the assumption that $D_{L1} \subset D_{L2} \subset \cdots \subset D_{L\tilde{M}}$ and $\Omega_{\hat{\rho}_1} \subset \Omega_{\hat{\rho}_2} \subset \cdots \subset \Omega_{\hat{\rho}_{\tilde{M}}}$, where $\Omega_{\hat{\rho}_{\tilde{M}}}$ is the final desired level set, may be useful. Even when it is difficult to find controllers that would meet the assumptions required by the proofs, there are many practical applications in which the approach proposed in this chapter would be stabilizing when the empirical models of Eq. 4.3 can sufficiently capture the nonlinear behavior of the system of Eq. 4.1. In addition, the values of N_d, M, and $e_{d,T}$ can be updated on-line or through experiments as described in the section "Application of Error-Triggered On-Line Model Identification to Plant Variations."*

Application of Error-Triggered On-Line Model Identification to Operating Region Changes: Application to a Chemical Process Example

This section uses a chemical process example to illustrate the application of error-triggered on-line model identification to LEMPC with expanding level sets (though this example only demonstrates Case 3 from the prior section, all three cases are conceptually similar in the sense that the process states vary throughout different regions of state-space under a controller developed from the

error-triggered on-line model identification strategy, so this example demonstrates the concept of operating region changes in general). The chemical process considered is the irreversible second-order exothermic reaction of A to B in a well-mixed, non-isothermal continuous stirred tank reactor (CSTR). The reactor feed enters with a volumetric flow rate F and consists of an inert solvent containing the reactant A with a concentration C_{A0} and a temperature T_0. The CSTR is heated and cooled at a heat rate Q through a jacket. The volume, density, and heat capacity of the liquid in the CSTR are assumed constant at V, ρ_L, and C_p, respectively. The dynamic equations describing the time evolution of the reactant concentration C_A and temperature T in the reactor have the form presented below:

$$\frac{dC_A}{dt} = \frac{F}{V}(C_{A0} - C_A) - k_0 e^{-E/RT} C_A^2 \tag{4.19a}$$

$$\frac{dT}{dt} = \frac{F}{V}(T_0 - T) - \frac{\Delta H k_0}{\rho_L C_p} e^{-E/RT} C_A^2 + \frac{Q}{\rho_L C_p V} \tag{4.19b}$$

where k_0 denotes the reaction pre-exponential factor, and E and ΔH denote the activation energy and the enthalpy of the reaction, respectively (see Table 4.3 for the process parameter values). The CSTR is controlled by an LEMPC that adjusts the values of the inlet concentration C_{A0} and the heat supply/removal rate Q. These manipulated inputs are bounded above and below as follows: $0.5 \leq C_{A0} \leq 7.5\ kmol/m^3$ and $-5.0 \times 10^5 \leq Q \leq 5.0 \times 10^5\ kJ/hr$. The CSTR is operated within a state-space region around the open-loop asymptotically stable steady-state $[C_{As}\ T_s] = [1.2\ kmol/m^3\ 438.0\ K]$ which corresponds to the steady-state input vector $[C_{A0s}\ Q_s] = [4.0\ kmol/m^3\ 0.0\ kJ/hr]$. The reactor states and inputs will be written in deviation variable form with respect to this steady-state as $x^T = [C_A - C_{As}\ T - T_s]$ and $u^T = [C_{A0} - C_{A0s}\ Q - Q_s]$. The explicit Euler method was used to numerically integrate the dynamic model of Eq. 4.19 and all empirical models used in this example with an integration time step of $h_c = 10^{-4}\ hr$.

The LEMPC objective is to maximize the production rate of the desired product B (the process profit). Thus, the cost function $L(x,u)$ in the LEMPC design is the average production rate of B,

Table 4.3: Parameter values of the CSTR.

$F = 5.0$	$\frac{m^3}{hr}$	$k_0 = 8.46 \times 10^6$	$\frac{m^3}{kmol\ hr}$
$T_0 = 300$	K	$\Delta H = -1.15 \times 10^4$	$\frac{kJ}{kmol}$
$V = 1.0$	m^3	$E = 5.0 \times 10^4$	$\frac{kJ}{kmol}$
$C_p = 0.231$	$\frac{kJ}{kg\ K}$	$\rho_L = 1000$	$\frac{kg}{m^3}$
$R = 8.314$	$\frac{kJ}{kmol\ K}$		

which is given by:

$$L(x,u) = \frac{1}{(t_{k+N} - t_k)} \int_{t_k}^{t_{k+N}} k_0 e^{-E/RT(\tau)} C_A^2(\tau)\, d\tau\ . \tag{4.20}$$

We also consider that the amount of reactant material available in a given period of operation of length $t_p = 1\ hr$ is limited by the following material constraint:

$$\frac{1}{t_p} \int_0^{t_p} u_1(\tau)\, d\tau = 0.0\ kmol/m^3. \tag{4.21}$$

Because the feed flow rate is fixed, this constraint requires that the amount of reactant fed to the reactor throughout one operating period be the same as the amount that would be fed for steady-state operation.

We assume that the nonlinear process model in Eq. 4.19 is unavailable and that to develop an LEMPC to meet the above objective and constraints, we must identify an empirical model. To construct an empirical state-space model that accurately predicts the process states within a region local to the initial state (the steady-state) of the CSTR, a sequence of step inputs was generated and applied to the CSTR and the resulting output sequence was collected. The ordinary multivariable output error state-space (MOESP)[43] algorithm using input and output data sequences was carried out to obtain a linear empirical model for the CSTR of Eq. 4.19. This initial ($i = 1$) model was validated using various step, impulse, and sinusoidal input responses and is described by the following matrices:

$$A_1 = \begin{bmatrix} -34.5 & -0.473 \\ 1430 & 18.1 \end{bmatrix},\ B_1 = \begin{bmatrix} 5.24 & -8.1 \times 10^{-6} \\ -11.6 & 0.457 \end{bmatrix} \tag{4.22}$$

Because it is assumed that only the empirical model is available, the Lyapunov-based controller designed for use in LEMPC is based on the empirical model of Eq. 4.22. The quadratic Lyapunov function $\hat{V}(x) = x^T P x$, where P is the following positive definite matrix:

$$P = \begin{bmatrix} 1060 & 22 \\ 22 & 0.52 \end{bmatrix} \tag{4.23}$$

was used to design a Lyapunov-based controller $h_{L1}^T(x) = [h_{L1,1}(x)\ h_{L1,2}(x)]$ for use in the LEMPC. To meet the material constraint of Eq. 4.21, the control law $h_{L1,1}(x)$ for the inlet reactant concentration was fixed to 0.0 $kmol/m^3$. The control law $h_{L1,2}(x)$ for the rate of heat input was developed using the following control law from:[27]

$$h_{L1,2}(x) = \begin{cases} -\dfrac{L_{\tilde{f}}\hat{V} + \sqrt{L_{\tilde{f}}\hat{V}^2 + L_{g_2}\hat{V}^4}}{L_{g_2}\hat{V}}, & \text{if } L_{g_2}\hat{V} \neq 0 \\ 0, & \text{if } L_{g_2}\hat{V} = 0 \end{cases} \tag{4.24}$$

where $\tilde{f} : R^n \to R^n$ and $g : R^n \to R^n \times R^m$ are defined based on the empirical model of Eq. 4.3 as follows:

$$\frac{dx(t)}{dt} = \underbrace{Ax}_{=:\tilde{f}(x)} + \underbrace{B}_{=:g(x)} u\ , \tag{4.25}$$

and $g_2(x)$ is the second column of the B matrix. $L_{\tilde{f}}\hat{V}$ and $L_{g_2}\hat{V}$ denote the Lie derivatives of the Lyapunov function $\hat{V}(x)$ with respect to $\tilde{f}(x)$ and $g_2(x)$, respectively. We assume that the stability region $\Omega_{\hat{\rho}_1}$ is not known a priori (this is the typical case in practice if the nonlinear process model is not known, because Ω_{ρ_1} is defined in the section "Lyapunov-Based Economic Model Predictive Control with Empirical Models" to be a region within which the controller h_{L1} designed based on the linear empirical models stabilizes the nonlinear system), so we initiate process operation within a level set denoted $\Omega_{\hat{\rho}_{e,1}} \subseteq \Omega_{\hat{\rho}_{e1}}$ within which the model prediction error is low. Extensive simulations were performed for the closed-loop system under the Lyapunov-based controller $h_{L1}(x)$ to define the level set $\Omega_{\hat{\rho}_{e,1}}$ with $\hat{\rho}_{e,1} = 55$. This is a region within which the linear model of Eq. 4.22

captures the nonlinear dynamics of Eq. 4.19 well. In all simulations below, we apply the LEMPC design in Eq. 4.6 but with the added material constraint of Eq. 4.21 to the process in Eq. 4.19 using a prediction horizon of $N = 10$ and a sampling period of $\Delta = 0.01$ hr (the objective function is defined by Eq. 4.20, with the bounds on C_{A0} and Q and the Lyapunov function noted above). The LEMPC optimization problem is solved at each sampling period using the interior point solver IPOPT.[119]

Though there is low prediction error in $\Omega_{\hat{\rho}_{e,1}}$ when the model of Eq. 4.22 is used, we would like to expand the level set of operation to improve the process profit. To do this, we note that if $\Omega_{\hat{\rho}_{e,1}}$ is not equal to $\Omega_{\hat{\rho}_{e1}}$, we can use a larger level set $\Omega_{\hat{\rho}_{e,2}} \subseteq \Omega_{\hat{\rho}_{e1}}$ in the LEMPC based on an empirical model while continuing to use the empirical model with $i = 1$. We denote the $q-th$ level set used from the start of process operation as $\Omega_{\hat{\rho}_{e,q}}$ (the final desired level set is $\Omega_{\hat{\rho}_{e,f}}$). Each time that the level set is expanded, we will calculate control actions based on the LEMPC of Eq. 4.6, but with the level set used in Eqs. 4.6e-4.6f as $\Omega_{\hat{\rho}_{e,q}}$. The values of $\hat{\rho}_{e,q}$ and the time intervals over which they will be applied are pre-determined, but the empirical model used with a given $\Omega_{\hat{\rho}_{e,q}}$ is not known a priori, but is determined during process operation using the moving horizon error detector to trigger model re-identification.

To demonstrate the need for re-identification of the empirical model as the region of process operation is expanded, the CSTR was operated in closed-loop under the LEMPC controller designed with the linear model of Eq. 4.22 within the region $\Omega_{\hat{\rho}_{e,1}}$ with $\hat{\rho}_{e,1} = 55$ for one hour of operation. Throughout this operating period, there was very low prediction error between the linear empirical model and the nonlinear CSTR model because this stability region had been chosen as one within which the plant-model mismatch was low. We subsequently increased the value of $\hat{\rho}_{e,1}$ used to define the Lyapunov-based constraints by 1 every Δ for the first 20 sampling periods of the second hour of operation (i.e., $\hat{\rho}_{e,1}$ was incrementally increased from $\hat{\rho}_{e,1} = 55$ to $\hat{\rho}_{e,21} = 75$ in 0.2 hr, where $\hat{\rho}_{e,2} = 56$ in the LEMPC of Eq. 4.6 at $t_k = 1$ hr, $\hat{\rho}_{e,3} = 57$ in the LEMPC of Eq. 4.6 at $t_k = 1.01$ hr, etc.) to optimize the process economics within a larger region of state-space. After reaching the level set with $\hat{\rho}_{e,21} = 75$, the system was maintained at that level set for the rest of

the second hour and throughout the third hour of operation as presented in Fig. 4.8. As the states moved out of the initial level set with $\hat{\rho}_{e,1} = 55$, the prediction error between the predicted states from Eq. 4.22 and the measured states of the CSTR increased and reached a value:

$$\frac{|T_p(3t_p) - T(3t_p)|}{|T(3t_p)|} + \frac{|C_{A_p}(3t_p) - C_A(3t_p)|}{|C_A(3t_p)|} = 0.3$$

at the end of the third hour. Because there are no disturbances or measurement noise in this simulation, the prediction error noted indicates that the total relative error in the two states is about 30% at the end of the third operating period, which shows that model re-identification should be used to better capture the nonlinear system dynamics in that region of state-space.

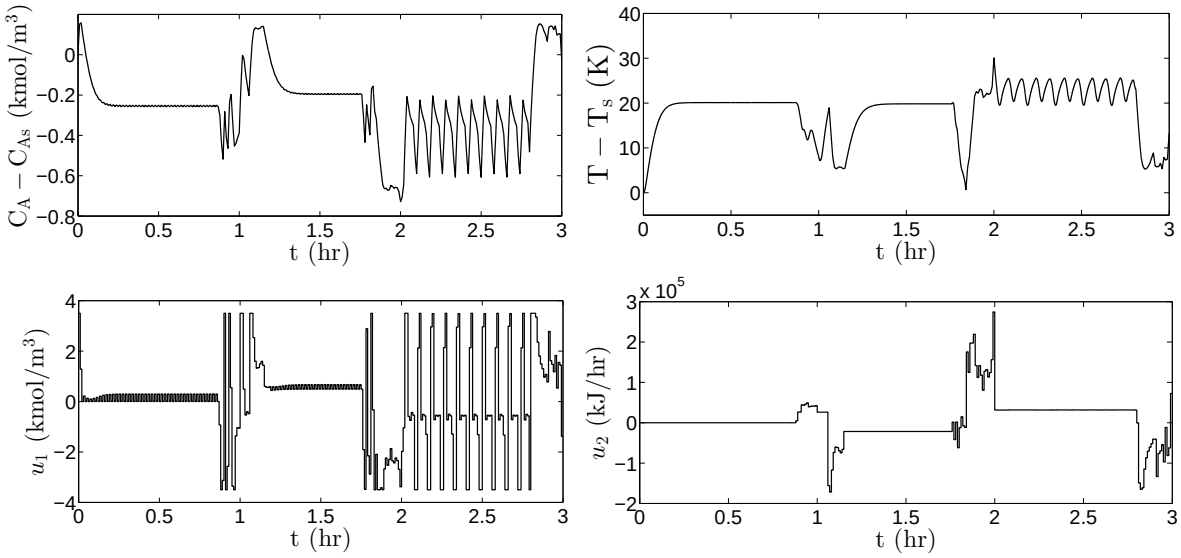

Figure 4.8: State and input trajectories of the CSTR controlled using the LEMPC with the empirical model of Eq. 4.22 starting at (C_{As}, T_s). The level set was changed from $\hat{\rho}_{e,1} = 55$ to $\hat{\rho}_{e,21} = 75$ gradually in the second hour.

After establishing the need for re-identification of a linear model as the allowable region of operation is expanded to increase profit, we now present three approaches for expanding the level sets from the level set with $\hat{\rho}_{e,1} = 55$ to a final desired level set with $\hat{\rho}_{e,f} = 155$ while gathering process input/output data and updating the model on-line. In the first approach, the level set is expanded suddenly to $\Omega_{\hat{\rho}_{e,f}}$. In the second approach, the level set is expanded incrementally to

$\Omega_{\hat{\rho}_{e,f}}$. In the third approach, the level set is incrementally expanded to $\Omega_{\hat{\rho}_{e,f}}$, with the expansion paused at intermediate level sets to allow sufficient input/output data to be collected throughout time in new regions of operation. The model identification process is triggered in the third approach by a moving horizon error detector. The collection of large amounts of input/output data in each region of operation allows the empirical models identified using the third approach to better capture the nonlinear process dynamics than the empirical models identified using the other approaches.

As mentioned above, the first approach investigated the sudden expansion of the level set $\Omega_{\hat{\rho}_{e,1}}$ with $\hat{\rho}_{e,1} = 55$ to $\Omega_{\hat{\rho}_{e,f}}$ with $\hat{\rho}_{e,f} = \hat{\rho}_{e,2} = 155$, after operating with $\hat{\rho}_{e,1} = 55$ for one hour. To maximize the profit in the new level set, the LEMPC of Eq. 4.6 predicted control actions that drove the state to regions of state-space where there was significant prediction error throughout the second hour of operation. At the end of this second hour, input/output data from the first two hours of operation was used to identify a new model and update the LEMPC with this new empirical model for the third hour of operation. The model obtained was:

$$A_2 = \begin{bmatrix} -46 & -0.610 \\ 2025 & 25.7 \end{bmatrix}, \; B_2 = \begin{bmatrix} 2.585 & -67 \times 10^{-6} \\ 65.36 & 0.639 \end{bmatrix} \tag{4.26}$$

Though all LEMPC optimization problems for the first approach were feasible and the closed-loop system was stable as shown in Fig. 4.9, the large prediction error throughout the second operating period resulting from the sudden expansion of the level set is undesirable. Therefore, the second approach that gradually increments the level sets was investigated. In this approach, after an hour of operation with $\hat{\rho}_{e,1} = 55$, the value of $\hat{\rho}_{e,1}$ was incrementally increased by 1 every sampling period for an hour to $\hat{\rho}_{e,f} = \hat{\rho}_{e,101} = 155$, while collecting input/output data. The prediction error during the second hour of operation was much less using this second approach than using the first approach. At the end of the second hour of operation, the input/output data from the first two hours of operation was used to identify the following empirical model that was used for the third hour of

operation:

$$A_2 = \begin{bmatrix} -47 & -0.643 \\ 1868 & 24.6 \end{bmatrix}, \; B_2 = \begin{bmatrix} 4.273 & -63 \times 10^{-6} \\ 16.65 & 0.632 \end{bmatrix} \tag{4.27}$$

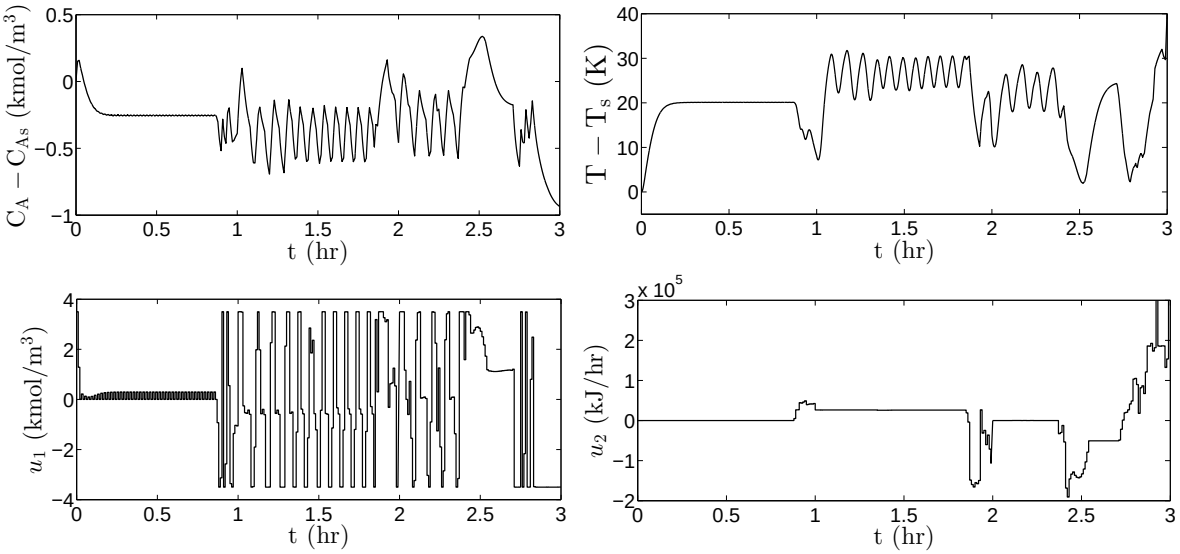

Figure 4.9: State and input trajectories of the CSTR controlled using the LEMPC with the empirical models in Eqs. 4.22 and 4.26. The level set was changed from $\hat{\rho}_{e,1} = 55$ to $\hat{\rho}_{e,2} = 155$ suddenly at the beginning of the second hour of operation (Approach 1).

Fig. 4.10 shows the state and input trajectories of the CSTR under the LEMPC of Eq. 4.6 using the second approach. The state and input trajectories for the first and second approaches are different, which shows that the empirical model used in the LEMPC and the way in which the level sets are expanded significantly affects the closed-loop process dynamics.

The third approach investigated is the gradual increase of the level set from $\hat{\rho}_{e,1} = 55$ to $\hat{\rho}_{e,f} = \hat{\rho}_{e,101} = 155$ throughout 10 hours of operation with error-triggered on-line model identification. First, the CSTR is operated at the level set with $\hat{\rho}_{e,1} = 55$ for one hour. Subsequently, the value of $\hat{\rho}_{e,1}$ is incrementally increased by 1 every sampling period for 20 sampling periods and then held at its new value for 1.8 hours (i.e., $\hat{\rho}_{e,21} = 75$ from $t_k = 1.19$ *hr* to 3 *hr*, $\hat{\rho}_{e,41} = 95$ from $t_k = 3.19$ *hr* to 5 *hr*, etc.). This increase and hold strategy is repeated until the final level set with $\hat{\rho}_{e,101} = 155$ is reached, and then the process is operated at the final level set for 2.8 hours. At the beginning of the third operating period, a moving horizon error detector is initiated to determine

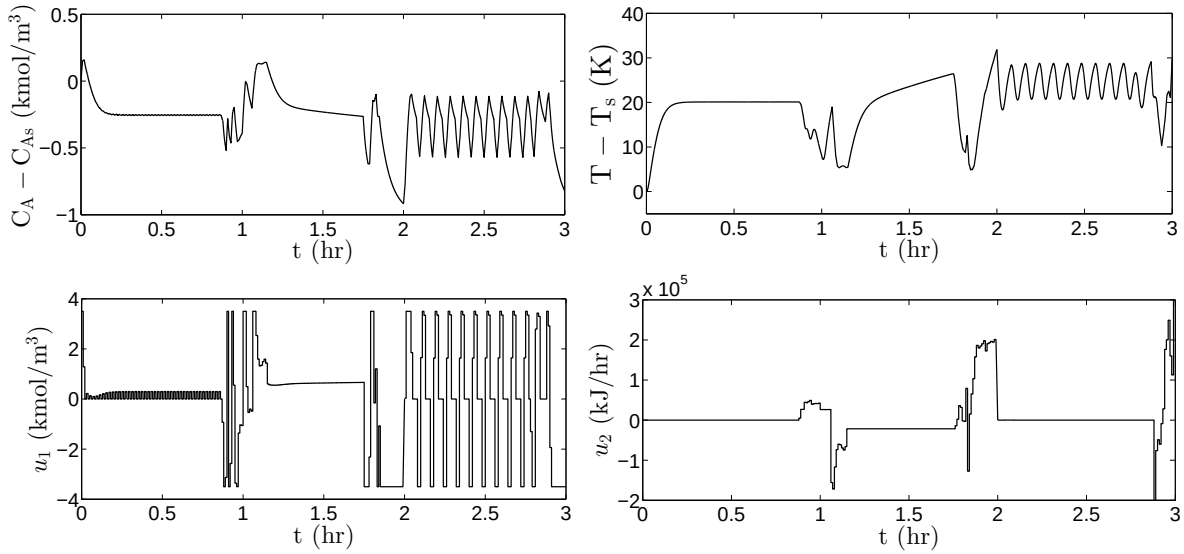

Figure 4.10: State and input trajectories of the CSTR controlled using the LEMPC with the empirical models in Eqs. 4.22 and 4.27. The level set was changed from $\hat{\rho}_{e,1} = 55$ to $\hat{\rho}_{e,101} = 155$ incrementally throughout the second hour of operation (Approach 2).

e_d at each sampling period, and to trigger re-identification of the process model when the value of e_d exceeds the threshold value of 3, which was chosen based on simulations that suggested that it was a reasonable indicator of significant plant-model mismatch. Each time that the on-line model identification is triggered, the previous two hours of input/output data is used to identify a new model. The moving horizon error detector calculates the relative prediction error in the concentration and temperature throughout the past 50 sampling periods and current sampling time as follows:

$$e_d(t_k) = \sum_{r=0}^{50} \frac{|T_p(t_{k-r}) - T(t_{k-r})|}{|T(t_{k-r})|} + \frac{|C_{A_p}(t_{k-r}) - C_A(t_{k-r})|}{|C_A(t_{k-r})|} \tag{4.28}$$

The predicted values of T and C_A were calculated using the first approach from Remark 8.

The moving horizon error detector triggered model re-identification four times throughout the gradual increase of the level set from $\hat{\rho}_{e,1} = 55$ to $\hat{\rho}_{e,101} = 155$ in the third approach, with the four

identified models as follows:

$$A_2 = \begin{bmatrix} -41 & -0.559 \\ 1424 & 18.149 \end{bmatrix}, B_2 = \begin{bmatrix} 4.92 & -7 \times 10^{-6} \\ -28 & 0.003 \end{bmatrix} \tag{4.29}$$

$$A_3 = \begin{bmatrix} -43 & -0.584 \\ 1658 & 20.997 \end{bmatrix}, B_3 = \begin{bmatrix} 3.64 & -49 \times 10^{-6} \\ 29.1 & 0.525 \end{bmatrix} \tag{4.30}$$

$$A_4 = \begin{bmatrix} -41 & -0.476 \\ 1691 & 18.0 \end{bmatrix}, B_4 = \begin{bmatrix} 3.53 & -53 \times 10^{-6} \\ 56.8 & 0.594 \end{bmatrix} \tag{4.31}$$

$$A_5 = \begin{bmatrix} -29 & -0.403 \\ 820 & 9.63 \end{bmatrix}, B_5 = \begin{bmatrix} 4.22 & -29 \times 10^{-6} \\ 57.9 & 0.443 \end{bmatrix} \tag{4.32}$$

When the empirical models were re-identified, the controller of Eq. 4.24 was updated based on the new empirical model. The same value of $\hat{V}$ was used for all simulations.

Fig. 4.11 shows the update scheme used in the third approach and indicates the four times at which the error-triggered model re-identification occurred. Once the model was updated at the end of the tenth operating period, no further model identification was triggered in the last two operating periods, indicating that the third approach was able to successfully expand the level sets while updating the model so that process operation could be moved to a new region of state-space where the corresponding empirical model locally had low plant-model mismatch. The figure also shows that the error-triggering is effective at determining the necessity of model updates, because the model identified at the end of the second period of operation was able to be used for four hours of operation and two sets of level set expansions since the prediction error was low and thus no model identification was needed. Fig. 4.12 shows the value of e_d throughout time under the third approach, which shows the growth of e_d when the model re-identification was triggered and provides further evidence that the prediction error was low at the end of the 12 hours of operation. In addition, Fig. 4.13 shows the evolution of the state-space trajectories within the initial level set

and into the expanded level sets during process operation.

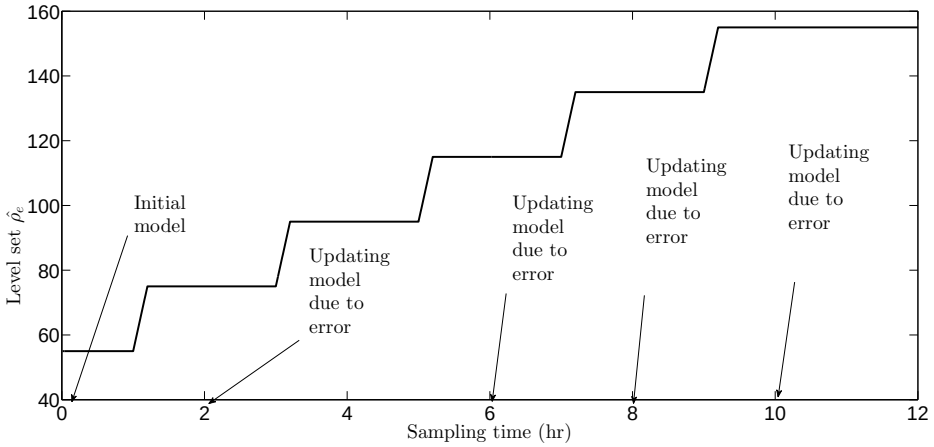

Figure 4.11: Plot showing the gradual expansion of the Lyapunov level set in Approach 3 and the times at which the model identification procedure was conducted over 12 hours of operation.

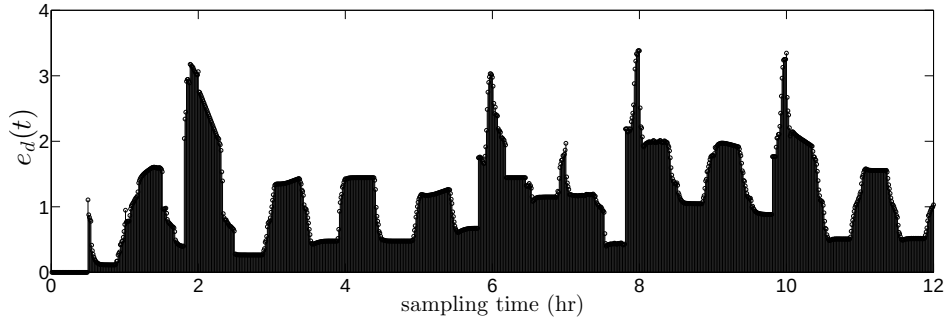

Figure 4.12: Value of e_d at each sampling time using Eq. 4.28 and the LEMPC design with error-triggered on-line model identification (Approach 3).

Fig. 4.14 shows the state and input trajectories of the CSTR using the LEMPC of Eq. 4.6 with the empirical models of Eq. 4.22 and Eqs. 4.29-4.32 for the third approach throughout the 12-hour simulation. Fig. 4.15 shows that the state and input trajectories of the CSTR under the LEMPC designed based on the first-principles model are similar to those under the LEMPC using the final empirical model of Eq. 4.32, when both use $\hat{\rho}_{e,f} = 155$ throughout the entire simulation (i.e., no level set expansion), and start from the same initial condition.

The three approaches presented above are compared in Table 4.4, which shows the time-averaged profit (J_e) and the maximum e_d throughout one hour of operation using the final identified

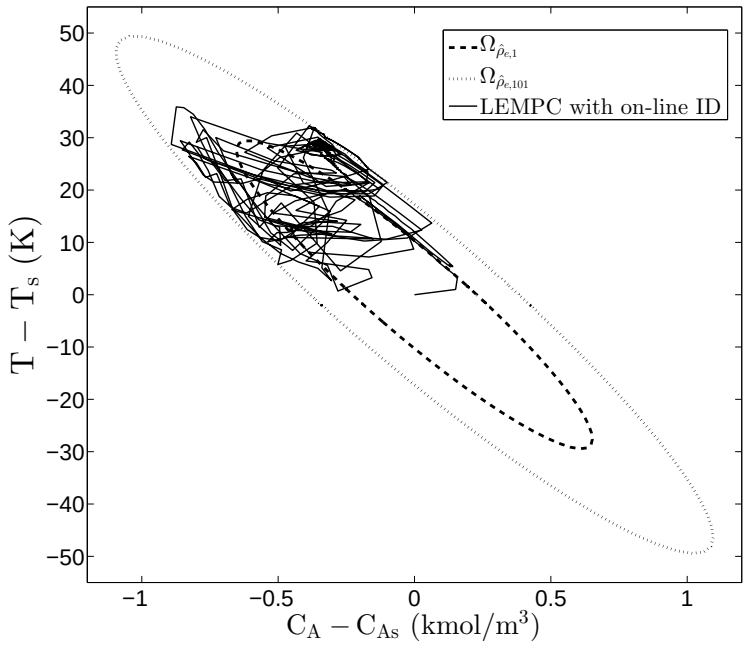

Figure 4.13: State-space representation of closed-loop state trajectories of the CSTR under the LEMPC with error-triggered on-line model identification for 12 *hr* starting at (C_{As}, T_s) (Approach 3).

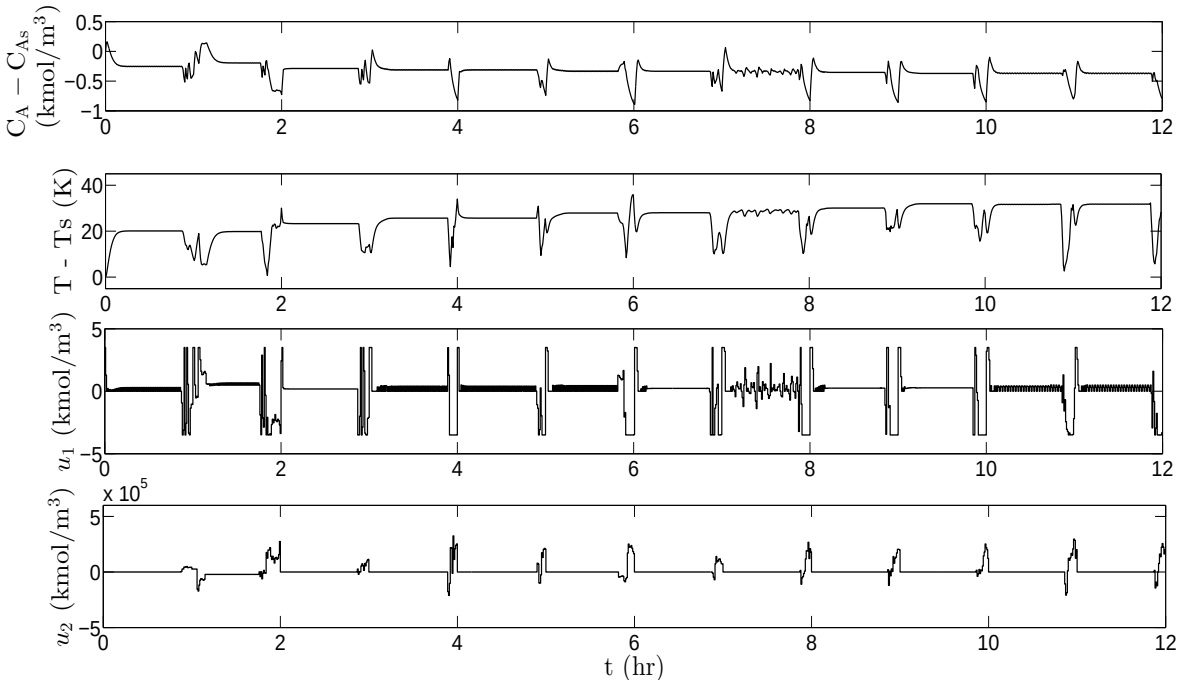

Figure 4.14: State and input trajectories of the CSTR controlled by the LEMPC with error-triggered on-line model identification over 12 *hr* operation (Approach 3).

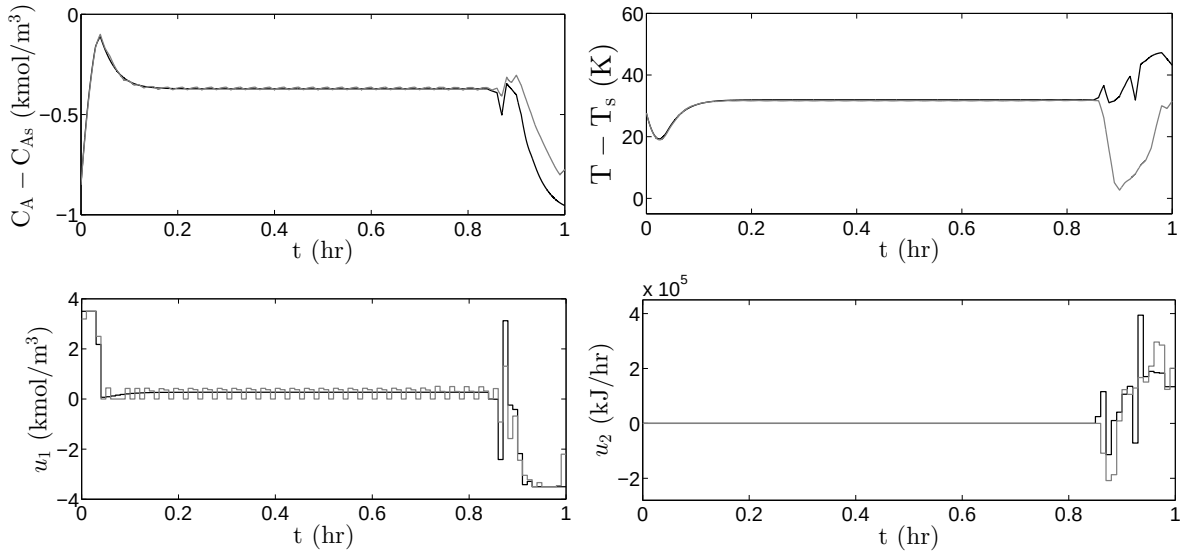

Figure 4.15: State and input trajectories of the CSTR controlled by the LEMPC using the first-principles model (black trajectories) and the LEMPC using the final identified model in Eq. 4.32 (gray trajectories) starting from $C_A - C_{As} = -0.8, T - T_s = 28$.

model for each approach and the level set with $\hat{\rho}_{e,f} = 155$ (J_e and e_d are calculated for the third hour of operation for the first two approaches, and for the twelfth hour of operation in the third approach). In addition, the profit resulting from using the nonlinear model of Eq. 4.19 is presented for comparison, initiated from the origin. Table 4.4 shows that the profit was greatest using the third approach, and was very close to that of the nonlinear system of Eq. 4.19 (the profit using the nonlinear model is only 0.7% greater than that using the third approach). In addition, Table 4.4 shows that the maximum value of e_d during process operation was greatest under the first approach and least under the third. The maximum value of e_d in the third approach is significantly lower than the threshold value of 3, further showing that the proposed approach was able to reduce the prediction error while maximizing profit.

Table 4.4: Average economic cost for the CSTR under LEMPC.

Approach	J_e	Max $e_d(t_k)$
1	15.621	11.7
2	15.70	5.98
3	16.49	1.73
Nonlinear Model	16.61	-

Remark 15 *In this example, the value of $\hat{\rho}_{e,f}$ was chosen because it allowed for a significant increase from $\hat{\rho}_{e,1}$ and thus was effective for illustrative purposes in this example at demonstrating the level set expansion procedure and the effect of the rate of expansion on the models identified. From the simulations, it can be seen that the nonlinear process was stabilized by the LEMPC with an empirical model within $\Omega_{\hat{\rho}_{e,f}}$ based on the various empirical models; however, choosing the value of $\hat{\rho}_{e,f}$ in general requires great care to prevent losing process closed-loop stability.*

Remark 16 *The time-varying nature of the trajectories calculated by the LEMPC in this example for the various level set expansion rates (Figs. 4.8-4.10 and 4.14-4.15) is due to economic considerations, as for the example in the section "Application of Error-Triggered On-Line Model Identification to Plant Variations: Application to a Chemical Process Example." As shown in these figures, closed-loop stability was maintained in all simulations, regardless of whether the empirical model was updated, but the error-triggered updating of the empirical models improves the predictions from the linear empirical model and can improve the process profit as shown in Table 4.4.*

4.5 Conclusion

In this chapter, a methodology for error-triggered on-line model identification for nonlinear process systems was proposed for use in model-based controller design based on linear empirical models. The error-triggering was conducted by a moving horizon error detector that quantifies the relative prediction error within its horizon and triggers model re-identification based on recent input/output data when the prediction error exceeds a threshold. The error-triggered on-line model identification procedure was shown to have many applications, including the improvement of state predictions for use in model-based control when plant variations occur and when the operating region changes. Both of these applications were demonstrated using a chemical process example under LEMPC. In the first example, it was shown that the error-triggering strategy was successful in indicating the need to re-identify the empirical model using the most recent input/output data as

the plant dynamics changed, which can also result in greater economic profit. The second example demonstrated that the proposed approach is able to maintain closed-loop stability while expanding the region of operation to improve profit, and also indicated that the rate at which the operating region is expanded can have a significant effect on the process performance and the accuracy of the identified empirical model.

Chapter 5

Fault-Tolerant Economic Model Predictive Control Using Error-Triggered On-line Model Identification

5.1 Introduction

Recent technological developments in the chemical and petrochemical industries have led to the creation of complex process networks to increase operational efficiency and meet the increasing energy demand. One approach for maximizing the efficiency of process operation is by integrating process control and process economic optimization. Economic model predictive control (EMPC) is a recent model-based feedback control strategy that integrates process control with dynamic economic optimization of the plant. EMPC promotes optimal time-varying operation of the plant and can incorporate constraints that ensure closed-loop stability (e.g.,[14,20,22,49]).

The first step in developing model-based feedback controllers is to establish a dynamic model representing the process dynamics, which can be done either from first principles or through system identification.[79] While first-principles models describe the underlying physico-chemical phenomena and develop detailed mathematical expressions for the observed process mechanisms, ob-

taining such models is a challenging task for complex and poorly understood processes. Instead, model identification provides suitable alternative models to be used for model-based feedback control when first-principles models are too complex or unavailable. Over the past four decades, various model identification methods have been developed to identify linear and nonlinear models from process data alone (e.g.,[1,76,79]).

Subspace model identification (SMI) refers to a class of system identification methods that are capable of identifying multiple-input multiple-output (MIMO) models based purely on input/output data.[16,43,44,56,76] SMI methods are non-iterative and account for multi-variable interactions.[39,76] Well-recognized SMI methods include numerical algorithms for subspace state-space system identification (N4SID),[39] the Canonical Variate Algorithm (CVA),[59] and the multi-variable output error state-space (MOESP) algorithm.[43,44] SMI methods have been widely used for industrial applications due to their reliability and numerical stability.[1,16,29,43] SMI methods have been used to provide models for various model-based feedback control systems such as model predictive control (MPC) and EMPC.[48,56]

A major problem that arises frequently in the chemical industry is actuator faults, in which authority over one or more actuators is lost. Detecting actuator faults and developing advanced fault-tolerant controllers for chemical process systems has been previously considered (e.g., in[120,121]). However, the existing works have assumed the availability of a first-principles model to develop fault-tolerant control methodologies. To date, no work on formulating fault-tolerant control strategies using empirical models has been considered. In the present chapter, we introduce a data-driven approach to overcome actuator faults in Lyapunov-based economic model predictive control (LEMPC) based on linear empirical models, which can be extended to other model-based feedback control designs. When actuator faults cause the prediction errors between the predicted states from the linear empirical model and the measured states to increase, model re-identification is triggered on-line by a moving horizon error detector if an error metric exceeds a pre-specified threshold. The proposed methodology is applied to two different chemical process examples to demonstrate the ability of the detector to indicate significant prediction errors when actuator faults occur and

update the model on-line in order to obtain more accurate predictions. The first example considers the application of the proposed scheme for the case where the value at which the actuator is stuck is known in a benchmark catalytic chemical reactor example where the actuator faults occur in the heat input causing shifts and variations in plant operating conditions. The second example demonstrates the application of the proposed scheme for the case where the value at which the actuator is stuck is unknown. Improved state predictions and economic performance were obtained by the proposed scheme as the updated models were able to capture process dynamics and compensate for the variations in the plant caused by the actuator loss.

5.2 Preliminaries

5.2.1 Notation

The operator $|\cdot|$ is used to denote the Euclidean norm of a vector. The transpose of a vector x is denoted by the symbol x^T. The symbol Ω_ρ represents a level set of a positive definite continuously differentiable scalar-valued function $V(x)$ ($\Omega_\rho := \{x \in R^n : V(x) \leq \rho\}$). A continuous function $\alpha : [0,a) \to [0,\infty)$ is said to belong to class $\mathscr{K}$ if it is strictly increasing and is zero only when evaluated at zero. The symbol diag(a) denotes a square diagonal matrix where the diagonal elements are the components of the vector a. The sampling period is denoted as $\Delta > 0$.

5.2.2 Class of Systems

This chapter considers a broad class of process systems described by first-order nonlinear ordinary differential equations of the following form:

$$\dot{x}(t) = f(x(t), u(t), w(t)) \tag{5.1}$$

where $x \in R^n$, $u \in R^m$, and $w \in R^l$ are the state vector of the system, manipulated input vector, and the disturbance vector, respectively. The disturbance vector is assumed to be bounded (i.e.,

$|w(t)| \leq \theta$ for all t). Physical limitations on actuation energy restrict the manipulated inputs to belong to the convex set $U := \{u \in R^m : u_i^{\min} \leq u_i \leq u_i^{\max},\ i = 1,\ \ldots,\ m\}$. The function f is assumed to be locally Lipschitz and the origin is taken to be an equilibrium of the nominal unforced system of Eq. 5.1 (i.e., $f(0,0,0) = 0$). We assume that measurements of the full state vector $x(t_k)$ are available at each sampling time $t_k = k\Delta$, $k = 0, 1, \ldots$.

This chapter is restricted to the class of stabilizable nonlinear systems. Specifically, we assume the existence of a locally Lipschitz feedback control law $h(x) \in U$ that can render the origin of the nominal ($w(t) \equiv 0$) closed-loop system of Eq. 5.1 locally asymptotically stable in the sense that there exists a continuously differentiable Lyapunov function $V : R^n \to R_+$ where the following inequalities hold:[30,111]

$$\alpha_1(|x|) \leq V(x) \leq \alpha_2(|x|), \tag{5.2a}$$

$$\frac{\partial V(x)}{\partial x} f(x, h(x), 0) \leq -\alpha_3(|x|), \tag{5.2b}$$

$$\left| \frac{\partial V(x)}{\partial x} \right| \leq \alpha_4(|x|) \tag{5.2c}$$

for all x in an open neighborhood D that includes the origin in its interior and $\alpha_j(\cdot)$, $j = 1, 2, 3, 4$, are class $\mathscr{K}$ functions. For various classes of nonlinear systems, several stabilizing control laws have been developed that take input constraints into consideration.[10,12,27] The stability region of the closed-loop system is defined to be a level set $\Omega_\rho \subset D$ where $\dot{V} < 0$. The origin of the closed-loop system is rendered practically stable when the control law $h(x)$ is applied in a sample-and-hold fashion for a sufficiently small sampling period.[31]

In this chapter, we apply an on-line model identification scheme to obtain empirical models that capture the evolution of the system of Eq. 5.1. The empirical models obtained are linear time-invariant (LTI) state-space models of the form:

$$\dot{x}(t) = A_i x(t) + B_i u(t) \tag{5.3}$$

where the constant matrices $A_i \in R^{n \times n}$ and $B_i \in R^{n \times m}$ correspond to the $i-th$ model identifi-

cation performed ($i = 1,\ldots,\tilde{M}$). We assume the existence of a set of stabilizing control laws $h_{L1}(x)$,$h_{L2}(x)$,...,$h_{L\tilde{M}}(x)$ designed based on the empirical models that can make the origin of the closed-loop system of Eq. 5.1 asymptotically stable and generate a continuously differentiable Lyapunov function $\hat{V} : R^n \to R_+$ where the following inequalities hold:[111]

$$\hat{\alpha}_1(|x|) \leq \hat{V}(x) \leq \hat{\alpha}_2(|x|), \tag{5.4a}$$

$$\frac{\partial \hat{V}(x)}{\partial x} f(x, h_{Li}(x), 0) \leq -\hat{\alpha}_{3_i}(|x|),\ i = 1,\ldots,\tilde{M} \tag{5.4b}$$

$$\left| \frac{\partial \hat{V}(x)}{\partial x} \right| \leq \hat{\alpha}_4(|x|) \tag{5.4c}$$

for all x in an open neighborhood D_{Li} that includes the origin in its interior. The functions $\hat{\alpha}_j(\cdot)$, $j = 1,2,4$, and $\hat{\alpha}_{3_i}$, $i = 1,\ldots,\tilde{M}$, are class $\mathscr{K}$ functions and the stability region of the system of Eq. 5.1 under the controller $h_{Li}(x)$ is defined as the level set $\Omega_{\hat{\rho}_i} \subset D_{Li}$, $i = 1,\ldots,\tilde{M}$.

5.2.3 Lyapunov-based EMPC

The formulation of EMPC to be used in this chapter incorporates Lyapunov-based stability constraints based on the explicit stabilizing controller $h(x)$. The resulting Lyapunov-based EMPC (LEMPC)[20] maximizes an economics-based cost function representing the plant economics and is

given by the following optimization problem:

$$\min_{u\in S(\Delta)} \quad \int_{t_k}^{t_{k+N}} L_e(\tilde{x}(\tau),u(\tau))\,d\tau \tag{5.5a}$$

$$\text{s.t.} \quad \dot{\tilde{x}}(t) = f(\tilde{x}(t),u(t),0) \tag{5.5b}$$

$$\tilde{x}(t_k) = x(t_k) \tag{5.5c}$$

$$u(t) \in U,\ \forall\, t \in [t_k,t_{k+N}) \tag{5.5d}$$

$$V(\tilde{x}(t)) \leq \rho_e,\ \forall\, t \in [t_k,t_{k+N})$$

$$\text{if } x(t_k) \in \Omega_{\rho_e} \tag{5.5e}$$

$$\frac{\partial V(x(t_k))}{\partial x} f(x(t_k),u(t_k),0) \leq \frac{\partial V(x(t_k))}{\partial x} f(x(t_k),h(x(t_k)),0)$$

$$\text{if } x(t_k) \notin \Omega_{\rho_e} \tag{5.5f}$$

where the decision variables are the input trajectories over the prediction horizon $N\Delta$ (i.e., $u \in S(\Delta)$ where $S(\Delta)$ signifies the class of piecewise-constant functions with period Δ). Control actions are implemented in a receding horizon fashion using process state predictions $\tilde{x}(t)$ from the dynamic model of the process (Eq. 5.5b) initiated from the state feedback measurement at each sampling time (Eq. 5.5c). Input constraints are taken into consideration in the LEMPC formulation in Eq. 5.5d.

The Mode 1 constraint (Eq. 5.5e) is activated when the state measurement is maintained within a subset of the stability region Ω_ρ that is referred to as Ω_{ρ_e}, and promotes time-varying process operation to maximize economics. When the closed-loop state exits Ω_{ρ_e}, the Mode 2 constraint (Eq. 5.5f) is activated to force the state back into Ω_{ρ_e} by computing control actions that decrease the Lyapunov function value. The stability region subset Ω_{ρ_e} is chosen to make Ω_ρ forward invariant in the presence of process disturbances.

5.3 EMPC Using Error-Triggered On-line Model Identification

The potential of EMPC for improving profits in the chemical process industries has motivated research in practical aspects of EMPC implementation, including the use of linear empirical models in EMPC.[48,118] However, all work on improving the practicality of EMPC with empirical models has assumed that no actuator faults occur, though the development of actuator faults poses unique challenges for linear empirical models utilized to obtain state predictions within EMPC. Because the models are developed with all actuators on-line based on process data only, there is no guarantee that when the underlying process dynamics change (i.e., an actuator output becomes fixed when it was previously varying) that the model developed based on data for the case that all actuators were varying will remain valid with the value of the faulty actuator fixed for all time, since this condition was not included in the original process data used to identify the model and the underlying process model is typically nonlinear such that nonlinear and coupled interactions between states and inputs exist. This can impact the accuracy of state predictions utilized within the EMPC after the fault occurs, which can negatively impact process profits as well as satisfaction of other constraints (including stability or state constraints). Though re-identification of the model when the fault is detected may appear to be a solution to the potential problems caused by the fault for the accuracy of the linear empirical models, re-identification would require the availability of a sufficient number of input/output data points corresponding to the new (after fault) operating conditions. Since sufficient after-fault data for model re-identification is not available until after the fault, there will be some time period during which the empirical model developed from data corresponding to the case that all actuators are on-line must continue to be utilized within the EMPC. Furthermore, depending on the severity of the fault and the empirical model in use at the time of the fault, the original empirical model may provide sufficiently accurate state predictions such that it is not necessary to interrupt the continuity of the control strategy by updating the model used within the controller. Therefore, a method for determining when the model should be updated as a result of the fault is necessary. In this chapter, we propose the use of the moving horizon error detector developed in[118] for this task; however, important changes to the implementation

strategy of the LEMPC with error-triggered on-line model identification must be made to address the issues specific to faults discussed above. In this development, we assume that a fault has occurred in an actuator that causes the actuator output to take some value, where it is known which actuator has experienced a fault. The proposed approach to develop fault-tolerant control for empirical model-based LEMPC may be applied in the case where the value of the faulty actuator's output is known and in the case where the value of the faulty actuator's output is unknown. We make no requirement on the number of faults that can occur at one time, as long as the number of on-line actuators allows sufficiently accurate linear empirical models to continue to be identified (observability assumption). Therefore, this method is flexible to handle multiple actuators experiencing faults simultaneously (and can also be extended to include re-commissioning of actuators that experienced faults and have been repaired) throughout time. The following section presents the LEMPC formulation using linear empirical models. After that, the formulation of the moving horizon error detector and the implementation strategy for on-line model identification to compensate for changes in the model due to actuator faults are introduced.

5.3.1 LEMPC Formulation Using Empirical Models

In this chapter, it is assumed that the plant model of Eq. 5.1 is unavailable and the process model to be incorporated in the LEMPC design is the $i-th$ empirical model ($i = 1,\ldots,\tilde{M}$). The empirical models and their corresponding $h_{Li}(x)$ and $\hat{V}(x)$ are used in the development of the stability constraints. The LEMPC design using the $i-th$ empirical model is presented by the following

optimization problem:[48]

$$\min_{u\in S(\Delta)} \quad \int_{t_k}^{t_{k+N}} L_e(\hat{x}(\tau),u(\tau))\,d\tau \tag{5.6a}$$

$$\text{s.t.} \quad \dot{\hat{x}}(t) = A_i\hat{x}(t) + B_i u(t) \tag{5.6b}$$

$$\hat{x}(t_k) = x(t_k) \tag{5.6c}$$

$$u(t) \in U,\ \forall\, t \in [t_k, t_{k+N}) \tag{5.6d}$$

$$\hat{V}(\hat{x}(t)) \leq \hat{\rho}_{ei},\ \forall\, t \in [t_k, t_{k+N})$$

$$\text{if } x(t_k) \in \Omega_{\hat{\rho}_{ei}} \tag{5.6e}$$

$$\frac{\partial \hat{V}(x(t_k))}{\partial x}\left(A_i x(t_k) + B_i u(t_k)\right) \leq \frac{\partial \hat{V}(x(t_k))}{\partial x}\left(A_i x(t_k) + B_i h_{Li}(x(t_k))\right)$$

$$\text{if } x(t_k) \notin \Omega_{\hat{\rho}_{ei}} \tag{5.6f}$$

where the notation follows that in Eq. 5.5, and $\hat{x}(t)$ denotes the state prediction using the linear empirical model (Eq. 5.6b), starting from the state feedback measurement (Eq. 5.6c). The subsets of the stability regions for the Mode 1 constraints $\Omega_{\hat{\rho}_{ei}} \subset \Omega_{\hat{\rho}_i}$ are chosen to make the stability region $\Omega_{\hat{\rho}_i}$ forward invariant in the presence of bounded process disturbances. Both $\Omega_{\hat{\rho}_i}$ and $\Omega_{\hat{\rho}_{ei}}$ that makes $\Omega_{\hat{\rho}_i}$ forward invariant can be difficult to determine in practice. Therefore, a conservative estimate of each can be chosen, or they can be adjusted on-line based on analyzing the process data to determine whether the LEMPC of Eq. 5.6 is able to maintain the state within an expected region of state-space.

5.3.2 Moving Horizon Error Detector

In this section, we describe the moving horizon error detector that quantifies prediction errors and triggers on-line model identification when necessary. Specifically, the moving horizon error detector tracks an error metric throughout the duration of process operation that is based on the difference between the predicted states using a linear empirical model and the measured states from

the process (relative prediction error). When this error exceeds an engineer-specified threshold $e_{d,T}$ (indicating significant plant/model mismatch), on-line model re-identification is triggered and performed using the most recent input/output data points, and the updated model is used in the LEMPC of Eq. 5.6. The error metric e_d calculated by the moving horizon error detector at each sampling period t_k using the most recent past state predictions and measurements in a moving horizon fashion is presented in the following equation:

$$e_d(t_k) = \sum_{r=0}^{M} \sum_{j=1}^{n} \frac{|x_{p,j}(t_{k-r}) - x_j(t_{k-r})|}{|x_j(t_{k-r})|} \tag{5.7}$$

where the horizon M is the number of sampling periods included in assessing the prediction error. $x_j(t_{k-r})$ and $x_{p,j}(t_{k-r})$, $r = 0,\ldots,M$, $j = 1,\ldots,n$, are the past process state measurements and the past state predictions from an empirical model between the sampling times t_{k-M} and t_k. Due to the fact that process states may vary in their orders of magnitude, the difference between the predicted states and the measured states is normalized by the magnitude of the measured state $|x_j(t_{k-r})|$. The purpose of summing over the horizon M is to average out the effect of small time-varying disturbances that may occur in practice and cause prediction errors to increase. For the detailed guidelines and the step-by-step procedure for determining the values of the horizon M and the error metric threshold $e_{d,T}$ for a given process, the reader may refer to.[118]

5.3.3 Implementation Strategy

In this section, we present the steps taken in the proposed on-line model identification scheme to overcome actuator faults in empirical model-based LEMPC as follows:

Step 1. Before an actuator fault occurs, an initial linear empirical model (A_1 and B_1) accounting for all actuators is obtained by exciting the system with a large number of inputs that have varying magnitudes and collecting the corresponding output data. This model is used to predict the process evolution within the LEMPC and to design the stabilizing controller h_{L1} and the corresponding $\hat{V}$ for the Lyapunov-based constraints of the LEMPC. The region $\Omega_{\hat{\rho}_{ei}}$ is chosen such that in this

region, plant-model mismatch is minimal.

Step 2. The process is operated under the LEMPC design using an empirical model and the moving horizon error detector is used to detect prediction errors.

Step 3. When an actuator fault occurs, the LEMPC receives information on which actuator is stuck. If the value at which the actuator is stuck is known, the corresponding input value in the LEMPC optimization problem is fixed to the fault value and the decision variables for this input are removed from the LEMPC optimization problem (i.e., the LEMPC no longer solves for the input corresponding to the faulty actuator). If the value at which the actuator is stuck is unknown, the LEMPC optimization problem continues to compute optimal control actions for all actuators (assuming that all actuators are active on-line) despite the fact that a fault has occurred in one of them (i.e., the LEMPC solves for all the inputs including the input corresponding to the faulty actuator despite the fact that it will not be implemented since this actuator is not under control).

Step 4. If $e_d(t_k)$ exceeds $e_{d,T}$, input and output data collected since the fault occurrence are used to identify a new model on-line for use in the LEMPC formulation and the design of the corresponding stabilizing controller h_{Li}. The new B_i matrix obtained will contain one less column since the number of manipulated inputs is reduced by one.

Step 5. Process operation under the LEMPC and the moving horizon error detector continues (i.e., return to Step *2* and proceed to Steps *3* through *5* if another actuator fault occurs).

Remark 17 *LEMPC may calculate time-varying input trajectories since the cost function of EMPC does not have its minimum at a steady-state of a process.[14] The persistent process state excitations caused by such time-varying input trajectories that may be generated under EMPC may make the input/output data convenient for use in on-line model identification.*

Remark 18 *Conditions guaranteeing feasibility and closed-loop stability of an LEMPC based on a linear empirical model that is not updated in time have been developed in.[48] These conditions include requirements that the empirical model must be sufficiently close to the linearization of the underlying nonlinear model. In the proposed methodology, when an actuator fault occurs, the underlying nonlinear model changes, but the process model cannot be immediately updated because*

no post-fault process input/output data is available. Therefore, it is not possible to assess if the previous linear empirical model is close to the linearization of the underlying nonlinear model after the fault has occurred, regardless of whether the value of the fault is known and it is fixed in the empirical model or the value of the fault is unknown and the empirical model is used assuming all inputs are active on-line. Due to this practical difficulty, proving guaranteed feasibility and closed-loop stability of the error-triggered on-line model identification for the LEMPC scheme has not been pursued. As a result, selecting $\hat{V}$, $\Omega_{\hat{\rho}_i}$, $\Omega_{\hat{\rho}_{ei}}$, *and* h_{Li} *to provide guaranteed closed-loop stability of the nonlinear process when used in the LEMPC can be challenging. However, appropriate parameters can be determined practically using closed-loop simulations with the linear empirical model in the LEMPC when a first-principles model is available for analyzing the accuracy of the state predictions and the ability of the LEMPC with an empirical model to maintain closed-loop stability of the nonlinear process, and then some conservatism can be added to the estimates of the parameters. Alternatively, a conservative estimate of* $\Omega_{\hat{\rho}_i}$ *and* $\Omega_{\hat{\rho}_{ei}}$ *can be utilized initially when a first-principles model is not available, and updated on-line if desired to reduce the conservatism after process operating data is available. In general, because process data is monitored frequently, the parameters can be tuned on-line if the closed-loop performance does not meet an engineer's expectations. Therefore, the lack of a rigorous closed-loop stability and feasibility proof for this LEMPC design does not pose practical limitations and would be expected to be effective in many practical applications.*

Remark 19 *The moving horizon error detector is also capable of initiating empirical model updates when significant plant variations, operating region changes, or disturbances that are not caused by actuator faults occur,*[118] *and it may also trigger model re-identification multiple times after a fault if the re-identified models were developed without sufficient post-fault input/output data to allow the model to adequately capture the post-fault process dynamics. When significant plant variations or disturbances or poorly identified post-fault models cause the prediction error to exceed the pre-defined threshold for the error metric* $e_d(t_k)$, *the same steps mentioned above are taken excluding Step 3 and the dimension of the updated* B_i *matrix remains the same as the*

B_i from the previous linear empirical model. Furthermore, any known and sudden disturbance that does not correspond to loss of a new actuator but which may change the underlying process dynamics (e.g., an actuator that has already become stuck at one value becomes stuck at another value due to a disturbance that affects the actuator position, or an on-off aspect of the process such as a pump or valve that is not manipulated by the control system has been changed) can also be handled with the implementation strategy detailed in this section (e.g., only data corresponding to the time after the known disturbance may be used in the model re-identification due to the change in the underlying process dynamics), except that the number of columns in the B_i matrix would not change if the disturbance did not affect the number of on-line actuators compared to the previous model re-identification. In practice, when an unknown disturbance or plant variation occurs and causes the prediction error to exceed the pre-defined threshold for the error metric $e_d(t_k)$, the time at which this unknown disturbance or plant variation started may also be unknown. Therefore, the number of input/output data points N_d utilized in each model identification after the threshold for the error metric $e_d(t_k)$ has been exceeded remains the same as the number utilized for obtaining the initial model (A_1 and B_1) since no extra information is available. If the re-identified model was developed without sufficient input/output data collected after the occurrence of the disturbance or plant variation, the threshold for the error metric $e_d(t_k)$ may be exceeded multiple times until enough input/output data collected after the occurrence of the disturbance or plant variation are available and the resulting identified model adequately captures the process dynamics. The ability of the moving horizon error detector to handle the many scenaria discussed in this remark, even simultaneously, makes it an integrated approach to handling a variety of practical considerations.

Remark 20 *In,[118] guidelines for determining M, $e_{d,T}$, and the number of input/output data points to utilize in model re-identification were presented assuming that the causes of plant/model mismatch are gradual changes such as plant variations, disturbances, or movement of the process state into new regions not captured by the original linear empirical model throughout time. However, actuator faults occur suddenly, which may cause an identified empirical model to rapidly become inadequate for representing the process dynamics. Therefore, process data and controller perfor-*

mance should be monitored after the fault to ensure that M, $e_{d,T}$, and the number of process data points chosen for model re-identification, determined using the non-faulty plant operating data and methods like those in,[118] remain valid for assessing the prediction error and obtaining sufficiently accurate models upon re-identification after the fault. If they do not, as in,[118] the values of M and $e_{d,T}$ can be increased or decreased on-line and the effect of this on the controller performance can be examined to arrive at updated values of M and $e_{d,T}$ when required. Furthermore, the last M data points including non-faulty data may continue to be used in evaluating the prediction error after the fault (due to the inability to set an error threshold on less than M post-fault data points alone after the fault since there would be no basis for the alternative error threshold, and the fact that very large prediction errors in the post-fault data will still trigger model re-identification if necessary before M post-fault data points are available even if pre-fault data is also included in the calculation of e_d). Similarly, when sufficient input/output data points are available after the fault for use for model re-identification, this number can be increased or decreased based on controller performance to ensure that it is still satisfactory after the fault. If the number of input/output data points N_d used for model re-identification before the fault is greater than the number of post-fault input/output data points available after the fault when model re-identification is first triggered by the moving horizon error detector, then only the post-fault data (i.e., less than the desired N_d) should be used for the re-identification. This is because the input/output model structure changes after the fault (i.e., there is one less input), with the result that the data corresponding to having one additional input from before the fault cannot be used in identifying a model corresponding to having one less input from after the fault. If a sufficiently accurate model is not identified due to the lack of sufficient post-fault data when the moving horizon error detector is triggered, it would be expected that the prediction error will eventually increase once again above $e_{d,T}$, triggering another model re-identification with additional post-fault data, so that eventually the linear empirical model used after the fault will have been developed with sufficient post-fault input/output data to allow for sufficiently accurate state predictions that no longer trigger model re-identification.

Remark 21 *Though the error-triggered model update strategy for actuator fault compensation*

is discussed in the context of LEMPC, it can be extended to other model-based control designs, including tracking MPC (MPC with a quadratic objective function), as well, as long as the process data available for updating the models when these other control designs are used contains enough information regarding the important process dynamics for use in identifying sufficiently accurate process models.

Remark 22 *It was previously noted that multiple simultaneous faults as well as actuator re-commissioning can be handled utilizing this strategy. The simultaneous faults may include those for which the value of the faulty actuator output is known, those for which it is unknown, or even a combination. For multiple simultaneous faults, Step 3 is applied to the various faulty actuators, and in Step 4, the number of columns in the B_i matrix is reduced by the number of faulty actuators. For actuator re-commissioning, model re-identification using the most recent N_d input/output data points since the last actuator fault (or the total number available since the last fault if the available number is less than N_d) can be performed, allowing the B_i matrix to include columns for all actuators that are now non-faulty. This model can then be utilized in the LEMPC, and the error-triggering procedure will update the model if the state predictions contain significant error due to the fact that the input/output data on which the model was based did not include the effects of the re-commissioned actuators taking output values different from the value at which they were stuck.*

Remark 23 *When the value at which a faulty actuator is stuck is unknown, other methods of accounting for this faulty actuator in the empirical model immediately after the fault could be utilized instead of continuing to solve for all actuator outputs as suggested in Step 3. The goal of Step 3 when the actuator output is unknown is to allow the LEMPC to continue computing control actions for the non-faulty actuators while generating input/output data that can be used to identify a model corresponding to the process dynamics subject to the fault, and this can be done with any reasonable assumption on the value of the faulty actuator outputs in the LEMPC.*

5.4 Application of Error-Triggered On-Line Model Identification when the Fault Value is Known: Catalytic Process Example

This section demonstrates the application of the proposed error-triggered on-line model identification for fault-tolerant LEMPC when the value at which the actuator is stuck is known. We consider the control of catalytic oxidation of ethylene (C_2H_4) in a continuous stirred tank reactor (CSTR). Ethylene is oxidized with air to produce the desired ethylene oxide (C_2H_4O) product as presented in the following chemical reactions:

$$C_2H_4 + \frac{1}{2}O_2 \xrightarrow{R_1} C_2H_4O \tag{R1}$$

$$C_2H_4 + 3O_2 \xrightarrow{R_2} 2CO_2 + 2H_2O \tag{R2}$$

$$C_2H_4O + \frac{5}{2}O_2 \xrightarrow{R_3} 2CO_2 + 2H_2O \tag{R3}$$

The reaction rates R_1, R_2, and R_3 are given by the following Arrhenius relationships:[85]

$$R_1 = k_1 \exp\left(\frac{-E_1}{R_g T}\right) P_E^{0.5} \tag{5.8a}$$

$$R_2 = k_2 \exp\left(\frac{-E_2}{R_g T}\right) P_E^{0.25} \tag{5.8b}$$

$$R_3 = k_3 \exp\left(\frac{-E_3}{R_g T}\right) P_{EO}^{0.5} \tag{5.8c}$$

where k_1, k_2, and k_3 are pre-exponential factors, E_1, E_2, and E_3 are activation energies for each reaction, R_g is the gas constant, and T is the absolute temperature. The reaction rates are presented in terms of partial pressures of ethylene (P_E) and of ethylene oxide (P_{EO}). The gas mixture inside the reactor is assumed to be ideal, and thus, the partial pressures in the reaction rates can be converted to molar concentrations using the ideal gas law. The dimensionless mass and energy balances for

this process are described by the following first-order ordinary differential equations:[86]

$$\frac{dx_1(t)}{dt} = u_1(1 - x_1x_4) \tag{5.9a}$$

$$\frac{dx_2(t)}{dt} = u_1(u_2 - x_2x_4) - A_1e^{\frac{\gamma_1}{x_4}}(x_2x_4)^{0.5} - A_2e^{\frac{\gamma_2}{x_4}}(x_2x_4)^{0.25} \tag{5.9b}$$

$$\frac{dx_3(t)}{dt} = -u_1x_3x_4 + A_1e^{\frac{\gamma_1}{x_4}}(x_2x_4)^{0.5} - A_3e^{\frac{\gamma_3}{x_4}}(x_3x_4)^{0.5} \tag{5.9c}$$

$$\frac{dx_4(t)}{dt} = \frac{u_1}{x_1}(1 - x_4) + \frac{B_1}{x_1}e^{\frac{\gamma_1}{x_4}}(x_2x_4)^{0.5} + \frac{B_2}{x_1}e^{\frac{\gamma_2}{x_4}}(x_2x_4)^{0.25} + \frac{B_3}{x_1}e^{\frac{\gamma_3}{x_4}}(x_3x_4)^{0.5} - \frac{B_4}{x_1}(x_4 - u_3) \tag{5.9d}$$

where x_1, x_2, x_3, and x_4 are the dimensionless gas density, ethylene concentration, ethylene oxide concentration, and temperature inside the reactor, respectively. The reactor manipulated inputs are the dimensionless volumetric flow rate of the inlet stream u_1, the dimensionless concentration of ethylene in the inlet stream u_2, and the dimensionless coolant temperature u_3. The manipulated inputs are constrained to belong to the following sets: $0.0704 \leq u_1 \leq 0.7042$, $0.2465 \leq u_2 \leq 2.4648$, $0.6 \leq u_3 \leq 1.1$. Table 5.1 lists the values of the process parameters. The reactor has an asymptotically stable steady-state at $[x_{1s}\ x_{2s}\ x_{3s}\ x_{4s}] = [0.998\ 0.424\ 0.032\ 1.002]$ corresponding to the manipulated input values of $[u_{1s}\ u_{2s}\ u_{3s}] = [0.35\ 0.5\ 1.0]$.

Table 5.1: Dimensionless Parameters of the Ethylene Oxidation CSTR.

$A_1 = 92.8$	$B_2 = 10.39$	$\gamma_2 = -7.12$
$A_2 = 12.66$	$B_3 = 2170.57$	$\gamma_3 = -11.07$
$A_3 = 2412.71$	$B_4 = 7.02$	
$B_1 = 7.32$	$\gamma_1 = -8.13$	

The control objective is to maximize the average yield of ethylene oxide by operating the reactor in a time-varying manner around the open-loop stable steady-state. Over a time period from t_0 to t_e, this average yield is given by:

$$Y(t_e) = \frac{\int_{t_0}^{t_e} u_1(\tau)x_3(\tau)x_4(\tau)\,d\tau}{\int_{t_0}^{t_e} u_1(\tau)u_2(\tau)\,d\tau} \tag{5.10}$$

t_e is an integer multiple of t_f which is the length of an operating period. In addition, we consider that there is a limitation on the amount of ethylene that may be fed to the rector during the length of an operating period t_f. Therefore, the time-averaged molar flow rate of ethylene that can be fed to the reactor should satisfy the following material constraint:

$$\frac{1}{t_f}\int_{(j-1)t_f}^{jt_f} u_1(\tau)u_2(\tau)\,d\tau = u_{1s}u_{2s} = 0.175 \tag{5.11}$$

where j is the operating period number ($j = 1, 2, \ldots$). Since the material constraint of Eq. 5.11 fixes the average amount of ethylene fed to the reactor over the operating period t_f, the economic cost that the LEMPC attempts to maximize such that the ethylene oxide yield is maximized becomes:

$$\int_{t_0}^{t_e} L_e(x,u) = \int_{t_0}^{t_e} u_1(\tau)x_3(\tau)x_4(\tau)d\tau \tag{5.12}$$

We assume that the reactor first-principles model in Eq. 5.9 is unavailable for control design. Therefore, the empirical model is used to design the LEMPC with the objective function and constraints mentioned above. To construct an empirical model that captures the process dynamics accurately in a region local to the stable steady-state, a large sequence of step inputs with varying magnitudes was applied to the reactor in order to excite the important dynamics and capture them in the empirical model. After collecting the input/output data points, the initial ($i = 1$) state-space linear empirical model of the reactor was obtained using the ordinary multivariable output error state-space (MOESP)[43] algorithm. Model validation was then conducted using various step, impulse, and sinusoidal input responses. The initial empirical model obtained is given by the

following constant matrices:

$$A_1 = \begin{bmatrix} -0.349 & 0.00051 & 0.00825 & -0.349 \\ -0.00488 & -0.374 & 0.0374 & -0.369 \\ 0.00109 & 0.0213 & -0.452 & 0.0653 \\ -0.0078 & 0.0259 & 0.0204 & -7.24 \end{bmatrix}$$
$$B_1 = \begin{bmatrix} -0.00011 & -0.000149 & -0.0239 \\ 0.0757 & 0.349 & -0.0194 \\ -0.0315 & 0.000208 & 0.00426 \\ -0.0173 & -0.00264 & 6.529 \end{bmatrix} \quad (5.13)$$

The stabilizing control law used in the LEMPC is designed based on the empirical model of Eq. 5.13 since we assumed that the reactor first-principles model of Eq. 5.9 is unavailable. The stabilizing control law is represented by the vector $h_{L1}^T(x) = [h_{L1,1}(x)\ h_{L1,2}(x)\ h_{L1,3}(x)]$. In order to meet the material constraint of Eq. 5.11 on the available feedstock, both $h_{L1,1}(x)$ and $h_{L1,2}(x)$ were set to their steady-state values. The linear quadratic regulator (LQR) was used in designing the third control law $h_{L1,3}(x)$ using the A_1 matrix and the third column of the B_1 matrix as the system matrices. Both LQR weighting matrices Q and R were taken to be the identity matrix. The resulting control law for the heat input is: $u_3 = h_{L1,3}(x) = -K(x-x_s) + u_{3s}$, with K equal to [-0.287 -0.276 0.023 0.405]. The closed-loop stability region is characterized using the quadratic Lyapunov function $\hat{V}(x) = (x-x_s)^T P(x-x_s)$ where the positive definite matrix P is P=diag[20 30 40 10]. Through extensive closed-loop simulations of the reactor system under the stabilizing control law $h_{L1}(x)$, the level sets $\Omega_{\hat{\rho}_1}$ and $\Omega_{\hat{\rho}_{e1}}$ were chosen to have $\hat{\rho}_1 = 96.1$ and $\hat{\rho}_{e1} = 87.4$. In these regions, the reactor first-principles nonlinear dynamics of Eq. 5.9 are well-captured by the linear empirical model of Eq. 5.13.

To compare the closed-loop performance of the process even in the presence of actuator faults when an LEMPC based on a linear empirical model is used instead of an LEMPC based on the first-principles model, two LEMPC schemes, one of the form of Eq. 5.6 and the other of the

form of Eq. 5.5, were designed for the CSTR with the cost function of Eq. 5.12 and the material constraint of Eq. 5.11 to compare closed-loop behavior. The first LEMPC initially utilized the model of Eq. 5.13 to predict the values of the process states throughout the prediction horizon, while the second LEMPC utilized the first-principles model of Eq. 5.9 (though both used the same Lyapunov-based controller and stability region). All LEMPC designs presented in this chemical process example use a prediction horizon of $N = 10$, a sampling period of $\Delta = 0.1$, and an operating period of 100 sampling periods ($t_f = 10$). The open-source optimization solver IPOPT[119] was used in solving the LEMPC optimization problems at each sampling time. The empirical LEMPC and the first-principles LEMPC were both applied to the CSTR model of Eq. 5.9. Closed-loop simulations of the reactor under each LEMPC design were performed starting from the open-loop stable steady-state $x_I^T = [x_{1I}\ x_{2I}\ x_{3I}\ x_{4I}] = [0.997\ 1.264\ 0.209\ 1.004]$. Simulations were performed using the Explicit Euler numerical integration method with an integration step size of $h = 10^{-4}$.

In order to demonstrate the effect of actuator faults on controlling the process using empirical models and the need to re-identify a new model on-line after a fault occurs, the reactor was simulated for four operating periods under the empirical LEMPC design. After three operating periods, an actuator fault is assumed to occur causing the heat input to stay at the steady-state value (i.e., $u_3 = 1$). After that, the reactor was operated in closed-loop using the empirical LEMPC design with u_3 set to its steady-state value in the empirical model defined by A_1 and B_1 (Eq. 5.13). For comparison, the closed-loop state and input trajectories were simulated for the first-principles LEMPC, including u_3 set to its steady-state value after three operating periods in the first-principles model for the LEMPC. For the first three operating periods (i.e., before the fault), the empirical and first-principles LEMPC's compute very similar input trajectories resulting in similar closed-loop state trajectories under both controllers, as shown in Figs. 5.1-5.2. This indicates that before the fault, the LEMPC with an empirical model is an effective control design for the reactor process. The reactor input and state trajectories under both the empirical and first-principles LEMPC's when $u_3 = u_{3s}$ after the first three operating periods are also depicted in Figs. 5.1-5.2, and they exhibit significant differences, indicating significant plant-model mismatch and resulting in less yield of

the final desired product under the empirical LEMPC. This demonstrates the need to re-identify the model on-line.

Based on the above simulations, it is expected that the closed-loop performance of the ethylene oxide production process under LEMPC with an empirical model would benefit from the use of the error-triggered on-line model identification procedure after a process fault. Therefore, simulations of the ethylene oxide process under the implementation strategy presented in this chapter were performed. Specifically, a moving horizon error detector was designed and initiated after $M = 40$ input/output data points were available to calculate the value of e_d at each sampling period to determine when it is necessary to trigger re-identification of the empirical process model. Simulations of the reactor suggested that significant plant-model mismatch was indicated when the value of e_d exceeded 3 and thus, this value was chosen as the threshold to trigger model re-identification. When on-line model identification was triggered, input/output data collected after the occurrence of the fault were used to identify a new model. The moving horizon error detector calculates the relative prediction error in the gas density in the reactor, ethylene concentration, ethylene oxide concentration, and the reactor temperature throughout the current and past 40 sampling periods as follows:

$$e_d(t_k) = \sum_{r=0}^{40} \Bigg[\frac{|x1_p(t_{k-r}) - x_1(t_{k-r})|}{|x_1(t_{k-r})|} + \frac{|x2_p(t_{k-r}) - x_2(t_{k-r})|}{|x_2(t_{k-r})|} + \frac{|x3_p(t_{k-r}) - x_3(t_{k-r})|}{|x_3(t_{k-r})|} + \frac{|x4_p(t_{k-r}) - x_4(t_{k-r})|}{|x_4(t_{k-r})|} \Bigg] \tag{5.14}$$

The initial empirical model utilized within the LEMPC coupled with the moving horizon error detector/on-line model re-identification strategy was again A_1 and B_1, and the reactor was again initiated from x_I. As in the above simulation, after three operating periods (i.e., at the beginning of the 4^{th} operating period), an actuator fault occurs, causing the heat input to stay at the steady-state value (i.e., $u_3 = 1$) for three operating periods. The LEMPC was apprised of the fault in the actuator corresponding to u_3 and the value of u_3 in the linear empirical model utilizing the A_1 and and B_1 matrices was subsequently set to the value u_{3s} at which it was stuck. The first six

operating periods depicted in Fig. 5.3 show the increase in e_d after the fault occurrence, leading it to eventually exceed its threshold and trigger on-line model re-identification that resulted in a sharp drop in the prediction error. The following model was identified using the post-fault input/output data:

$$A_2 = \begin{bmatrix} -149.8 & -1.30 & -6.71 & -0.347 \\ -2276 & 20.3 & 72.9 & -0.235 \\ 1469 & -13.4 & -59.8 & 0.0220 \\ -120.3 & -1.10 & 14.2 & -7.31 \end{bmatrix}, \quad B_2 = \begin{bmatrix} -0.0021 & -0.004 \\ 0.0454 & 0.202 \\ 0.0018 & 0.062 \\ 0.0188 & 0.008 \end{bmatrix} \tag{5.15}$$

Notably, in accordance with Step *4* of the implementation strategy presented in this chapter, the B_2 matrix has one less column than the B_1 matrix due to the loss of availability of u_3 as a manipulated input.

It was noted in Remark 19 that the error-triggered on-line model re-identification procedure can be used not only for handling actuator faults, but also for handling other disturbances and plant variations, even sudden changes in the process dynamics that do not affect the number of on-line actuators. Therefore, the error-triggered on-line model re-identification procedure for use in LEMPC provides a unified framework for dealing with many different root causes of reduced accuracy of state predictions from linear empirical models. To demonstrate how this unified framework can be implemented, we followed the six operating periods related to the process fault discussed above with six more operating periods (for a total simulation length of 12 operating periods) in which the actuator u_3 remained stuck (i.e., unavailable as a manipulated input by the LEMPC), but we assumed that it was subjected to disturbances that caused it to take two other known values throughout these six operating periods (e.g., a valve utilized in setting u_3 experienced a large degree of stiction but slipped to two new values due to changes in the forces applied to it twice throughout the six operating periods). Specifically, the value of u_3 changed to its maximum value of 1.1 at the beginning of the 7^{th} operating period and remained stuck at this value for three operating periods, and then it changed to the value of 0.75 at the beginning of the 10^{th} operating period and remained

stuck at this value for another three operating periods. Throughout the six operating periods during which the value of u_3 experienced these disturbances, only one model re-identification was triggered by the moving horizon error detector, leading to a drop in the prediction error around the beginning of the 11^{th} operating period as shown in Fig. 5.3 when the following model was identified:

$$A_3 = \begin{bmatrix} -27.39 & 15.4 & 7.29 & -25.8 \\ 33.39 & -18.2 & 12.3 & 30.14 \\ -16.95 & -4.20 & -201 & 2.004 \\ -168.1 & 87.1 & -26.4 & -155.9 \end{bmatrix}, \quad B_3 = \begin{bmatrix} 0.1771 & -0.541 \\ 0.2206 & -0.260 \\ -0.018 & 0.0397 \\ -0.203 & 0.8383 \end{bmatrix} \tag{5.16}$$

This model re-identification was triggered when $u_3 = 0.75$ (i.e., no model re-identification was triggered when $u_3 = 1.1$), showing that the error-triggering was successful at deciding the necessity of model updates, because even though u_3 changed its value at the beginning of the 7^{th} operating period, no re-identification was required since the error did not exceed the threshold of $e_d = 3$. Because this model re-identification was not related to loss of a new actuator, B_3 has the same dimension as B_2.

The input and state trajectories for the entire 12 operating periods of the reactor process of Eq. 5.9 under the LEMPC of Eq. 5.6 with the empirical models of Eqs. 5.13, 5.15, and 5.16 subject to the actuator fault and disturbances in the value at which u_3 was stuck are presented in Figs. 5.4-5.5. The values of e_d throughout the 12 operating periods is presented in Fig. 5.3, showing the rises of the e_d values that triggered the model re-identifications and the rapid decreases of the values of $e_d(t_k)$ after each on-line model re-identification. These figures show the successful implementation of a unified framework using the moving horizon error detector and error-triggered model updates within LEMPC for handling both faults and other disturbances throughout time.

In addition to decreasing the plant-model mismatch due to faults and disturbances, the on-line model identification improved the process economic performance compared to not updating the model as presented in Table 5.2. The table lists the average yield and the maximum value of $e_d(t_k)$

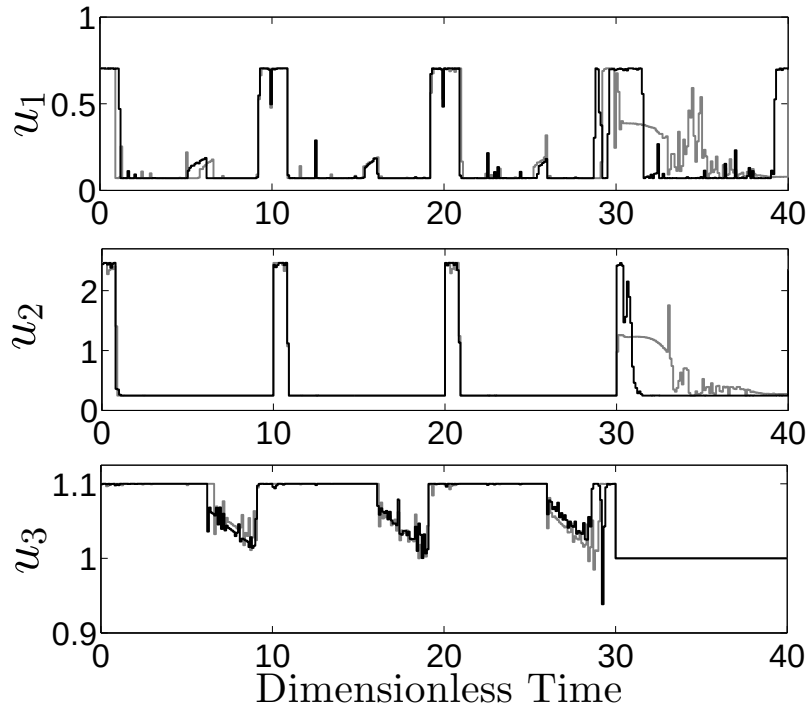

Figure 5.1: Closed-loop input trajectories for four operating periods of the reactor of Eq. 5.9 initiated from x_I under the LEMPC designed with the first-principles model (solid black trajectories) and the LEMPC designed with the empirical model in Eq. 5.13 (solid gray trajectories) where an actuator fault occurs at the end of the 3^{rd} operating period.

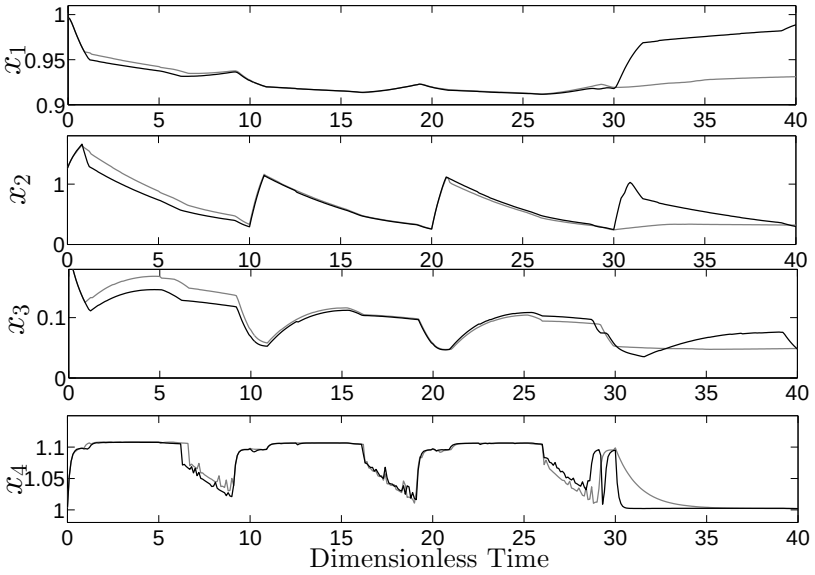

Figure 5.2: Closed-loop state trajectories for four operating periods of the reactor of Eq. 5.9 initiated from x_I under the LEMPC designed with the first-principles model (solid black trajectories) and the LEMPC designed with the empirical model in Eq. 5.13 (solid gray trajectories) where an actuator fault occurs at the end of the 3^{rd} operating period.

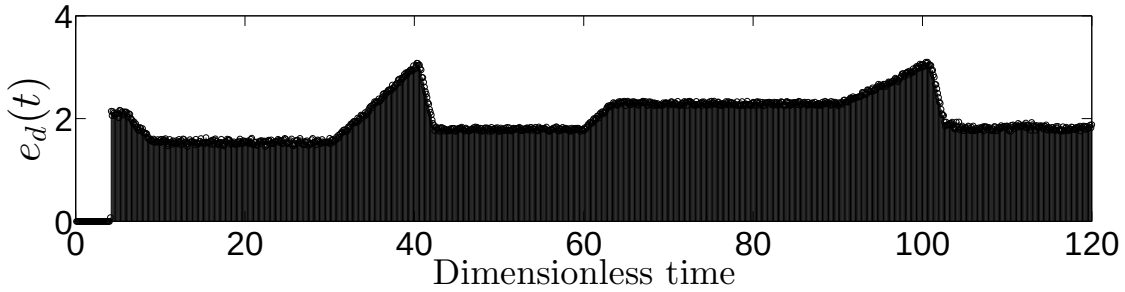

Figure 5.3: Value of error metric e_d at each sampling using the detector of Eq. 5.14 for the LEMPC integrated with the error-triggered on-line model identification.

for the two operating periods after the first on-line model re-identification (when u_3 is stuck at the value of 1) and after the second model identification (when u_3 is stuck at the value of 0.75). The results listed are for three approaches: the "One Empirical Model" approach, in which no model re-identification is conducted and the initial empirical model (A_1 and B_1) is used throughout the 12 operating periods despite the faults, the "On-line Model ID" approach, in which the proposed on-line model re-identification approach is conducted, and the "Nonlinear Model" approach, in which the first-principles model of Eq. 5.9 is used in the LEMPC including the changes in the u_3. These results show the significant improvement in process yield resulting from updating the empirical model on-line compared to using the same initial empirical model throughout process operation despite the faults.

Table 5.2: Relative prediction error and average yield for the CSTR under LEMPC.

	After 1^{st} on-line ID		After 2^{nd} on-line ID	
Approach	Y	Max $e_d(t_k)$	Y	Max $e_d(t_k)$
One Empirical Model	7.16	4.76	7.23	5.03
On-line Model ID	8.31	1.98	8.21	1.82
Nonlinear Model	8.43	-	8.39	-

Remark 24 *In this example, the controller h_{L1} was not redesigned after the actuator fault as noted in Step 4 of the on-line model identification scheme because the closed-loop state never left $\Omega_{\hat{\rho}_{e1}}$ during the simulation. The example in the next section exemplified the change in the Lyapunov-based control law when the fault occurs.*

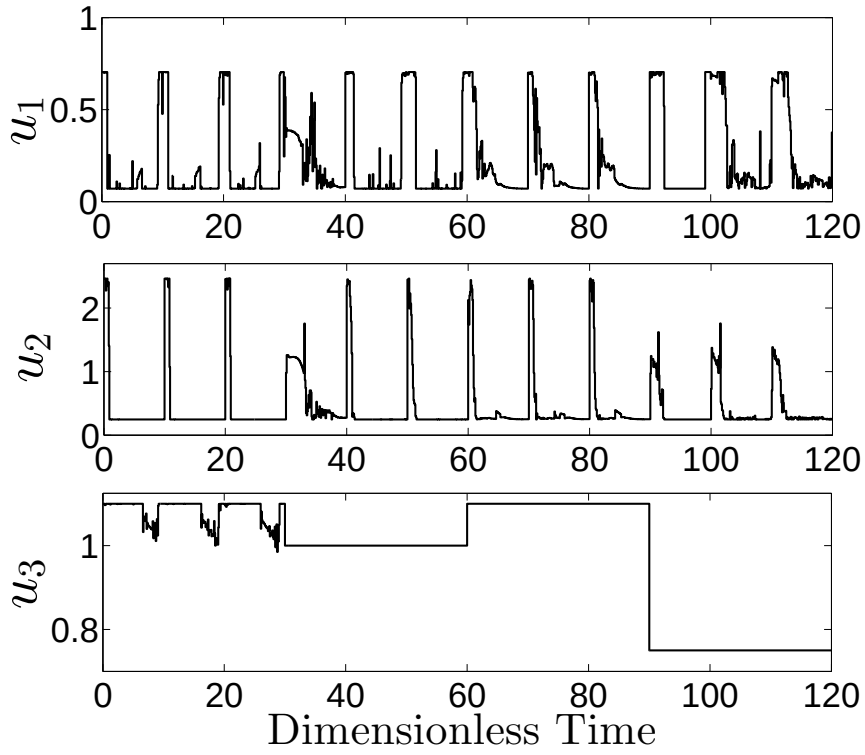

Figure 5.4: Closed-loop input trajectories of the reactor of Eq. 5.9 under the LEMPC using the error-triggered on-line model identification starting from $x_I^T = [x_{1I}\ x_{2I}\ x_{3I}\ x_{4I}] = [0.997\ 1.264\ 0.209\ 1.004]$.

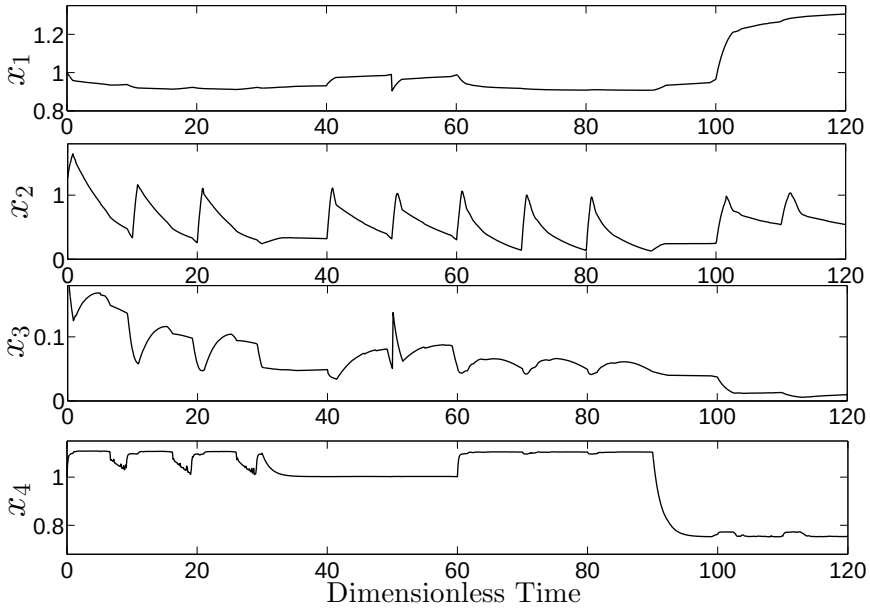

Figure 5.5: Closed-loop state trajectories of the reactor of Eq. 5.9 under the LEMPC using the error-triggered on-line model identification starting from $x_I^T = [x_{1I}\ x_{2I}\ x_{3I}\ x_{4I}] = [0.997\ 1.264\ 0.209\ 1.004]$.

5.5 Application of Error-Triggered On-Line Model Identification when the Fault Value is Unknown: CSTR Example

In this section, we use a chemical process example to demonstrate the application of the proposed error-triggered on-line model identification for fault-tolerant LEMPC when the value at which the actuator is stuck is unknown. The example is a non-isothermal, well-mixed continuous stirred tank reactor (CSTR) in which an irreversible second-order exothermic reaction takes place converting the reactant A to the desired product B. An inert solvent containing the reactant A with a concentration C_{A0} is fed to the reactor at a feed volumetric flow rate F and a temperature T_0. The CSTR is heated/cooled by a heating jacket that supplies/removes heat at a heat rate Q. The liquid inside the CSTR is assumed to have constant heat capacity C_p, volume V, and density ρ_L. The CSTR dynamic model, derived from mass and energy balances, that describes the reactant concentration C_A and temperature T evolution with time is presented below:

$$\frac{dC_A}{dt} = \frac{F}{V}(C_{A0} - C_A) - k_0 e^{-E/R_g T} C_A^2 \tag{5.17a}$$

$$\frac{dT}{dt} = \frac{F}{V}(T_0 - T) - \frac{\Delta H k_0}{\rho_L C_p} e^{-E/R_g T} C_A^2 + \frac{Q}{\rho_L C_p V} \tag{5.17b}$$

where the parameters k_0, E and ΔH denote the reaction pre-exponential factor, activation energy and the enthalpy of the reaction, respectively. The values of the process parameters are listed in Table 5.3. The reactor inlet concentration C_{A0} and heat supply/removal rate Q are the manipulated inputs, which are constrained by the following maximum and minimum values: $0.5 \leq C_{A0} \leq 7.5\ kmol/m^3$ and $-5.0 \times 10^5 \leq Q \leq 5.0 \times 10^5\ kJ/hr$. The reactor is operated around the open-loop asymptotically stable steady-state $[C_{As}\ T_s] = [1.2\ kmol/m^3\ 438.0\ K]$ which corresponds to the input values $[C_{A0s}\ Q_s] = [4.0\ kmol/m^3\ 0.0\ kJ/hr]$. We rewrite the CSTR state and input vectors in deviation from this steady-state as $x^T = [C_A - C_{As}\ T - T_s]$ and $u^T = [C_{A0} - C_{A0s}\ Q - Q_s]$, in order to translate the origin to be the equilibrium of the unforced system. The process dynamic model of Eq. 5.17 and all empirical models in this example are numerically integrated using the explicit

Euler method with an integration time step of $h_c = 10^{-4}\ hr$.

Table 5.3: Parameter values of the CSTR.

$F = 5.0$	$\frac{m^3}{hr}$	$k_0 = 8.46 \times 10^6$	$\frac{m^3}{kmol\ hr}$
$T_0 = 300$	K	$\Delta H = -1.15 \times 10^4$	$\frac{kJ}{kmol}$
$V = 1.0$	m^3	$E = 5.0 \times 10^4$	$\frac{kJ}{kmol}$
$C_p = 0.231$	$\frac{kJ}{kg\ K}$	$\rho_L = 1000$	$\frac{kg}{m^3}$
$R = 8.314$	$\frac{kJ}{kmol\ K}$		

The control objective is to maximize the time-averaged production rate of the desired product B (the process profit). Therefore, the production rate of B is used to design the cost function of the LEMPC and is given by:

$$\int_{t_k}^{t_{k+N}} L_e(x,u)\, d\tau = \frac{1}{(t_{k+N}-t_k)} \int_{t_k}^{t_{k+N}} k_0 e^{-E/R_g T(\tau)} C_A^2(\tau)\, d\tau\ . \tag{5.18}$$

We also consider that there is a limitation on the amount of reactant material that may be fed to the reactor in a given period of operation of length $t_p = 1\ hr$. Therefore, the inlet concentration input trajectory is restricted by the following material constraint:

$$\frac{1}{t_p} \int_0^{t_p} u_1(\tau)\, d\tau = 0.0\ kmol/m^3. \tag{5.19}$$

The purpose of this constraint is to limit the amount of reactant material fed to the reactor over each operating period $t_p = 1\ hr$ to be equal to the amount that would be fed for steady-state operation.

The reactor first-principles model in Eq. 5.17 is assumed to be unavailable, with the result that an empirical model for the system must be identified to develop an LEMPC with the above objective and constraints. Therefore, a series of step inputs were generated and applied to the CSTR and the corresponding outputs were collected in order to identify a linear time-invariant state-space model that captures the process dynamics in a state-space region around the steady-state. Using these input and output data points, the ordinary multivariable output error state-space

(MOESP)[43] algorithm was implemented to produce a linear empirical model for the reactor of Eq. 5.17. This initial ($i = 1$) model of the reactor is described by the following matrices:

$$A_1 = \begin{bmatrix} -34.5 & -0.473 \\ 1430 & 18.1 \end{bmatrix}, \; B_1 = \begin{bmatrix} 5.24 & -8.1 \times 10^{-6} \\ -11.6 & 0.457 \end{bmatrix} \tag{5.20}$$

Model validation was conducted using step, impulse, and sinusoidal inputs. This empirical model is used to design the Lyapunov-based controller for the LEMPC design since it is assumed that the reactor first-principles model of Eq. 5.17 is unavailable. The Lyapunov-based controller consisted of both inputs following the control law $h_{L1}^T(x) = [h_{L1,1}(x) \; h_{L1,2}(x)]$, where the reactant inlet concentration $h_{L1,1}(x)$ was fixed at 0.0 $kmol/m^3$ to meet the material constraint of Eq. 5.19. For the heat rate supply/removal rate, the following control law was used:[27]

$$h_{L1,2}(x) = \begin{cases} -\dfrac{L_{\tilde{f}}\hat{V} + \sqrt{L_{\tilde{f}}\hat{V}^2 + L_{g_2}\hat{V}^4}}{L_{g_2}\hat{V}}, & \text{if } L_{g_2}\hat{V} \neq 0 \\ 0, & \text{if } L_{g_2}\hat{V} = 0 \end{cases} \tag{5.21}$$

where the vector function $\tilde{f} : R^n \to R^n$ and the matrix function $g : R^n \to R^{n \times m}$ are defined as follows:

$$\frac{dx(t)}{dt} = \underbrace{Ax}_{=:\tilde{f}(x)} + \underbrace{B}_{=:g(x)} u \, , \tag{5.22}$$

and $g_2(x)$ is the second column of the B matrix. $L_{\tilde{f}}\hat{V}$ and $L_{g_2}\hat{V}$ are the Lie derivatives of the Lyapunov function $\hat{V}(x)$ with respect to $\tilde{f}(x)$ and $g_2(x)$, respectively. A quadratic Lyapunov function of the form $\hat{V}(x) = x^T P x$ is used, where P is the following positive definite matrix:

$$P = \begin{bmatrix} 1060 & 22 \\ 22 & 0.52 \end{bmatrix} \tag{5.23}$$

Through extensive closed-loop simulations of the reactor system under the control law $h_{L1}(x)$,

the level sets $\Omega_{\hat{\rho}_{e1}}$ and $\Omega_{\hat{\rho}_1}$ of the Lyapunov function $\hat{V}$ were chosen to have $\hat{\rho}_{e1} = 55$ and $\hat{\rho}_1 = 64.32$. In this region, the nonlinear dynamics of Eq. 5.17 are well-captured by the linear empirical model of Eq. 5.20.

In this example, the LEMPC design in Eq. 5.6 that also incorporates the material constraint of Eq. 5.19 is applied to the process in Eq. 5.17. We will demonstrate the case where a fault occurs in u_2. When such a fault occurs, another stabilizing control law that is based on u_1 needs to be designed to implement Mode 2 of the LEMPC if the closed-loop state exits $\Omega_{\hat{\rho}_{e1}}$. The stabilizing control law is of the following form:

$$h_{L1,1}(x) = \begin{cases} -\dfrac{L_{\tilde{f}}\hat{V} + \sqrt{L_{\tilde{f}}\hat{V}^2 + L_{g_1}\hat{V}^4}}{L_{g_1}\hat{V}}, & \text{if } L_{g_1}\hat{V} \neq 0 \\ 0, & \text{if } L_{g_1}\hat{V} = 0 \end{cases} \tag{5.24}$$

where $g_1(x)$ is the first column of the B matrix and $\hat{V}$, $\Omega_{\hat{\rho}_{e1}}$ and $\Omega_{\hat{\rho}_1}$ are the same as mentioned above. After the fault occurs, u_1 is the only manipulated input that is available both to maximize the profit and also to keep the state inside the stability region $\Omega_{\hat{\rho}_1}$, and therefore, the manipulated input trajectories calculated by the LEMPC with an empirical model may require u_1 to utilize more material than it is constrained to use by the material constraint of Eq. 5.19 (i.e., the LEMPC optimization problem may become infeasible in the second half of the operating periods after the occurrence of the fault in u_2). When the optimization problem becomes infeasible, a different optimization problem is solved to determine the value of u_1 to apply to the process, with the form of Eq. 5.6, without the material constraint of Eq. 5.19, and with the stage cost $L_e(x,u) = u_1^2(\tau)$ instead of the stage cost in Eq. 5.18. Mode 2 is continuously implemented so that this control design minimizes the amount of feedstock material utilized while seeking to stabilize the closed-loop system. For all of the simulations presented below, the LEMPC is designed using a prediction horizon of $N = 10$ and a sampling period of $\Delta = 0.01\ hr$. The open-source optimization solver IPOPT[119] was used in solving the LEMPC optimization problems at each sampling time.

The CSTR was initialized from the open-loop stable steady-state and was controlled using the

LEMPC designed with the cost function of Eq. 5.18 and the material constraint of Eq. 5.19. The LEMPC utilizes the model of Eq. 5.20 to predict the values of the process states throughout the prediction horizon. A moving horizon error detector that calculates e_d at each sampling time to determine when it is necessary to trigger re-identification of the empirical process model was designed and initiated after $M = 50$ input/output data points were available. Simulations of the CSTR suggested that significant plant-model mismatch was indicated when the value of e_d exceeded 3 and thus, this value was chosen as the threshold to trigger model re-identification. The moving horizon error detector calculates the relative prediction error in the concentration and temperature throughout the past 50 sampling periods and current sampling time as follows:

$$e_d(t_k) = \sum_{r=0}^{50} \left[\frac{|T_p(t_{k-r}) - T(t_{k-r})|}{|T(t_{k-r})|} + \frac{|C_{A_p}(t_{k-r}) - C_A(t_{k-r})|}{|C_A(t_{k-r})|} \right] \tag{5.25}$$

The initial empirical model utilized within the LEMPC coupled with the moving horizon error detector/on-line model re-identification strategy was A_1 and B_1. After two operating periods (i.e., at the beginning of the 3^{rd} operating period), an actuator fault occurs, causing the heat input to stay at the value of $Q = 4.0 \times 10^4$ kJ/hr for the next two operating periods. As mentioned above, this example assumes that the value at which Q became stuck is unknown, and therefore, the LEMPC continues to solve for both u_1 and u_2 after the fault, but only u_1 is implemented since a fault has occurred in u_2. Fig. 5.10 shows the increase in e_d after the fault occurrence, leading it to eventually exceed its threshold and trigger on-line model re-identification, using input/output data collected after the occurrence of the fault, which resulted in a sharp drop in the prediction error. The following model was identified using the post-fault input/output data:

$$A_2 = \begin{bmatrix} 678.6 \times 10^{-3} & 12.89 \\ -4.378 \times 10^{-3} & 1.168 \end{bmatrix}, \; B_2 = \begin{bmatrix} 26.35 \times 10^{-3} \\ -1.700 \times 10^{-7} \end{bmatrix} \tag{5.26}$$

Notably, in accordance with Step *4* of the implementation strategy presented in this chapter, the B_2 matrix has one less column than the B_1 matrix due to the loss of availability of u_2 as a manipulated input. When the empirical models were re-identified, the controller of Eq. 5.21

was replaced with that of Eq. 5.24 based on the new empirical model. The same value of $\hat{V}$ was used for all simulations. The input and state trajectories for the reactor process under the LEMPC of Eq. 5.6 with the empirical models of Eqs. 5.20 and 5.26 (with the changes in the LEMPC when infeasibility occurs as noted above) subject to the actuator fault in u_2 are presented in Figs. 5.6-5.9. Fig. 5.10 shows the value of e_d throughout time under the proposed approach, which shows the growth of e_d that triggered the model re-identification. The new model (A_2 and B_2) that was obtained from input and output data collected after the fault occurrence was able to capture the process dynamics corresponding to the new conditions and caused the values of $e_d(t_k)$ to decrease rapidly afterwards. In addition, Fig. 5.11 shows the evolution of the state-space trajectories within the level sets $\Omega_{\hat{\rho}_1}$ and $\Omega_{\hat{\rho}_{e1}}$ during process operation. This figure shows that the state was maintained within the stability region $\Omega_{\hat{\rho}_1}$ under the proposed scheme. Infeasibility of the LEMPC with the material constraint occurred in the third and fourth hours of operation, during which the material constraint of Eq. 5.19 was violated by 0.08 $kmol/m^3$ and 0.047 $kmol/m^3$, respectively (i.e., $\frac{1}{1\ hr}\int_{2\ hr}^{3\ hr} u_1(\tau)\ d\tau = 0.08\ kmol/m^3$ for the third hour and $\frac{1}{1\ hr}\int_{3\ hr}^{4\ hr} u_1(\tau)\ d\tau = 0.047\ kmol/m^3$ for the fourth hour), resulting in use of the modified LEMPC design discussed above.

In addition to decreasing the plant-model mismatch due to faults, the on-line model identification procedure improved the process economic performance compared to not updating the model as presented in Table 5.4. The results listed are for two approaches: the "One Empirical Model" approach, in which no model re-identification is conducted and the initial empirical model (A_1 and B_1) is used throughout the operating periods, despite the fault (i.e., the LEMPC calculates both u_1 and u_2 despite the fault) and the "On-line Model ID" approach, in which the proposed on-line model re-identification approach is employed. These results show the significant improvement in the profit resulting from updating the empirical model on-line compared to using the same initial empirical model throughout process operation despite the faults. Table 5.4 shows the time-averaged profit (denoted by J_e), the maximum value of e_d and the amount of material used ($\frac{1}{1\ hr}\int_{3\ hr}^{4\ hr} u_1(\tau)\ d\tau$) for each approach throughout the last hour of operation, where J_e in this table

is given by:

$$J_e = \frac{1}{1\ hr}\int_{3\ hr}^{4\ hr} k_0 e^{-E/R_g T(\tau)} C_A^2(\tau) d\tau. \tag{5.27}$$

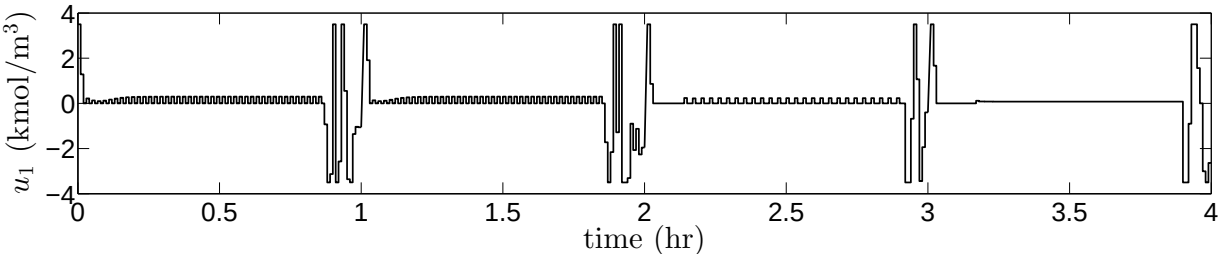

Figure 5.6: Closed-loop input trajectory ($u_1 = C_{A0} - C_{A0s}$) of the reactor of Eq. 5.17 under the LEMPC using the error-triggered on-line model identification starting from $[C_{As}\ T_s] = [1.2\ kmol/m^3\ 438.0\ K]$ with $Q = 4.0 \times 10^4\ kJ/hr$ after the fault.

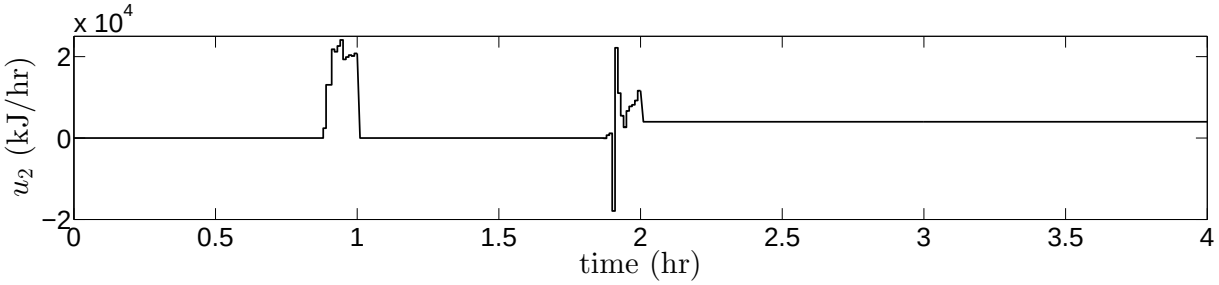

Figure 5.7: Closed-loop input trajectory ($u_2 = Q - Q_s$) of the reactor of Eq. 5.17 under the LEMPC using the error-triggered on-line model identification starting from $[C_{As}\ T_s] = [1.2\ kmol/m^3\ 438.0\ K]$ with $Q = 4.0 \times 10^4\ kJ/hr$ after the fault.

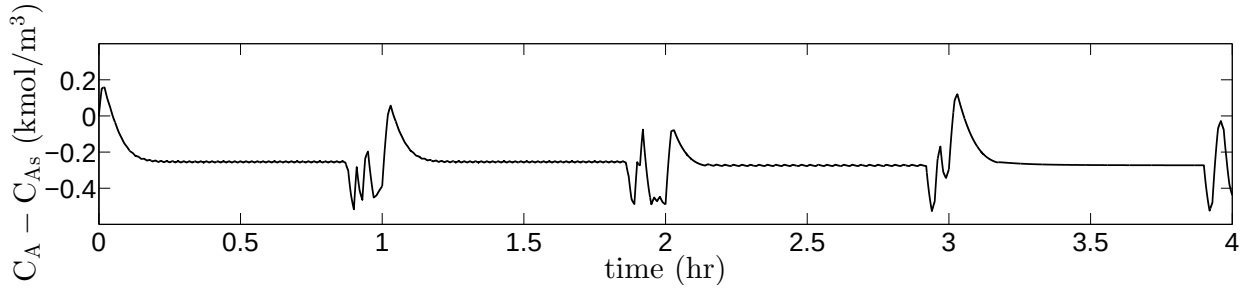

Figure 5.8: Closed-loop state trajectory ($x_1 = C_A - C_{As}$) of the reactor of Eq. 5.17 under the LEMPC using the error-triggered on-line model identification starting from $[C_{As}\ T_s] = [1.2\ kmol/m^3\ 438.0\ K]$ with $Q = 4.0 \times 10^4\ kJ/hr$ after the fault.

To demonstrate the ability of the moving horizon error detector to indicate significant prediction errors and determine when it is necessary to update the model on-line, another simulation of the

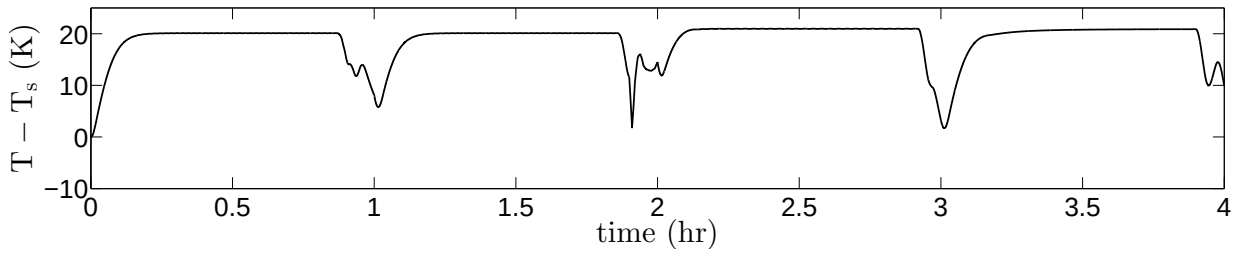

Figure 5.9: Closed-loop state trajectory ($x_2 = T - T_s$) of the reactor of Eq. 5.17 under the LEMPC using the error-triggered on-line model identification starting from $[C_{As}\ T_s] = [1.2\ kmol/m^3\ 438.0\ K]$ with $Q = 4.0 \times 10^4\ kJ/hr$ after the fault.

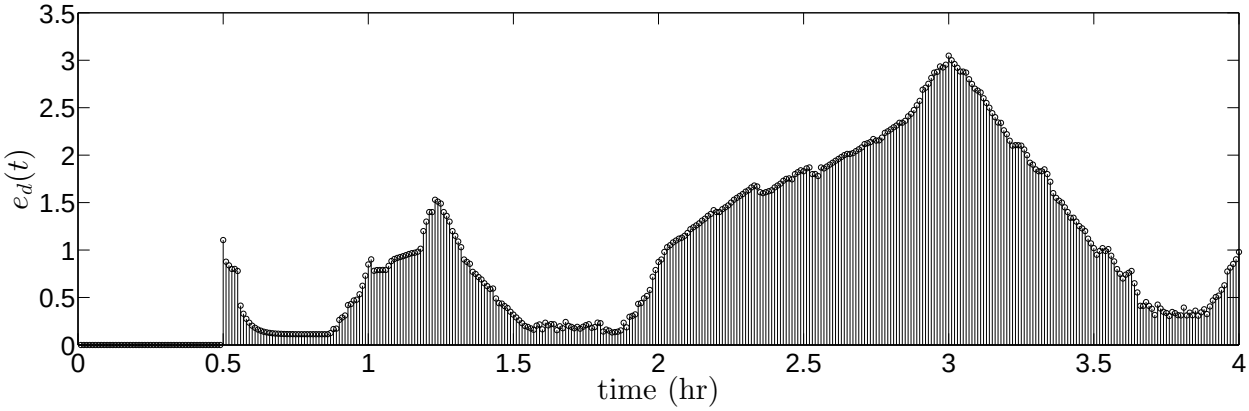

Figure 5.10: Value of error metric e_d at each sampling using the detector of Eq. 5.25 for the LEMPC integrated with the error-triggered on-line model identification with $Q = 4.0 \times 10^4\ kJ/hr$ after the fault.

Table 5.4: Relative prediction error, average profit and amount of material used for the CSTR under LEMPC during the 4^{th} hour of operation.

Approach	J_e	Max $e_d(t_k)$	$\frac{1}{1\ hr}\int_{3\ hr}^{4\ hr} u_1(\tau)\, d\tau$
One Empirical Model	14.94	3.92	0.089
On-line Model ID	15.49	3.01	0.047

CSTR of Eq. 5.17 is considered. The CSTR was initialized from the same open-loop stable steady-state and was controlled using the same LEMPC architecture mentioned above with the same initial model (A_1 and B_1). The moving horizon error detector was initiated after $M = 50$ input/output data points were available to calculate the values of e_d. After two operating periods, an actuator fault is assumed to occur causing the heat input to remain at $Q = 1.0 \times 10^4\ kJ/hr$ for the next two operating periods. The LEMPC continued to compute optimal control actions for both u_1 and u_2.

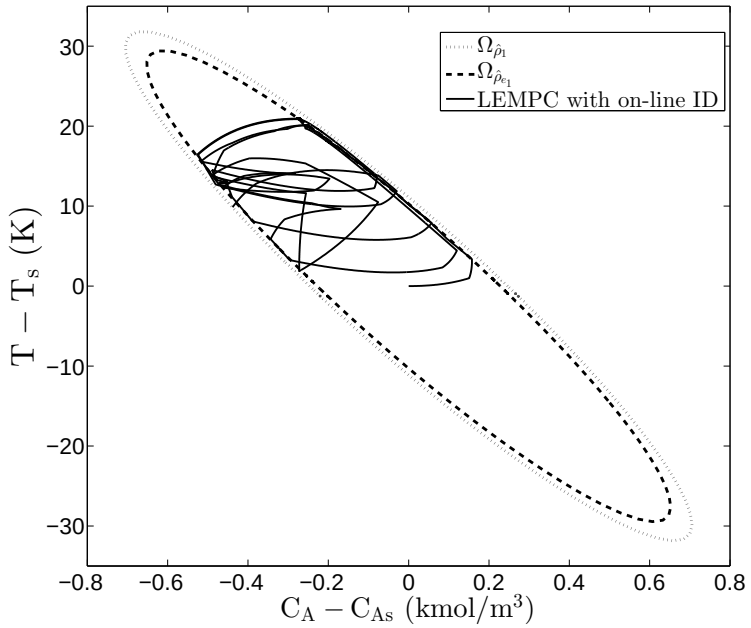

Figure 5.11: State trajectories in the state-space coordinates of the closed-loop CSTR of Eq. 5.17 under the LEMPC with error-triggered on-line model identification starting from $[C_{As}\ T_s] = [1.2\ kmol/m^3\ 438.0\ K]$ with $Q = 4.0 \times 10^4\ kJ/hr$ after the fault.

This caused values of e_d to increase as can be seen in Fig. 5.12. However, no re-identification was required since the error did not exceed the threshold of $e_d = 3$ showing that the error-triggering was successful at deciding the necessity of model updates. The state-space trajectories of the reactor process under the LEMPC subject to the actuator fault in the value of u_2 are presented in Fig. 5.13. The figure shows that the state was maintained within the stability region even after the fault occurrence. In this simulation, the material constraint was not violated after the fault occurrence (i.e., $\frac{1}{1\ hr}\int_{2\ hr}^{3\ hr} u_1(\tau)\ d\tau = 0.0\ kmol/m^3$ for the third hour and $\frac{1}{1\ hr}\int_{3\ hr}^{4\ hr} u_1(\tau)\ d\tau = 0.0\ kmol/m^3$ for the fourth hour).

5.6 Conclusion

In this chapter, we proposed an on-line model identification methodology that updates the empirical models used in LEMPC on-line to overcome actuator faults. Empirical models were updated on-line based on significant prediction errors indicated by a moving horizon error detector. The error-

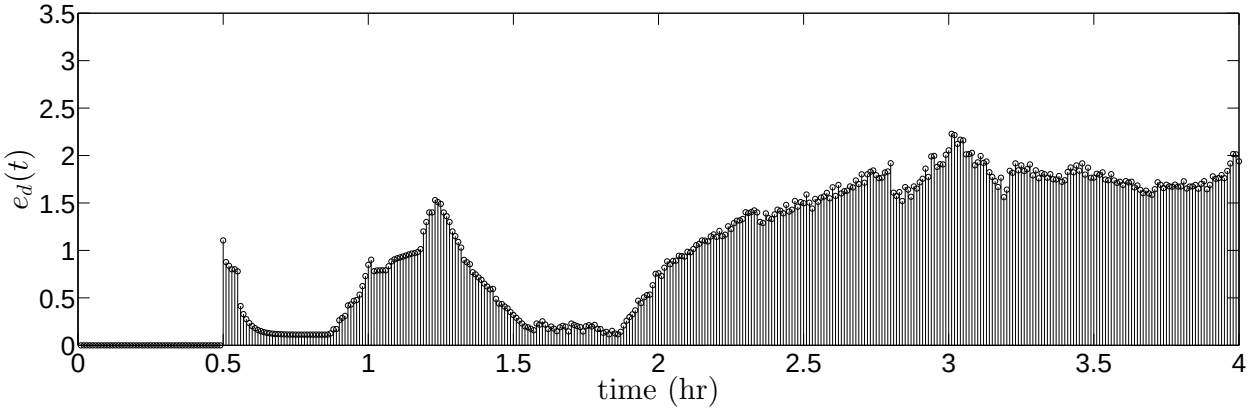

Figure 5.12: Value of error metric e_d at each sampling using the detector of Eq. 5.25 for the LEMPC integrated with the error-triggered on-line model identification with $Q = 1.0 \times 10^4\ kJ/hr$ after the fault.

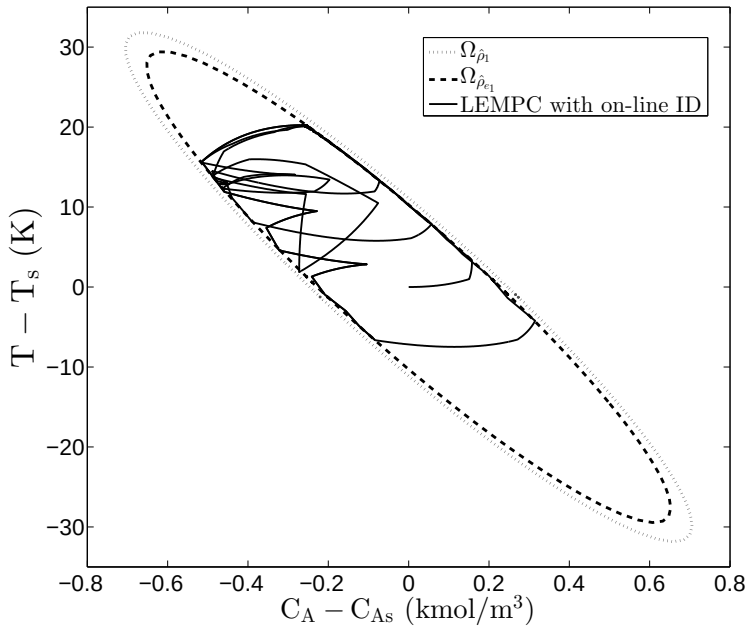

Figure 5.13: State trajectories in the state-space coordinates of the closed-loop CSTR of Eq. 5.17 under the LEMPC with error-triggered on-line model identification starting from $[C_{As}\ T_s] = [1.2\ kmol/m^3\ 438.0\ K]$ with $Q = 1.0 \times 10^4\ kJ/hr$ after the fault.

triggered on-line model identification methodology can be applied to overcome different actuator fault scenaria that occur in practice, including the case where the value at which the actuator is stuck is known and the case where the value at which the actuator is stuck is unknown. Applications were demonstrated for both cases using two chemical process examples under LEMPC. In the first example, a benchmark chemical process was used to demonstrate the application of the proposed

scheme in the case where the value at which the actuator is stuck is known. In the second example, another chemical process was used to demonstrate the application of the proposed scheme in the case where the value at which the actuator is stuck is unknown. The chemical process examples presented the ability of the proposed scheme to detect when it is necessary to update the empirical model on-line in response to operational variations caused by actuator faults and/or disturbances. Improved state predictions and economic performance were obtained under the proposed scheme compared to using one empirical model throughout operation despite the actuator faults. The examples show the successful implementation of a unified framework using the moving horizon error detector and error-triggered model updates within LEMPC for handling faults.

Chapter 6

Integrating Production Scheduling and Process Operation via Economic Model Predictive Control

6.1 Introduction

Dynamic product demand changes have made it necessary to increase the operational management efficiency and plant economic performance in the chemical and petrochemical industry. This has led process systems engineers in both academia and industry to develop technologies that aim to economically optimize process operation and allow for real-time energy management. Integrating feedback process control strategies with plant economic optimization serves as one approach for achieving optimal process operation. Economic model predictive control (EMPC) is a fairly recent control strategy that integrates dynamic economic plant optimization and a feedback control policy by utilizing an economics-based cost and the process dynamic model to predict the plant evolution. EMPC has gained attention due to its ability to yield optimal time-varying operation while accounting for operational constraints and ensuring closed-loop stability (e.g.,[14,22,49,122–127]).

Production management subject to demand changes plays a crucial role in industry.[90–93] Shifts

in demand and supply of certain products occur constantly and finding reliable methods to achieve the desired production has become necessary.[94,95] It has become common in the chemical industry to produce multiple products from the same plant in both batch and continuous processes[91,93] such as the production of multiple grades of polyethylene.[96] Various studies have considered the integration of planning and scheduling in supply chain optimization to achieve economically optimal operational management in response to the desired demand.[90,93–95] Some methods proposed in this context have been inspired by process control design methodologies, such as modeling the dynamic production in supply chains and using classical process control strategies to manage and control the supply chain.[97] In addition, several frameworks that use advanced control and optimization strategies have been proposed for scheduling in order to optimize the decision-making process while accounting for practical constraints and limitations.[93,94] Furthermore, a rolling horizon approach solved using multiparametric programming with uncertainties in both the disturbances and initial states was investigated for reactive scheduling.[98] Scheduling of industrial electricity use, with a case study for the energy-intensive chlor-alkali process, was also investigated in[99] by considering contracts between industrial consumers and electricity producers with price penalties in use over the contract in the scheduling problem.

After solving the planning and scheduling problem, process control strategies are used to drive the plant to follow the desired production schedule. Scheduling and control are two crucial elements that serve the same overall goal of maximizing plant economics while meeting the customer demand. Linking the control problem with the scheduling problem by accounting for the control layer in the scheduling layer to improve economics has been considered.[100] Solving the control and scheduling problems simultaneously while accounting for the nonlinear dynamics of processes in order to find optimal steady-states and optimal product and states transitions has been considered.[101,102] Integrating process design with control and scheduling has also been investigated.[103] Extensive research efforts have been dedicated recently to developing reliable methods that could track desired production set-points that correspond to different operating conditions.[91,105,106] The use of multiple Lyapunov-based nonlinear controllers to achieve the desired schedule where each

nonlinear controller is equipped with a Lyapunov function corresponding to the region of operation has been studied in.[107] Demand management through production scheduling and closed-loop process control while accounting for the cost of transition between different production levels has also been proposed in.[106] This concept can be used for demand response of industrial electricity customers.[108] In addition, several studies have considered the use of model predictive control (MPC) in tracking the desired production schedule while accounting for input/output constraints.[90,91,105] The use of a low-dimensional time scale-bridging model (SBM) in a scheduling-oriented MPC in order to link control with scheduling and capture the closed-loop dynamics over the longer time scales of the scheduling problem has been considered in.[90] Integrating scheduling and control for continuous processes under dynamic product demand changes was proposed where a model predictive control was used to track the schedule set-points.[91] Another application of combining scheduling with control is for a post-combustion CO_2 capture process.[110]

Typically, only a subset of the components of the total process state vector is required to follow a production schedule. Therefore, there is a potential in many processes to meet the desired schedule while achieving economically optimal process operation. In this chapter, we propose an approach that achieves maximizing plant economics while meeting the desired production schedule using economic model predictive control (EMPC). The EMPC framework tracks production schedules for the desired states while maximizing economics with respect to the rest of the states within manifolds in the process state-space that maintain the requested schedule. Practical considerations that should be introduced at the operating or scheduling level when the EMPC for schedule management is used are discussed. Sufficient conditions for feasibility and closed-loop stability of a nonlinear process under the proposed LEMPC formulation are derived for the case that the times at which the schedule switches occur are known *a priori* and the case that they are not. The LEMPC with production schedule management method is applied to a chemical process example and closed-loop simulations demonstrate closed-loop stability of the process while following the desired production schedule and maximizing economics.

6.2 Preliminaries

6.2.1 Notation

The symbol x^T is used to denote the transpose of the vector x. The 2-norm of a vector is denoted by the operator $|\cdot|$. A continuous function $\alpha : [0,a) \to [0,\infty)$ is called a class $\mathscr{K}$ function if it is strictly increasing and $\alpha(0) = 0$. The symbol Ω_ρ is used to denote a level set of a sufficiently smooth scalar function $V(x)$ ($\Omega_\rho := \{x \in R^n : V(x) \leq \rho\}$). The symbol $\Delta > 0$ denotes the sampling period.

6.2.2 Class of Systems

The class of nonlinear systems considered in this chapter is described by nonlinear ordinary differential equations of the following form:

$$\frac{dx}{dt} = f(x,u,w) \tag{6.1}$$

where $x \in R^n$ and $u \in R^m$ are the system state and manipulated input vectors respectively. The vector $w \in R^l$ denotes the disturbance vector. Actuator constraints on the control energy available are considered by restricting the control actions to belong to the convex set $U := \{u \in R^m : u_i^{\min} \leq u_i \leq u_i^{\max},\ i = 1,\ldots,m\}$. The disturbance vector is assumed to be bounded (i.e., $w \in W := \{w \in R^l :\ |w(t)| \leq \theta\ \forall\ t\}$). The origin is taken to be an equilibrium of the unforced system of Eq. 6.1 (i.e., $f(0,0,0) = 0$). At each sampling time $t_k = k\Delta$, $k = 0,1,\ldots$, measurements of the state vector $x(t_k)$ are assumed to be available.

The class of nonlinear systems studied is restricted to stabilizable nonlinear systems for which there exists a controller $h(x) \in U$ that can render the origin of the nominal ($w(t) \equiv 0$) closed-loop system of Eq. 6.1 asymptotically stable in the sense that there exists a sufficiently smooth Lyapunov

function $V : R^n \rightarrow R_+$ that satisfies the following inequalities:[30,111]

$$\alpha_1(|x|) \leq V(x) \leq \alpha_2(|x|), \tag{6.2a}$$

$$\frac{\partial V(x)}{\partial x} f(x, h(x), 0) \leq -\alpha_3(|x|), \tag{6.2b}$$

$$\left| \frac{\partial V(x)}{\partial x} \right| \leq \alpha_4(|x|) \tag{6.2c}$$

for all x in an open neighborhood $D \subseteq R^n$ that includes the origin and $\alpha_j(\cdot)$, $j = 1,\ 2,\ 3,\ 4$, are class $\mathscr{K}$ functions. Various stabilizing controllers that take into account input constraints have been developed for several classes of nonlinear systems.[10,12,27] The stability region of the closed-loop system is taken to be the level set $\Omega_\rho \subset D$ where $\dot{V} < 0$. The origin of the system of Eq. 6.1 is rendered practically stable[31] when the controller $h(x)$ is applied in a sample-and-hold fashion for a sufficiently small sampling period. The function f is assumed to be locally Lipschitz on $\Omega_\rho \times U \times W$.

In this chapter, it is assumed that the values of the first n_s states of the state vector x (i.e., $x_i,\ i = 1, \ldots, n_s$) are required to be maintained at certain values $x_{i_{desired}},\ i = 1, \ldots, n_s$, which change at specific points in time corresponding to a production schedule. For every set of values $x_{i_{desired}},\ i = 1, \ldots, n_s$, within the schedule, we assume that a steady-state of the nominal system of Eq. 6.1 exists at which the states $x_i,\ i = 1, \ldots, n_s$, have the required values. The origin of the system of Eq. 6.1 can be translated to have its equilibrium at each of these steady-states corresponding to the schedule. We assume that for each steady-state, there exists a stabilizing controller that can make that steady-state asymptotically stable, with a corresponding Lyapunov function. With some abuse of notation, we will denote in this chapter the deviation of the state from the currently desired steady-state by x and will use the notation (e.g., f, V, h, D, Ω_ρ, and α_j, $j = 1,\ 2,\ 3,\ 4$) developed in the above discussion for the case that the equilibrium was at the origin of the original system to denote analogous regions or functions for each deviation variable x. With this convention, it is assumed that the Lyapunov function and stabilizing controller for each steady-state satisfy Eq. 6.2.

Because f is Lipschitz continuous, V is sufficiently smooth, and x, u, and w are bounded within compact sets, there exist $M > 0$, $L_x > 0$, $L_w > 0$, $L'_x > 0$ and $L'_w > 0$ such that:

$$|f(x,u,w)| \leq M \tag{6.3}$$

$$|f(x_1,u,w) - f(x_2,u,0)| \leq L_x|x_1 - x_2| + L_w|w| \tag{6.4}$$

$$\begin{aligned} &\left|\frac{\partial V(x_1)}{\partial x} f(x_1,u,w) - \frac{\partial V(x_2)}{\partial x} f(x_2,u,0)\right| \\ &\qquad \leq L'_x|x_1 - x_2| + L'_w|w| \end{aligned} \tag{6.5}$$

for all $x, x_1, x_2 \in \Omega_\rho$, $u \in U$, and $|w| \leq \theta$.

6.2.3 Economic Model Predictive Control

Economic model predictive control (EMPC) is a model predictive control (MPC) strategy for which the objective function is based on economics and does not have its minimum at the economically optimal steady-state of the process. To address feasibility and closed-loop stability of a process under such a controller, a variety of constraints have been investigated, but a general formulation of EMPC is as follows:[114]

$$\min_{u \in S(\Delta)} \int_{t_k}^{t_{k+N}} -L_e(\tilde{x}(\tau), u(\tau))\, d\tau + V_f(\tilde{x}(t_{k+N})) \tag{6.6a}$$

$$\text{s.t.} \quad \dot{\tilde{x}}(t) = f(\tilde{x}(t), u(t), 0) \tag{6.6b}$$

$$\tilde{x}(t_k) = x(t_k) \tag{6.6c}$$

$$u(t) \in U, \ \forall\, t \in [t_k, t_{k+N}) \tag{6.6d}$$

$$g(\tilde{x}(t), u(t)) \leq 0, \ \forall\, t \in [t_k, t_{k+N}] \tag{6.6e}$$

where the stage cost $L_e(\tilde{x}(\tau), u(\tau))$ (Eq. 6.6a) represents the process profit, and $V_f(\tilde{x}(t_{k+N}))$ is a terminal penalty evaluated at the predicted state $\tilde{x}$ at the end of the prediction horizon of length N (where the prediction $\tilde{x}(t)$ is the solution of the nominal process model of Eq. 6.6b at time t given

the initial condition of Eq. 6.6c obtained from a state measurement at time t_k). The constraint of Eq. 6.6d ensures that the process inputs, which are the decision variables u ($u(\cdot) \in S(\Delta)$ signifies that the decision variables are piecewise constant vectors with period Δ) of the EMPC meet the input constraints. The function $g(x,u)$ represents any additional constraints that may be included within the EMPC. Three constraints that are often used within EMPC for stability purposes and can be represented by g are a terminal equality constraint,[50] a terminal region constraint,[49] and Lyapunov-based constraints[20] (for the terminal equality constraint and Lyapunov-based constraints, V_f is not usually included[114]). Other types of constraints or considerations for EMPC are addressed in.[14,114]

6.2.4 Lyapunov-based EMPC

Though this chapter will address scheduling management in the context of EMPC in general, the formulation of EMPC with Lyapunov-based stability constraints (termed Lyapunov-based EMPC (LEMPC)[20]) will receive special focus because it is straightforward for this method to prove feasibility and closed-loop stability of a process under this EMPC formulation in the presence of disturbances with an *a priori* characterization of the set of initial conditions for which recursive feasibility is guaranteed. The formulation of LEMPC, incorporating Lyapunov-based stability con-

straints based on the explicit controller $h(x)$, is as follows:

$$\min_{u\in S(\Delta)} \int_{t_k}^{t_{k+N}} -L_e(\tilde{x}(\tau),u(\tau))\, d\tau \tag{6.7a}$$

$$\text{s.t.} \quad \dot{\tilde{x}}(t) = f(\tilde{x}(t),u(t),0) \tag{6.7b}$$

$$\tilde{x}(t_k) = x(t_k) \tag{6.7c}$$

$$u(t) \in U,\ \forall\, t \in [t_k,t_{k+N}) \tag{6.7d}$$

$$V(\tilde{x}(t)) \leq \rho_e,\ \forall\, t \in [t_k,t_{k+N})$$

$$\text{if } x(t_k) \in \Omega_{\rho_e} \tag{6.7e}$$

$$\frac{\partial V(x(t_k))}{\partial x} f(x(t_k),u(t_k),0) \leq \frac{\partial V(x(t_k))}{\partial x} f(x(t_k),h(x(t_k)),0)$$

$$\text{if } x(t_k) \notin \Omega_{\rho_e} \tag{6.7f}$$

where the notation follows that in Eq. 6.6. When a state measurement is received, either the Mode 1 (Eq. 6.7e) or the Mode 2 (Eq. 6.7f) constraint is activated based on the state location in the state-space. Mode 1 promotes time-varying operation to maximize profit while maintaining the state within the region $\Omega_{\rho_e} \subset \Omega_\rho$. Mode 2 is activated when the closed-loop state escapes the Ω_{ρ_e} region to force the state back into Ω_{ρ_e} by computing control actions that decrease the Lyapunov function value. Ω_{ρ_e} is chosen to make Ω_ρ forward invariant in the presence of disturbances. For additional discussion of LEMPC and a more rigorous closed-loop stability analysis, the reader can refer to.[20] The control actions calculated from the LEMPC design are applied in sample-and-hold in a receding horizon fashion.

6.3 Schedule Management Using EMPC

In this section, we discuss the formulation of the proposed EMPC for schedule management, along with practical and theoretical considerations. We will refer to the states that are required to follow

a certain schedule as the scheduled states, and to those that do not have this requirement as the free states.

6.3.1 Formulation of EMPC for Schedule Management

In this section, we present several ideas for formulating an EMPC for schedule management, all of which are designed to meet the constraint of the scheduling problem (i.e., the first n_s states $x_i,\ i = 1,\ldots,n_s$, of the state vector are required to be maintained at desired values $x_{i_{desired}}, i = 1,\ldots,n_s$), while simultaneously varying the remaining $n-n_s$ free states in a manner that optimizes the process economics and ensures satisfaction of all process constraints. Using the EMPC framework, meeting the schedule is thus considered to be a constraint on some states, rather than the goal of process operation. As noted in the section "Class of Systems," we assume that the origin of the system of Eq. 6.1 is translated to be at a steady-state where the schedule is met so that $x_{i_{desired}} = 0,\ i = 1,\ldots,n_s$.

To illustrate the manner in which the free states may vary to maximize process economics while the scheduled states satisfy the requested schedule, Fig. 6.1 presents an example with three states (x_1,x_2,x_3), in which the state x_1 must follow a certain schedule. The original steady-state is at the origin, and $x_{1_{desired}} = 0$. The process is initially operated in a manner that keeps x_1 small while allowing x_2 and x_3 to vary to maximize the process economics. At t_1, the state is at the dot on the x_3 axis, and the schedule for x_1 changes from $x_1 = 0$ to a new value of x_1 that corresponds to the x_1 value of the plane to the right of the origin in Fig. 6.1. As illustrated in this figure, the state is driven to this plane to meet the required schedule, and then moves around within the plane to optimize the process economics while continuing to meet the schedule.

Perhaps the most intuitive EMPC formulation for schedule management is one that uses a hard constraint for the scheduled states to enforce that they must meet the schedule at all times (except for a time during the transient between two steady-states), with either a terminal equality constraint or terminal region constraint around the steady-state corresponding to the scheduled values for stability purposes. This allows the free states to maximize process economics as long as they reach

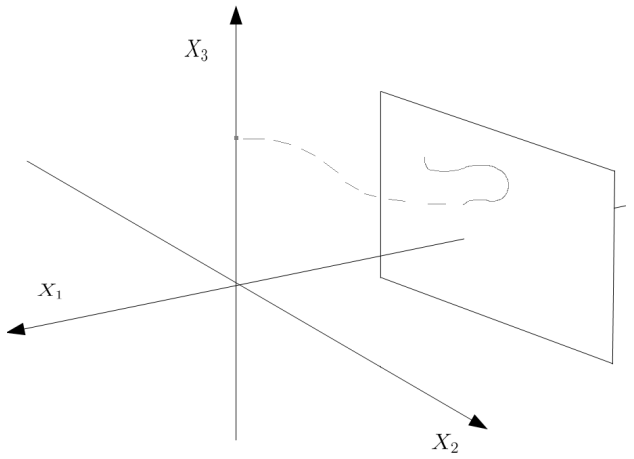

Figure 6.1: Illustration of a possible state trajectory for the closed-loop process under the EMPC for schedule management. The process is initiated from the dot on the x_3 axis and subsequently travels along the dotted line to the plane on the right of the figure in which x_1 is fixed, driving x_1 to the value required by the schedule. The state subsequently moves within the plane of fixed x_1 (solid line in the figure) to maximize the process economics with the remaining states while continuing to meet the schedule.

the steady-state values at the end of the prediction horizon. Though this method of enforcing the schedule as a hard constraint is intuitively appealing because it ensures that the schedule can be met for a system without disturbances when the problem is feasible, it may result in feasibility issues at a plant where plant-model mismatch, measurement noise, and process disturbances are unavoidable. To avoid this, the schedule constraints and terminal equality and region constraints discussed above could be implemented as soft constraints using the standard EMPC formulation of Eq. 6.6. In such a case, however, the set of initial conditions from which feasibility and closed-loop stability of a process under the EMPC could be proven would not be as straightforward to obtain as when the soft constraints are utilized in the context of LEMPC (Eq. 6.7), so the details of an LEMPC formulation for schedule management will be the subject of the rest of this section.

The formulation of an LEMPC that achieves the scheduling objective using a soft constraint on the schedule (i.e., the LEMPC seeks to drive the n_s states $x_i,\ i = 1,\ldots,n_s$, quickly to the values required by the production schedule and to maintain the states close to $x_{i_{desired}}, i = 1,\ldots,n_s$,

thereafter) is as follows:

$$\min_{u\in S(\Delta)} \int_{t_k}^{t_{k+N}} -L_e(\tilde{x}(\tau),u(\tau)) + \sum_{i=1}^{n_s} \alpha_{Wi}(\tilde{x}_i(\tau))^2 \, d\tau \tag{6.8a}$$

$$\text{s.t.} \quad \dot{\tilde{x}}(t) = f(\tilde{x}(t),u(t),0) \tag{6.8b}$$

$$\tilde{x}(t_k) = x(t_k) \tag{6.8c}$$

$$u(t) \in U, \ \forall \ t \in [t_k, t_{k+N}) \tag{6.8d}$$

$$V(\tilde{x}(t)) \leq \rho_e, \ \forall \ t \in [t_k, t_{k+N})$$

$$\text{if } x(t_k) \in \Omega_{\rho_e} \tag{6.8e}$$

$$\frac{\partial V(x(t_k))}{\partial x} f(x(t_k),u(t_k),0)$$

$$\leq \frac{\partial V(x(t_k))}{\partial x} f(x(t_k),h(x(t_k)),0)$$

$$\text{if } x(t_k) \notin \Omega_{\rho_e} \text{ or } |x_i(t_k)| \geq \gamma_i, \ i = 1,\ldots,n_s$$

$$\text{or } t_k \geq t' \tag{6.8f}$$

where the notation follows that in Eq. 6.7. The LEMPC cost function consists of two components: the first component $L_e(\tilde{x}(\tau),u(\tau))$ represents the process profit, and the second component penalizes deviations of the states $x_i, \ i = 1,\ldots,n_s$, from the desired values $x_{i_{desired}} = 0, \ i = 1,\ldots,n_s$. To achieve a quick approach of the states $x_i, \ i = 1,\ldots,n_s$, to the required values, subject to the process dynamics, the weighting coefficients $\alpha_{Wi}, \ i = 1,\ldots,n_s$, can be chosen such that following the schedule (i.e., $x_i = x_{i_{desired}}, i = 1,\ldots,n_s$) is prioritized more than optimizing the process economics through the cost function L_e. The time t' in the constraint of Eq. 6.8f will be discussed in later sections.

The states of a process operated under the LEMPC of Eq. 6.8 that are required to meet a schedule must be maintained sufficiently close to the desired values to meet the schedule, and also must never leave the stability region Ω_ρ to ensure closed-loop stability. The Mode 1 and Mode 2 constraints in Eqs. 6.8e and 6.8f ensure that both of these requirements are met. As in Eq. 6.7, the Mode 1 and Mode 2 constraints are activated based on whether the measurement of the closed-

loop state at t_k is within Ω_{ρ_e}, which ensures that the state never leaves Ω_ρ. In addition, because the first n_s states meet their production schedule at the origin, and repeated application of the Mode 2 constraint drives the state to a small neighborhood $\Omega_{\rho_{\min}}$ of the origin,[20] the Mode 2 constraint is also activated whenever the measured value of any state that is required to meet a schedule deviates from this schedule by more than an allowable amount γ_i, $i = 1,\ldots,n_s$. This ensures that any deviation from the schedule causes the state to be driven back toward the origin, where all required states are within γ_i, $i = 1,\ldots,n_s$, and the schedule is thus sufficiently followed (this is guaranteed only if each γ_i is greater than or equal to the maximum magnitude of the corresponding state x_i in $\Omega_{\rho_{\min}}$).

When the state measurements at t_k of the first n_s states are within γ_i, $i = 1,\ldots,n_s$, of their scheduled values and the full process state is within Ω_{ρ_e}, the Mode 1 constraint is active, and the Mode 2 constraint is not applied. This allows control actions to be computed that vary the states to achieve economic optimality while meeting the schedule. If the weights α_{Wi}, $i = 1,\ldots,n_s$, are appropriately chosen, the LEMPC will choose control actions that prevent the values of x_i, $i = 1,\ldots,n_s$, from becoming large, which means that the economic optimization will primarily adjust the $n - n_s$ states that do not need to follow a schedule to attain economic optimality while continuing to keep the x_i, $i = 1,\ldots,n_s$, close to their scheduled values.

6.3.2 Schedule Changes Under EMPC for Schedule Management

Regardless of the formulation chosen for the EMPC for schedule management (Eq. 6.6 incorporating a terminal equality constraint or terminal region constraint with a hard constraint for the scheduled states, or a soft constraint formulation in the form of Eq. 6.6 or Eq. 6.8), a key feature of the EMPC is that it must be capable of handling changes in $x_{i,desired}$, $i = 1,\ldots,n_s$, according to the schedule to meet changes in demand or product or resource pricing. For all of the EMPC formulations, this requires a change in the objective function and/or constraints of the problem. Specifically, the terminal region or equality constraints and schedule constraint will be updated if a hard constraint formulation is used, penalties on deviations from the terminal conditions will be

updated in the objective function if a soft constraint is used, or the Lyapunov-based constraints will be reformulated with respect to the Lyapunov-based controller for the new steady-state if the LEMPC of Eq. 6.8 is used. The time at which this change is required may or may not be known by the controller *a priori*. Thus, some consideration must be made for the EMPC for schedule management to determine the manner in which the switching of the control problem should occur to avoid feasibility issues, both when the controller has prior knowledge of the switching time and when it does not.

As mentioned previously, an EMPC formulation for schedule management of the form of Eq. 6.6 but with either soft or hard constraints on the schedule and terminal equality or region constraints is difficult to evaluate for feasibility considerations when operated for a process without a schedule change. This is a limitation once again when the schedule changes because the set of points for which recursive feasibility is guaranteed in the presence of process disturbances is difficult to characterize. In addition, the set of initial conditions from which the EMPC to be implemented after the schedule change will be feasible is also difficult to characterize, so the question of when it is possible to change the schedule while maintaining feasibility of the control problem is difficult to answer even for nominal operation. However, for the LEMPC of Eq. 6.8, the conditions under which closed-loop feasibility can be maintained when the time at which it is desired to change $x_{i,desired}$ is known in advance by the controller and when it is not can be explicitly derived.

When the LEMPC begins to drive the closed-loop state to a steady-state at which new values of the scheduled states are met, the LEMPC of Eq. 6.8 is updated so that it is written with respect to the Lyapunov-based controller and process model with the origin at the steady-state corresponding to the new desired values of the scheduled states. For a feasible solution to the LEMPC for schedule management to be guaranteed when this updated LEMPC begins to be used, the closed-loop state must be contained within the stability region of the new steady-state when the LEMPC being utilized is updated. To see this, suppose that the LEMPC of Eq. 6.8 is designed with respect to a certain steady-state and is denoted as $LEMPC_1$, and has stability region Ω_{ρ_1}. At time t_1, the LEMPC will be updated so that it maintains the closed-loop state within the stability region around

a new steady-state for which the corresponding LEMPC is denoted $LEMPC_2$ and is the LEMPC of Eq. 6.8 but with the parameters updated for the new steady-state (e.g., the stability region is Ω_{ρ_2}). To ensure that $x(t_1) \in \Omega_{\rho_1}$ and Ω_{ρ_2} to guarantee that there is a feasible solution to $LEMPC_2$ at t_1, the stability regions for $LEMPC_1$ and $LEMPC_2$ must intersect at $x(t_1)$ to ensure that closed-loop stability is maintained at this state under both $LEMPC_1$ and $LEMPC_2$.

Fig. 6.2 illustrates the overlapping of the level sets just described for the case that three schedule changes occur. The steady-states are denoted as X_{s1}, X_{s2}, and X_{s3}, with corresponding stability regions Ω_{ρ_1}, Ω_{ρ_2}, and Ω_{ρ_3}. In the figure, it is assumed that the process is driven to each steady-state and then operated very close to that steady-state for some period of time. This means that at t_1, the state at t_1 (which is the steady-state corresponding to the prior desired value of the scheduled states) must be within the stability region of the new steady-state (e.g., $X_{s2} \in \Omega_{\rho_1}$ and Ω_{ρ_2}, and $X_{s3} \in \Omega_{\rho_2}$ and Ω_{ρ_3}) to ensure feasibility and closed-loop stability of the process.

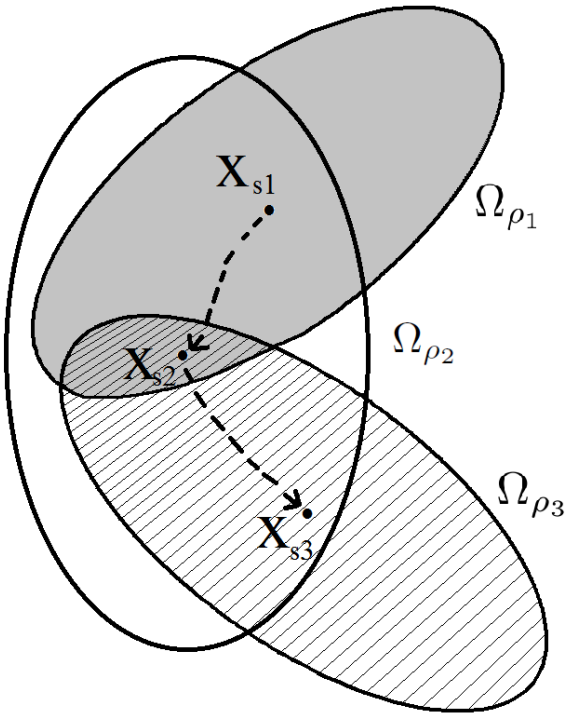

Figure 6.2: Illustration of intersection of level sets corresponding to each steady-state where the process schedule is met.

Ideally, the LEMPC would be updated to start driving the process state toward the next steady-

state in the schedule at the switching time t_s at which it is desired to start producing $x_{i,desired}$, $i = 1,\ldots,n_s$, at the values corresponding to this new steady-state (i.e., ideally, $t_1 = t_s$). However, because feasibility of the optimization problem at t_1 is ensured only if $x(t_1) \in \Omega_{\rho_1}$ and Ω_{ρ_2}, it is only possible for $t_1 = t_s$ when the LEMPC knows t_s far enough in advance to be able to drive the state into $\Omega_{\rho_1} \cap \Omega_{\rho_2}$ before t_s. If, for example, the LEMPC has no knowledge of t_s until t_s, the LEMPC may need to drive the state into $\Omega_{\rho_1} \cap \Omega_{\rho_2}$ after t_s, so that t_1 may be greater than t_s and thus there may be periods of time during which it is desired to start operating the process at the next $x_{i,desired}$, $i = 1,\ldots,n_s$, but this cannot yet occur while maintaining controller feasibility. More will be said regarding a method for choosing Ω_{ρ_2} to ensure that a region $\Omega_{\rho_1} \cap \Omega_{\rho_2}$ exists into which the LEMPC can be guaranteed to drive the process state in finite time in the section "Feasibility and Stability Analysis."

6.3.3 Scheduling and Operations Considerations with EMPC for Schedule Management

Several practical considerations for EMPC for schedule management that must be accounted for either at the scheduling level or at the operations level when developing the set of steady-states, Lyapunov-based control laws, and level sets to send to the controller are as follows:

- **The EMPC for schedule management requires that a region exists in which the EMPCs designed for both the current and next steady-states are both feasible, and that the state can be driven by the EMPC for schedule management into this region.**

  Notwithstanding that it may be possible for a variety of EMPC formulations to meet this criteria in practice even if it is not easily provable theoretically, for provable feasibility of the EMPC scheduling problem, the LEMPC formulation should be used and the feasibility issue should be addressed at the scheduling or operations level, depending on the difference between the timescale on which the schedule changes and the timescale of the process dynamics, and depending on the impact of the transient on the profit of the process.

When the process dynamics are determined to be on a timescale comparable to the timescale of schedule changes, or the manner in which transitions between regions of state-space occur is determined to significantly affect the process economics in a manner that would alter the schedule chosen if it were taken into account, it may be desirable to include considerations related to the process dynamics and level set intersections in the scheduling problem. The scheduling problem is often formulated as a mixed-integer linear program, but could be modified to include some representation of level set intersection (e.g., if the level sets are determined *a priori*, then constraints could be devised that permit the next steady-state in the schedule to only be one for which the level sets intersect; this ensures that, for example, a schedule developed for the steady-states in Fig. 6.2 does not request the production of X_{s1} followed immediately by the production of X_{s3} because Ω_{ρ_3} does not contain X_{s1}). It may be that one or more of the level sets that are found for the steady-states corresponding to demanded products do not intersect any of the other level sets corresponding to demanded products. In this case, it may be necessary to develop additional state-space points which do not correspond to any marketable product but which have level sets that allow for any gaps in state-space where the level sets of the demanded products do not intersect to be bridged. If this is required, such intermediate points can also be considered for inclusion in the scheduling problem, possibly with constraints that try to limit the time spent approaching these intermediate points or the number of the intermediate points approached in the schedule. For example, if a schedule requires production only of X_{s1} and X_{s3} in Fig. 6.2 without the production of X_{s2}, then it is not necessary to use the LEMPC for schedule management with the desired steady-state at X_{s2} all the way until the state reaches X_{s2}. Rather, the LEMPC with the desired steady-state at X_{s2} can be applied for an amount of time that ensures that the closed-loop state enters Ω_{ρ_3}, and then the LEMPC with the desired steady-state at X_{s3} can be applied. Because it may be necessary, for example, to produce a product that is not in immediate demand in order to transition between the production of two more heavily demanded products, accurate forecasting of data used to set the schedule (e.g., demand and pricing)

sufficiently long in advance are essential for determining an appropriate schedule for this LEMPC strategy, so that frequent changes to the schedule can be avoided, particularly if the changes require intermediate products to be produced. The scheduling problem may also include a representation of the process dynamics if it is on a timescale comparable to that on which the schedule is changed, to choose the best schedule accounting for the time spent with off-specification production due to the process dynamics.

If the process dynamics are much faster than the timescale on which scheduling changes occur, it may be decided to relegate the issue of moving between level sets to an operational issue after the schedule is determined. Thus, a standard scheduling problem can be solved without knowledge of the process dynamics or intersecting level sets, but then before sending the steady-states corresponding to the various desired production levels to the controller, the set of steady-states can be evaluated to determine whether their level sets intersect or whether it is necessary to add additional intermediate steady-states to the operating procedure as noted in the prior paragraph to drive the state through state-space without losing controller feasibility. If the time of switching from each production level to the next is known, this can also be considered in the development of the set of steady-states used in the operating procedure so that the production stays as close to the target values that were determined by the scheduling problem for the lengths of time determined by this problem as possible.

- **EMPC for schedule management in general cannot guarantee that scheduled states are at their values for all time.**

  Though this may at first seem to be a limitation of the method, when the schedule is changed under any controller, there will be some length of time in which the process state is transitioning to its new value at a speed determined by the process dynamics. In addition, if it is required to drive the state into the intersection of the level sets for the prior and new steady-states (e.g., t_s is not known *a priori*), there will be some time required after the new schedule is requested not only to move to the new schedule, but also to move toward the region of

intersection, and this time cannot be known *a priori* without closed-loop simulations. In general, the soft constraint formulation offers the flexibility to highly penalize the deviation of the states from the scheduled values so that the EMPC will calculate control actions that attempt to move the process state as quickly as possible to the new steady-state, given the process dynamics. In the presence of disturbances, there is no controller that can keep the values of some or all states at precise values for all times, but high penalties would again cause an EMPC for schedule management to drive the predicted state (and ideally the actual closed-loop state) toward a region where the schedule is met as quickly as possible. For the LEMPC for schedule management, because the feasible region is characterizable *a priori*, closed-loop off-line simulations can be used to determine a worst-case rate of approach to the next scheduled steady-state. If there are concerns regarding the time that the process is not operating with the states at the schedule due to disturbances, simulations can be performed to evaluate the effect of the choice of γ_i on product quality. In general, the magnitude of γ_i may be evaluated considering regular deviations of the scheduled states from their scheduled values due to process disturbances. If γ_i is very small relative to the state deviations, the Mode 2 constraint may be triggered almost constantly because of process disturbances, which would enforce steady-state operation and not allow for the possible economic benefits of EMPC for schedule management. It may be desirable to choose γ_i in a manner that prevents Mode 2 from activating regularly due to common disturbances if this does not significantly affect the product quality.

- **EMPC for schedule management requires a steady-state to be chosen for the process among many where the values of only the first n_s states are specified.**

  The steady-state to operate around may be chosen as the economically optimal steady-state at which the schedule is met, subject to practical constraints (e.g., limitations on the temperature for safety reasons).

6.3.4 Feasibility and Stability Analysis

In this section, we prove feasibility and closed-loop stability of a process under the proposed LEMPC for schedule management. We first present two propositions required for the feasibility and stability proofs, and then present a theorem on the feasibility and stability results.

Proposition 9 *(c.f.[20,117]). Consider the systems*

$$\dot{x}_a(t) = f(x_a(t), u(t), w(t)) \tag{6.9a}$$

$$\dot{x}_b(t) = f(x_b(t), u(t), 0) \tag{6.9b}$$

with initial states $x_a(t_0) = x_b(t_0) \in \Omega_\rho$. There exists a $\mathscr{K}$ function $f_W(\cdot)$ such that

$$|x_a(t) - x_b(t)| \leq f_W(t - t_0) \tag{6.10}$$

for all $x_a(t), x_b(t) \in \Omega_\rho$ and all $w(t) \in W$ with

$$f_W(\tau) = \frac{L_w \theta}{L_x}(e^{L_x \tau} - 1) \tag{6.11}$$

Proposition 10 *(c.f.[20,117]) Consider the Lyapunov function $V(\cdot)$ of the nominal system of Eq. 6.1 under the controller $h(x)$. There exists a quadratic function $f_V(\cdot)$ such that*

$$V(x) \leq V(\hat{x}) + f_V(|x - \hat{x}|) \tag{6.12}$$

for all $x, \hat{x} \in \Omega_\rho$ with

$$f_V(s) = \alpha_4(\alpha_1^{-1}(\rho))s + M_v s^2 \tag{6.13}$$

where M_v is a positive constant.

Theorem 3 *(c.f.[20]) Consider the system of Eq. 6.1 in closed-loop under the LEMPC design of Eq. 6.8 based on a controller $h(x)$ that satisfies the conditions of Eq. 6.2. Let $\varepsilon_w > 0$, $\Delta > 0$,*

$\rho > \rho_e \geq \rho_{\min} \geq \rho_s > 0$ *satisfy*

$$\rho_e \leq \rho - f_V(f_W(\Delta)) \tag{6.14}$$

and

$$-\alpha_3(\alpha_2^{-1}(\rho_s)) + L_x' M\Delta + L_w'\theta \leq -\varepsilon_w/\Delta \tag{6.15}$$

If $x(t_0) \in \Omega_\rho$ *and* $N \geq 1$ *where*

$$\rho_{\min} = \max\{V(x(t+\Delta)) : V(x(t)) \leq \rho_s\} \tag{6.16}$$

then the state $x(t)$ *of the closed-loop system is always bounded in* Ω_ρ *and is ultimately bounded in* $\Omega_{\rho_{\min}}$.

Proof 6.1 *In this proof, we examine feasibility and closed-loop stability of the LEMPC of Eq. 6.8 for operation around one steady-state corresponding to one set of desired values of the scheduled states.*

We first discuss the feasibility of the LEMPC of Eq. 6.8. This LEMPC is guaranteed to be feasible at all times if the state is maintained in Ω_ρ*, as will be subsequently shown, because the Lyapunov-based control law implemented in sample-and-hold is a feasible solution (i.e.,* $u = h(x(t_k)),\ t \in [t_k, t_{k+1})$ *and* $u = h(\tilde{x}(t_j)),\ t \in [t_j, t_{j+1}),\ j = k+1, \ldots, k+N-1$*, is always a feasible solution). This feasibility, however, is only ensured when the initial value of the state at the time* t_0 *at which the LEMPC of Eq. 6.8 first begins to be used is within* Ω_ρ *because the Lyapunov-based controller* $h(x)$ *implemented in sample-and-hold is only guaranteed to maintain closed-loop stability of states within* Ω_ρ.

Closed-loop stability is guaranteed at all times by the LEMPC formulation of Eq. 6.8. Before t'*, the state is always guaranteed to be within* Ω_ρ *from the use of the Mode 1 and Mode 2 constraints when the state leaves* Ω_{ρ_e} *using the same proof as in.*[20] *The requirement that the contractive constraint be enforced whenever* $|x_i(t_k)| \geq \gamma_i$ *ensures that the Lyapunov function of the closed-loop state decreases whenever the state leaves this bound, which ensures that the state can always be*

driven back into a region where this bound is met in finite time. Furthermore, the contractive constraint always forces the state to $\Omega_{\rho_{\min}}$, so after t', it is guaranteed to be driven into this small region containing the origin.

The fact that feasibility of the LEMPC design of Eq. 6.8 hinges on whether $x(t_0) \in \Omega_\rho$ shows that when there is a plan to switch the schedule and thus to adjust the V, Ω_{ρ_e}, Ω_ρ, $h(x)$, f, and origin used in Eq. 6.8, the state at the switching time must be within the stability region of the new steady-state. In general, it is difficult to characterize the points that may be accessed by the LEMPC within Ω_ρ without extensive closed-loop simulations from various initial conditions. The only region within the stability region of the first steady-state in which it is guaranteed that a process can be forced to operate is $\Omega_{\rho_{\min}}$, such that if the state is always driven into this region first and the new stability region overlaps this region, it can be guaranteed that a feasible solution to the new problem will exist. Another advantage of including $\Omega_{\rho_{\min}}$ within the overlap of the level sets is that any prior scheduled value of the state can be requested in the future and can be reached, since each stability region includes both $\Omega_{\rho_{\min}}$ of the set-point that it is designed with respect to, and also that of at least one other schedule. This motivates the following theorem, which characterizes the conditions under which the LEMPC formulation of Eq. 6.8 can be updated to drive the state to new values of the scheduled states without losing controller feasibility at t_1, both when t_s is known *a priori* and when it is not. In this theorem, the time length t_h is defined as the worst-case time for a Lyapunov-based controller implemented in sample-and-hold with sampling period Δ to drive the state from any initial condition in the stability region into $\Omega_{\rho_{\min}}$, and it can be assessed with closed-loop simulations using initial conditions throughout the stability (feasible) region of the LEMPC for schedule management.

Theorem 4 *Consider the process of Eq. 6.1 operated under the LEMPC of Eq. 6.8 formulated with respect to a steady-state having stability region Ω_{ρ_1} with $\Omega_{\rho_{\min}} \subseteq \Omega_{\rho_1}$ where $\Omega_{\rho_{\min}}$ is defined as in Eq. 6.16 for the steady-state with stability region Ω_{ρ_1}. If also $\Omega_{\rho_{\min}} \subseteq \Omega_{\rho_2}$ and t_s is known a priori such that t' can be chosen as $t' = t_s - t_h$, then $x(t_s) \in \Omega_{\rho_{\min}}$ and the LEMPC of Eq. 6.8 formulated with respect to a steady-state having stability region Ω_{ρ_2} is feasible at $t_1 = t_s$. If t_s is not known a*

priori, then if $t' = t_s$ and $t_1 = t_s + t_h$ and $\Omega_{\rho_{\min}} \subseteq \Omega_{\rho_1}$ and also $\Omega_{\rho_{\min}} \subseteq \Omega_{\rho_2}$, $x(t_1) \in \Omega_{\rho_{\min}}$ and the LEMPC of Eq. 6.8 formulated with respect to a steady-state having stability region Ω_{ρ_2} is feasible at t_1.

Proof 6.2 *The proof of this theorem relies on many concepts from the proof of Theorem 3. Specifically, if t_s is known a priori and $t' = t_s - t_h$, then if the Lyapunov-based controller were applied in sample-and-hold with sampling period Δ, the process state would be within $\Omega_{\rho_{\min}} \subseteq \Omega_{\rho_1} \cap \Omega_{\rho_2}$ by t_s, regardless of the location of the initial state in Ω_{ρ_1} from the definition of t_h. The Mode 2 constraint of Eq. 6.8f, when implemented repeatedly, ensures that the applied control action drives the closed-loop state into $\Omega_{\rho_{\min}}$ in a finite time at a rate no less than the rate at which a Lyapunov-based controller implemented in sample-and-hold would drive the state to this region. Thus, if the Mode 2 constraint begins to be implemented repeatedly at t', the closed-loop state under the LEMPC of Eq. 6.8 will enter $\Omega_{\rho_{\min}}$ by t_s and then since $x(t_s) \in \Omega_{\rho_2}$, from Theorem 3, the LEMPC for the next steady-state will be feasible at t_s. Using similar logic, if t_s is not known a priori but the Mode 2 constraint is applied repeatedly starting at $t' = t_s$, then by $t_1 = t_s + t_h$, the closed-loop state has entered $\Omega_{\rho_{\min}} \subseteq \Omega_{\rho_2}$, and the LEMPC for the next steady-state is then feasible by Theorem 3.*

6.4 Application to a Chemical Process Example

In this section, we provide a chemical engineering example to illustrate the application of the proposed EMPC with production schedule management. Specifically, a non-isothermal continuously stirred tank reactor (CSTR) where an irreversible second-order exothermic reaction takes place is considered. The reactor converts the reactant A to the product B ($A \rightarrow B$). An inert solvent containing the reactant A with a concentration of C_{A0} is fed to the reactor at a feed temperature of T_0. The CSTR is coated with a heating jacket that supplies or removes heat from the reactor at a heat rate Q. The reactor has a constant volume of V, and the volumetric flow rate of the entering and exiting streams is F. The liquid has a constant density of ρ_L and a heat capacity of C_p. The CSTR first-principles dynamic model derived from mass and energy balances for this process is of the

following form:

$$\frac{dC_A}{dt} = \frac{F}{V}(C_{A0} - C_A) - k_0 e^{-E/RT} C_A^2 \tag{6.17a}$$

$$\frac{dC_B}{dt} = k_0 e^{-E/RT} C_A^2 - \frac{F}{V} C_B \tag{6.17b}$$

$$\frac{dT}{dt} = \frac{F}{V}(T_0 - T) - \frac{\Delta H k_0}{\rho_L C_p} e^{-E/RT} C_A^2 + \frac{Q}{\rho_L C_p V} \tag{6.17c}$$

where C_A and C_B are the reactant and product concentrations. The temperature in the reactor is T and the reaction pre-exponential factor is k_0. E and ΔH are the activation energy and the enthalpy of the reaction, respectively (process parameter values are listed in Table 6.1). The CSTR is operated around an open-loop asymptotically stable steady-state that occurs at $[C_{As}\ C_{Bs}\ T_s] = [1.22\ kmol/m^3\ 2.78\ kmol/m^3\ 438.0\ K]$ which corresponds to an input vector of $[C_{A0s}\ Q_s] = [4.0\ kmol/m^3\ 0.0\ kJ/hr]$.

Table 6.1: Parameter values of the CSTR.

$F = 5.0$	$\frac{m^3}{hr}$	$k_0 = 8.46 \times 10^6$	$\frac{m^3}{kmol\ hr}$
$T_0 = 300$	K	$\Delta H = -1.15 \times 10^4$	$\frac{kJ}{kmol}$
$V = 1.0$	m^3	$E = 5.0 \times 10^4$	$\frac{kJ}{kmol}$
$C_p = 0.231$	$\frac{kJ}{kg\ K}$	$\rho_L = 1000$	$\frac{kg}{m^3}$
$R = 8.314$	$\frac{kJ}{kmol\ K}$		

The inlet concentration C_{A0} and the heat supply/removal rate Q are the manipulated inputs which are upper and lower bounded by physical limitations on actuators as follows: $0.5 \leq C_{A0} \leq 7.5\ kmol/m^3$ and $-5.0 \times 10^5 \leq Q \leq 5.0 \times 10^5\ kJ/hr$. The CSTR state and input vectors in deviation variable form are defined as follows: $x^T = [C_A - C_{As}\ C_B - C_{Bs}\ T - T_s]$ and $u^T = [C_{A0} - C_{A0s}\ Q - Q_s]$. In the simulations below, the process model of Eq. 6.17 was integrated numerically using the explicit Euler method with an integration time step of $h_c = 10^{-4}\ hr$. The control objective of the LEMPC is to minimize the heat supply and removal rate while meeting a desired production schedule of the desired product B. Therefore, the economic measure used as the LEMPC cost

function is given by:

$$\frac{1}{(t_{k+N}-t_k)}\int_{t_k}^{t_{k+N}}[\alpha Q(\tau)^2+\beta(C_B(\tau)-C_{B_{desired}})^2]d\tau \tag{6.18}$$

where α and β are weighting constants. Owing to practical considerations, we consider that a limited amount of reactant material is available for a given operating period of $t_p = 1\ hr$. Therefore, the time-averaged concentration of reactant fed to the reactor over the operating period should satisfy the following material constraint:

$$\frac{1}{t_p}\int_0^{t_p} u_1(\tau)\, d\tau = 0.0\, kmol/m^3. \tag{6.19}$$

To ensure closed-loop stability of the process considered, a Lyapunov-based controller is designed. In this example, only one stability region and Lyapunov-based controller, designed with respect to the open-loop asymptotically stable steady-state described above, was used, even when the schedule was switched. As will be shown below, there were no feasibility or closed-loop stability issues for the simulations performed, illustrating that the requirement that there be different but overlapping level sets for each schedule change for closed-loop stability and feasibility of the controller is met. An estimate of the closed-loop system stability region can be obtained utilizing the Lyapunov function established under the Lyapunov-based controller. In this example, Eq. 6.17b indicates that the concentration of the desired product C_B is affected by the concentration of the reactant C_A and the temperature T but not vice versa. Since the inputs of the system affect the reactant concentration and temperature differential equations directly in Eq. 6.17a and Eq. 6.17c, the stability analysis of the closed-loop system can be established on the basis of the (C_A, T) subsystem. Therefore we define a reduced state vector as $\hat{x}^T = [C_A - C_{As}\ T - T_s]$. The Lyapunov-based controller design can be represented as a vector with two components: $h^T(\hat{x}) = [h_1(\hat{x})\ h_2(\hat{x})]$. The inlet concentration control law $h_1(\hat{x})$ was set to its steady-state value ($h_1(\hat{x}) = 0.0\ kmol/m^3$) in order to meet the material constraint of Eq. 6.19. The stabilizing Lyapunov-based control law for the rate of heat input $h_2(\hat{x})$ is the following:[38]

$$h_2(\hat{x}) = \begin{cases} -\dfrac{L_f V + \sqrt{L_f V^2 + L_g V^4}}{L_g V}, & \text{if } L_g V \neq 0 \\ 0, & \text{if } L_g V = 0 \end{cases} \tag{6.20}$$

$L_f V$ and $L_g V$ denote the Lie derivatives of the Lyapunov function $V(\hat{x})$ with respect to $f(\hat{x})$ and $g(\hat{x})$ respectively, where $f(\hat{x})$ signifies the terms in Eqs. 6.17a and 6.17c (in deviation form) not including the inputs, and $g(\hat{x})$ signifies the terms multiplying the inputs in those equations. A quadratic Lyapunov function of the form $V(\hat{x}) = \hat{x}^T P \hat{x}$ was used to characterize the stability region of the closed-loop system with the following positive definite P matrix:

$$P = \begin{bmatrix} 1060 & 22 \\ 22 & 0.52 \end{bmatrix} \tag{6.21}$$

Extensive closed-loop simulations were conducted under the Lyapunov-based controller $h(\hat{x})$. The regions needed in designing stability constraints in the LEMPC controller were Ω_ρ with $\rho = 368$ and Ω_{ρ_e} with $\rho_e = 340$. In the simulation below, the LEMPC design had a sampling period of $\Delta = 0.1$ hr and a prediction horizon of $N = 10$.

It is assumed that the production schedule requires a change in the concentration of the desired product C_B every two hours (i.e., $C_{B_{desired}} = 3$ $kmol/m^3$ for the first two hours of operation, 1.5 $kmol/m^3$ for the next two, then 2.5 $kmol/m^3$, 2.7 $kmol/m^3$, and 2 $kmol/m^3$ for times between 4 and 6 hr, 6 and 8 hr, and 8 and 10 hr, respectively). The proposed LEMPC scheme was applied to the CSTR of Eq. 6.17 in order to produce C_B concentrations that meet the desired schedule. The CSTR was initiated from the steady-state and the LEMPC optimization problem at each sampling time was solved using the interior-point solver IPOPT.[119] The weighting coefficients in the objective function were chosen to be $\alpha = 1$ and $\beta = 10,000$ in order to balance the difference in magnitude between Q and $C_B - C_{B_{desired}}$. The resulting concentration of the output (C_B) is presented in Fig. 6.3, which demonstrates the ability of the proposed scheme to achieve the desired production schedule while taking into account allowable trajectories from the process dynamics.

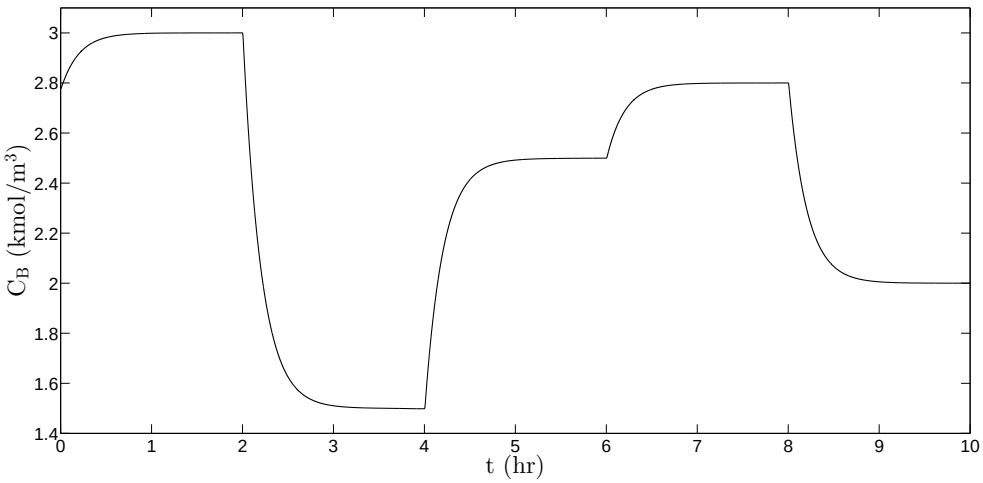

Figure 6.3: Concentration of product B in time for the CSTR of Eq. 6.17 under the LEMPC of Eq. 6.8 with the material constraint of Eq. 6.19, following the production schedule with changes in the required value of C_B every two hours.

The closed-loop input trajectories for the CSTR under the LEMPC throughout the ten hours of operation are presented in Fig. 6.4. The trajectories show that the inputs were able to meet the material constraint while driving the value of C_B to $C_{B_{desired}}$. They also show that the use of heating (Q) was effectively minimized as required by Eq. 6.18, with u_2 remaining at low values for the majority of the time of operation. The trajectories of the reactant concentration and reactor temperature in deviations from the steady-state values ($C_A - C_{As}, T - T_s$) are presented in Fig. 6.5. This figure shows that T and C_A evolved in a time-varying fashion, even after C_B reached $C_{B_{desired}}$, to maintain C_B at its required value while meeting the material constraint and minimizing the objective function.

To present the ability of this scheme to maintain the process within the stability region, the state-space trajectories of the reactant concentration and reactor temperature in deviations from the steady-state values ($C_A - C_{As}, T - T_s$) are presented in Fig. 6.6. The Lyapunov function values throughout the ten hours of operation are presented in Fig. 6.7.

The simulations discussed above manipulated two inputs while maintaining the time-averaged inlet concentration at its steady-state value. The traditional approach for achieving the desired production schedule, when the time-averaged inlet concentration is constrained to equal the steady-

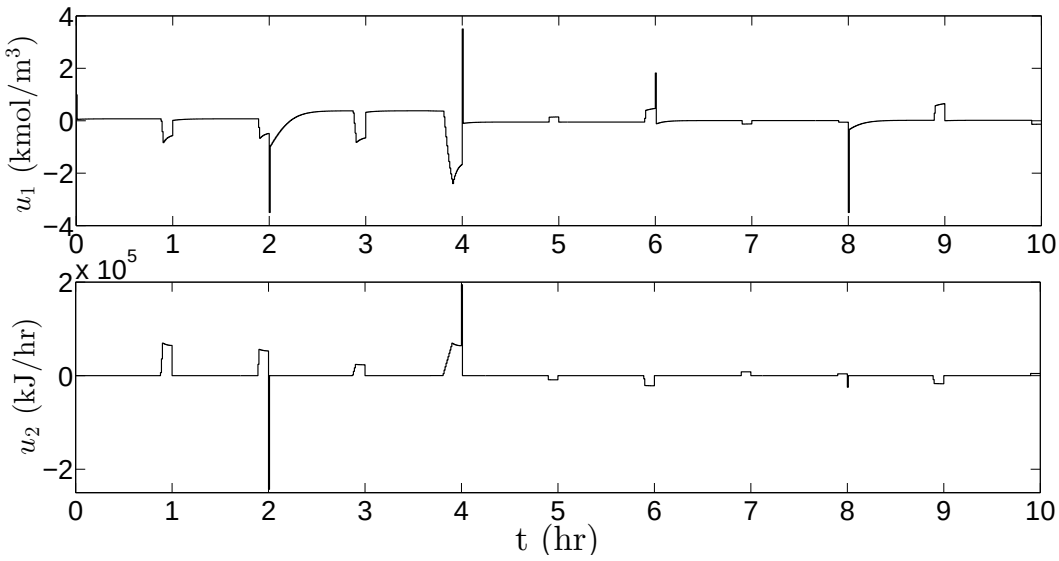

Figure 6.4: Input trajectories for the CSTR of Eq. 6.17 under the LEMPC of Eq. 6.8 with the material constraint of Eq. 6.19, following the production schedule with changes in the required value of C_B every two hours.

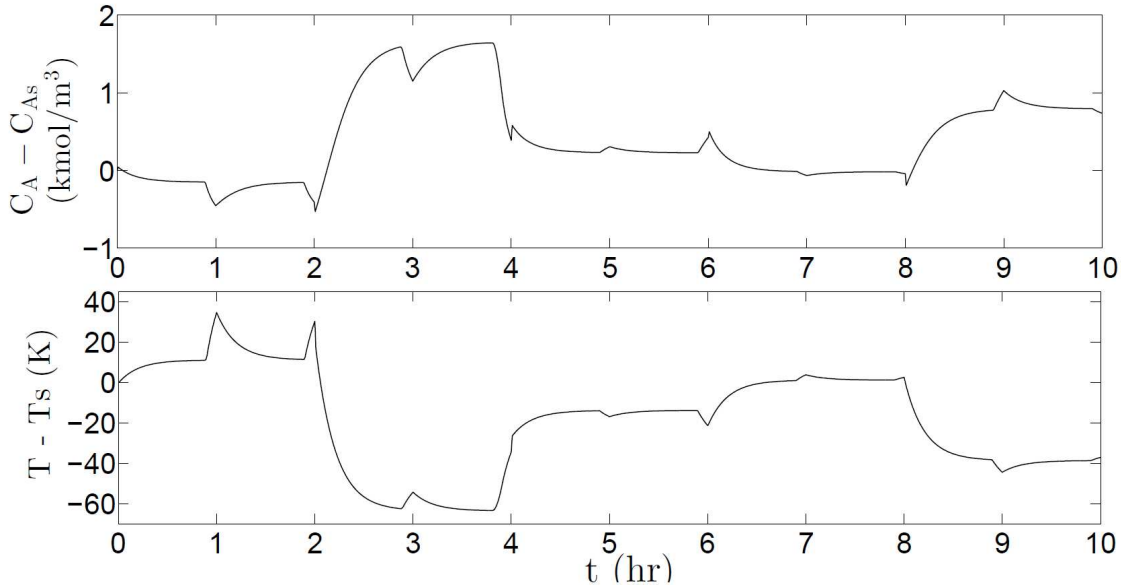

Figure 6.5: State trajectories for the CSTR of Eq. 6.17 under the LEMPC of Eq. 6.8 with the material constraint of Eq. 6.19, following the production schedule with changes in the required value of C_B every two hours.

state value, is to fix the inlet concentration to its steady-state value C_{A0s} and manipulate the heat input to achieve the desired schedule. This can lead to using more heat to achieve the same desired schedule since the problem involves only one manipulated input. Using the same optimization

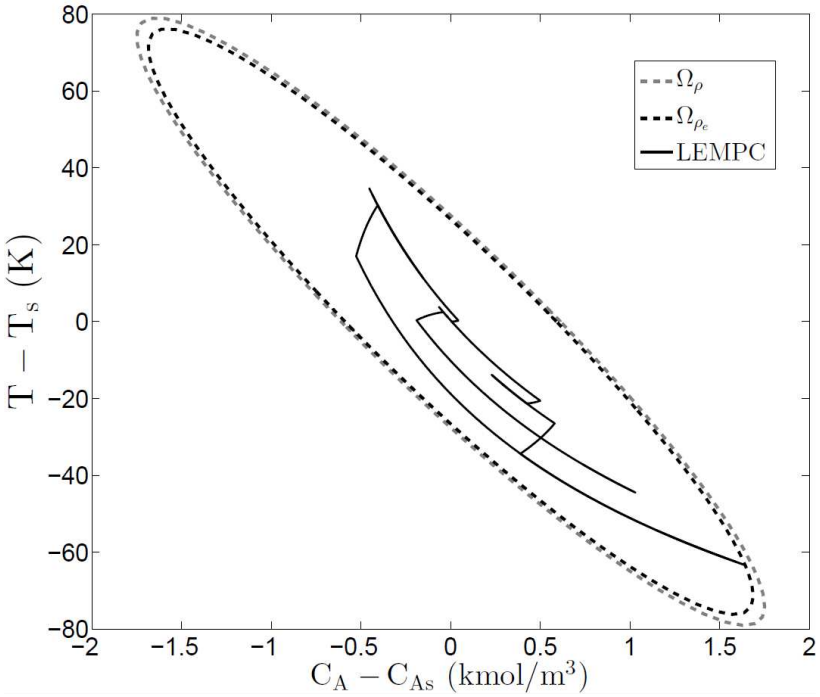

Figure 6.6: The state-space profile for the closed-loop CSTR of Eq. 6.17 under the LEMPC of Eq. 6.8 with the material constraint of Eq. 6.19 following the production schedule for the 10 *hr* operating period starting at $[C_A(0), T(0)] = [1.2\ kmol/m^3, 438\ K]$.

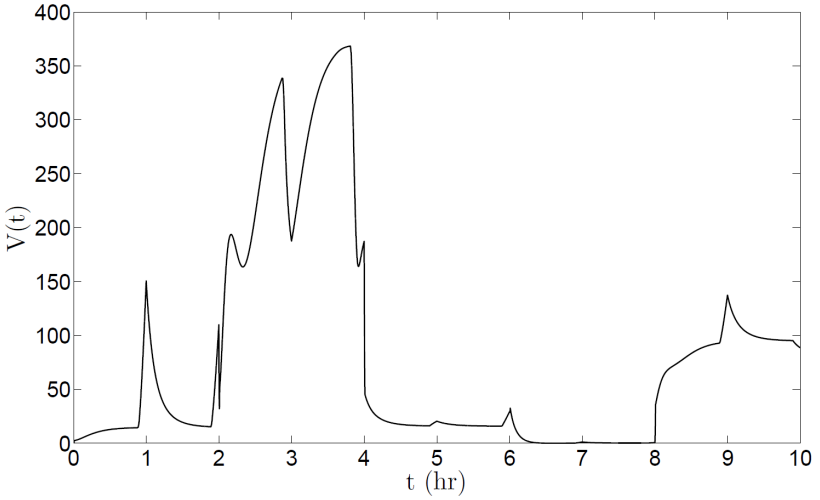

Figure 6.7: The Lyapunov function value as a function of time for the closed-loop CSTR of Eq. 6.17 under the LEMPC of Eq. 6.8 with the material constraint of Eq. 6.19 starting at $[C_A(0), T(0)] = [1.2\ kmol/m^3, 438\ K]$ following the production schedule with changes in the required value of C_B every two hours.

problem formulation as in the simulations above (with the same objective function and starting conditions) except with u_1 set to C_{A0s}, the total heat used in producing the first schedule for the

first two hours was 1.1378×10^6 kJ. However, when both inputs are manipulated to achieve the desired schedule, as demonstrated in the simulations above, the total heat used for producing the first schedule for the first two hours was 1.1176×10^6 kJ which requested 2% less heat usage. Even though the total amount of reactant fed to the reactor throughout the two hours of operation was the same in both cases, allowing the inlet concentration to be manipulated in a time-varying manner introduces extra flexibility that was utilized by the EMPC to minimize the objective function even further. Introducing more flexibility by allowing more inputs to be manipulated in a time-varying manner and also optimizing economics with respect to a subset of the state vector can in general enhance the economic performance. Although for this example the increase in the number of manipulated inputs resulted in only 2% economic benefit, using an EMPC for schedule management with multiple manipulated inputs can present higher economic performance in plants involving many more states where the desired production schedule is requested only over a subset of the entire state vector.

In the simulation presented above, we only imposed the Mode 2 constraint if the closed-loop state exited Ω_{ρ_e} because, as demonstrated through the results in Fig. 6.3, the high penalty on the deviation of the value of C_B from its steady-state value in the objective function (Eq. 5.18) was effective at driving the concentration of the product B to its scheduled value and maintaining it there with every change in the production level required by the schedule, without the need to utilize the Mode 2 constraint to enforce this tracking capability. In addition, there were no disturbances in this simulation to move the closed-loop state away from the schedule or out of Ω_{ρ_e}, so the Mode 2 constraint was never activated. In order to demonstrate the application of the Mode 2 constraints, another simulation that involved significant plant disturbances was considered. Specifically, we considered the case where the production schedule required a change in the concentration of the desired product C_B from $C_{B_{desired}} = 3\ kmol/m^3$ to $2.78\ kmol/m^3$ for the next three hours. The CSTR was initiated from $[C_{As}\ C_{Bs}\ T_s] = [1\ kmol/m^3\ 3\ kmol/m^3\ 468.37\ K]$ and no disturbances were imposed in the first hour of operation. After that, we implemented a constraint of the form of Eq. 6.8f requiring that the closed-loop state stay at the scheduled value of $C_B = 2.78\ kmol/m^3$, and that if

it deviates from this value by more than 0.01 $kmol/m^3$ (i.e., $\gamma = 0.01$), that the Mode 2 constraint should be activated to drive the closed-loop state back toward the schedule. A bounded disturbance vector $w^T = [w_1 \; w_2 \; w_3]$ was added to the right-hand side of Eq. 6.17 (stationary bounded Gaussian white noise with variances $\sigma_1 = 1$ $kmol/m^3$, $\sigma_2 = 1$ $kmol/m^3$, and $\sigma_3 = 40$ K with bounds $|w_1| \leq 1$, $|w_2| \leq 1$, and $|w_3| \leq 40$). Disturbances were added for the first 40 sampling periods of the second and third hours of operation which caused the concentration of C_B to be driven outside of the desired product quality in which case Mode 2 was activated to drive the concentration of C_B back inside $\gamma = 0.01$. The LEMPC was effective at maintaining C_B near the scheduled value of the state at all times as presented in Fig. 6.8.

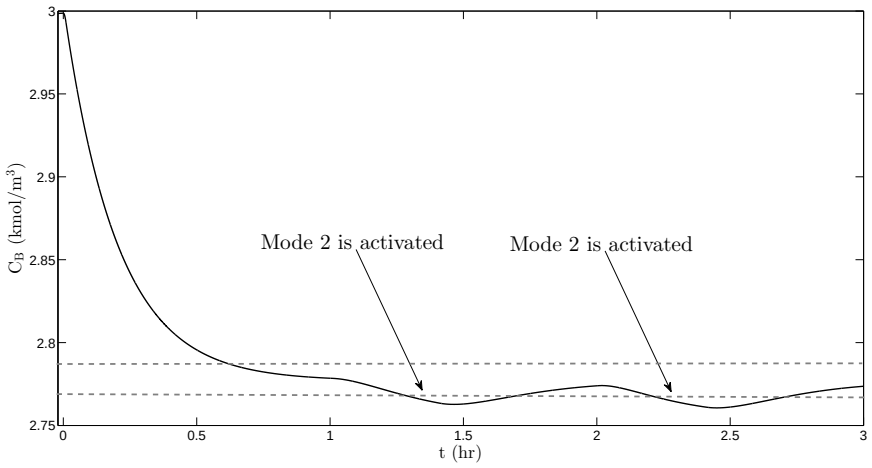

Figure 6.8: Concentration of product B in time for the CSTR of Eq. 6.17 under the LEMPC of Eq. 6.8 with the material constraint of Eq. 5.19, following the desired production schedule of $C_B = 2.78$ $kmol/m^3$ with $\gamma = 0.01$ subject to plant disturbances starting at $t = 1$ hr.

Remark 25 *The LEMPC for schedule management is particularly beneficial when the economics-based term in the cost function does not have its minimum at a steady-state of the process (i.e., time-varying operation is more profitable than steady-state operation). In traditional tracking MPC's that are designed to drive the closed-loop state to a steady-state, a quadratic cost function is used. In this chemical process example, the cost function has a quadratic form, but the process is not operated at steady-state (Fig. 6.5 shows that the unscheduled states evolve dynamically after C_B reaches the schedule), but in general non-quadratic stage costs can be utilized within EMPC,*

which distinguishes it from tracking MPC (see, e.g.,[48,112,118] *for examples of the implementation of EMPC's for the same chemical process utilized in the example in the present manuscript but for which the objective function is a non-quadratic function to be maximized).*

6.5 Conclusion

In this chapter, the concept of improving process profit while meeting a schedule with EMPC for production schedule management was proposed for nonlinear systems in which some of the states are constrained to follow a certain desired production schedule. Several formulations of EMPC for schedule management, with practical considerations, were discussed with a focus on LEMPC with a soft constraint for the schedule because for this formulation, sufficient conditions to guarantee closed-loop stability of a process and feasibility of the controller could be derived. A chemical process example demonstrated that the proposed approach can handle significant changes in the desired values of the scheduled states throughout time to achieve the requested production schedule while maintaining closed-loop stability.

Chapter 7

Conclusions

Motivated by the potential benefits of applying EMPC in industrial practice, this dissertation developed novel EMPC designs that utilized advanced data-driven linear and nonlinear system identification methods to obtain the process model needed for the EMPC feedback control strategy. On-line model identification was used to obtain more accurate models when the linear empirical models were not capable of capturing the nonlinear dynamics as a result of significant plant disturbances and variations, actuator faults, or changing the region of operation. In addition, we developed an EMPC framework that tracks production schedule for the desired states while maximizing economics with respect to the rest of the states.

Specifically, in Chapter 2, an LEMPC method formulated with empirical models was considered for nonlinear process systems. Under the assumption that the error between the empirical linear model and the one of the linearization of the nonlinear model at the steady-state around which time-varying operation is considered, sufficient conditions such that the LEMPC formulated with the empirical linear model will guarantee closed-loop stability of the nonlinear system in the sense of boundedness of the closed-loop state in a compact set were derived. A chemical process example demonstrated the application of the proposed method and extensive simulation results were given. From these results, a similar closed-loop behavior between the chemical process under the LEMPC with the nonlinear model and under the LEMPC with an empirical model was

observed with comparable closed-loop economic performance. However, a significant decrease in the computation time required to solve the LEMPC with a linear model compared to LEMPC with a nonlinear model was observed. In all of the simulations, the LEMPC with the linear model maintained closed-loop stability and obtained better closed-loop economic performance than that obtained at steady-state.

Subsequently, in Chapter 3, a nonlinear system identification technique was developed for general nonlinear systems with affine inputs using a polynomial nonlinear state-space (PNLSS) model with additional constraints on the numerical stability of the identified model so that the identification process would produce empirical models that could be numerically integrated with explicit methods without using a very small integration step size. The motivation for this is that such models have an advantage in model predictive control applications, in contrast to the models identified with standard techniques that may require a step size too small for real-time use. This chapter demonstrates the benefits of the proposed system identification method in model predictive control by developing the formulation of an LEMPC scheme that uses an empirical model derived from the PNLSS method accounting for model well-conditioning to predict the process dynamics. A stability analysis of the closed-loop system under this controller provided sufficient conditions such that closed-loop stability in the sense of boundedness of the closed-loop state in a compact set is established. A chemical process example demonstrated that incorporating the well-conditioned empirical model in place of a first-principles model in LEMPC has significant computational advantages such that the LEMPC with the empirical model can be used for real-time control, with minimal reduction in profit compared to using the first-principles model.

In Chapter 4, a methodology for error-triggered on-line model identification for nonlinear process systems was proposed for use in model-based controller design based on linear empirical models. The error-triggering was conducted by a moving horizon error detector that quantifies the relative prediction error within its horizon and triggers model re-identification based on recent input/output data when the prediction error exceeds a threshold. The error-triggered on-line model identification procedure was shown to have many applications, including the improvement of state

predictions for use in model-based control when plant variations occur and when the operating region changes. Both of these applications were demonstrated using a chemical process example under LEMPC. In the first example, it was shown that the error-triggering strategy was successful in indicating the need to re-identify the empirical model using the most recent input/output data as the plant dynamics changed, which can also result in greater economic profit. The second example demonstrated that the proposed approach is able to maintain closed-loop stability while expanding the region of operation to improve profit, and also indicated that the rate at which the operating region is expanded can have a significant effect on the process performance and the accuracy of the identified empirical model.

Subsequently, Chapter 5 proposed an on-line model identification methodology that updates the empirical models used in LEMPC on-line in order to overcome actuator faults. Empirical models were updated on-line based on significant prediction errors indicated by a moving horizon error detector. The error-triggered on-line model identification methodology can be applied to overcome different actuator faults scenaria that occur in practice, including the case where the value at which the actuator is stuck is known and the case where the value at which the actuator is stuck is unknown. Applications of each of such cases was demonstrated using two chemical process examples under LEMPC. In the first example, a benchmark chemical process was used to demonstrate the application of the proposed scheme in the case where the value at which the actuator is stuck is known. In the second example, another chemical process was used to demonstrate the application of the proposed scheme in the case where the value at which the actuator is stuck is unknown. The chemical process examples presented the ability of the proposed scheme to detect when it is necessary to update the empirical model on-line in response to operational variations caused by actuator faults and/or disturbances. Improved state predictions and economic performance were obtained under the proposed scheme compared to using one empirical model throughout operation despite the actuator faults. The examples show the successful implementation of a unified framework using the moving horizon error detector and error-triggered model updates within LEMPC for handling faults.

Finally, in Chapter 6, the concept of improving process profit while meeting a schedule with EMPC for production schedule management was proposed for nonlinear systems in which some of the states are constrained to follow a certain desired production schedule. Several formulations of EMPC for schedule management, with practical considerations, were discussed with a focus on LEMPC with a soft constraint for the schedule because for this formulation, sufficient conditions to guarantee closed-loop stability of a process and feasibility of the controller could be derived. A chemical process example demonstrated that the proposed approach can handle significant changes in the desired values of the scheduled states throughout time to achieve the requested production schedule while maintaining closed-loop stability.

Bibliography

[1] S. R. Anderson and V. Kadirkamanathan. Modelling and identification of non-linear deterministic systems in the delta-domain. *Automatica*, 43:1859 – 1868, 2007.

[2] D. Angeli, R. Amrit, and J. B. Rawlings. On average performance and stability of economic model predictive control. *IEEE Transactions on Automatic Control*, 57:1615–1626, 2012.

[3] K. J. Åström and P. Eykhoff. System identification–a survey. *Automatica*, 7:123 – 162, 1971.

[4] H. Anders, Z. Liu, and L. Vandenberghe. Subspace system identification via weighted nuclear norm optimization *51st IEEE Conference on Decision and Control*, 3439-3444, 2012.

[5] L. Vandenberghe. Convex optimization techniques in system identification. *IFAC Proceedings Volumes*, 45:71-76, 2012.

[6] S. Aumi and P. Mhaskar. Integrating data-based modeling and nonlinear control tools for batch process control. *AIChE Journal*, 58:2105–2119, 2012.

[7] S. A. Billings. *Nonlinear System Identification: NARMAX Methods in the Time, Frequency, and Spatio-Temporal Domains*. John Wiley & Sons, 2013.

[8] H. H. J. Bloemen, T. J. J. Van Den Boom, and H. B. Verbruggen. Model-based predictive control for Hammerstein-Wiener systems. *International Journal of Control*, 74:482–495, 2001.

[9] C.T. Chou and M. Verheagen. Subspace algorithms for the identification of multivariable dynamic errors-in-variables models. *Automatica*, 33:1857 – 1869, 1997.

[10] P. D. Christofides and N. H. El-Farra. *Control of Nonlinear and Hybrid Process Systems: Designs for Uncertainty, Constraints and Time-Delays*. Springer-Verlag, Berlin, Germany, 2005.

[11] F. J. Doyle, R. K. Pearson, and B. A. Ogunnaike. *Identification and control using Volterra models*. Springer, 2002.

[12] N. H. El-Farra and P. D. Christofides. Bounded robust control of constrained multivariable nonlinear processes. *Chemical Engineering Science*, 58:3025–3047, 2003.

[13] M. Ellis and P. D. Christofides. On finite-time and infinite-time cost improvement of economic model predictive control for nonlinear systems. *Automatica*, in press, DOI: 10.1016/j.automatica.2014.08.011.

[14] M. Ellis, H. Durand, and P. D. Christofides. A tutorial review of economic model predictive control methods. *Journal of Process Control*, 24:1156–1178, 2014.

[15] S. Engell. Feedback control for optimal process operation. *Journal of Process Control*, 17:203–219, 2007.

[16] W. Favoreel, B. De Moor, and P. Van Overschee. Subspace state space system identification for industrial processes. *Journal of Process Control*, 10:149 – 155, 2000.

[17] K. P. Fruzzetti, A. Palazoğlu, and K. A. McDonald. Nonlinear model predictive control using Hammerstein models. *Journal of Process Control*, 7:31 – 41, 1997.

[18] L. Grüne and M. Stieler. Asymptotic stability and transient optimality of economic MPC without terminal conditions. *Journal of Process Control*, 24:1187–1196, 2014.

[19] K. Hariprasad, S. Bhartiya, and R. D. Gudi. A gap metric based multiple model approach for nonlinear switched systems. *Journal of Process Control*, 22:1743 – 1754, 2012.

[20] M. Heidarinejad, J. Liu, and P. D. Christofides. Economic model predictive control of nonlinear process systems using Lyapunov techniques. *AIChE Journal*, 58:855–870, 2012.

[21] B. Huang and R. Kadali. *Dynamic modeling, predictive control and performance monitoring*. Lecture Notes in Control and Information Sciences. Springer, London, 2008.

[22] R. Huang, E. Harinath, and L. T. Biegler. Lyapunov stability of economically oriented NMPC for cyclic processes. *Journal of Process Control*, 21:501–509, 2011.

[23] X. Jin, B. Huang, and D. S. Shook. Multiple model LPV approach to nonlinear process identification with EM algorithm. *Journal of Process Control*, 21:182 – 193, 2011.

[24] H. K. Khalil. *Nonlinear Systems*. Prentice Hall, Upper Saddle River, NJ, third edition, 2002.

[25] P. Kokotović and M. Arcak. Constructive nonlinear control: a historical perspective. *Automatica*, 37:637–662, 2001.

[26] W.E. Larimore. Canonical Variate Analysis in identification, filtering, and adaptive control. In *Proceedings of the 29th IEEE Conference on Decision and Control, 1990.*, pages 596–604 vol.2, Dec 1990.

[27] Y. Lin and E. D. Sontag. A universal formula for stabilization with bounded controls. *Systems & Control Letters*, 16:393–397, 1991.

[28] L. Ljung. *System identification: theory for the user*. Prentice Hall, Upper Saddle River, NJ, 1999.

[29] I. Markovsky, J. C. Willems, P. Rapisarda, and B. L. M. De Moor. Algorithms for deterministic balanced subspace identification. *Automatica*, 41:755 – 766, 2005.

[30] J. L. Massera. Contributions to stability theory. *Annals of Mathematics*, 64:182–206, 1956.

[31] D. Muñoz de la Peña and P. D. Christofides. Lyapunov-based model predictive control of nonlinear systems subject to data losses. *IEEE Transactions on Automatic Control*, 53:2076–2089, 2008.

[32] M. A. Müller, D. Angeli, and F. Allgöwer. On the performance of economic model predictive control with self-tuning terminal cost. *Journal of Process Control*, 24:1179–1186, 2014.

[33] R. Murray-Smith and T Johansen. *Multiple Model Approaches to Nonlinear Modelling and Control*. CRC press, 1997.

[34] S. J. Norquay, A. Palazoğlu, and J. A. Romagnoli. Model predictive control based on Wiener models. *Chemical Engineering Science*, 53:75 – 84, 1998.

[35] B. A. Ogunnaike and W. H. Ray. *Process dynamics, modeling, and control*. Oxford University Press, New York, 1994.

[36] R. K. Pearson. Selecting nonlinear model structures for computer control. *Journal of Process Control*, 13:1–26, 2003.

[37] S. J. Qin. An overview of subspace identification. *Computers and Chemical Engineering*, 30:1502 – 1513, 2006.

[38] E. D. Sontag. A 'universal' construction of Artstein's theorem on nonlinear stabilization. *Systems & Control Letters*, 13:117–123, 1989.

[39] P. Van Overschee and B. De Moor. N4SID: Subspace algorithms for the identification of combined deterministic-stochastic systems. *Automatica*, 30:75 – 93, 1994.

[40] P. Van Overschee and B. De Moor. *Subspace identification for linear systems: Theory, Implementation, Application*. 1996.

[41] M. Verhaegen. Identification of the deterministic part of MIMO state space models given in innovations form from input-output data. *Automatica*, 30:61 – 74, 1994.

[42] M. Verhaegen and E. Deprettere. A fast, recursive MIMO state space model identification algorithm. In *Proceedings of the 30th IEEE Conference on Decision and Control*, pages 1349–1354, 1991.

[43] M. Verhaegen and P. Dewilde. Subspace model identification Part 1. The output-error state-space model identification class of algorithms. *International Journal of Control*, 56:1187–1210, 1992.

[44] M. Viberg. Subspace-based methods for the identification of linear time-invariant systems. *Automatica*, 31:1835 – 1851, 1995.

[45] A. Wächter and L. T. Biegler. On the implementation of an interior-point filter line-search algorithm for large-scale nonlinear programming. *Mathematical Programming*, 106:25–57, 2006.

[46] C. Yu, R. J. Roy, H. Kaufman, and B. W. Bequette. Multiple-model adaptive predictive control of mean arterial pressure and cardiac output. *IEEE Transactions on Biomedical Engineering*, 39:765–778, 1992.

[47] V. A. Akpan and G. D. Hassapis. Nonlinear model identification and adaptive model predictive control using neural networks. *ISA Transactions*, 50:177–194, 2011.

[48] A. Alanqar, M. Ellis, and P. D. Christofides. Economic model predictive control of nonlinear process systems using empirical models. *AIChE Journal*, 61:816–830, 2015.

[49] R. Amrit, J. B. Rawlings, and D. Angeli. Economic optimization using model predictive control with a terminal cost. *Annual Reviews in Control*, 35:178–186, 2011.

[50] M. Diehl, R. Amrit, and J. B. Rawlings. A Lyapunov function for economic optimizing model predictive control. *IEEE Transactions on Automatic Control*, 56:703–707, 2011.

[51] F. J. Doyle, R. K. Pearson, and B. A. Ogunnaike. *Identification and Control Using Volterra Models*. Springer, 2002.

[52] A. Dutta, Y. Zhong, B. Depraetere, K. Van Vaerenbergh, C. Ionescu, B. Wyns, G. Pinte, A. Nowe, J. Swevers, and R. De Keyser. Model-based and model-free learning strategies for wet clutch control. *Mechatronics*, 24:1008–1020, 2014.

[53] M. Ellis and P. D. Christofides. Optimal time-varying operation of nonlinear process systems with economic model predictive control. *Industrial & Engineering Chemistry Research*, 53:4991–5001, 2014.

[54] M. Ellis and P. D. Christofides. Real-time economic model predictive control of nonlinear process systems. *AIChE Journal*, 61:555–571, 2015.

[55] G. Harnack, L. Lauwers, R. Pintelon, and J. Schoukens. Identification of nonlinear feedback systems using a structured polynomial nonlinear state space model. In *Proceedings of the 15th IFAC Symposium on System Identification*, pages 332–337, Saint-Malo, France, 2009.

[56] B. Huang and R. Kadali. *Dynamic Modeling, Predictive Control and Performance Monitoring: A Data-driven Subspace Approach*. Springer-Verlag, London, 2008.

[57] R. Huang, L. T. Biegler, and E. Harinath. Robust stability of economically oriented infinite horizon NMPC that include cyclic processes. *Journal of Process Control*, 22:51–59, 2012.

[58] S. V. Lapin. Identification of time-varying nonlinear systems using Chebyshev polynomials. *Journal of Computational and Applied Mathematics*, 49:121–126, 1993.

[59] W. E. Larimore. Canonical variate analysis in identification, filtering, and adaptive control. In *Proceedings of the 29th IEEE Conference on Decision and Control*, pages 596–604, Honolulu, Hawaii, 1990.

[60] M. Ławryńczuk. Computationally efficient nonlinear predictive control based on neural Wiener models. *Neurocomputing*, 74:401–417, 2010.

[61] M. Ławryńczuk. Practical nonlinear predictive control algorithms for neural Wiener models. *Journal of Process Control*, 23:696–714, 2013.

[62] G. P. Liu, V. Kadirkamanathan, and S. A. Billings. On-line identification of nonlinear systems using Volterra polynomial basis function neural networks. *Neural Networks*, 11:1645–1657, 1998.

[63] S. Mahmoodi, J. Poshtan, M. R. Jahed-Motlagh, and A. Montazeri. Nonlinear model predictive control of a pH neutralization process based on Wiener–Laguerre model. *Chemical Engineering Journal*, 146:328–337, 2009.

[64] A. Marconato, J. Sjöberg, and J. Schoukens. Initialization of nonlinear state-space models applied to the Wiener–Hammerstein benchmark. *Control Engineering Practice*, 20:1126–1132, 2012.

[65] N. A. Mardi and L. Wang. Subspace-based model predictive control of time-varying systems. In *Proceedings of the 48th IEEE Conference on Decision and Control, held jointly with the 28th Chinese Control Conference*, pages 4005–4010, Shanghai, China, 2009.

[66] M.A. Müller, D. Angeli, and F. Allgöwer. On convergence of averagely constrained economic MPC and necessity of dissipativity for optimal steady-state operation. In *Proceedings of American Control Conference*, pages 3141–3146, Washington, DC, 2013.

[67] J. Paduart, L. Lauwers, R. Pintelon, and J. Schoukens. Identification of a Wiener–Hammerstein system using the polynomial nonlinear state space approach. *Control Engineering Practice*, 20:1133–1139, 2012.

[68] J. Paduart, L. Lauwers, J. Swevers, K. Smolders, J. Schoukens, and R. Pintelon. Identification of nonlinear systems using polynomial nonlinear state space models. *Automatica*, 46:647–656, 2010.

[69] A. Patrikar and J. Provence. Nonlinear system identification and adaptive control using polynomial networks. *Mathematical and Computer Modelling*, 23:159–173, 1996.

[70] R. S. Patwardhan, S. Lakshminarayanan, and S. L. Shah. Constrained nonlinear MPC using Hammerstein and Wiener models: PLS framework. *AIChE Journal*, 44:1611–1622, 1998.

[71] B. L. Pence, H. K. Fathy, and J. L. Stein. Recursive maximum likelihood parameter estimation for state space systems using polynomial chaos theory. *Automatica*, 47:2420–2424, 2011.

[72] J. B. Rawlings, D. Angeli, and C. N. Bates. Fundamentals of economic model predictive control. In *Proceedings of the 51st IEEE Conference on Decision and Control*, pages 3851–3861, Maui, Hawaii, 2012.

[73] T. B. Schön, A. Wills, and B. Ninness. System identification of nonlinear state-space models. *Automatica*, 47:39–49, 2011.

[74] G. R. Sriniwas and Y. Arkun. A global solution to the nonlinear model predictive control algorithms using polynomial ARX models. *Computers and Chemical Engineering*, 21:431–439, 1997.

[75] A. Van Mulders, J. Schoukens, M. Volckaert, and M. Diehl. Two nonlinear optimization methods for black box identification compared. *Automatica*, 46:1675–1681, 2010.

[76] P. Van Overschee and B. De Moor. *Subspace Identification for Linear Systems: Theory, Implementation, Application*. Kluwer Academic Publishers, Boston, MA, 1996.

[77] W. D. Widanage, J. Stoev, A. Van Mulders, J. Schoukens, and G. Pinte. Nonlinear system-identification of the filling phase of a wet-clutch system. *Control Engineering Practice*, 19:1506–1516, 2011.

[78] J. Zhang, S. Liu, and J. Liu. Economic model predictive control with triggered evaluations: State and output feedback. *Journal of Process Control*, 24:1197–1206, 2014.

[79] B. A. Ogunnaike and W. H. Ray. *Process Dynamics, Modeling, and Control*. Oxford University Press, New York, 1994.

[80] G. Mercère, S. Lecoeuche, and M. Lovera. Recursive subspace identification based on instrumental variable unconstrained quadratic optimization. *International Journal of Adaptive Control and Signal Processing*, 18:771–797, 2004.

[81] M. Lovera, T. Gustafsson, and M. Verhaegen. Recursive subspace identification of linear and non-linear Wiener state-space models. *Automatica*, 36:1639–1650, 2000.

[82] M. Moonen, B. De Moor, L. Vandenberghe, and J. Vandewalle. On- and off-line identification of linear state-space models. *International Journal of Control*, 49:219–232, 1989.

[83] P. Kokotović and M. Arcak. Constructive nonlinear control: A historical perspective. *Automatica*, 37:637–662, 2001.

[84] D. Q. Mayne, J. B. Rawlings, C. V. Rao, and P. O. M. Scokaert. Constrained model predictive control: Stability and optimality. *Automatica*, 36:789–814, 2000.

[85] F. Alfani and J. J. Carberry. An exploratory kinetic study of ethylene oxidation over an unmoderated supported silver catalyst. *La Chimica e L'Industria*, 52:1192–1196, 1970.

[86] F. Özgülşen, R. A. Adomaitis, and A. Çinar. A numerical method for determining optimal parameter values in forced periodic operation. *Chemical Engineering Science*, 47:605–613, 1992.

[87] J. E. Bailey, F. J. M. Horn, and R. C. Lin. Cyclic operation of reaction systems: Effects of heat and mass transfer resistance. *AIChE Journal*, 17:818–825, 1971.

[88] P. L. Silveston. Periodic operation of chemical reactors-a review of the experimental literature. *Sādhanā*, 10:217–246, 1987.

[89] A. Alanqar, M. Ellis, and P. D. Christofides. Economic model predictive control of nonlinear process systems using multiple empirical models. In *Proceedings of the American Control Conference*, pages 4953–4958, Chicago, IL, 2015.

[90] M. Baldea, J. Du, J. Park, and I. Harjunkoski. Integrated production scheduling and model predictive control of continuous processes. *AIChE Journal*. 2015;61:4179-4190.

[91] M.A. Gutiérrez-Limón, A. Flores-Tlacuahuac A, and I.E. Grossmann. A reactive optimization strategy for the simultaneous planning, scheduling and control of short-period continuous reactors. *Computers & Chemical Engineering*. 2016;84:507-515.

[92] A.F. Merchan, S. Velez, and C.T. Maravelias. Tightening methods for continuous-time mixed-integer programming models for chemical production scheduling. *AIChE Journal*. 2013;59:4461-4467.

[93] K. Subramanian, J.B. Rawlings, and C.T. Maravelias. Economic model predictive control for inventory management in supply chains. *Computers & Chemical Engineering*. 2014;64:71-80.

[94] E. Perea-López, B.E. Ydstie, and I.E. Grossmann. A model predictive control strategy for supply chain optimization. *Computers & Chemical Engineering*. 2003;27:1201-1218.

[95] K. Subramanian, J.B. Rawlings, and C.T. Maravelias, J. Flores-Cerrillo, and L. Megan. Integration of control theory and scheduling methods for supply chain management. *Computers & Chemical Engineering*. 2013;51:4-20.

[96] K.B. McAuley and J.F. MacGregor. Optimal grade transitions in a gas phase polyethylene reactor. *AIChE Journal*. 1992;38:1564-1576.

[97] E. Perea, I. Grossmann, E. Ydstie, and T. Tahmassebi. Dynamic modeling and classical control theory for supply chain management. *Computers & Chemical Engineering*. 2000;24:1143-1149.

[98] G.M. Kopanos and E.N. Pistikopoulos. Reactive scheduling by a multiparametric programming rolling horizon framework: A case of a network of combined heat and power units. *Industrial & Engineering Chemistry Research*. 2014;53:4366-4386.

[99] X. Wang, N.H. El-Farra, and A. Palazoglu. Optimal scheduling of demand responsive industrial production with hybrid renewable energy systems. *Renewable Energy*. 2017; 100:53-64.

[100] J. Du, J. Park, I. Harjunkoski, and M. Baldea. A time scale-bridging approach for integrating production scheduling and process control. *Computers & Chemical Engineering*. 2015;79:59-69.

[101] A. Flores-Tlacuahuac and I.E. Grossmann. Simultaneous cyclic scheduling and control of a multiproduct CSTR. *Industrial & Engineering Chemistry Research*. 2006;45:6698-6712.

[102] A. Flores-Tlacuahuac and I.E. Grossmann. Simultaneous scheduling and control of multiproduct continuous parallel lines. *Industrial & Engineering Chemistry Research*. 2010;49:7909-7921,.

[103] E.N. Pistikopoulos and N.A. Diangelakis. Towards the integration of process design, control and scheduling: Are we getting closer? *Computers & Chemical Engineering*. 2016;91:85-92.

[104] R.C. Pattison, C.R. Touretzky, T. Johansson, I. Harjunkoski, and M. Baldea. Optimal process operations in fast-changing electricity markets: Framework for scheduling with low-order dynamic models and an air separation application. *Industrial & Engineering Chemistry Research*. 2016;55:4562-4584.

[105] M. Baldea and I. Harjunkoski. Integrated production scheduling and process control: A systematic review. *Computers & Chemical Engineering*. 2014;71:377-390.

[106] C. Tong, A. Palazoglu, N.H. El-Farra, and X. Yan. Energy demand management for process systems through production scheduling and control. *AIChE Journal*. 2015;61:3756-3769.

[107] M.W. McConley, B.D. Appleby, M.A. Dahleh, and E. Feron. A computationally efficient Lyapunov-based scheduling procedure for control of nonlinear systems with stability guarantees. *IEEE Transactions on Automatic Control*. 2000;45:33-49.

[108] C. Tong, N.H. El-Farra, and A. Palazoglu. Energy demand response of process systems through production scheduling and control. In: *Proceedings of the 9th IFAC Symposium on Advanced Control of Chemical Processes*. Whistler, Canada: 2015;385-390.

[109] C.R. Touretzky and M. Baldea. Integrating scheduling and control for economic MPC of buildings with energy storage. *Journal of Process Control*. 2014;24:1292-1300.

[110] Z. He, M.H. Sahraei, and L.A. Ricardez-Sandoval. Flexible operation and simultaneous scheduling and control of a CO_2 capture plant using model predictive control. *International Journal of Greenhouse Gas Control*. 2016;48:300-311.

[111] H.K. Khalil. *Nonlinear Systems* (third edition). Upper Saddle River, NJ: Prentice Hall, 2002.

[112] A. Alanqar, H. Durand, and P. D. Christofides. On identification of well-conditioned nonlinear systems: Application to economic model predictive control of nonlinear processes. *AIChE Journal*, 61:3353-3373, 2015

[113] L.E. Sterman and B.E. Ydstie. Periodic forcing of the CSTR: An application of the generalized Π-criterion. *AIChE Journal*. 1991;37:986-996.

[114] M. Ellis, H. Durand, and P.D. Christofides. Elucidation of the role of constraints in economic model predictive control. *Annual Reviews in Control*. 2016;41:208-217.

[115] S.F. Hafstein. A constructive converse Lyapunov theorem on asymptotic stability for nonlinear autonomous ordinary differential equations. *Dynamical Systems*. 2005;20:281-299.

[116] M. Ellis, J. Zhang, J. Liu, and P.D. Christofides. Robust moving horizon estimation based output feedback economic model predictive control. *Systems & Control Letters*. 2014;68:101-109.

[117] P. Mhaskar P, J. Liu, and P.D. Christofides. *Fault-Tolerant Process Control: Methods and Applications*. London, England: Springer-Verlag, 2013.

[118] A. Alanqar, H. Durand, and P. D. Christofides. Error-triggered on-line model identification for model-based feedback control. *AIChE Journal*, 63:949–966, 2017.

[119] A. Wächter and L. T. Biegler. On the implementation of an interior-point filter line-search algorithm for large-scale nonlinear programming. *Mathematical Programming*, 106:25–57, 2006.

[120] L. Lao, M. Ellis, and P. D. Christofides. Proactive fault-tolerant model predictive control. *AIChE Journal*, 59:2810–2820, 2013.

[121] P. Mhaskar, A. Gani, N. H. El-Farra, C. McFall, P. D. Christofides, and J. F. Davis. Integrated fault-detection and fault-tolerant control of process systems. *AIChE Journal*, 52:2129–2148, 2006.

[122] A. Alanqar, H. Durand, F. Albalawi, and P. D. Christofides. An economic model predictive control approach to integrated production management and process operation. *AIChE Journal*, in press, 2017

[123] A. Alanqar, H. Durand, and P. D. Christofides. Fault-Tolerant Economic Model Predictive Control Using Error-Triggered On-line Model Identification. *Industrial & Engineering Chemistry Research J.*, submitted, 2017.

[124] A. Alanqar, H. Durand, and P. D. Christofides. Handling Plant Variation via Error-Triggered On-line Model Identification: Application to Economic Model Predictive Control *IFAC-PapersOnLine*, 49:790-795, 2016

[125] A. Alanqar, H. Durand, and P. D. Christofides. Fault-Tolerant Economic Model Predictive Control Using Empirical Models *IFAC-PapersOnLine*, in press, 2017

[126] A. Alanqar, H. Durand, and P. D. Christofides. Error-triggered on-line model identification in economic model predictive control *American Control Conference (ACC)*, 1770-1777, 2016

[127] A. Alanqar, H. Durand, F. Albalawi, and P. D. Christofides. Integrating production scheduling and proceAlbalawiss operation via economic model predictive control *IEEE 55th Conference on Decision and Control (CDC)*, 3190-3195, 2016